UNIVERSITY OF BIRMINGHAM

ADVANCED IN VITRO AND IN SILICO MODELS TO EXPLORE MECHANISMS OF DEEP VEIN THROMBOSIS

By

HOSAM ALDEN BAKSAMAWI

A thesis submitted to The University of Birmingham for the degree of

DOCTOR OF PHILOSOPHY

School of Chemical Engineering

College of Engineering and Physical Sciences

The University of Birmingham

October 2023

Abstract:

Deep vein thrombosis is a significant global medical issue associated with high levels of illness and death. Investigating DVT mechanisms and discovering innovative approaches for its prevention and treatment rely extensively on animal models; however, using animals in research is associated with technical and ethical challenges, which raise the critical need to create *in vitro* and *in silico* models that mimic the formation of thrombi in deep veins without relying on animals. Here, a microfluidics *in-vitro* method allows for the investigation of valve flexibility through an *in-situ* fabrication process, which provides independent control over the rigidity of valve leaflets and enables testing under pulsatile flow conditions. Symmetrical valves exhibit platelet accumulation on valve tips, while asymmetrical valves show platelet accumulation within the valve pocket. This model has been further developed by incorporating moving valve leaflets to replicate venous hydrodynamics alongside an endothelial cell monolayer. Employing a pulsatile flow, typical of veins, these experiments reveal that unstimulated human platelets, reconstituted with whole blood, accumulate on the luminal side of leaflet tips in proportion to leaflet flexibility. Thrombin-induced platelet activation results in robust accrual at leaflet tips. GPIbα-vWF interaction blockade abolishes platelet deposition. Histamine-induced endothelial stimulation prompts platelet accrual at the basal side of leaflets, illustrating human thrombi location and indicating a dependence on leaflet flexibility and GPIbα-vWF interaction. An in-silico model has also been developed to simulate particle agglomeration within elastic valves, replicating venous valve geometry and fluid dynamics. The findings support the hypothesis that fluid dynamics near the valve leaflets primarily drive clot formation.

These approaches combine experimental and numerical models to increase our understanding of DVT initiation phenomena, highlighting crucial aspects of thrombus formation. Also, It offers a feasible alternative to animal models in research.

ACKNOWLEDGEMENTS

First and foremost, I extend my deepest gratitude to my supervisors, Dr Daniele Vigolo, Dr Alessio Alexiadis, and Dr Alexander Brill, for their outstanding support throughout my PhD journey.

I am also profoundly thankful to the School of Chemical Engineering at the University of Birmingham and the Birmingham Platelets Group for providing the essential resources and environment for conducting my laboratory experiments. Special appreciation goes to the National Centre for the Replacement, Refinement, and Reduction of Animals in Research (NC3Rs) for their sponsorship, which was key in the pursuit of my research.

I have been truly fortunate to be surrounded by exceptional colleagues who showed great understanding during the challenging times, particularly in the face of the pandemic and the premature birth of my son, Khaled. The blessing of fatherhood served as a constant source of inspiration, propelling me to strive for excellence in all aspects of life.

My deepest appreciation extends to my wife, Dr Hadil Abuwarda, whose extraordinary support has been a constant pillar of strength throughout my PhD journey. Her belief in me played an important role in reaching this significant milestone, and I consider myself genuinely fortunate to have her by my side.

I would also like to express a special and heartfelt appreciation to my beloved parents, Khaled and Haifaa, as well as my sister, brother, and my extened family. Your enduring support and encouragement have been a consistent source of motivation and resilience during my entire PhD journey.

LIST OF PAPERS AND CONFERENCES

- Schofield, Z., **Baksamawi, H.A**., Campos, J., Alexiadis, A., Nash, G.B., Brill, A. and Vigolo, D. (2020) 'The role of valve stiffness in the insurgence of deep vein thrombosis', *Communications Materials*, *1*(1), p.65.
- **Baksamawi, H.A**., Ariane, M., Brill, A., Vigolo, D. and Alexiadis, A. (2021) 'Modelling particle agglomeration on through elastic valves under flow', *ChemEngineering*, *5*(3), p.40.
- **Baksamawi, H.A**., Alexiadis, A., Vigolo, D. and Brill, A. (2023) 'Platelet accumulation in an endothelium-coated elastic vein valve model of deep vein thrombosis is mediated by GPIb α—VWF interaction', *Frontiers in Cardiovascular Medicine*, *10*, p.1167884.

The most recent findings were selected for an oral presentation at the following conferences:

- **Baksamawi, H.A**., Alexiadis, A., Vigolo, D. and Brill, A. (2023) 'Platelet accumulation in an endothelium-coated elastic vein valve model of deep vein thrombosis is mediated by GPIb α—VWF interaction': Selected for an oral presentation at the BSHT Annual Scientific Meeting, Birmingham, 2023.
- **Baksamawi, H.A**., Alexiadis, A., Vigolo, D. and Brill, A. (2023) 'Platelet accumulation in an endothelium-coated elastic vein valve model of deep vein thrombosis is mediated by GPIb α—VWF interaction': Selected for an oral presentation at the LASA Annual Winter Meeting, which includes a 3Rs, Cambridge, 2023.

Table of Contents

Chapter 1. Introduction **1**

1.1. Background of haemostasis 2

1.1.1. Primarily haemostasis 2

1.1.2. Secondary haemostasis 2

1.1.3. Tertiary haemostasis 5

1.2. Roles of von Willebrand factor (vWF) and fibrinogen in haemostasis 6

1.2.1. vWF 6

1.2.2. Fibrinogen 7

1.3. The role of platelets in haemostasis 8

1.3.1. The principal surface receptors of the platelet 10

1.3.1.1. Glycoprotein (GP)Ib-IX-V 10

1.3.1.2. Integrins 12

1.3.1.3. Glycoprotein VI 13

1.3.1.4. G protein-coupled receptors (GPCRs) 13

1.3.1.4.1. The PARs family 14

1.3.1.5. Toll-like receptors (TLRs) 14

1.3.2. Platelet granules 19

1.4. Background of deep vein thrombosis (DVT) 20

1.5. DVT within the umbrella of cardiovascular diseases 21

1.6. Exploration of Deep Vein Thrombosis (DVT) 23
1.6.1. DVT epidemiology 23
1.6.2. Aetiology and risk factors for DVT 26
1.6.3. Challenges associated with DVT. 27
1.7. DVT and Virchow's triad 29
1.7.1. Blood flow stasis 30
1.7.2. Hypercoagulability 31
1.7.3. Endothelial dysfunction 31
1.7.4. Blood flow stasis along with hypoxia and endothelium activation 32
1.8. Venous versus arterial thrombosis 35
1.8.1. An overview of the arterial thrombosis route 35
1.9. Blood vessel anatomy 40
1.9.1. The tunica intima 42
1.9.1.1. Endothelial cells 42
1.9.2. The tunica media 43
1.9.2.1. Extracellular matrix (ECM) 43
1.9.2.2. Smooth muscle cells (SMCs) 44
1.9.3. Tunica adventitia 45
1.10. Blood flow 45
1.10.1. Platelet adhesion and aggregation are influenced by WSR 47
1.10.2. The role of venous valves in DVT 49
1.11. Models of DVT 54

1.11.1. *In-Vivo* models of DVT 54

1.11.1.1. Challenges of using IVC models for DVT 57

1.11.1.2. Ethical consideration 59

1.11.2. *In-Vitro* models of DVT 60

1.11.2.1. Human microscopic venous valves (MVVs) 61

1.11.2.2. The importance of developing DVT *in vitro* models 62

1.11.3. *In-Silico* models of DVT 67

1.11.3.1. Mesh free approach 68

1.11.3.2. Previous numerical models of vein valves 69

Chapter 2. Material and Methods **74**

2.1. *In Vitro* 75

2.1.1. Master Mould Fabrication 75

2.1.2. Preparation and modification of PDMS and PEGDA surfaces 77

2.1.2.1. Valve fabrication 78

2.1.2.1.1. Microfluidic devices without cells 78

2.1.2.1.2. Microfluidic devices to be coated with HUVECs monolayer 80

2.1.3. Coating with HUVEC 81

2.1.3.1. Preparation of the Human umbilical vein endothelial cells (HUVECs) 82

2.1.3.2. Functionalisation and sterilisation of the microfluidic device 83

2.1.4. Blood preparation 84

2.1.5. Immunostaining 85

2.1.6. Imaging 86

2.1.6.1. Filter cubes specifications and applications 88

2.1.6.2. Image Quantification and statistical analysis 90

2.2. *In silico* 90

2.2.1. The theory of Discrete Multiphysics 90

2.2.1.1. Smoothed Particle Hydrodynamics (SPH) 91

2.2.1.2. Lattice Spring Model (LSM) 93

2.2.1.3. Coupling SPH and LSM (Fluid-structure interaction) 93

2.2.1.4. Solid-solid interaction (agglomeration) 97

2.2.2. The valve model and geometry 97

Chapter 3. A Microfluidic approach to investigate deep vein thrombosis 102

3.1. Introduction 103

3.2. Result and discussion 104

3.2.1. Analysing the blood aggregation on or behind the fabricated flexible valves 104

3.2.1.1. Symmetrical valve 105

3.2.1.2. Asymmetrical valve 108

3.3. Summary and conclusion 111

Chapter 4. Modelling particle agglomeration on through elastic valves under flow 113

4.1. Introduction 114

4.2. Results and discussion 116

4.2.1. Hydrodynamics 116

4.2.2. Particle agglomeration 118

4.2.3. Larger agglomerates 120

4.3. Conclusion 122

Chapter 5. Cellular Elastic Vein Valve (CEVV) model **123**

5.1. Introduction 124

5.2. Results and Discussion 126

5.2.1. HUVECs growth on PDMS surfaces 126

5.2.2. HUVECs growth within the microfluidic channels 129

5.2.3. HUVECs growth within the microfluidic channels with the presence of a flexible valve 131

5.3. Capability of CEVV model for the blood experiment 141

Chapter 6. Platelet accumulation in an endothelium-coated elastic vein valve model of deep vein thrombosis is mediated by GPIbα – vWF interaction **143**

6.1. Introduction 144

6.2. Results 146

6.2.1. Cellular elastic vein valve model 146

6.2.2. Unchallenged platelets accumulate at the luminal side of leaflet tips 148

6.2.3. Thrombin activation enhances platelet accumulation 151

6.2.4. Accumulation of activated platelets depends on GPIbα—vWF A1 domain interaction. 145

6.2.5. Endothelial activation promotes platelet accumulation at the space behind valve leaflets 154

6.3. Discussion 155

6.4. Conclusion 160

Chapter 7. General conclusions and further work **162**

7.1. Summary and conclusion 163

7.2. Further work 167

Chapter 8. List of references **172**

Apendex **198**

Table of Figures

Figure 1.1. Coagulation cascade consists of intrinsic, extrinsic, and common pathways. **4**

Figure 1.2. Inhibition and activation pathways of producing Plasmin from Plasminogen. Plasmin will facilitate tertiary haemostasis known as fibrinolysis, or clot lysis (Gil, 2019; Ziliotto, Bernardi and Piazza, 2021). **5**

Figure 1.3. In the human GPIb-IX-V complex, the subunits GPIbα, GPIbβ, GPIX, and GPV are present in the respective ratio of 1:2:1:1. This figure is adopted from Lu et al., 2023 ..... **11**

Figure 1.4. Thrombosis is the principal underlying pathology in major cardiovascular disorders, Heart attack, stroke, and VET. Global public awareness of venous thrombosis (DVT and PE) is lower than that of arterial thrombosis (heart attack and stroke) **22**

Figure 1.5. Illustration of a healthy human deep vein with flexible valve versus deep vein thrombosis; the usual site of thrombus formation is behind the valve leaflets in the sinus area. When this blood clot becomes unstable, it could break down and detach from its original site, and then the created emboli travel with the blood flow; if it reaches the lung, it could block the pulmonary artery and cause sudden death. Created with BioRender.com **25**

Figure 1.6. Virchow's triad includes hypercoagulability, blood flow stasis, and endothelial dysfunction.. ..... **30**

Figure 1.7. Illustration of the systemic circulation. A, Healthy Skeletal contraction muscles are responsible for returning blood to the heart aided by the flexible valves to prevent blood backflow. B, The arterial bloodstream is influenced by the heart beating and the arterial vessel wall contractibility. Created with BioRender.com **40**

Figure 1.8. The diagram illustrates the composition of the three main types of blood vessels: artery, vein, and capillary. Shows that the arterial wall is thicker than the venous wall. The diagram adopted from Jouda, Larrea Murillo and Wang. 2022 .....**42**

Figure 1.9. The hydrodynamics of a valve encompass discrete periods of valve leaflet movement (shown in blue): opening, equilibrium, closed, and closing. The fluid pressure gradient within the vessel modulates these periods. The diagram and description are adopted from Bazigou and Makinen, 2013 .....**52**

Figure 1.10. (A) illustrates a human deep vein with a flexible valve clarifying the sinus area of the valvular valve leaflets. **(B)** the schematic diagram illustrates the characteristic vortical flow pattern observed during streamlined flow in the deep venous system. The oxygen tension is represented by a colour gradient ranging from red to blue, with darker blue shades indicating higher levels of hypoxia. Diagram **B**, and its description are adopted from Bovill and Van Der Vliet, 2011 .....**53**

Figure 1.11. The bloodstream hydrodynamic forces promote the initiation of blood clots in arteries and veins (Diamond, 2016; Pandian *et al*., 2018) **60**

Figure 2.1. (A) Shows a duplex image of the femoral vein valve, with arrowheads highlighting the valve leaflets in a partially open position and the presence of valve sinuses on the opposite side. **(B&C)** The AutoCAD microfluidic channel design, with a wide sinus area, includes **(Bi)** a 2 cm channel length, **(Ci)** a 700 µm valve region length, **(Cii)** a 300 µm channel width **(Ciii)** and a maximum width of 500 µm in the valve region. **(D)** The AutoCAD design of the valve mask, **(Di)** a valve leaflet length of 530 µm. Figure **2.1. (A)** is adopted from Dalsing and Kistner, 2019.

.....**76**

Figure 2.2. The fundamental stages involved developing a sophisticated microfluidic channel with an elastic valve **79**

Figure 2.3. The temperature inside the PDMS channel was maintained at 37°C. The blue line indicates the temperature of the thermocouple surface, and the orange line indicates the temperature of the PDMS channel's inner surface **80**

Figure 2.4. Valve fabrication, **(A)** Optical images of the microfluidic channel spotting the anchors and the valve region **(B)** Optical image of mask alignment through the fluorescent light of an inverted microscope. The mask was designed to produce the desired valve shape through a 10× objective. **(C)** Optical image of the created flexible valve. The length of the valve is about 330 µm, however this length will increase when the hydrogel swells in the growth medium, the width of each leaflet starts at about 900 µm, and it narrows towards the tip..**81**

Figure 2.5. A schematic diagram illustrating the imaging configuration of the microfluidic device. After being positioned on a dedicated platform, the device was connected to a temperature controller, which maintains channel temperature at approximately 37℃. The inlet tubing links to a blood container, and the outlet tubing directs flow to a waste container. The pressure controller modulates flow rates between 0 and 120 mbar per second while maintaining a constant backflow at 60 mbar. The PCO-edge 5.5 interfaces with the fluorescence microscope and displays the valve area on-screen. A Rhodamine B filter cube (Filter 1) was employed for precise valve alignment during the microfluidic device setup. Subsequently, a DAPI filter cube (Filter 2) facilitated *in situ* polymerisation during experimentation. Two Nikon objectives contributed to the experiments: Nikon Plan Fluor 20X/0.45 and Plan Fluor 10X/0.30, each offering distinct magnification and numerical aperture characteristics for versatile imaging capabilities. Overall, the detailed setup ensures controlled temperature conditions, regulated flow dynamics, and accurate imaging procedures for robust experimentation within the microfluidic device **87**

Figure 2.6. Diagram illustrating **(A)** 12-6 potential used for the no-penetration conditions and **(B)** the 4-2 potential used for particle agglomeration. In both cases, the cut-off is selected so that only the white area of the diagram is used in the potential. This implies that **(A)** is only repulsive because only the positive part is considered, while in **(B)** the negative part of the force which is attractive; particles tend to agglomerate at the location where the force is zero, which is where is the minimum of the potential is located. **96**

Figure 2.7. 2D geometry and structure of dual venous valve: **(a)** geometry showing the location of the contraction forces and **(b)** geometry showing the computational particles and their location in the model. **99**

Figure 3.1. (A) Time-lapse images capture the gradual platelet accumulation on rigid, symmetrical valves. This platelet aggregate rapidly forms within 30–40 seconds under pulsed flow conditions, as indicated by the accumulation of fluorescently labelled platelets at the leaflet tips. Subsequently, it gradually grows until eventual detachment (in this instance, occurring after 93 seconds). An arrow highlights the platelet aggregate, and the scale bar represents 100 µm. **(B)** The progression of the platelet aggregate's growth over time is illustrated, with an initial rapid expansion followed by a plateau and, eventually, detachment (marked by a sudden decline in the fluorescence signal). At its maximum size, the surface area coverage extended to approximately 1200 µm² on the valve tip.....**107**

Figure 3.2. (A) Time-lapse images of blood aggregate building up over time on asymmetrical valves. The aggregation formed slowly behind one of the leaflets. The arrow indicates the main agglomeration site, and the scale bar represents 100 µm. **(B)** The agglomeration detected approximately after 20 minutes; the size of blood agglomeration started to increase progressively to reach its peak after 40 minutes. The error bars represent standard error. **110**

Figure 4.1. Velocity magnitude in the valve during opening and closing phases. **117**

Figure 4.2. Dependence of the average size of particle agglomerates on the pair potential values between $\varepsilon = 10^{-8}$ J and $\varepsilon = 10^{-5}$ J as the simulation is running. **118**

Figure 4.3. Average size of the agglomerates associated with different pair potential values between $\varepsilon = 10^{-8}$ J and $\varepsilon = 10^{-6}$ J at specific times (t=12.5s). Above the value of $\varepsilon = 10^{-8}$ J, agglomeration starts, and the size of the agglomerates increases linearly with log(ε). **120**

Figure 4.4. Simulation and experiment (platelets, fluorescently labelled, agglomeration in Schofield *et al*. 2020) snapshots illustrating the aggregates near the valve's leaflet at different time points. The arrows indicate the aggregates near the valve leaflets. **115**

Figure 5.1. Golden standards for advancing *in vitro* deep vein thrombosis (DVT) models involve developing microfluidic channels equipped with flexible valves, ensuring all surfaces are covered with functional endothelial cells, and incorporating pulsatile flow of human blood. **126**

Figure 5.2. Brightfield microscopy images of HUVEC growth on different groups of samples after 16 hours of incubation. **(A)** HUVECs were cultured directly on the PDMS surface showing patches of HUVEC growth. **(B)** HUVECs were cultured on a PDMS coated with 0.1% modified Gelatine (PH =9) showing patches of HUVEC growth. **(C)** HUVECs were cultured on PDMS coated with 0.1% Gelatine showing monolayer of HUVEC growth. **(D)** HUVECs were cultured on PDMS coated with MaxGel™ ECM mixture, and the scale bar represents 100 µm showing patches of HUVEC growth. **128**

Figure 5.3. (A, B, C) Brightfield microscopy was employed to observe the growth of HUVECs and the formation of lumens within the microfluidic channel. This experiment examined three distinct protocols for treating the microfluidic channels: **(A)** channels coated solely with 1% Gelatin, **(B)** channels treated with 1% APTES for twenty minutes before Gelatin coating, and **(C)** channels subjected to a longer 1% APTES treatment duration for thirty minutes followed by Gelatin coating. **(Ai, Bi, Ci)** beginning of the cell seeding at 0 hr, **(Aii, Bii, Cii)** cells started to attach to the channel surface at 2 hrs, and **(Aiii, Biii, Ciii)** HUVEC growth after perfusing the growth medium at 1µl min^{-1}, **(Ciii)** confluence lumen formed after 16 hrs. The scale bar represents 150 µm. **129**

Figure 5.4. (A, B & C) Brightfield microscopy images display human umbilical vein endothelial cells (HUVECs) attachment to the microfluidic channel and the valve leaflets. Prior to cell culture, the surfaces of the microfluidic channel were treated with different solutions: **(A)** the channel was treated with 70% ethanol, **(B)** 60% isopropanol, and **(C)** hydrogen peroxide.

Despite the treatments, HUVEC attachment appeared poor on all treated surfaces. The scale bar indicates 100 µm.. .....**132**

Figure 5.5. (Ai, Bi, Ci) Bright field images of HUVECs growth within the microfluidic channel and valve leaflets obtained from three microfluidic devices. The scale bar represents 100 µm. **(Dii, Diii, Div)**, **(Eii, Eiii, Eiv)** and **(Fii, Fiii, Fiv)** Confocal microscopy images of HUVECs growth within the microfluidic channel and valve leaflets, CD31 (green), and nucleus (Hoechst, blue) the cells attracted and clumped on the valve leaflets eventually died. The figures represent a single z-slice taken from the top plane. The scale bar represents 300 µm. **135**

Figure 5.6. (A, B, C) Brightfield microscopy images of HUVECs growth and lumen formation within the microfluidic channel. **(A)** Beginning of the cell seeding at 0 hr, **(B)** cells started to attach and grow within the channel at 4 hrs, and growth medium perfused at 1µl min^{-1}, **(C)** confluence lumen formed after 16 hrs. **(D, E)** Confocal microscopy images of HUVECs growth within the microfluidic channel and valve leaflets. Where **(D)** shows the nucleus (Hoechst, blue) and **(E)** shows VE-Cadherin (green), and nucleus (Hoechst, blue). The scale bar represents 150 µm......**136**

Figure 5.7. Brightfield microscopy images of HUVECs growth and lumen formation within the microfluidic channel, the valve leaflets were swollen in the growth medium and lost their mobility. The left and right images display varying degrees of deformability in the valve leaflets. The scale bar represents 150 µm......**137**

Figure 5.8. Brightfield microscopy images of HUVECs growth and lumen formation within the microfluidic channel. **(A)** beginning of the cell seeding at 0 hr, **(B)** cells started to attach and grow within the channel at 4 hrs, and growth medium perfused at 1µl min^{-1}, **(C)** confluence lumen formed after 20 hrs. scale bar represents 100 µm. **(Di, Dii, Diii, Div)** and (Ei, Eii, Eiii, Eiv) confocal microscopy images of HUVECs growth within the microfluidic channel and valve leaflets. **(Fi, Fii, Fiii)** showing 2D cross-sections of the 3D confocal images of the valve area. VE-Cadherin (green), nucleus (Hoechst, blue), and CD31 (red). The scale bar represents 150 µm. **139**

Figure 5.9. (A) Bright field and confocal microscopy images of HUVECs growth within the microfluidic channel and valve consist of one leaflet. **(Bi, Bii, Biii, and Biv)** Confocal microscopy images of HUVECs growth within the microfluidic channel and valve leaflets.VE-Cadherin (green), nucleus (Hoechst, blue), and CD31 (red) Scale bar represent 150 µm.. ..**140**

Figure 5.10. The valve opening – closing cycle at a rate of one cycle per second achieved by using pulsed blood flow between 0 and 120 mbar. Time-lapse images of the valve leaflets made of PEGDA of molecular weight of (Mn 700) and Gelatine hydrolysate Enzymatic, along with HUVECs monolayer grown within the microfluidic device and on the valve leaflets. **A-** closed phase (time = 0 s), **B-** opening phase (time = 0.25 s), **C-** equilibrium phase (time = 0.5 s) and **D-** closing phase (time = 0.75 s) then complete the cycle. The scale bar represents 150 µm. **141**

Figure 5.11. Fluorescence microscopy images of HUVECs; nucleus (Hoechst, blue). The HUVEC monolayer was stable after 10 minutes of perfusing whole blood with pulsatile flow with maximum wall shear rate of ~100 s^{-1}. The scale bar represents 150 µm. **142**

Figure 6.1. Subdivision of the valve into four areas (two for each leaflet) for quantitation, TL represent the leaflet's tip and luminal side, TS represent the leaflet's tip and sinus side. ..**147**

Figure 6.2. Deposition of unchallenged platelets on symmetrical, non-symmetrical valves and deposition of platelets treated with eptifibatide. Blood reconstituted with fluorescently labelled platelets was perfused through either symmetrical **(A)** or non-symmetrical, the arrow points to the rigid leaflet**(B)** valves, and resting platelets were preincubated with 9 mM eptifibatide **(C)** through a symmetrical valve for 5 min. Quantitation of resting platelet accumulation on more flexible (TL area, circles; TS area, open triangles) and less flexible/immobile (TL area, squares; TS area, Xs) leaflets of the symmetrical **(D)** or non-symmetrical **(E)** valve. **(F, G)** Quantitation of eptifibatide-treated platelet accumulation at the TL **(F)** and TS **(G)** regions. Scale bar 100 µm. Error bars represent SEM, n = 3.....**150**

Figure 6.3. Deposition of platelets is increased by thrombin. Platelets were preincubated with 0.1 U/ml thrombin **(A, C)**, and with 0.1 U/ml thrombin + 9 µM eptifibatide **(B, D)**, Blood

reconstituted with fluorescently labelled platelets was perfused through a symmetrical valve for 5 min. **(C, D)**, left row represents TL region, and the right row represents TS region; (TL, circles; TS, open triangles). Scale bar 100 µm. Error bars represent SEM, n = 3 .....**152**

Figure 6.4. Deposition of platelets is mediated by the VWF-GPIbα axis. Platelets were preincubated with OS-1 peptide (M3456 CTERMALHNLC, Alta Bioscience, 12 µM) (A), or with 0.1 U/ml thrombin + OS-1 peptide (B) for 5 min, fluorescently labelled platelets, reconstituted with whole blood, and perfused through a symmetrical valve for 5 min. (C,D), Quantitation of platelet accumulation on more flexible (TL area, circles; TS area, open triangles) and less flexible (TL area, squares; TS area, Xs) leaflets. Scale bar 100 µm. Error bars represent SEM, n = 3. .....**153**

Figure 6.5. Histamine increases platelet deposition in the valve pockets (TS area). (A) HUVECs inside the chamber were incubated with histamine (10 µM, 15 min), and whole blood reconstituted with resting platelets was perfused through a symmetrical valve for 5 min. (B, C) quantitation of platelet accumulation on more flexible (circles) and less flexible (squares) leaflets, TL and TS region, respectively. Scale bar 100 µm. Error bars represent SEM, n = 3. .....**155**

Figure A.1: AUC at TL and TS areas of flexible and less/non-flexible leaflets. AUC of platelets deposited at the TL and TS areas of **(A)** symmetrical valve, **(B)** non-symmetrical valve, **(C)** resting platelets + eptifibatide, **(D)** thrombin-activated platelets, **(E)** thrombin-activated platelets + eptifibatide, **(F)** resting platelets treated with OS-1, **(G)** thrombin-activated platelets treated with OS-1, and **(H)** histamine-treated HUVECs is presented as mean ± SD. Statistical comparison was performed by unpaired Student's t-test. **199**

Figure A.2: Passage through the flow system does not activate platelets. Expression of CD41/GPIIb-IIIa, P-selectin, active CD41/GPIIb/IIIa (PAC-1), CD42b/GPIba and phosphatidylserine (annexin V) on platelets in the whole blood was analyzed before and after passage through the microfluidics chamber. Red dashed line represents the level of expression before the passage. Bars represent mean fluorescence intensity (MFI), mean ± SD. Statistical comparison was performed by unpaired Student's t-test **200**

List of Tables:

Table 1.1. Comparison between GPIbα, GPαIIbβ3, GPVI (glycoprotein VI), PAR1 (protease-activated receptor 1) and PAR4 (protease-activated receptor 4).. .....**16**

Table 1.2. Comparison between alpha granules, dense granules, and lysosomal granules...**19**

Table 1.3. Cases of conditions or factors, along with the potential consequences, that may trigger thrombosis **34**

Table 1.4. Venous thrombosis versus arterial thrombosis.....**37**

Table 1.5. Some examples of large animal models in DVT investigations **55**

Table 1.6. *In vitro* models for DVT, including their valve, fluid type and the presence of endothelial cells **65**

Table 1.7. Comparison between different *In silico* models specified with flexible valves.....**70**

Table 2.1. HUVECs growth medium formulae.....**82**

Table 2.2. Fluorescence filter cube specifications.....**88**

Table 2.3. Camera PCO-edge settings were applied to record the experiments. **89**

Table 2.4. Model's numerical parameters. **100**

Abbreviations

ADAMTS13	A Disintegrin and Metalloprotease with a ThromboSpondin type 1 motif, member 13
ADP	Adenosine Diphosphate
AIDS	acquired immunodeficiency syndrome
APTES	(3-aminopropyl)-trimethoxysilane
BSA	bovine serum albumin
CEVV	Cellular Elastic Vein Valve model
DMP	Discrete Multiphysics
DOACs	direct oral anticoagulants
DPBS	Dulbecco's phosphate-buffered saline
DVT	Deep Vein Thrombosis
ECM	Extracellular matrix
ECs	Endothelial cells
FBS	Fetal bovine serum
FSI	Fluid-structure interaction
GP	Glycoprotein
GPCRs	G protein-coupled receptors
HAT	hospital-acquired thrombosis
HUVECs	Human umbilical vein endothelial cells
ISTH	The International Society on Thrombosis and Haemostasis
IVC	inferior vena cava
LSM	Lattice Spring Model
MVVs	microscopic venous valves
NC3Rs	the Replacement, Refinement, and Reduction of Animals in Research
PARs	Protease-activated receptors
PBS	phosphate-buffered saline
PDMS	Polydimethylsiloxane
PE	Pulmonary Embolism
PEGDA	poly (ethylene glycol) diacrylate

PI	photo-initiator
SMCs	Smooth muscle cells
SPH	Smoothed Particle Hydrodynamics
TL	leaflet's tip and luminal side
TLRs	Toll-like receptors
TS	leaflet's tip and sinus side
VKA	vitamin K antagonist
VTE	Venous Thromboembolism
vWF	von Willebrand factor
WPBs	Weibel-Palade bodies
WSR	Wall shear rate
WSS	Wall shear stress

CHAPTER 1: INTRODUCTION

1.1. Background of Haemostasis

In humans, blood circulates within a highly pressurised closed cardiovascular system, and any rupture in the vessel wall can result in a sudden and severe loss of blood caused by the pressure differential at the injury site (Fogelson and Neeves, 2015). Haemostasis is a vital process, that prevents and stops bleeding, activated by damaged blood vessels, including vascular spasm, creating a platelet plug and initiating coagulation, and is considered the main mechanism preventing bleeding (haemorrhage) (Jin and Gopinath, 2016). Preserving the balance between procoagulants, anticoagulants, and fibrinolysis, the fluid state of blood is maintained, whereas disturbing this balance will result in either blood clot formation (thrombosis) or haemorrhage (Shaydakov, Sigmon and Blebea. 2022). The coagulation process includes three phases: primary haemostasis, secondary haemostasis and tertiary haemostasis (Winter, Flax and Harris, 2017).

1.1.1. Primarily haemostasis

Platelet, von Willebrand factor (vWF) and collagen are the principal contributors to the primary haemostatic response (Mccarty *et al.*, 2006). At the location of blood vessel injury, the subendothelial layer is exposed to vWF, which directly facilitates the platelet's attraction and activation. Platelet activation occurs via interactions between platelet glycoprotein (GP) Ibα receptor and vWF. Activated platelets also provide surfaces for coagulation proteins deposition (Green, 2006). During this stage of haemostasis, GPIbα-vWF bonds are formed and broken, creating a slow rolling motion of the activated platelets on the endothelial surfaces of the injured vessel site (Cowman *et al.*, 2017).

1.1.2. Secondary haemostasis

The coagulation cascade, a pivotal process for haemostasis, is triggered by two pathways, intrinsic and extrinsic. Both pathways converge in common final steps leading to fibrin formation (Wu *et al.*, 2022). Tissue factor (TF) is a principle trigger of the coagulation cascade. TF is produced by smooth muscle cells, endothelial cells, monocytes and macrophages (Schecter *et al.*, 1997). Binding the TF to factor VIIa initiates the extrinsic pathway (Figure 1.1). while the intrinsic pathway can be initiated via the 'contact phase.' In this process, the protein FXII can either self-activate (autoproteolysis) or engage in reciprocal interaction with another protein, prekallikrein (preKK), on a negatively charged surface. Despite FXII deficiency not leading to spontaneous bleeding, this activation might impact haemostasis and could play a role in thrombosis (Gershom *et al.*, 2010). Both pathways eventually end with the activation of factor X. In the presence of Factor Va, Factor X is capable of converting prothrombin into thrombin. The intrinsic and common pathways are signified by activated partial thromboplastin time (aPTT), while the extrinsic and common pathways of blood clotting are signified by prothrombin time (PT) (Hoffman, 2003). aPTT and PT tests are measured in seconds and used to detect fibrin formation in the blood. However, these tests do not assess the events of early tertiary haemostasis (Winter, Flax and Harris, 2017).

Blood coagulation proteins found in plasma that rely on vitamin K, including factors X, IX, VII, prothrombin, and proteins C, S, and Z, exhibit a comparable amino-terminal module. This module contains all the y-carboxyglutamic acid (Gla) residues created through a post-translational conversion that relies on vitamin K and plays a crucial part in the binding of Calcium ions (Ca^{2+}) (Harlos *et al.*, 1987). The mediating role of Ca^{2+} in the coagulation cascade is shown in Figure 1.1 (Wu *et al.*, 2022).

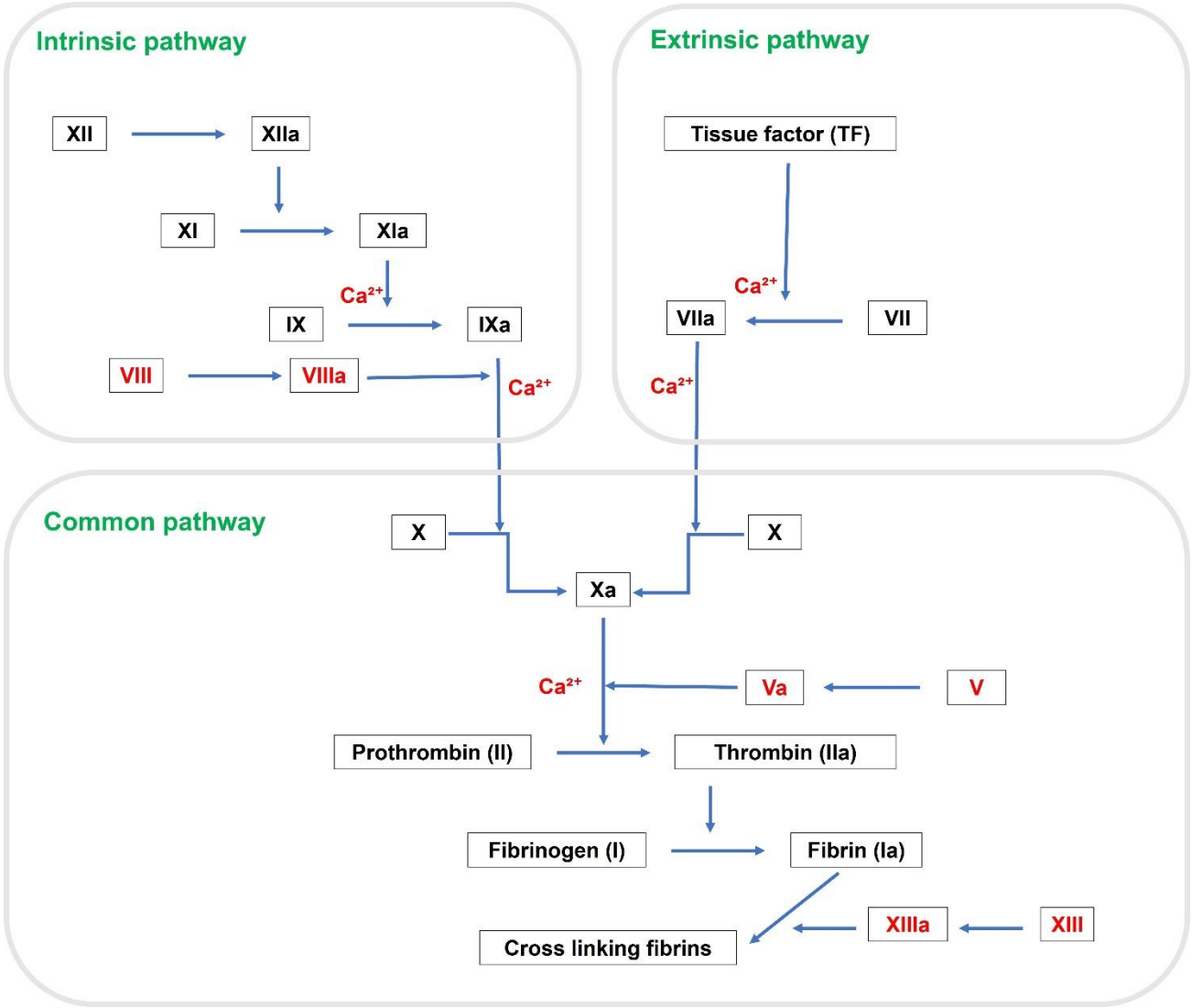

Figure 1.1. Coagulation cascade consists of intrinsic, extrinsic, and common pathways. Figure taken from (Wu et al., 2022).

1.1.3. Tertiary haemostasis

After blood clot formation, fibrinolysis is stimulated to lyse the clot and restore the vessel lumen size to its original dimensions (Gil, 2019). Fibrinolysis is facilitated by plasmin, which is produced by tissue-type plasminogen activator (t-PA) and urokinase-type plasminogen activator (u-PA). Plasminogen activator inhibitor-1 (PAI-1) is capable to control t-PA and u-PA enzymes (Figure 1.2) (Ziliotto, Bernardi and Piazza, 2021). During the cleaving of fibrin polymers, plasmin yields fibrin degradation component that affect platelet accumulation and fibrin polymerisation. The outcome of this process leads to the destabilisation of the platelet clot, which is eventually dissolved (breakdown) within the bloodstream, as unstable platelet aggregation cannot withstand the high-shear stress (Gil, 2019).

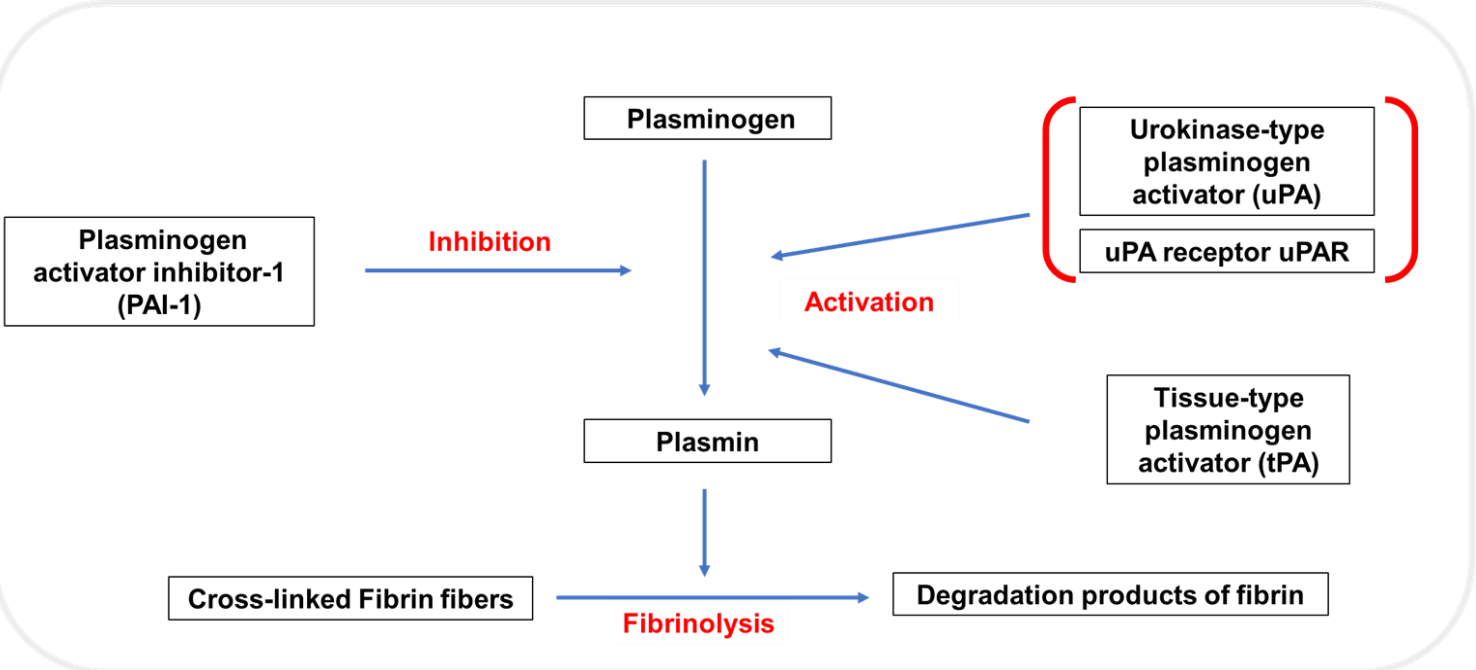

Figure 1.2 Inhibition and activation pathways of producing Plasmin from Plasminogen. Plasmin will facilitate tertiary haemostasis known as fibrinolysis, or clot lysis (Gil, 2019; Ziliotto, Bernardi and Piazza, 2021).

1.2. Roles of von Willebrand factor (vWF) and fibrinogen in haemostasis

1.2.1. vWF

vWF is a large protein crucial for platelet recruitment in haemostasis events(Dong *et al.*, 2018). Higher levels of vWF are present in large vessels than in capillaries (Pusztaszeri, Seelentag and Bosman, 2006). A molecule of human vWF monomer consists of 2050 amino acids (Martin, Morales and Cruz, 2007). vWF is reserved in Weibel-Palade bodies of endothelial cells and platelet α-granules. Each subunit of vWF consists of the following domains; D'-D3-A1-A2-A3-D4-B1-B2-B3-C1-C2 (Andrews and Berndt, 2008), the central part of it contains a triplicate repeat sequence, known as A domains, A1 domain binds platelet's GPIbα, collagen, sulfatides and heparin, while A2 domain of vWF contains a cleavage site for ADAMTS13 (A Disintegrin and Metalloprotease with a ThromboSpondin type 1 motif, member 13) (Auton *et al.*, 2010; Tischer, Moon-Tasson and Auton, 2023), which controls the size of vWF multimers. Under elevated hydrodynamic stress, the A2 domain can experience adequate lengthening or even unfolding, enabling the Interacting with platelets through the A1 domain (Dong *et al.*, 2018). The pro-adhesive properties of vWF are proportional to its size. vWF is cleaved by ADAMTS13, a metalloprotease that belongs to the metalloproteinase family. Cleavage of vWF by ADAMTS13 requires unveiling of vWF by shear forces. Individuals with reduced levels of ADAMTS13 may suffer from thrombotic thrombocytopenic purpura (TTP), distinguished by huge von Willebrand Factor (vWF) multimers in the bloodstream (Lee *et al.*, 2012).

vWF is capable to promote platelet adhesion at the site of injury. Once vWF exposed on the sub-endothelium, or in the presence of pathological shear, its binding to GPIbα (Mccarty *et al.*, 2006). It takes place when GPIbα binding site, located within the A1 domain of vWF, becomes exposed to high fluid shear and when the multimeric protein is immobilised (Auton

et al., 2010). Circulating vWF alone does not facilitate platelet adhesion and aggregation. Its functional properties become active only upon exposure to fluid shear and surface adsorption (Kang *et al.*, 2007). This interaction is reversible, allowing platelet translocation in the blood stream (Maxwell *et al.*, 2007).

1.2.2. Fibrinogen

Fibrinogen is a protein facilitating both adhesion and aggregation of platelets. Fibrinogen is vital in maintaining haemostasis which abnormal levels of fibrinogen in plasma are directly linked to an increased likelihood of venous and arterial thrombosis (Huffman *et al.*, 2015). In humans, fibrinogen is present in blood at high concentrations (2–5 mg/mL), but with acute inflammation the fibrinogen concentration can rise above 7 mg/mL (Kattula S, JR and Wolberg AS, 2017).

Each fibrinogen molecule consists of three sets of polypeptide sequences, 2Aα, 2Bβ, and 2γ, attached by twenty nine disulfide bridges forming a molecule with 340 kDa molecular weight (Kattula S, JR and Wolberg AS, 2017). During the blood clotting process, thrombin turns soluble fibrinogen into insoluble fibrin (Bailey, Astbury and Rudall., 1943). Where thrombin induces fibrin production close or at the platelet surface, fibrin will be able to bind αIIbβ3 (Adair *et al.*, 2020) in particular, thrombin cleaves two fibrinopeptides of fibrinogen from Aα- and Bβ- sequences, this cleavage exposes two knobs on fibrin monomer which bind permanently to the related holes on another fibrin monomer. This interaction results in the formation of half-staggered fibrin oligomers. The polymerisation process proceeds to form larger oligomers called protofibrils. When the protofibrils reach a length of 0.5 mm, they undergo lateral aggregation to form fibres and create a protein framework that serves as a scaffold for blood clots (Asquith *et al.*, 2022), where platelets attach to the highly elastic

polymeric network via integrin αIIbβ3 (Tutwiler *et al.*, 2016) and then clot contraction occurs, which is a process that refers to squeezing the size of the created blood aggregate, also increasing its stiffness and density, which eventually leads to a reduction in the clot porosity and permeability, where the red blood cells (RBCs) accumulated at the core of the clot (Litvinov and Weisel, 2023). Clot contraction is the principal action for preventing blood loss and restoring blood flow (Tutwiler *et al.*, 2016). The binding sites of αIIbβ3 for fibrin, which play a role in clot contraction, are different from the binding site of αIIbβ3 for fibrinogen during the process of platelet aggregation (Litvinov and Weisel, 2023).

There is an imperative contrast between the mechanisms responsible for initiating platelet adhesion on vWF and immobilised fibrinogen under altered flow conditions (Maxwell *et al.*, 2007). vWF initially promotes a slow and steady motion on the surface, which proves highly effective in capturing platelets during extremely high shear stress scenarios, ultimately resulting in irreversible attachment. On the other hand, platelet attachment to fibrinogen is immediate and irreversible, though its efficiency reduces gradually as shear stress increases (Savage, Saldívar and Ruggeri, 1996).

1.3. The role of platelets in haemostasis

Anucleate blood platelets, found exclusively in mammals, appeared moderately recently in evolutionary history, around 400 million years ago; this evolutionary development equipped mammals with advanced haemostatic capabilities, improving their chances of survival (Italiano *et al.*, 2003). Platelets were known as cellular dust. Recently, platelets have become widely recognised for their vital role in diverse biological processes such as haemostasis, injury healing and inflammation (Machlus and Italiano, 2013). Human platelets are small discoid anucleate cells with thickness of 0.5 μm, and diameter of ∼2 μm (Fogelson and

Neeves, 2015). Under normal health condition, most platelets circulate in the body in a non-active state, eventually being removed at the end of their lifecycle. The lifecycle of platelets in the blood of a healthy adult human is around 8–10 days, which requires constant production of platelets to keep the platelet quantity in the range of 150,000 – 400,000 platelets per µL of blood (Adair *et al.*, 2020). In the event of blood vessel injury, the first haemostasis step is platelet activation and aggregation. Adhered platelets become activated due to their contact with extracellular matrix proteins and are additionally stimulated by agonists released from their dense granules, such as Serotonin, Calcium ions and adenosine diphosphate (ADP). In the process of amplifying platelet activation, ADP mediate both autocrine and paracrine. Upon ADP binding to its specific receptors (P2Y1 and P2Y12) on the surface of the platelet, it promotes stable platelet aggregation, exerting its autocrine effect. ADP can also bind to the ADP receptors on neighbouring platelets, leading to a paracrine effect recruiting other platelets (Badimon, 2018). Platelet activation through multiple pathways directs various responses, including diverse essential functions; The ADP molecules released from the activated platelets into the surrounding environment attaches to P2Y1 and P2Y12 receptors. Conversions in the platelet surface membrane facilitating the production of thrombin as well as the activation of the platelet receptors PAR1 and PAR4, also release intra-platelet Ca2+ (Patrono *et al.*, 2017). During platelet activation, the distribution of lipids in the plasma membrane changes, exposing a significant quantity of phosphatidylserine (PS) on the membrane's external surface and directed the coagulation process to the site of injury (Bevers and Williamson, 2016). The exposed PS enhance both; the transformation of factor X to factor Xa via the alliance of factor IXa, factor VIIIa, and Ca2+, also converting prothrombin to thrombin via the alliance of factor Xa, factor Va, and Ca2+ (Bevers, Comfurius and Zwaal, 1983). The outcome; platelets attached to the damaged blood vessel surface and form

aggregates through the interaction between soluble fibrinogen (FB) or other proteins with activated αIIbβ3 receptors (Adair *et al.*, 2020). Platelets activated through haemostasis process, which lead to changes in platelet shape and dynamic nature. Thus, the platelets can recognise wound surfaces and rapidly respond by adhering to the site of injury and preventing blood loss, which is the main role of platelets in preventing haemorrhage (Dorsam and Kunapuli, 2004; Thomas, 2019).

1.3.1. The principal surface receptors of the platelet

The main functions of platelets in blood vessel injury are adhesion and aggregation, where platelet surface receptors are involved in haemostasis and thrombosis event (Rivera *et al.*, 2009).

1.3.1.1. Glycoprotein (GP)Ib-IX-V

GP Ib-IX-V part of the Lucine-rich repeat family, exclusively expressed, and activated on the surface of platelets. GPIb-IX-V complex stands as one of the most prevalent platelet membrane receptor complexes. Each platelet expresses approximately 25 000 copies of this receptor, which play a pivotal role in platelet adhesion, the primary step of haemostasis (Amelirad *et al.*, 2019). GPIbα, GPIbβ, GPIX and GPV are the subunits that comprise the GPIb-IX-V complex in a 1:2:1:1 ratio, which makes the GPIb-IX-V complex able to bind several ligands. The molecular structure of GPIb-IX-V complex has recently been discovered (Figure 1.3), which helps to understand its molecular arrangement and three-dimensional architecture in resting platelets (Lu *et al.*, 2023).

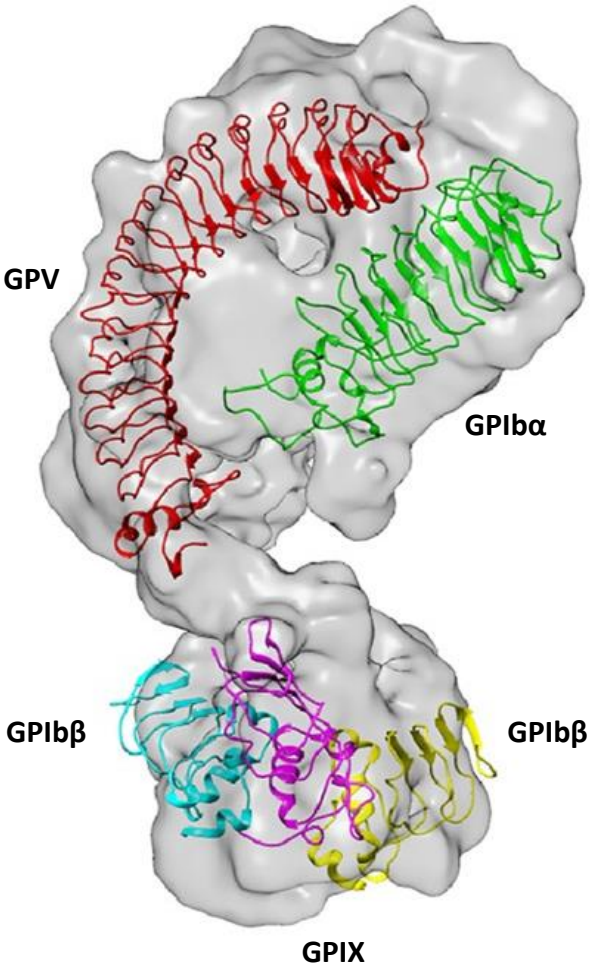

Figure 1.3. In the human GPIb-IX-V complex, the subunits GPIbα, GPIbβ, GPIX, and GPV are present in the respective ratio of 1:2:1:1. This figure is adopted from Lu et al., 2023.

GPIbα is the main subunit in the GPIb-IX-V complex, which contains the binding domain for vWF. The primary attachment of platelets on the site of injury occurs via pivotal interaction between vWF and GPIbα (Klaeske *et al.*, 2023; Tischer, Moon-Tasson and Auton, 2023). GPIbα is mandatory to decrease the speed of platelets that get in touch with the injured surface under high flow conditions, by this means extending the time needed for the other platelet

receptors to interact, such as the interaction between GPαIIbβ3 and vWF and the interaction between GPαIIbβ3 and fibrinogen. This results in gathering of additional platelets and the a growth platelet plug at the site of injury (Savage, Saldívar and Ruggeri, 1996).

1.3.1.2. Integrins

Integrins represent a group of transmembrane glycoprotein receptors which can transfer information from the external surface of a cell across the plasma membrane to the internal surface and vice versa. Integrins consist of α, and β subunits and integrin families are defined by the β subunit. Multiple cell types express integrins. Human platelets express β1 (α2β1, α5β1, and α6β1) and β3 (αvβ3 and αIIbβ3) integrins (Huang *et al.*, 2019). Platelet integrins play a key role in the process of haemostasis. Integrins are abundantly expressed on the surface of platelets and are essential for mediating platelet interactions with subendothelial matrix components, they also facilitate platelet-platelet interactions which is necessary for platelet aggregation and formation of a haemostatic plug (Lecut *et al.*, 2004). The production of integrins with low-affinity binding state occurs on the resting platelets to prevent interactions with fibrinogen and other ligands. Upon activation, platelet integrins transition to a high-affinity state, allowing them to interact and bind ligands (Nieswandt *et al.*, 2001).

Glycoprotein GPIIbIIIa, also known as the GPαIIbβ3, is the dominant integrin on platelets. GPαIIbβ3 plays an essential role in platelet interactions with adhesive proteins (Blair, Michelson and Frelinger, 2018), such as vWf, fibronectin, and fibrinogen (Michelson and Barnard, 1987). Integrin αIIbβ3 is a heterodimer complex dependent on Ca^{+2}, where bonding of Ca^{+2} to metal ions results in disassembling these integrins into monomeric glycoproteins (Jennings and Phillips, 1982).

Integrin α2β1 is important for platelet adhesion to the collagen within subendothelial extracellular matrix (ECM) and facilitating the interactions with the GPVI (Nieswandt and Watson, 2003). However, unlike platelet aggregation in solution, platelet adhesion to surface-immobilized fibrinogen does not need pre-activation of the platelets. Therefore, resting platelets has the capability to adhere to fibrinogen-coated surfaces but not the soluble fibrinogen (Bonnefoy *et al.*, 2000).

Controlling platelet aggregation requires precise regulation of the activation of integrin αIIbβ3 at the site of injury (Ginsberg, 2014). Eptifibatide, tirofiban, and abciximab, anti-platelets drug, which target αIIbβ3, have effectively reduced mortality and ischemic complications in individuals with myocardial infarction. However, their medical use in acute coronary syndrome associated with a significant bleeding risk (Adair *et al.*, 2020).

1.3.1.3. Glycoprotein VI

Glycoprotein VI (GPVI) or glycoprotein VI–Fc-receptor γ-chain complex interacts with collagen contributing to platelet recruitment and activation. GPVI is appear on the platelet membrane in a monomeric and dimeric form. Platelet activation leads to a shift towards the dimeric form, which can be identified using dimer-specific antibodies (Feitsma *et al.*, 2022). Also, GPVI interacts with laminin and fibrin and controls several platelet functions, including adhesion, aggregation, and procoagulant activity. When GPVI binds to its ligands, it forms clusters on the surface of platelets (Mammadova-Bach *et al.*, 2020).

1.3.1.4. G protein-coupled receptors (GPCRs)

GPCRs are the biggest family of human membrane proteins (GPCRs). Despite their vital significance, only a small fraction of GPCRs have been structurally characterised, and the

mechanisms behind their functioning remain poorly understood (Do *et al.*, 2022). Protease-activated receptors (PARs) are a cluster of GPCRs, which mediate responses related to inflammation, haemostasis, and thrombosis (Grimsey, Soto and Trejo, 2011).

1.3.1.4.1. The PARs family

PARs in the cardiovascular system are expressed in smooth muscle cells, endothelial cells, leukocytes, and platelets (Arachiche *et al.*, 2013). PARs family comprises four members: PAR1, PAR2, PAR3, and PAR4. PAR1 was first identified in 1991 and is the most extensively investigated member of the PARs group (Grimsey, Soto and Trejo, 2011). Proteases such as thrombin are significant regulators that can cleave PARs and control various biological processes such as cell behaviour. In humans, platelets exclusively generate PAR1 and PAR4, potentially viable targets for developing therapies to prevent platelet aggregation. PAR1 is called the thrombin receptor, as thrombin is the first identified protease to trigger PAR1 (Han, Nieman and Kerlin, 2021). Thrombin can activate platelets by the cleavage of PAR1, PAR4 or both. Within human platelets, PAR1 acts as a strong substrate for thrombin due to its hirudin-like sequence that strongly attached to thrombin exosite I. Also, PAR1 acts as a co-factor facilitating the cleavage and activation of PAR4 at lower thrombin concentration (≤10 nM)(Arachiche *et al.*, 2013).

1.3.1.5. Toll-like receptors (TLRs)

Toll-like receptors (TLRs) are a group of receptors that identify patterns associated with pathogens and damage. Activating these receptors is essential to trigging the inflammatory response against these hazardous signals. The TLR family encompasses ten well-known receptors, and there are indications that some of them is expressed either on or within human platelets. Platelet-TLRs, such as TLRs 1, 3, 5, 6, and 8, exhibit relatively low expression levels,

whereas TLRs 2, 4, and 9 are more abundantly expressed. Limited research on TLRs 7 and 10 makes it challenging to ascertain their presence and abundance within platelets (Hally *et al.*, 2020).

In the Table 1.1 a comparison between some of the platelet's receptors; GPIbα, GPαIIbβ3, GPVI (glycoprotein VI), PAR1 (protease-activated receptor 1) and PAR4 (protease-activated receptor 4).

Table 1.1. Comparison between GPIbα, GPαIIbβ3, GPVI (glycoprotein VI), PAR1 (protease-activated receptor 1) and PAR4 (protease-activated receptor 4).

	GPIbα	**GPαIIbβ3**	**GPαIIβ1**	**GPVI**	**PAR1 and PAR4**
Family	Lucine Rich Repeat family (Amelirad *et al*., 2019)	Integrins (Huang *et al*., 2019)	Integrins (Huang *et al*., 2019)	glycoprotein VI–Fc-receptor γ-chain complex (Feitsma *et al*., 2022)	The cluster of G protein-coupled receptors (GPCRs) (Grimsey, Soto and Trejo, 2011)
Main role	Platelets Adhesion on the site of injury (Klaeske *et al*., 2023) (Tischer, Moon-Tasson and Auton, 2023) triggers platelet	Platelets aggregation (Ginsberg, 2014) and firm adhesion of platelets on the	Firm adhesion of platelets on the ECM surface (Nieswandt and Watson, 2003)	Maximum platelets activation (Feitsma *et al*., 2022)	Platelets activation and aggregation (Grimsey, Soto and Trejo, 2011)

	activation and encourages thrombus formation. (Auton *et al.*, 2010).	ECM surface (Nieswandt and Watson, 2003)			
Ligands	vWF (Auton *et al.*, 2010).	Fibrinogen, vWF (Savage, Almus-Jacobs and Ruggeri, 1998)	Collagen (Nieswandt and Watson, 2003)	Collagen (Feitsma *et al*., 2022)	Thrombin (Grimsey, Soto and Trejo, 2011)

	A1 domain GPIbα-vWF interaction is initiated under high shear rates >1000/s) (Jamasbi et al., 2017) (Savage, Almus-Jacobs and Ruggeri, 1998) GPIbα-vWF unstable bonds (Cowman *et al*., 2017) but necessary to decrease the platelets velocity (Savage, Saldívar and Ruggeri, 1996)	GPIIb/IIIa-vWF interactions contribute predominantly to thrombus growth (Jamasbi *et al*., 2017) GPIIb/IIIa-vWF stable bonds (Cowman *et al*., 2017) GPIIb/IIIa- Fibrinogen stable bonds (Savage, Saldívar and Ruggeri, 1996)			

1.3.2. Platelet granules

One of the critical processes that occur during platelet activation and aggregation is platelet degranulation. This process involves alpha granules, dense granules, and lysosomal granules (Table 1.2). During degranulation, the contents of these granules are released and support further platelet activation (Badimon, 2018). Platelets contain up to 50 a-granules comprising about 10% of their volume and more than 300 proteins, haemostatic and adhesive molecules (Guerrero *et al.*, 2014). Dense granules (δ-granules) release nonprotein components for example ADP and Calcium ions (Ca^{+2}) that important to initiate platelet aggregation (Deppermann *et al.*, 2013).

Table 1.2. Comparison between alpha granules, dense granules, and lysosomal granules

	Content	**Role**
Dense granules (δ-granules)	ADP, ATP, Calcium ions (Ca^{+2}) and Serotonin (Deppermann *et al.*, 2013).	Platelet aggregation (Deppermann *et al.*, 2013).
Alpha Granules (α-granules)	P-selectin, thrombospondin, vWF, fibrinogen, fibronectin, coagulation factors, inflammatory peptides, and pro-, and anti-angiogenic factors (Guerrero *et al*., 2014)	Upon activation, the contents of alpha granules are relocated to the platelet membrane, leading amplification, and preservation of the platelet adhesion process. This relocation promotes platelet interaction with white blood cells, facilitating immune responses and

		inflammatory processes (Badimon, 2018).
Lysosomal granules	Lysosomal enzymes (Badimon, 2018)	Facilitating immune responses (Badimon, 2018)

1.4. Background of deep vein thrombosis (DVT)

Historically, the Greek philosopher Aristotle is acknowledged to have the first observation of blood clotting (Cohen. 1985). Plato observed that when blood cools outside the body, it forms structures or "fibres"; these findings passed down over 2000 years (Sorrentino *et al.*, 2015). Even though there is no recorded evidence of other well-known Greek physicians like Hippocrates and Oribasius or Roman physicians such as Galen or Caelius Aurelianus reporting cases that suggested diagnosis cases of deep vein thrombosis, the same absence of documentation can be seen in the medical practices of ancient Egypt, Persia, and South America. However, considering the likelihood that this blood clotting disease has existed since ancient times, it is probable that DVT is as old as humanity itself (Galanaud, Laroche and Righini, 2013). Hence, prior to the eighteenth century, revealing venous thrombosis was rare (Bagot and Arya, 2008). The earliest well-reported case of DVT dates back to the year 1271, Since then, the quantity of reported DVT occurrences has increased, with a notable prevalence among pregnant and postpartum women (Galanaud, Laroche and Righini, 2013), It is a primary medical concern with the most severe complication of pulmonary embolism. Then, in 1855, the advancement in this field started with an observation made by a famous German pathologist Rudolf Virchow, who identified the three fundamental causes of intravascular thrombosis; hypercoagulability of the blood, injury to the blood vessels wall,

and blood stasis (McLachlin *et al.*, 1960; Dexter, 1973; Bagot and Arya, 2008; Byrnes and Wolberg, 2017) known as Virchow's triad. These factors are widely acknowledged and continue to play an essential role in understanding thrombosis (Bagot and Arya, 2008).

1.5. DVT within the umbrella of cardiovascular diseases

Cardiovascular diseases constitute a significant proportion of non-infectious illnesses, where thrombosis known as the highest frequent underlying pathology (Raskob *et al*., 2014). Thrombosis is the blood clot formation in the vascular system, partially or wholly obstructing blood vessels, affecting both veins and arteries, this disturbance in blood flow can lead to various clinical complications. Maintaining normal blood circulation within vessels depends on a balance between numerous factors such as platelets, coagulation factors, and the endothelial cells. Upset the delicate balance will increase the likelihood of either arterial or venous thrombosis, or, on the opposite, bleeding (Ashorobi, Ameer and Fernandez. 2022). Also, thrombus development and degradation depend on dynamic processes that involve competition between prothrombotic and antithrombotic factors (Chi *et al.*, 2017). Thrombosis carries significant medical implications. In arteries, acute arterial thrombosis is the primary cause of myocardial infarction, and about eighty per cent of strokes (Mackman, 2008). In veins, venous thromboembolism is the third major contributor to cardiovascular-associated deaths (Takhviji *et al.*, 2021) Figure 1.4. The underlying mechanisms that precipitate in thrombosis still need to be explained, which is essential in developing safer and more efficient antithrombotic medications (Mackman, 2008).

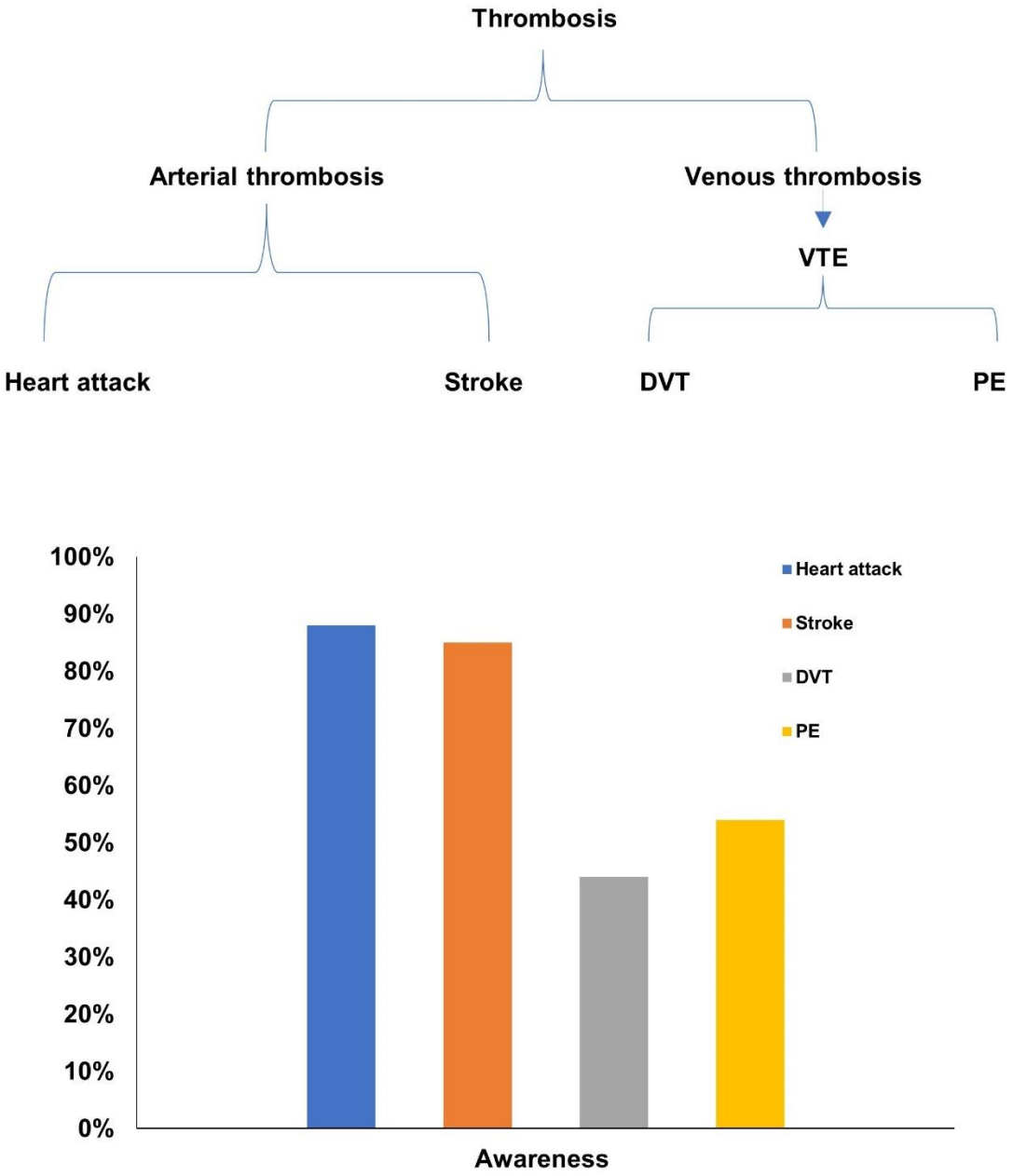

Figure 1.4. Thrombosis is the principal underlying pathology in major cardiovascular disorders, Heart attack, stroke, and VET. Global public awareness of venous thrombosis (DVT and PE) is lower than that of arterial thrombosis (heart attack and stroke).

1.6. Exploration of Deep Vein Thrombosis (DVT)

1.6.1. DVT epidemiology

Venous thromboembolism (VTE) is a significant life-threatening cardiovascular disease (Nishiwaki *et al.*, 2021). VTE encompasses both deep vein thrombosis (DVT) and pulmonary embolism (PE) as a related condition (Siegal *et al.*, 2021; Shen *et al.*, 2021; DeRoo *et al.*, 2023). VTE is believed to cause almost 25,000 deaths per year in the United Kingdom. While the specific death rate is uncertain, the overall number of fatalities attributed to VTE in the UK is five times higher than the combination of overall fatalities from traffic accidents, acquired immunodeficiency syndrome (AIDS) and breast cancer (Hunt, 2009). DVT occurs when a thrombus (blood clot) formed in deep veins, frequently in the legs (Figure 1.5), such as the iliac, popliteal and femoral veins (Raskob *et al.*, 2021) and rarely, in the upper-limb DVT can occur as a result of venous catheterisation (Vyas and Goyal. 2022). PE, a serious DVT complication, results from the thrombus evolving loose and separating from its original site and travelling with the bloodstream, blocking branches of the pulmonary artery, possibly leading to sudden death (Pandian *et al.*, 2018; Siegal *et al.*, 2021). Approximately 95% of emboli are originated from the deep venous system of the lower limbs (Cook *et al.*, 2000). DVT can also lead to disabilities that affect the life quality of individuals (Cook and Crowther, 2010; Payne and Brill, 2017; Das and Biradar, 2018). On average, approximately 1 in 1,000 adults are affected by this condition (Cushman, 2007). Patients diagnosed with PE are at a significantly elevated risk of early mortality compared to those with DVT alone, with an 18-fold increase in mortality rates observed in the former group (Heit, Spencer and White, 2016). In comparison to DVT alone, the presence of PE with or without DVT is an indicator of decreased survival in patients for a duration of up to three months following its start. This suggests that the treatment approach for individuals with PE and DVT should differ to

effectively address the potential impact on survival (Heit *et al.*, 1999). Patients with COVID-19 face an increased risk of mortality following VTE. Specifically, in individuals admitted to the intensive care unit, and requiring mechanical ventilation, the risk escalates by threefold (Tsao *et al*., 2023). Therefore, it is crucial to prioritise prophylaxis measures for hospitalised patients (Heit, 2002). For example, a considerable proportion of patients admitted to the hospital for general, medical operation, and rehabilitation services, and later they suffered from hospital-acquired thrombosis (HAT), did not get a risk assessment for VTE, or received appropriate thromboprophylaxis through their initial admission process. Analysis performed at a public hospital in New Zealand between 2015 and 2019 revealed that out of the 213 patients diagnosed with HAT, only approximately 54.5% of patients, through their initial admission process, undertook partial or informal risk assessment evaluation. However, only 15% received a formal risk assessment. Regarding thromboprophylaxis, 46.2% of patients received simple form of treatment during their initial admission, while 56.8% received appropriate thromboprophylaxis (Kemp *et al.*, 2023). Another study conducted in the European Union (EU) to estimate the total burden of VTE per annum confirmed that 59% of the VET deaths cases followed undiagnosed PE (Cohen *et al*., 2007). Figure 1.4 shows that public awareness of PE and DVT is low, with only 54% and 44% awareness, respectively. In contrast, there is a much high awareness of 88% for heart attack and 85% for stroke. The United Kingdom is constantly classified as the top nation that provides a high awareness of all heart attacks, strokes, and VTE (Wendelboe and Raskob, 2016). Greater attention should be given to VTE due to its enormous impact on public health crosses a range of income levels in countries, including low, middle, and high-income nations, making it a significant economic burden (Raskob *et al*.,2014).

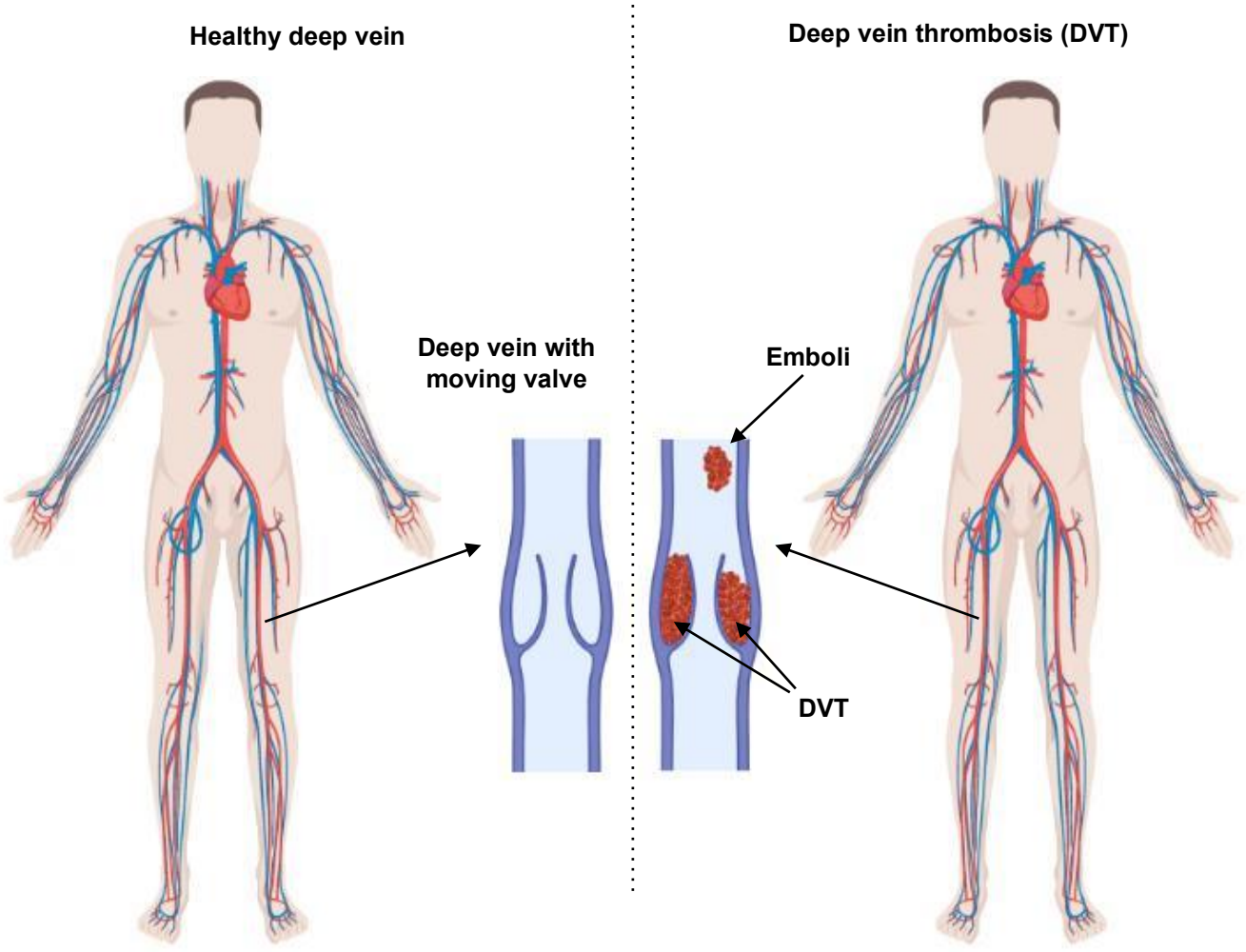

Figure 1.5. Illustration of a healthy human deep vein with flexible valve versus deep vein thrombosis; the usual site of thrombus formation is behind the valve leaflets in the sinus area. When this blood clot becomes unstable, it could break down and detach from its original site, and then the created emboli travel with the blood flow; if it reaches the lung, it could block the pulmonary artery and cause sudden death. Created with BioRender.com

1.6.2. Aetiology and risk factors for DVT

VTE is a complex multifactorial disease whose underlying pathophysiology that is remain incompletely understood. Emerging evidence suggests the involvement of a sophisticated interaction between blood clotting routes, inflammation and innate immune system (Dyer *et al.*, 2018). As previously mentioned, PE is a DVT complication; therefore, it is widely believed that the risk factors of both conditions are similar (Brink *et al*., 2023). According to statistical records, there is an increased likelihood of getting a DVT in individuals over 45 years. (Cushman, 2007). However, solid, and constant evidence shows that the worldwide occurrence of VTE increases with age, particularly among elderly people (Raskob et al., 2014). Other risk factors observed include such conditions as trauma (Vella *et al.*, 2020; Godat *et al.*, 2023), varicose veins and immobility (Westling *et al.*, 2002), obesity, diabetes (Ageno *et al.*, 2008), pregnancy (Cook and Crowther, 2010), and genetic risk factors, such as prothrombin or Factor V Leiden mutation (Mackman, 2012; Takhviji *et al.*, 2021). Extended air travel lasting more than 4-6 hours has been linked to a marginal elevation in the risk of VTE, with an estimated incidence of approximately 1 case per 4656 flights (Heit, Spencer and White, 2016).

When multiple triggering conditions or risk factors are present, the likelihood of getting venous thrombosis is typically amplified. For example, In patients admitted to the hospital for acute medical illness combined with recent trauma, surgery, smoking or active cancer, the risk of thrombosis becomes higher (Heit, Spencer and White, 2016). Likewise, PE often remains clinically undetected, occurring without prior suspicion in 70% to 80% of hospitalised patients who eventually die (Cook *et al.*, 2000). Recent reports indicate an association between COVID-19 and DVT in hospitalised patients (Terpos *et al.*, 2020; Rashidi *et al.*, 2021); however, the full understanding of the pathogenesis behind thrombosis in patients infected

with Coronavirus remains incomplete (Goudswaard *et al.*, 2023). Overall, in a substantial proportion of cases, the exact cause of a patient's VTE may remain unclear (Shaydakov *et al.*, 2022), with about 25% of the VTE cases designated as idiopathic (White, 2003), while up to 50% of DVT cases has no identifiable risk factors (Mazzolai *et al.*, 2022).

1.6.3. Challenges associated with DVT.

One of the difficulties of VTE prevention, especially in acute cases, is the absence of clinical signs, with the first sign being sudden death (Cohen *et al*., 2007; Vyas V, Goyal A., 2022). Whereas the general symptoms related to DVT condition are lower limbs swelling with discomfort (Audu, Wakefield and Coleman, 2019), health care professionals typically confirm the diagnosis of DVT by ultrasound imaging and measuring the plasma level of D-dimer, a indicator of on-going fibrin degradation (Chi *et al.*, 2017; Lapointe *et al.*, 2023).

The main prophylaxis and treatment options are anticoagulant drugs. However, such drugs are associated with complications, primarily causing bleeding even when anti-coagulant medications are kept within the usual therapeutic range (Crowther and Warkentin, 2008; Lapointe *et al.*, 2023). It has been reported that after direct oral anti-coagulant treatment, the cases of clinical bleeding, and major bleeding increased significantly from 6.6% to 10.2% and from 1.1% to 4.0%, respectively (Chen *et al.*, 2023). Bleeding is considered a clinical bleeding event when it does not meet the criteria for major bleeding, which were addressed by the International Society on Thrombosis and Haemostasis (ISTH), comprising mortal bleeding and/or the decrease in haemoglobin levels which require blood transfusions (Schulman and Kearon, 2005).

The management of VTE has experienced a significant changeover due to the recent

introduction of direct oral anticoagulants (DOACs). These medications are given at consistent doses and do not require regular hospital monitoring in sharp contrast to injectable anticoagulants, typically low-molecular-weight heparin, and the subsequent treatment with a vitamin K antagonist (VKA), typically warfarin. These types of VET treatments are highly expensive and require hospital monitoring (Weitz, Jaffer and Fredenburgh, 2017; Clay *et al.*, 2018). Recent guidelines recommended that patients with DVT discontinue anticoagulant treatment after three months if their DVT was triggered by a specific factor or event categorised as 'provoked'. On the other hand, for those with idiopathic DVT, treatment with anticoagulants should be selectively extended(Chen *et al.*, 2023). For example, the optimal treatment duration with anticoagulant medications for cancer associated VTE patients remains unclear. While these patients are at an increased risk of recurrent VTE events occurring multiple times, there is potential for significant bleeding due to anticoagulant therapy within this group (Vedovati *et al.*, 2023). The use of inferior vena cava (IVC) filters has been recommended as an option to prevent PE in patients who cannot undergo or have failed anticoagulation therapy. IVC filters have been employed for over 40 years, and their utilization is increasing. However, these filters' effectiveness and safety are debatable, as they are associated with various complications, including filter orientation, relocation, vein wall breach and filter-induced thrombosis (Wang *et al.*, 2020).

Recent studies, both *in vivo* and *in vitro*, have highlighted the capability of an innovative therapy involving chymase inhibition to resolve DVT without increasing the risk of bleeding, however new drugs still need clinical evaluation (Lapointe *et al.*, 2023). Despite extensive studies in the DVT field during the last decade(Date, Ettelaie and Maraveyas, 2017; Payne and Brill, 2017; Ponomaryov *et al.*, 2017; Schönfelder, Jäckel and Wenzel, 2017; Rajeeva Pandian

et al., 2020; Schofield *et al.*, 2020; Wu *et al.*, 2020), DVT mechanisms are still incompletely understood and further investigations are warranted to provide a thorough understanding of this disease.

1.7. DVT and Virchow's triad:

The initiation of thrombosis in blood vessels is prompted by critical factors, including hypercoagulability, dysfunction of blood vessel walls, and blood flow stasis (Sasano et al., 2021); these factors are classified within Virchow's triad (Figure.1.6) (McLachlin *et al.*, 1960; Bagot and Arya, 2008; Byrnes and Wolberg, 2017). Inflammation was included as a contributing factor to DVT, where white cell induced damage to the endothelium cells(Stewart, Ritchie and Lynch, 1974). Every factor of Virchow's triad can play a significant role in thrombus formation, but typically not as a sole initiator, the combined effect of two or more factors within the triad promotes blood clot formation (Date, Ettelaie and Maraveyas, 2017; Lurie *et al.*, 2019). In some cases, venous thrombosis can be triggered by all Virchow Triad factors, for example, the effect of cancer and its treatment, which release the procoagulant factors into the bloodstream, and alterations to blood flow in which mean damage or activate the endothelial cells (Thomas *et al.*, 2015).

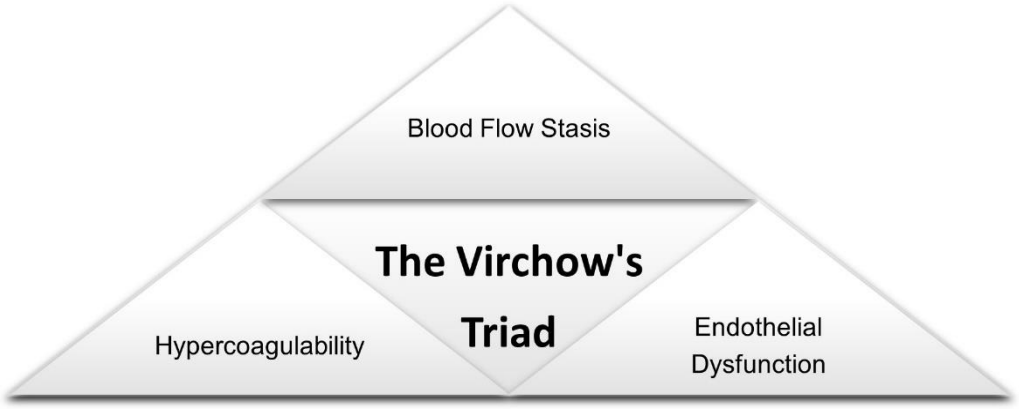

Figure 1.6. Virchow's triad includes hypercoagulability, blood flow stasis and endothelial dysfunction.

1.7.1. Blood flow stasis:

The local haemodynamic conditions of blood flow and the rheological properties of the blood strongly contribute to blood cell adhesion to the vascular endothelial layer (Skilbeck *et al.*, 2004). Hence, Investigating the stasis of blood flow, particularly in the valvular pocket of the venous cusps, is essential as it significantly contributes to clot initiation. Clots originating in this region have a significant risk of leading to PE (Rajeeva Pandian *et al.*, 2020). Reduced blood flow is classified as the leading factor in triggering DVT (Payne and Brill, 2017). However, clot formation is not solely attributed to reduced blood flow, as blood flow tends to be more static during sleep, and does not induce clot formation (Brooks *et al.*, 2009). The development of thrombosis isn't immediate after a single day of bed rest; however, immobility for over 72 hours is a significant factor in triggering DVT, likewise, the risk increases by 3% with each additional day of hospitalisation (Budnik and Brill, 2018). Therefore, the interaction between blood flow stasis and the other components of Virchow's triad is critical for initiating thrombosis, such as, stasis induces hypoxia as the supply of new portions of fresh blood is limited, which may lead to hypercoagulability (Brooks *et al.*, 2009). The presence of stagnant

blood flow within venous valves is confirmed by contrast agents employed in venography procedures, which remain within the veins for an extended duration of up to 60 minutes in elderly individuals, displaying an actual pattern of escalating stasis as age increases (Bovill and Van Der Vliet, 2011). Hypoxia is recognised as the primary pathogenic mechanism connecting stagnant blood flow to deep vein thrombosis (DVT). Endothelium is crucial for circulatory balance and thrombus prevention, recent evidence underlines hypoxia leads to endothelial dysfunction, contributing to DVT progression. Nevertheless, the precise molecular mechanisms linking hypoxia-induced endothelial dysfunction to DVT are largely unidentified (Tang *et al.*, 2023).

1.7.2. Hypercoagulability

Hypercoagulability or thrombophilia is caused by a variety of factors, either inherited or acquired, in which the blood has an abnormal ability to form clots (Dautaj *et al.*, 2019). Blood coagulation, the normal ability to form clots, starts immediately after vessel injury to ensure haemostasis and eventually stop blood loos(Neubauer and Zieger, 2022). More than 50% of all inherited thrombophilia disorders are due to factor V Leiden mutation and prothrombin gene mutation. It is possible for patients to have multiple inherited thrombophilia disorders, such as factor V Leiden mutation is often seen in combination with protein C and protein S deficiencies (McLendon *et al*., 2023).

1.7.3. Endothelial dysfunction:

Vascular endothelial cells have antithrombotic and profibrinolytic properties, which are crucial for maintaining the smooth flow of blood. EC express thrombomodulin, an important anticoagulant protein, with higher concentrations found in valve pockets compared to adjacent areas. Valvular EC also expresses greater amount of endothelial protein C receptor.

These increased levels of anticoagulant proteins help reduce blood aggregation in the vulnerable valvular sinus, where the protective effect of laminar shear-mediated anticoagulation is absent (Byrnes and Wolberg, 2017). EC plays a crucial role in regulating the haemostatic balance of the circulatory system and preventing thrombosis by expressing a variety of mediators that inhibit platelet activation and defeat aggregation; hence, weakened EC function may disrupt this delicate balance by shifting the production of prothrombotic and antithrombotic factors, thereby promoting the development of thrombosis (Date, Ettelaie and Maraveyas, 2017; Fang *et al.*, 2021). Endothelial activation may trigger DVT by increasing platelet and immune cell adhesion to the endothelial surface(Savage, Saldívar and Ruggeri, 1996), and DVT, in turn, can also cause endothelial dysfunction (Henke and Wakefield, 2009). A recent study highlights a significant divergence between procoagulant and anticoagulant factors within the valvular sinus endothelium compared to the endothelium of the vein lumen. Thus, valvular sinus endothelium demonstrates a discernible shift towards a thromboresistant phenotype. Moreover, it also considers the potential impact of the ageing process, a known risk factor for DVT, in altering the thromboresistance phenotype of the endothelial cells in the valvular pocket. (Brooks *et al.*, 2009).

1.7.4. Blood flow stasis along with hypoxia and endothelium activation:

Prolonged blood flow stasis impacts vascular endothelium by disrupting the healthy state of the endothelial cells (Henke and Wakefield, 2009) or inducing hypoxia due to reduced oxygen levels in the surrounding environment; this is observed behind valve leaflets (Table 1.3) (Malone and Agutter, 2016). This hypoxic environment increases the thrombus formation likelihood due to changes in shear stress, eventually promoting prothrombotic attributes (Brooks *et al.*, 2009; Henke and Wakefield, 2009; Malone and Agutter, 2016). Hypoxia triggers

the stimulation of different type of cells within the venous wall, including EC and mast cells (MCs). This activation prompts the production of adhesion receptors also releasing the components of Weibel–Palade bodies (WPBs), which found in endothelial cells (Budnik and Brill, 2018).

Table 1.3. Cases of conditions or factors, along with the potential consequences, that may trigger thrombosis.

Conditions or factors	Consequence		References
Bloodstream stasis in the valvular pocket	Hypoxia		(Brooks *et al*., 2009; Reitsma, Versteeg and Middeldorp, 2012)
Hypoxia	Activates endothelium		(Mackman, 2012; Falanga, Schieppati and Russo, 2019)
Inflammation and/or cancer			
Activation of the endothelium.	A decrease in anticoagulant expression. Promoted synthesis of tissue factor (TF).	An increase in hypercoagulability, which leads to the formation of a thrombus.	(Malone and Agutter, 2016)

1.8. Venous versus arterial thrombosis

Venous and arterial thrombosis are known to be two separate pathophysiological entities, each with its own unique mechanism of development. Venous thrombosis has been associated with activation of the clotting system, while arterial thrombosis has primarily been attributed to platelet activation (Prandoni, 2009). Numerous studies have highlighted that these conditions share multiple risk factors, including metabolic syndrome, infections, obesity, and age. Further evidence for the association between the two is provided by the observation that patients diagnosed with VTE manifest a greater propensity towards experiencing arterial thrombosis events, and vice versa(Franchini and Mannucci, 2008). For example, elderly age, a well-documented risk factor for atherosclerosis, has been recognised as a distinct risk factor for VTE. Also, several studies have shown a connection between VTE and chronic arterial disease of the lower limbs. Atherosclerosis is linked to the activation of both platelet and blood coagulation, and increased plasma fibrin levels, all of which can contribute to thrombotic complications (Prandoni, 2009). Platelets and fibrin comprise the primary components of arterial thrombi (Chernysh *et al.*, 2020), while venous thrombi are distinguishable by their structure, primarily composed of RBCs and fibrin (Byrnes and Wolberg, 2017).

1.8.1. An overview of the arterial thrombosis route

Arterial thrombosis is the blood clot formation in the arteries (Ashorobi, Ameer and Fernandez. 2022). It is mainly driven by interactions between the arterial wall and circulating blood cells (Delbosc *et al.*, 2017) and frequently occurs because of arterial wall injury or atherosclerotic plaque rupture, this is considered the leading cause of death and disability worldwide. Atherosclerosis is driven by lipoprotein accumulation leading to fatty plaque

formation(Bentzon *et al.*, 2014). In addition, the pathogenesis of atherosclerosis includes oxidative stress, platelet activation and inflammatory cell enrolment (Martin-Ventura *et al.*, 2017). Following the rupture of an atherosclerotic plaque, platelets are attracted to the site by interacting with collagen and vWF, which leads to platelet adhesion and initiates a rapid accumulation of more platelets contributing to the expansion of the thrombus. Parallelly, platelets undergo activation through several pathways, including the activation of the platelet receptor PAR1 (protease-activated receptor 1) by the enzyme thrombin, which is generated through the blood coagulation cascade. Upon stimulation, platelets granular contents will be released, thereby amplifying platelet recruitment, adhesion, activation, and aggregation (Mackman, 2008). Atheroma, a collection of smooth muscle cells (SMC) that could trap lipids, has been connected to inflammation. This finding improves our understanding of how various risk factors contribute to atherosclerosis development (Libby and Hansson., 2019). Platelets might play a significant role in the inflammatory processes that contribute to the formation of atherosclerotic lesions, as platelets can adhere to non-denuded endothelium, this adhesion triggers platelet activation (Massberg *et al.*, 2002).

Table 1.4. Venous thrombosis versus arterial thrombosis

	Arterial thrombosis	**Venous thrombosis**
Site of event	Arteries	Veins
Pathogenesis and primary triggers	Developing a blood clot due to platelet activation (Prandoni, 2009) and fibrin deposition in a diseased arterial wall (e.g., the breakdown of an atherosclerotic plaque) (Mackman, 2008).	Developing a blood clot due to activation of the clotting system (Prandoni, 2009) initiated by stasis blood flow, endothelial injury, or hypercoagulable states (Sasano *et al*., 2021)
Thrombus component	Fibrin and high content of platelets (Chernysh *et al.*, 2020)	High content of RBCs in addition to fibrin, platelets, and leukocytes (Byrnes and Wolberg, 2017). Unlike arterial clots, venous clots typically have a relatively lower number of platelets (Raskob *et al*., 2014).
Risk factors	Atherosclerosis (Bentzon *et al*., 2014), injuries of the intima of the vessel wall (Delbosc *et al.*, 2017) , smoking, hypertension, hyperlipidaemia (Weintraub, 2009), diabetes	Provoked events of VTE occur after triggering factors in the prior three months, including immobilization, trauma, surgery, cancer, or hospitalization, especially for a major surgery. Conversely, unprovoked

	and a complex genetic susceptibility to the arterial disease (family history)(Bentzon *et al.*, 2014) Hypertension is linked to vascular remodelling and promoted vascular stiffness, which is closely associated with cardiovascular events (Martínez-Revelles *et al.*, 2017)	events of VTE take place when these conditions are absent (Lutsey and Zakai, 2023)
Symptoms	Sudden onset of symptoms: chest (Macinnes and Miller, 1984; Martin-Ventura *et al.*, 2017) and ischaemic limb pain (Galbraith *et al.*, 1985).	Slow clinical onset (Bovill and Van Der Vliet, 2011), with common symptoms encompassing pain, swelling, increased visibility of skin veins, erythema, cyanosis, and may be accompanied by unexplained fever, with possible complications such as PE with its common symptom of chest pain and breathing difficulty. However, clinical signs and symptoms of the condition exhibit a wide range of variability (Mazzolai *et al.*, 2018).
Medical complications	Myocardial infarction (heart attack), stroke, limb ischemia (Bentzon *et al.*, 2014) (Mackman, 2008)	DVT and PE (Takhviji *et al.*, 2021).

Diagnosis	Electrocardiogram (ECG) and Cardiac biochemical indicators levels such as troponin (Badimon, 2018)	Ultrasound, high plasma D-dimer levels, CT scan and MRI venography (Mazzolai *et al.*, 2018)
Treatment	Antiplatelet medications (e.g., aspirin and oral platelet Glycoprotein αIIbβ3 receptor inhibitors)(Van De Graaff and Steinhubl, 2001), anticoagulants (e.g., heparin, enoxaparin, apixaban (Pohl *et al.*, 2023) and warfarin (Mazzolai *et al.*, 2018), balloon angioplasty, stenting (Abe *et al.*, 2014), bypass surgery (She *et al.*, 2020)	Anticoagulants (e.g., warfarin, heparin) or/and oral anticoagulants (e.g., inhibitors of FXa or thrombin) (Mazzolai *et al.*, 2018)

1.9. Blood vessel anatomy

The cardiovascular system operates under pressure as a closed system, including blood vessels regulating blood flow to and from the heart, as depicted in Figure 1.7. It has two main loops: pulmonary circulation and systemic circulation (Chaudhry, Miao and Rehman., 2022)

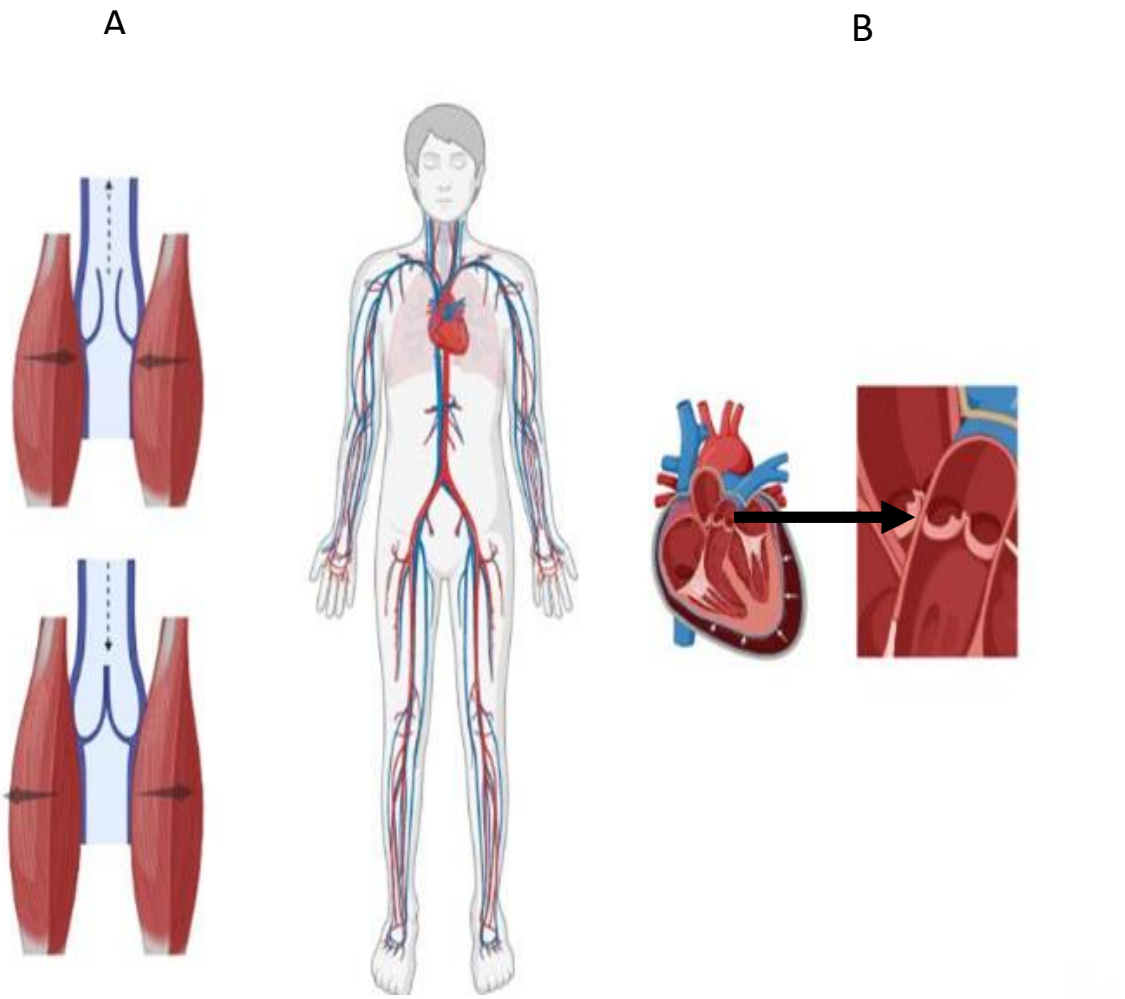

Figure 1.7. Illustration of the systemic circulation. **A,** Healthy Skeletal contraction muscles are responsible for returning blood to the heart aided by the flexible valves to prevent blood backflow. **B,** The arterial bloodstream is influenced by the heart beating and the arterial vessel wall contractibility. Created with BioRender.com

Blood vessels play a pivotal role in transporting nutrients to organs and tissues and eliminating waste products via the bloodstream. Its primary function involves facilitating the oxygenation process within the body, where deoxygenated blood travels through veins returning to the right side of the heart and eventually reaching the lungs. On the other hand, oxygenated blood from the lungs is directed to the left side of the heart and distributed throughout the body via arteries (Tucker, Arora, and Mahajan., 2023). The heart is the primary generator of blood flow in arteries, propelling it through arterioles, capillaries, and venules before it is returned to the heart via the venous system (Pugsley and Tabrizchi, 2000). The heart valves regulate blood flow by opening and closing in coordination with the heart's beating (Figure 1.7, B)(Bazigou and Makinen, 2013). Simultaneously, blood flows from the superficial veins to the deep veins and moves towards the heart, driven by flexible bicuspidate valves extending from the internal wall, ensuring unidirectional bloodstream. Further, muscle contractions in the calf, foot, and thigh support pushing the blood towards the heart, pulling over the effects of gravity and the elevated hydrostatic venous pressure (Figure 1.7, A) (MacColl and Khalil, 2015), particularly from the lower extremities (Bazigou and Makinen, 2013).

Most blood vessels are composed of three distinguishable histological areas, each area is called a "tunic" derived from the Latin phrase "a membrane or related structure covering or lining a body part or organ". These areas are known as the tunica intima, tunica media, and tunica adventitia, arranged from the inner lumen of the blood vessel outward (Pugsley and Tabrizchi, 2000) refer to Figure 1.8.

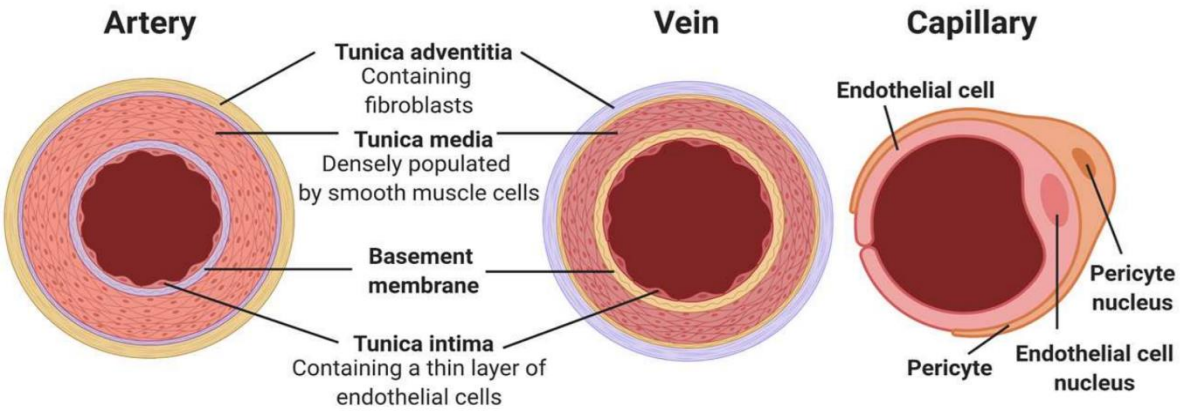

Figure 1.8. The diagram illustrates the composition of the three main types of blood vessels: artery, vein, and capillary. Shows that the arterial wall is thicker than the venous wall. The diagram adopted from Jouda, Larrea Murillo and Wang. 2022.

1.9.1. The tunica intima

The tunica intima, the innermost layer of the blood vessel wall, is in direct contact with the lumen and interacts with its contents. It comprises primarily of a one layer of ECs (Taylor and Bordoni., 2020) shown in Figure 1.8.

1.9.1.1. Endothelial cells

The endothelium is crucial in preserving vascular integrity and promoting overall vascular healthy conditions (Khursigara *et al.*, 2020). The endothelium is a continuous lining of vascular ECs that spreads from the heart to the tiniest capillaries, forming the internal surface of the blood circulatory system (Rajendran *et al.*, 2013), and therefore, ECs make direct contact with the bloodstream (Khursigara *et al.*, 2020). If the ECs from a single human body were lined up sequentially, they would extend more than four times around the Earth. Moreover, the endothelium, far from being an inert cell layer, exhibits outstanding metabolic activity and plays a crucial role in diverse homeostatic activities. These include regulating vasomotor tone,

transporting cells and nutrients, maintaining blood fluidity, controlling vessel wall integrity and permeability, and forming new blood vessels(Aird, 2005). Also, ECs are the primary source of vWF, collected in specialised granules called Weibel-Palade bodies (WPBs). When exposed to shear stress or vessel wall damage, ECs promptly release vWF and various inflammatory and angiogenic factors. vWF contributes to haemostasis and thrombosis by facilitating platelet adhesion and aggregation at locations of vascular damage and by protecting the circulating coagulation factor VIII (FVIII) from being cleavage (Khursigara *et al.*, 2020) (Schillemans *et al*., 2018). WPBs contain a lot of proteins such as P selectin, Eotaxin-3, Interleukin-8 (IL-8), Angiopoietin-2, Osteoprotegerin, Endothelin-1, Calcitonin gene-related peptide and Tissue-type plasminogen activator (tPA) and Endothelin-converting enzyme (Valentijn *et al*., 2011).

1.9.2. The tunica media

Tunica intima is based on a subendothelial layer, which can vary in thickness and contain extracellular matrix (ECM)/collagen, SMC, and elastic fibres. The tunica intima is detached from the tunica media by a layer of elastic fibres known as internal elastic membrane. The internal elastic membrane is most prominent in muscular arteries and is relatively thin throughout the venous system (Figure 1.8) (Taylor and Bordoni., 2020).

1.9.2.1. Extracellular matrix (ECM)

The initial stage of the haemostatic cascade involves platelet engagement to the exposed ECM at locations of blood vessel damage. Collagen is a critical protein component within the ECM that significantly contributes to platelet recruitment. *In vitro*, studies have demonstrated that collagen facilitates platelet adhesion through direct pathway GPVI binds to collagen and indirect pathways integrin α2β1- and the integrin αIIbβ3 binds to collagen via vWF. Also,

collagen triggers platelet activation, leading to their aggregation and procoagulant activity, adhesion, and aggregation of platelets on collagen involve a coordinated process that encompasses various platelet agonists acting through distinct receptors including integrins, G-protein–coupled receptors and GPVI (Nieswandt and Watson, 2003)

1.9.2.2. Smooth muscle cells (SMCs)

SMCs represent the predominant cellular component within the Tunica media of the blood vessel wall. They are present in all types of vessels except for capillaries, which can be distinguished by the presence of smoothelin (Table 1.5) (Van Der Loop *et al.*, 1997). Smoothelin found in the vascular SMC is called smoothelin-B, and it is expressed exclusively in blood vessels. Its expression is greater in the SMC of arteries than in veins. Not all vascular SMC exhibit smoothelin-B expression. Studies have shown that smoothelin-B can interact with α-smooth muscle actin in vascular SMC; this suggests its potential significance in the contraction process (Li and Hui, 2009).

SMCs in blood vessels exhibit significant phenotypic plasticity, and the dominant phenotype in young and healthy blood vessels is contractile, providing sufficient autoregulating of blood pressure and blood flow. However, vascular cells can experience a phenotypic switch throughout an individual's lifespan to a synthetic, mostly noncontractile state. This transformation is often triggered by proinflammatory stimuli, dietary factors, or other influences, leading to atherosclerosis or vessel remodelling (Brozovich *et al.*, 2016).

SMCs are crucial in producing essential ECM components, including proteoglycans, collagen, and elastin. Also, they are responsible for maintaining the balance between ECM production and degradation during the development of atherosclerosis (Badimon, 2018), and their exposure to thrombin and thrombosis-related products can trigger inflammatory activation

in smooth muscle cells, in addition to their ability to synthesis procoagulant substances (Libby and Simon., 2001).

1.9.3. Tunica adventitia

The external layer of the vessel wall, known as the tunica externa or tunica adventitia, plays a pivotal role in maintaining the vessel's integrity (Taylor and Bordoni., 2020). It primarily comprises fibro-elastic connective tissue (Pugsley and Tabrizchi, 2000). Also, collagen is an important element of tunica adventitia and facilitates attaching the vessel to neighbouring structures and tissues (Taylor and Bordoni., 2020).

1.10. Blood flow

Blood flow inside the vessels is largely laminar, it contributes to changing the morphological characteristics of the ECs. This laminar flow generates shear stresses; the highest shear stresses occur near the vessel wall, impacting the appearance and activity of endothelial cells of the vascular wall (Lowe, 2003), where the shear stress promotes the maintenance and health of ECs (Savage, Saldívar and Ruggeri, 1996; Byrnes and Wolberg, 2017; Teixeira, Padilla and Vianna, 2017). Blood is a complex fluid, and its viscosity is influenced by haematocrit and RBCs, aggregation, and deformability. Blood viscosity exhibits shear thinning behaviour, wherein viscosity decreases with an increase in shear rate. In other words, blood viscosity is typically inversely proportional to the shear rate (Panteleev *et al.*, 2021). This could be explained when blood shear rates are low, the potential of RBC aggregation may increase, this, in turn, will raise the viscosity to very high values(Simão *et al.*, 2016). The shear rate is a widely used parameter to quantify blood flow, representing the rate of velocity change between adjacent fluid layers in a direction vertical to the flow. It estimates the relative motion between different layers of the flowing fluid, and according to current understanding,

low and moderate blood flow velocities are observed in healthy, unobstructed blood vessels, while high shear rates (>2000 s^{-1}) are noticed in narrowed arteries, particularly in the circumstance of thrombotic events(Yakusheva *et al.*, 2022). Wall shear stress (WSS) refers to the force applied by flowing blood to the inner surface of blood vessels (Sache *et al.*, 2023), affecting the function, gene expression and structure of the ECs (Reneman, Arts and Hoeks, 2006). ECs lining blood vessels and heart chambers can sense fluid shear stress. In response to variations in shear stress, these cells exhibit modified cytosolic calcium levels and nitric oxide release, which is crucial for regulating vascular contractility. Irregularities in nitric oxide production or release are strongly associated with hypertension (Nauli *et al.*, 2008).

In all theoretical discussions and nearly all investigations concerning the interplay between shear stress (τ) and the functioning of ECs, whether conducted *in vitro* or *in vivo*, the shear stress is commonly determined using Poiseuille's law through the following equation (Reneman, Arts and Hoeks, 2006):

$$\tau = \frac{4\,\eta\,q}{\pi r^3} \tag{1.1}$$

Where τ is shear stress, η is medium viscosity, q is measured flow, and lumen radius r.

This is applied in circular cross-sections of vessels, similarly WSS calculated by using the average velocity or the maximal velocity (Potters *et al*., 2014):

$$\tau = \frac{8\,\mu V_m}{D} = \frac{4\,\mu V_{max}}{D} \tag{1.2}$$

Where μ is viscosity, *D* the diameter and (V_m, V_{max}) are respectively the mean velocity and the maximum velocity of the blood.

Eventually, WSS can be calculated from the WSR and blood viscosity (Du *et al*., 2020)

$$\tau = \mu . \gamma \quad (1.3)$$

Where τ is shear stress, μ is viscosity and γ shear rate.

Of note, blood is a mixture of cellular elements, including red and white blood cells, as well as platelets. These blood cells, suspended within the plasma, show an almost Newtonian behaviour. On the other hand, whole blood displays non-Newtonian aspects, revealed by the aggregation of RBCs occurs at low shear rates, conversely, the deformability of RBCs and their propensity to align with the flow direction arises under higher shear rates (Simão *et al.*, 2016).

1.10.1. Platelet adhesion and aggregation are influenced by WSR.

The mechanisms involved in initiating platelet aggregation are related to the value of the vessel WSR; when the shear rate remains below 1000 s^{-1} , the process mainly relies on activating integrin αIIbβ3 receptors. Within the range of 1000 to 10,000 s^{-1}, platelet activation relies on both GPIb and integrin αIIbβ3. At extremely high shear rates above 10,000 s^{-1}, platelet aggregation is solely mediated by the interaction between vWF and GPIb, without the need of platelet activation and the crucial function of integrin αIIbβ3, where immobilised vWF in combination with soluble multimeric vWF can initiate the formation of large, unstable aggregates of nonactivated platelets (Maxwell *et al.*, 2007).

High shear rate plays a role in arterial thrombosis via activating the platelets. Particularly in atherosclerosis with narrowed vessel lumens, these regions experience increased shear stress compared to average circulation (Ruggeri and Mendolicchio, 2007). Also, the arterial stenotic flows exhibit distinctive characteristics, including significant pressure drops when stenosis exceeds 75%, resulting in angina, helical flows due to asymmetric lesions and instances of turbulence when the Reynolds number exceeds 300–400 during specific phases (Diamond, 2016).

$$Re = \frac{\rho DV}{\mu} \quad (1.4)$$

Where ρ is fluid density, V is velocity, D is vessel diameter, and μ is dynamic viscosity.

Also, it has recently been discovered that different types of lesions (circle and ellipse) in both small and large blood vessels of mice and humans lead to exceptionally high shear rates at the wound's edge, where haemostasis happens. These shear levels arise beyond those observed in healthy vessels during normal conditions. They are even higher than those found in diseased arteries with advanced atherosclerotic plaques, where elevated shear rates are typically very high at the apex of stenosis (Yakusheva *et al.*, 2022). Also, about a 90% reduction in the lumen of a coronary artery can result in shear rates ranging from 20,000 s^{-1}, to 40,000 s^{-1}, at or near the site of stenosis. These values are approximately 100 times higher than those observed without obstruction and ten times higher than those found in micro arterioles. During platelet adhesion and aggregation at this high WSR, aggregates remain stable with adhering and aggregated platelets experiencing stretching forces at the points of contact with surfaces or other platelets. This stretching leads to the formation of elongated structures that can exceed 10 µm in length. These elongated structures play a crucial role in supporting additional platelet adhesion and aggregation by facilitating binding with vWF (Ruggeri *et al.*, 2006).

A high shear rate induces the unfolding of vWF multimers, thus facilitating platelets binding and forming aggregates (Qiu *et al.*, 2015). Blood flow stasis, opposite to high shear stress, can arise from the occlusion of blood vessels caused by the formation of atherosclerotic plaques in arteries (Pandian *et al.*, 2018). Venous thrombosis, in difference to arterial thrombosis, mainly happens in reduced or stagnant blood flow, where venous flows are slow with WSR around 100–200 s^{-1} and WSS between 1 and 8 dyne/cm2. This maintains a

consistent blood flow and sometimes could reach a blood stasis, where velocity becomes zero, a condition of higher risk for developing DVT (Diamond, 2016). Venous thrombosis occurs near venous valves behind the valve leaflets, where the pulsatile bloodstream conditions are abrupted, and hypoxic ECs is associated with the creation of blood clot, or it can also occur due to the dysfunction of valves in the deep veins, leads to changing of the flow patterns and create a thrombotic environment (Pandian *et al.*, 2018). Eventually, venous thrombosis occurs under low shear stress on the mechanically non-activated endothelial surface, whereas arterial thrombosis develops under high shear stress in the areas where the endothelium is denuded and subendothelial matrix proteins are exposed (Lowe, 2003; Mackman, 2012).

1.10.2. The role of venous valves in DVT

Bicuspid valves are projections of the inner vessel wall, tunica intima (Nuñez-borque, Fernandez-bravo and Yuste-montalvo, 2022), which consist of collagen and elastin fibres and valvular interstitial cells, which share similarities with SMCs. Pathological changes in biomechanical conditions, such as WSS and blood pressure, can contribute to numerous valvular disorders. These disorders are characterised by fibrosis triggered by phlebitis, causing stiffening of the leaflet structure and increased valve rigidity (Soifer *et al.*, 2017). Venous valves are essential in controlling the unidirectional bloodstream in the legs. Performing as gate, their structures, cusps, and mechanical effects are vital in sustaining blood flow in a single direction. Their operation is influenced by the contraction of skeletal muscles surrounding the veins, facilitating blood movement from superficial veins to deep veins and ahead towards the heart. Simultaneously, the valves prevent excessive pressure build-up in the capillaries and veins during muscle contractions, maintaining a balanced flow (Lurie *et al.*, 2003). In the case of everyday activities, blood flow in the veins displays a pulsatile nature,

particularly when the body is in a proper standing position. This position is when muscle contractions significantly facilitate the mechanical operation of the venous valve (Wu *et al.*, 2020). These venous valves open and close at a rate of about twenty cycle per minute (Aird, 2007). Conditions like immobility promote the risk of developing thrombosis (Payne and Brill, 2017). Immobilisation can reduce the pulsatile rhythm, especially in the legs, which decreases blood flow velocity. Consequently, this condition can lead to a raised stasis level in the veins, especially within the valve sinus (McLachlin *et al.*, 1960; Lurie *et al.*, 2003). Since endothelium on the valve cusps relies solely on blood within the pocket or lumen for its oxygenation, the endothelium facing the pocket may experience hypoxia during non-pulsatile blood flow, while the endothelium facing the lumen receives sufficient oxygenation. Hence the pulsatility of venous flow is a powerful natural defensive mechanism against thrombus formation in the sinus area of the venous valve (Hamer, Malone and Silver., 1981).

Ultrasound technology has shed light on the mechanics of venous valve function and has distinguished how leaflet movement affects the bloodstream by categorising the valve cycle into four periods: opening, equilibrium, closing, and closed. The hydrodynamic forces on either side of the valve cusps influencing the position of the valve leaflets (Figure 1.9) (Bazigou and Makinen, 2013). In the opening period of the valve cycle, valvular leaflets transition from a closed to an open position as it moves towards the sinus wall. In the equilibrium period, the valve reaches its fully open position, and the valve leaflets cause differences in the luminal vein section. Hence the change in the valve leaflet's position alters the hydrodynamics of blood flow, especially at the top edges of the leaflets. It leads to the creation of vortices, which persist during the closing period of the valve cycle and play a pivotal role in reducing stasis in the sinus pocket (Lurie *et al.*, 2003). Likewise, vortices can significantly alter flow patterns,

thereby increasing the collision likelihood between the blood cells and the vessel walls surfaces and establish a preferable site for platelets adhesion and subsequent aggregation (Skilbeck *et al.*, 2004). Therefore, it is important to study the flow pattens created at the valve region, and the role of valve leaflets flexibility in local haemodynamic. Nevertheless, the region encompassing the sinus pocket undergoes the least magnitude of fluid shear stress, whereas the base area of the sinus side of the leaflet encounters the highest level of tissue stress particularly in regions characterized by negligible fluid shear stress (Figure 1.10 A). Thus, changes in the WSS and local blood pressure can cause valvular diseases leading to fibrosis, which increases stiffness of the leaflet and impacts mostly the closed period (Soifer *et al.*, 2017). *In vitro* studies have provided insights into the flow dynamics around the valve region, confirming the formation of intricate vortex patterns in the sinus area. As shown in Figure 1.10 B, the flow passing through the valve leaflets generates a primary vortex when a part of the bloodstream curves into the valve pocket. This primary vortex, in turn, gives rise to a smaller secondary vortex that rotates in the opposite direction at the bottom of the valvular sinus. Notably, secondary vortex exhibits a slow rotation and coincides with the sinus region that experiences the most significant hypoxia during blood flow. Furthermore, it has been observed that RBCs introduced into the infused fluid tend to accumulate within this secondary vortex, resulting in their clustering (Bovill and Van Der Vliet, 2011).

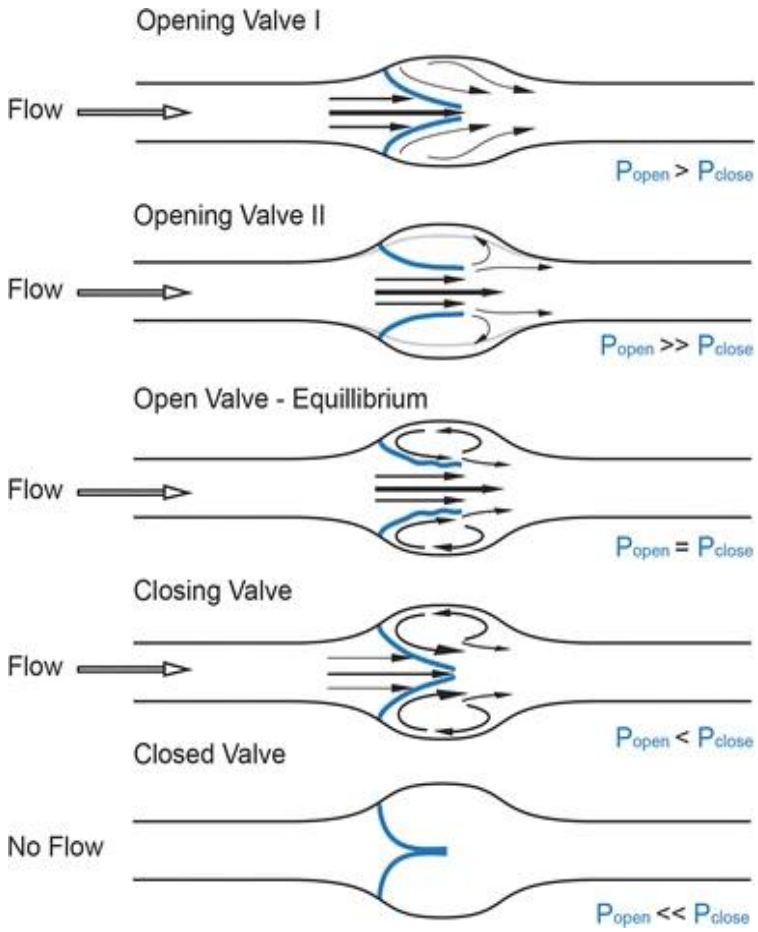

Figure 1.9. The hydrodynamics of a valve encompass discrete periods of valve leaflet movement (shown in blue): opening, equilibrium, closed, and closing. The fluid pressure gradient within the vessel modulates these phases. The diagram and description are adopted from Bazigou and Makinen, 2013.

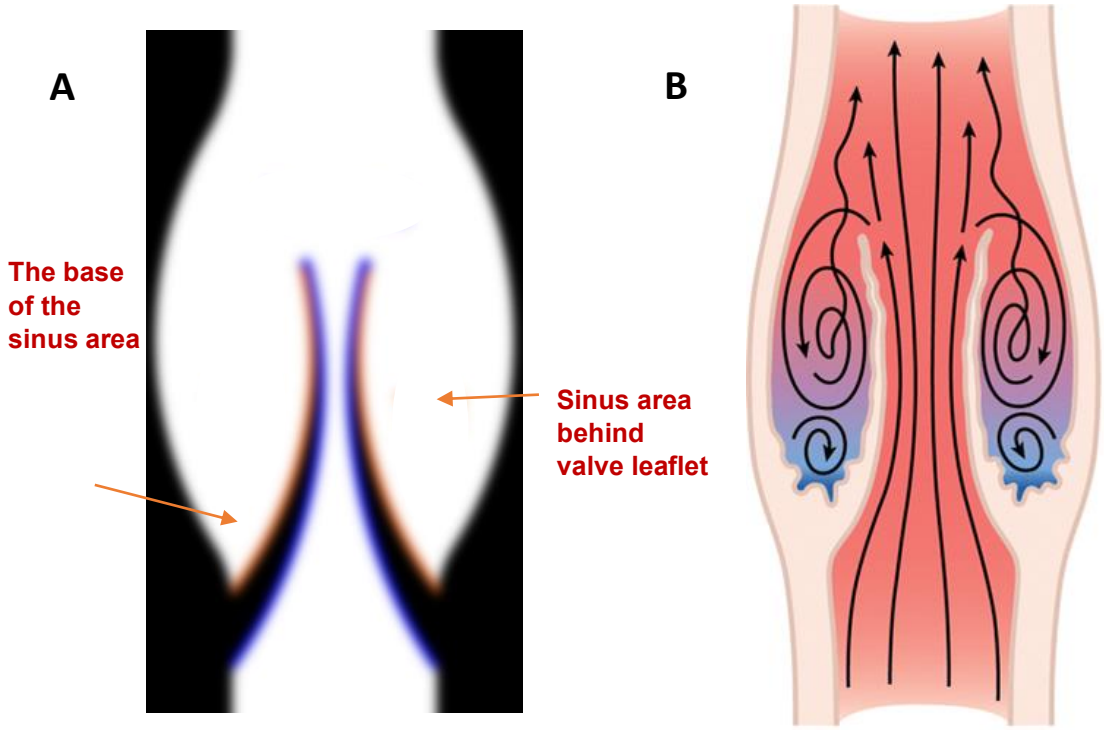

Figure 1.10. (A) Illustrates a human deep vein with a flexible valve clarifying the sinus area of the valvular valve leaflets. **(B)** The schematic diagram illustrates the characteristic vortical flow pattern observed during efficient flow in the deep veins. The oxygen tension is represented by a colour gradient ranging from red to blue, with darker blue shades indicating higher levels of hypoxia. Diagram **B** and its description are adopted from Bovill and Van Der Vliet, 2011.

1.11. Models of DVT

1.11.1. *In Vivo* models of DVT:

Animal models have been widely used to explore the mechanisms of thrombosis and haemostasis, as well as in evaluating the effectiveness and safety of antithrombotic drugs for potential human treatments (Dörffler-Melly *et al.*, 2000). Unfortunately, invertebrates like *Drosophila* and *Caenorhabditis elegans* cannot perform as suitable *in vivo* models to investigate mammalian haemostasis due to considerable differences in the components of haemostasis between these invertebrates and mammals (Jagadeeswaran *et al*., 2007). Studying thrombosis using animal models, start with zebrafish to nonhuman primates, is critical for detecting pathological paths and finding the most suitable treatment with minimal impact on haemostasis (Jagadeeswaran *et al.*, 2016). Generally, rodents are most frequently used in venous thrombosis research, while the pig, due to its similarity in size and vascular and coagulation reactivity to humans, is considered the most closely comparable model for human studies (Kang *et al*., 2003) refer to Table 1.5.

Table 1.5. Some examples of large animal models in DVT investigations

Animal model	Method	Thrombosis	Outcome	References
PIG	Endothelial denudation with 80% stenosis	High occurrence of thrombosis	Investigating anticoagulant treatments	Kang *et al*., 2003
	Endothelial denudation with 50% stenosis	Low occurrence of thrombosis	Assessing procoagulant effects of conditions or treatments	
Dog	Thrombogenic embolization coils	Create Deep Venous Thrombi or Pulmonary Emboli	Imaging deep venous thrombi and pulmonary emboli with radioactive material	(Kanke *et al.*, 1991; Knight, Maurer and Romano, 1996; Knight *et al.*, 2000)
	Measure the oxygen level in the valve pocket in static and pulsate conditions.	Thrombus formation on a valve cusp	Through non-pulsatile bloodstream, the ECs facing the pocket, or inner surface, can experience hypoxia while the ECs facing the lumen, or the inner	(Hamer, Malone and Silver., 1981)

			cavity of the blood vessel, remains adequately oxygenated. Early thrombus formation on a valve leaflet was observed after just two hours of non-pulsatile flow.	
Baboon	Thrombogenic reagents and ligation (stasis). Duplex imaging of the IVC and the iliac veins was performed to assess their status.	The experimental animals were administered HPC4 as a protein C inhibitor, and tumour necrosis factor developed thrombosis in the left iliac vein, which extended into IVC.	Establish a DVT model. This model allows for further investigation of agents that have the potential to modify thrombus formation.	(Wakefield *et al*., 1991)

Mice and rats are the highest used animals in DVT studies due to their widespread availability, relatively low cost, easy breeding, availability of advanced techniques of genetic manipulations (Dörffler-Melly *et al.*, 2000), and relative similarity of the haemostatic and thrombotic mechanisms with humans (Emeis *et al*., 2007). However, DVT does not occur naturally in mice, like other animals, therefore, various physical or chemical methods are employed to induce DVT in mice, including changes of the vein wall, to generate thrombosis (Rys, Blostein and Lemarié, 2018). Among murine models of DVT, flow restriction in the abdominal IVC is most used (Diaz *et al.*, 2019).

Thrombus is generated by inducing either complete (stasis model) or partial (stenosis model) blood flow cessation in the IVC (Payne and Brill, 2017). In the IVC stenosis model, residual blood flow through the IVC is left. This model is particularly suitable for studying thrombus development. IVC stenosis model consider the closest model that mimics human DVT initiation, as it develops thrombi without inducing endothelial injury. The main disadvantage of the model is the variability of thrombus size and lack of thrombus development in a proportion of mice (Brandt *et al*., 2014). This issue is absent in the complete stasis model, which is considered to recapitulate the conditions of human DVT less accurately, and it can represent complete occlusion (Diaz *et al.*, 2012).

1.11.1.1. Challenges of using IVC models for DVT

Developing a novel mouse model that initiates venous thrombosis through reduced venous blood flow without disrupting the endothelium has been a crucial advancement in comprehending deep vein thrombosis (DVT) (Brühl *et al.*, 2012). The initial approach referred to as the "IVC ligation (stasis) model," involved blocking all branches of the IVC to generate thrombus formation by restricting blood flow re-entry and promoting, this model is effective

in producing consistent thrombus sizes and measurable amounts of thrombus. Furthermore, to ensure accuracy and minimise variability in thrombus sizes, it is important to close the side branches of the IVC. Hence, ultrasonography measures the size of the thrombus and monitors the progression and resolution of thrombus formation over time within the same animal (Rys, Blostein and Lemarié, 2018).

However, interrupting the IVC branches, or not, in mouse models of DVT has sparked an argument within the scientific community. Ensuring consistency in thrombus size is essential, especially when evaluating the effectiveness of new drugs and comparing them to established treatments (Diaz *et al.*, 2015). The IVC stenosis model of venous thrombosis is created by a significant reduction of bloodstream, reaching about 80-90%, and leads to blood clot formation at the stenosis location. This model holds clinical relevance for studying deep vein thrombosis (DVT) in humans. It effectively reproduces vital features observed in DVT, such as local inflammation manifested by endothelial activation and the recruitment of platelets and immune cells to the vessel wall, which play essential roles in initiating thrombosis. However, the main limitation of this model is the absence of innate thrombus formation in some animals and the variability in blood clot size, that can impact the consistency of results. Additionally, researchers have yet to concurrence regarding the closure of side branches in this model (Campos and Brill., 2020).

VTE is a complex disease involving various factors such as mechanical and hemodynamic factors, coagulation, and inflammation cascade, which occur over a long time. Due to this complexity, no animal model currently exists that can fully replicate the diverse pathology seen in humans. However, small animal models, particularly rodents, are typically used to study and evaluate different aspects of thrombogenesis, and thrombolysis and test new

pharmacological therapies (Schwein *et al*., 2020), and despite using animal models, mechanisms of DVT initiation remain incompletely understood (Rajeeva Pandian *et al.*, 2020), this is in particular due to difference in venous characteristics between mice and humans, for example, the presence of valves in the human vein and their absence in mice, or horizontal spinal orientation of mice making the impact of gravity different from humans (Payne and Brill, 2017), also the vascular anatomy in mice exhibits significant variability, especially regarding the quantity of side and back branches and the width of the IVC (Campos and Brill., 2020), in addition, events occur faster in mice as it has a high metabolic rate and a short life span, compared to humans (Diaz *et al.*, 2012).

1.11.1.2. Ethical consideration

In 1824, the Society for the Preservation of Cruelty to Animals was founded in England, marking the establishment of the first organisation dedicated to the protection of animals. Subsequently, in 1876, the British Cruelty to Animal Act was proposed, serving as an early legal measure to regulate the utilisation of animals in research within Great Britain. Ethical animal experimentation issues in North America were not extensively explored until 1909 when the first publication addressing these concerns emerged (Miziara *et al.*, 2012). Significant progress in addressing ethical considerations in animal research occurred in 1959 with the publication of a seminal book by William M.S. Russell and Rex L. Burch. Their work introduced the "3 Rs" principle ‘Replacement, Reduction, and Refinement’ as a guiding framework for conducting animal research (Russell and Burch., 1959) (Camenzind and Eggel, 2022). Although the principles were acknowledged, widespread acceptance and implementation of these principles gained substantial global traction only in recent years. In 2010, the World Organization for Animal Health (OIE) established standards for the "Use of

Animals in Research and Education" within Chapter 7.8 of its Terrestrial Animal Health Code, further reinforcing the significance of ethical considerations in animal research (Bayne *et al.*, 2015). Ethical considerations establish a framework promoting responsible and conscientious utilisation of animals in research, with a primary focus on safeguarding animal welfare, optimising resource utilisation by minimising their use when feasible, and actively following alternative methodologies to advance scientific understanding while upholding ethical standards (Olsson *et al*., 2012) however, the European Union is even more strict to implementing the replacement of animals in research as soon as it is scientifically achievable and acceptable (Herrmann, 2019).

1.11.2. *In-Vitro* models of DVT:

Microfluidic platforms are constructed structures as hollow rectangular channels with micrometre-scale dimensions. These dimensions are typically achieved through soft lithography, a standard microfabrication technique. These devices are designed to replicate

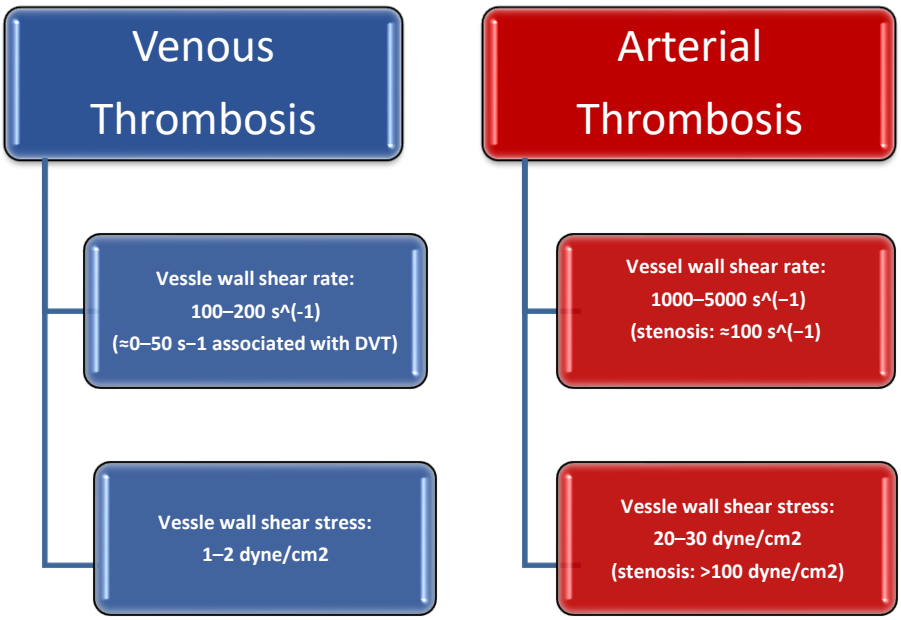

Figure 1.11. The bloodstream hydrodynamic forces promote the initiation of blood clots in arteries and veins (Diamond, 2016; Pandian *et al*., 2018).

the characteristics of human blood vessels (Fiddes *et al*., 2010). These microfluidic devices can also perfuse blood at high arterial and low venous wall shear rates (WSRs), as shown in Figure 1.11 (Diamond, 2016; Pandian *et al*., 2018). They have found recent applications in *in vitro* models of DVT research (Rajeeva Pandian *et al*., 2020), provided by the opportunity to culture human endothelial cells (Jain *et al*., 2018). This innovative approach effectively replicates human vessels, incorporating features like human tissue and flow dynamics (Van Den Berg *et al*., 2019).

The rheological properties of whole blood profoundly affect vascular biology, platelet function, and the signalling pathways crucial for haemostasis. Notably, many in vitro devices have not combined the natural flow of human blood in their reviews, primarily due to technological challenges (Jain *et al.*, 2018). Utilising microfluidic devices has an advantage in their ability to study thrombus formation and coagulation in fabricated vessels on chips using small volumes of blood, also these chips are biocompatible, allowing the culture of a monolayer of human cells within the microfluidic devices (Jain *et al.*, 2018).

The innovative *in vitro* model, involving the utilization of microfluidics alongside in situ fabrication techniques, was previously pioneered by Schofield *et al.* (2020), refer to materials and methods. This approach facilitates a more comprehensive comprehension of valve flexibility, the flow patterns established within the channels, and their influence on the accumulation of particles around the valve.

1.11.2.1. Human microscopic venous valves (MVVs)

Venous valves are commonly considered to be lacking in veins smaller than two millimetres. Therefore, recent research into DVT primarily concentrates on evaluating valves' competency

in larger veins. Even the small superficial veins in the human legs possess a significant number of valves. However, most of these valves, bicuspid valves of ~18μm in diameter, are located within venous channels with a luminal diameter of less than 100μm (Phillips, Jones *et al*., 2004). The first description of microscopic venous valves (MVVs) in human digits (fingers and toes) was in 1934. Since then, they have been observed in various locations within the human body and animals. The specific distribution of MVVs suggest their function in preventing blood backflow in tiny veins and determining the bloodstream from postcapillary venules back into the capillary network (Caggiati *et al*., 2006).

Due to the challenges of fluid mechanical analysis in mice models, using *in silico* and *in vitro* models for MVVs can provide valuable insights. These models can help us investigate whether these valves, comparable to the larger valves in deep veins, are susceptible to thrombus formation. Computational modelling techniques can be employed to investigate the blood flow dynamics in MVVs regions, unravelling their unique and complex fluid behaviour. Findings from these analyses can be used as a foundation for the future development of *in vitro* models specifically created to represent MVVs (Rajeeva Pandian and Jain., 2022).

1.11.2.2. The importance of developing DVT *in vitro* models

Human blood is widely applied *in vitro* flow assays, while *in vivo* studies are often conducted using mice as experimental models. Although it is feasible to employ murine blood for *in vitro* flow assays, which can be validated using related murine blood *in vivo* models, the same approach cannot be applied to human blood. These differences emphasise the importance of developing advanced *in vitro* models that accurately replicate pathological conditions, including human-specific flow patterns, to bridge the gap between *in vivo* and *in vitro* models. The observed differences in rheological values between mouse and human vessels, WSRs

reported in human studies range from 40 to 150 s^{-1}, with 14 to 20 mm vessel diameters. In comparison, a study found a significant difference between humans and male mice, with WSRs of 140 s^{-1} in humans and 2500 s^{-1} in male mice for a 700 µm diameter, which has a different effect on platelet function and, consequently, thrombosis. For instance, mouse platelets enhance platelets adhesion via integrins at high WSR compare to human platelets (Panteleev *et al.*, 2021) also, using murine blood demonstrated that venous thrombi exhibit lower platelet density than arterial thrombi. This disparity is attributed to the influence of wall shear rates, which play a crucial role in platelet aggregation and adhesion to the ECM (Pandian *et al.*, 2018).

The future priority of animal-based scientific research is expected that ethics and legislation will continue to influence the progress and development of replacement research methods (Herrmann, 2019). Likewise, this project is funded by the National Centre for the Replacement, Refinement, and Reduction of Animals in Research (NC3Rs), aims at developing a new technique to avoid animal usage in DVT research. NC3Rs is a scientific organisation established by the UK government to explore, advance, and advocate novel scientific methods aligned with replacement, reduction, and refinement of the utilisation of animals in research. Similarly, NC3Rs encourage animal welfare and reduce their unnecessary inclusion in research (Prescott and Lidster, 2017).

In general, valve pockets of large veins of the leg are likely to experience any changes of the blood flow, such as turbulence or complete stagnation. In addition, these valve pockets are widely believed to be the primary site of origin for most venous thrombi, so studying the altered blood flow, valves and their dynamics is enthusiastically proposed for a better understanding of this poorly investigated component of Virchow's Triad (Kattula S, JR and

Wolberg AS, 2017). However, there is a current need for *in vitro* models investigating the initiation mechanisms of DVT that integrate three crucial parameters into a single system: a flexible valve, whole blood flow, and endothelium (refer to Table 1.6). Our project is progressing with the usage of *in vitro* models of DVT. These models were fabricated using microfluidic devices with flexible valves. The promising challenge is to add HUVECs to the system to coat the inner surfaces of the channels, which are equipped with flexible valves to mimic the characteristics of human veins more accurately.

Table 1.6. *In vitro* models for DVT, including their valve, fluid type and the presence of endothelial cells.

***In vitro* model's summary**	**Valve type**	**Fluid type**	**Endothelium**	**References**
Microfluidic devices assessing the impact of RBCs on venous thrombosis, it has been observed that in microchannels designed to mimic the geometries of venous valve pockets, the presence of vortical flows results in an atypical local distribution of RBCs, and blood stasis.	Rigid valve	Dilute RBC suspension, 5% haematocrit.	Not included	(Sanchez *et al*., 2022)
Microfluidic devices replicate the dynamic motion of valves and the compression of vessels caused by muscle contractions. Understanding the impact of altered blood flow on thrombus formation in the valve pocket	Valve with flexible leaflets	Whole blood	Not included	(Hu *et al.*, 2020)
Microfluidic devices combining blood flow through venous valves coated with ECs and show varying responses in different regions upon administering anticoagulant drugs. Importantly, blood clot formation within the venous valves exhibited an amplified resistance to anticoagulation.	Rigid valve	Whole blood	HUVECs	(Rajeeva Pandian *et al.*, 2020)

A microfluidic device resembling human venous valves mimicking their dynamics and dimensions. The model exhibited flow patterns within the valve sinus, characterised by primary and secondary vortices. The results indicate that RBCs facilitate the transportation of platelets into the primary vortex and promoting their adhesion to the fibrin network created within the valve pocket. GPVI is essential for the adherence of platelets to fibrin and further activation, leading to the lengthening of thrombus beyond the valve sinus.	Rigid valve	Plasma, RBC suspension, platelet rich plasma, reconstituted blood, or whole blood	Not included	(Lehmann *et al.*, 2018)

1.11.3. *In-Silico* models of DVT

Fluid-structure interaction (FSI) has been used for the numerical simulation of the leaflets of the human valve and their interface with the bloodstream (Soifer *et al.*, 2017). In solid-liquid flow simulations, three phenomena are observed and categorised into groups: contact forces, solid mechanics, and fluid dynamics (Alexiadis, 2015). Recently, many papers have been dedicated to the computational modelling of thrombosis, specifically the site and mechanisms of blood clot formation, to discover the conditions that eventually trigger thrombosis (Yesudasan and Averett, 2019).

In silico simulations can be employed to model the hydrodynamics of blood flow and its interactions with the solid structure (Marom, 2015), where the formation of solid cluster, membrane deformation, and hydrodynamics in unique DVT model have been simulated (Ariane *et al.*, 2017b) such approach provides a more precise means of measuring hydrodynamics, which can sometimes be challenging to detect in both *in vivo* or *in vitro* models (Liu *et al*., 2020). Accordingly, enhancing advanced *in silico* simulations is crucial for investigating thrombosis (Ariane *et al*., 2017b). Veins show an innate elasticity, allowing their lumens to collapse when subjected to exterior forces and distend when interior pressures increase. The fluid flow within these flexible structures is controlled by a combination of forces, including exterior stresses, structural characteristics, the material properties of the fluid, and the presence and function of internal valves; hence, the interplay of viscous forces and fluid pressure results in a continuous movement of these flexible structures (Wijeratne and Hoo, 2008). This interaction can impact the development of DVT, where the characteristics of the valve leaflets, including their flexibility and length, and the blood flow mechanisms play a key role in the growth of thrombus (Ariane *et al*., 2017b)

1.11.3.1. Mesh free approach

Simulations of biological valves generally involve the interaction between a solid structure and the surrounding flow. This is an example of a computational problem commonly referred to as a FSI. Traditionally, two main categories of algorithms are used to solve FSI problems: conforming mesh methods and non-conforming mesh methods. Conforming mesh methods require meshes conforming to the interface as the Interface conditions are treated as physical boundary conditions, and due to solid structure movement/deformation the re-meshing is needed. On the other hand, non-conforming mesh methods study the boundary position and interface conditions as restrictions on model equations, also, separate grids re-meshing is not needed as fluid and solid equations able to be solved independently (Hou, Wang and Layton, 2012). This work uses a third novel approach does not count on meshes called discrete multi-physics to simultaneously capture valve deformation, fluid dynamics and the formation of solid aggregates. This method utilizes computational particles for the flow and the structure without relying on a mesh, and classifying the status particles as a solid or a liquid relies entirely on the forces acting upon each contributed particle. Liquid particles are considered by pressure and viscous forces, while solid particles are characterised by elastic forces. Modifying the forces acting on specific sets of particles that able to shift between liquid and solid states. DMP was used for simulating the valves and the agglomerants, this choice of DMP aligns with its successful application for similar problems (Ariane *et al*., 2017b). Primarily discrete multi-physics model capable to combine Lattice Spring Model (LSM), and Smoothed Particle Hydrodynamics (SPH) in one hybrid model for simulating dispersed solid-liquid flows, this model has been applied successfully on biological fluids, demonstrating its ability to capture the essential characteristics of the flow phenomena (Alexiadis., 2015).

1.11.3.2. Previous numerical models of vein valves

There is a need for developing *in silico* models investigating the initiation mechanisms of DVT that integrate three crucial parameters into a single system: a flexible valve, hydrodynamics, and the initiation circumstances of blood clot. For a comparative analysis among various in-silico models, each equipped with flexible valves (see Table 1.7).

Table 1.7. Comparison between different *in silico* models specified with flexible valves.

The purpose of study	Method	Valve	Blood aggregate formation	References
The simulation is designed to show up how the formation of clots influences the flow dynamics in a vein segment equipped with multiple valves. The study incorporates different time intervals coordinated with the cycles of contraction and expansion in the vein wall, providing valuable insights into the individual responses of each venous valve to these variations.	Rely on meshes	3D model (Series of three valves)	Resulted of the interaction between the viscous forces inside the venous valves edges and the fluid dynamic viscosity	(Simão *et al*., 2016)
Understanding how pathological stiffening of valve leaflets affects valve biomechanics and the interactions between neighbouring valves in different situations.	Rely on meshes	• 2D model (Two sequential venous valves)	N/A	(Soifer *et al*., 2017)

		• 2D model (Two parallel venous valves)		
Initiate the formation of solid aggregates at the valve leaflet and in the flow, then highlight how the presence of the clot influences the hydrodynamics.	Mesh free	2D model (One valve)	Agglomeration seed placed in three locations independently, and then the clot creation accelerated by applying higher clustering probabilities.	(Ariane *et al.*, 2017a)
The study examines how varying diameters and lengths of a free clot affect the flow dynamics around the valve leaflets. A free blood clot significantly changes the fluid	Mesh free	2D model (Two valves)	A solid particle (embolus-like structure) is	(Ariane *et al.*, 2018b)

dynamics and affects the behaviour of the valve leaflets. The free clot's ability to remain within the valve chamber is strongly linked to its length.			introduced into the flow.	
The stiffness and length of valve leaflets are key factors affecting mechanical stress and flow stagnation. Rigid and shorter leaflets may not effectively prevent blood reflux but reduce stagnant blood volume, potentially lowering thrombosis risk.	Mesh free	2D model (One valve)	Introduce an agglomeration seed in two locations, then the agglomeration algorithm applied.	(Ariane *et al.*, 2017b)

Our project further developed the original *in silico* models for DVT (Ariane *et al.*, 2017a; Ariane *et al.*, 2017b), by introducing particle agglomeration around the valve leaflets and studying the effects of hydrodynamics on this phenomena. To the best of our knowledge, this represents the first DVT model to include agglomeration.

CHAPTER 2

MATERIALS AND METHODS

Declaration: Some of the content presented in this chapter have been published:

Platelet accumulation in an endothelium-coated elastic vein valve model of deep vein thrombosis is mediated by GPIb α—VWF interaction.

Baksamawi, H.A., Alexiadis, A., Vigolo, D. and Brill, A., 2023.

Frontiers in cardiovascular medicine, 10, p.1167884. Published: 27 April 2023

DOI: https://doi.org/10.3389/fcvm.2023.1167884

Modelling particle agglomeration on through elastic valves under flow.

Baksamawi, H.A., Ariane, M., Brill, A., Vigolo, D. and Alexiadis, A., 2021.

ChemEngineering, 5(3), p.40. Published: 26 July 2021

DOI: https://doi.org/10.3390/chemengineering5030040

2.1. *In vitro*

2.1.1 Master Mould Fabrication

In nature, human venous valve anatomy is unique in its structure. It has thin and strong leaflets and an expanded sinus area (refer to Figure 2.1. A). Also, the number of valves within the veins is varied in the lower limbs, for example, in the femoral and popliteal veins, as they represent the most prominent intramuscular veins, with one to five valves and one to three valves, respectively. On the other hand, most of the iliac veins have no venous valves (Dalsing and Kistner, 2019).

The designs, along with the geometries of the microfluidic channels and the valves, have been created using AutoCAD software (Autodesk Inc, US). Designing the microfluidic system, a clinical image of the femoral vein, as illustrated in Figure 1, was used as a model to develop an AutoCAD design that replicates the shape of the bicuspid leaflets and the arrangement of the sinus area. The design of the microfluidic channels was modified to mimic the geometry of the human femoral vein and valve leaflets, considering the sinus area.

The created design of microfluidic channels and valves was printed on top of a special transparency photomask (Microlithography Services Ltd, UK). The desired geometries of the microfluidic channels were drawn with a width of 300µm. The valve region geometries have a maximum width of 520 µm and 700 µm in length (Figure 2.1 B, C, D). The thickness of the channels depends on the spin coating speed.

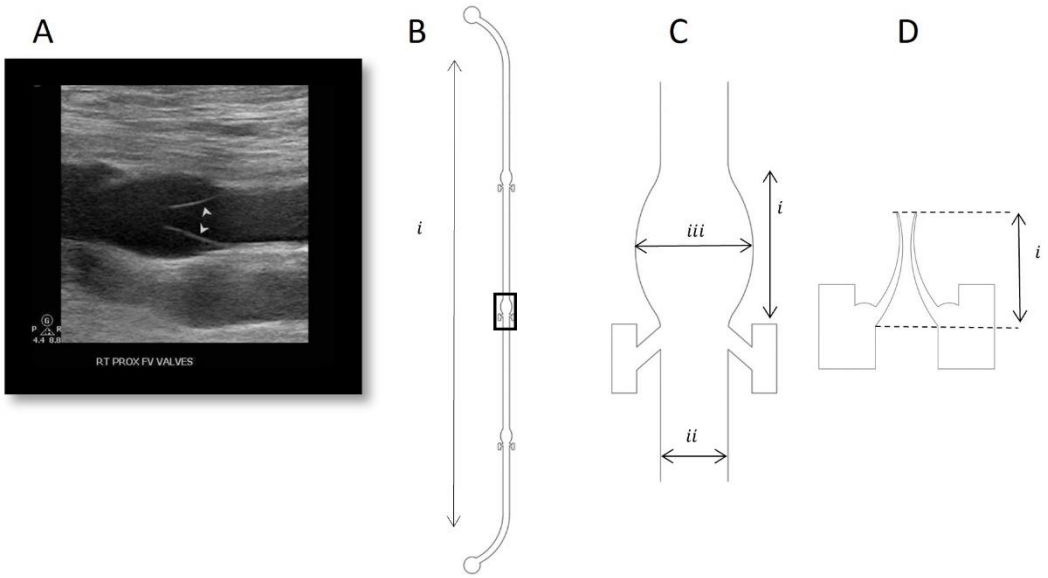

Figure 2.1. (A) Shows a duplex image of the femoral vein valve, with arrowheads highlighting the valve leaflets in a partially open position and the presence of valve sinuses on the opposite side. **(B&C)** The AutoCAD microfluidic channel design, with a wide sinus area, includes **(Bi)** a 2 cm channel length, **(Ci)** a 700 µm valve region length, **(Cii)** a 300 µm channel width **(Ciii)** and a maximum width of 500 µm in the valve region. **(D)** The AutoCAD design of the valve mask, **(Di)** a valve leaflet length of 530 µm. Figure **2.1. (A)** is adopted from Dalsing and Kistner, 2019.

Preparation of master moulds was carried out in the clean room to minimize contamination as much as possible. The silicon wafer (d=100 mm, Si-Mat, Germany) was cleaned using acetone (Sigma Aldrich, UK) followed by isopropanol (Sigma Aldrich, UK). Then the silicon wafer was dried with nitrogen gas. Then the silicon wafer was baked at 160°C for 15 minutes to dehydrate the surfaces. The wafer was left at room temperature for 5 minutes to cool down. To create a master mould with an approximate thickness of 120 µm, 5 g of SU8-2075 (MicroChem, Westborough, USA) was poured onto the centre of the silicon wafer and spin-coated at 2100 rpm for 30 seconds. The silicon wafer was soft baked at 65°C for 5 mins and 95°C for 14 mins, and the wafer was left at room temperature to cool down for 10 mins. Later the photo mask (MicroLithography Services Ltd, UK) is aligned with the silicon wafer using a

mask aligner (Canon PLA-501FA Mask Aligner) and exposed to ultraviolet (UV) light for 20 seconds, with an exposure power of 11.5 W/sq.cm, for total exposure energy of 230 mJ/ sq.cm. Post-exposure bake was at 65°C for 4 mins and 95°C for 9 mins. The wafer was allowed to cool down and then developed in SU8 developer (PEGMEA) (MicroChem, Westborough, USA) for approximately 8 minutes until all SU8 2075 had visibly disappeared. Then the wafer was washed in fresh PGMEA followed by isopropanol (Sigma Aldrich, UK) to ensure the development was precisely completed. Finally, the master mould was dried in nitrogen gas and was ready to be used for the soft lithography process to get the desired PDMS devices. The thickness of the channels was variant 120 $\pm$ 15µm. The master moulds that were used to run the lab experiment had a thickness of ≈120 µm. Throughout the project, 12 master moulds were made, while up to 20 PDMS devices were created weekly.

2.1.2. Preparation and modification of PDMS and PEGDA surfaces

Polydimethylsiloxane (PDMS) is a cheaper and more elastic than other materials, such as glass and silicon (Dogru *et al*., 2020; Duffy *et al*., 1998). The microfluidic devices were manufactured by using soft lithography. First, the PDMS base and the curing agent (Sylgard 184, Dow Corning) with a weight ratio of 10:1 was mixed. Then, the PDMS mixture was poured on top of the mould. Regarding the mixing procedure, air bubbles were created within the PDMS mixture. The mould was kept under vacuum condition for 20 minutes, followed by oven heat treatment at 70°C for 1:30 hrs. Next, a biopsy puncher (1.5 mm) was used to make the inlet and outlet of the cured PDMS layer that was removed from its initial mould. This layer represents the top layer of the fabricated microfluidic device.

For the bottom layer, a glass slide spin-coated with ≈250 µm of PDMS (30 s at 1500 rpm) and left it to cure in an oven at 70°C for 90 min was used. To create the device, both layers were

treated with a corona discharge for 1-1.5 minutes at a power of 30 Watts (PZ2 Handheld Device, Relyon Plasma GmbH, Germany) and bonded together. Then the device was placed on a hot plate for 10 minutes to induce irreversible bonding.

A limitation of microfluidic devices is that the cross-section of the microfluidic channel is a rectangular, whereas the cross-sections of the blood vessel are circular (Fiddes *et al.*, 2010).

2.1.2.1 Valve fabrication:

2.1.2.1.1. Microfluidic devices without cells

Permeability of PDMS material facilitates the presence of Oxygen from the surrounding atmosphere and thus prevents poly (ethylene glycol) diacrylate (PEGDA) polymerisation, and a consistent non-polymerised PEGDA layer will be created along the channel walls (Duprat *et al*., 2015). For this reason, the microfluidic channel was provided with anchors to guarantee that the created valves were attached securely to the channel wall. First, PEGDA (Mn ≈ 525, Sigma Aldrich, UK), was diluted with distilled water. Then, 2-hydroxy-2-methyl propiophenone (photo-initiator) (Sigma Aldrich, UK) was added at specific values to achieve the desired polymerization. The channel was filled with the prepared mixture. Exposure time to the UV light with wavelength λ ≈ 365 nm by using (Lumencor SOLA, USA) is significant to successfully cure the PEGDA mixture almost as the valve mask shape aligned previously in their specific site in the channel. The flexible valve is created, and the microfluidic device is ready to run the polystyrene particles and blood experiments (Figure 2.2).

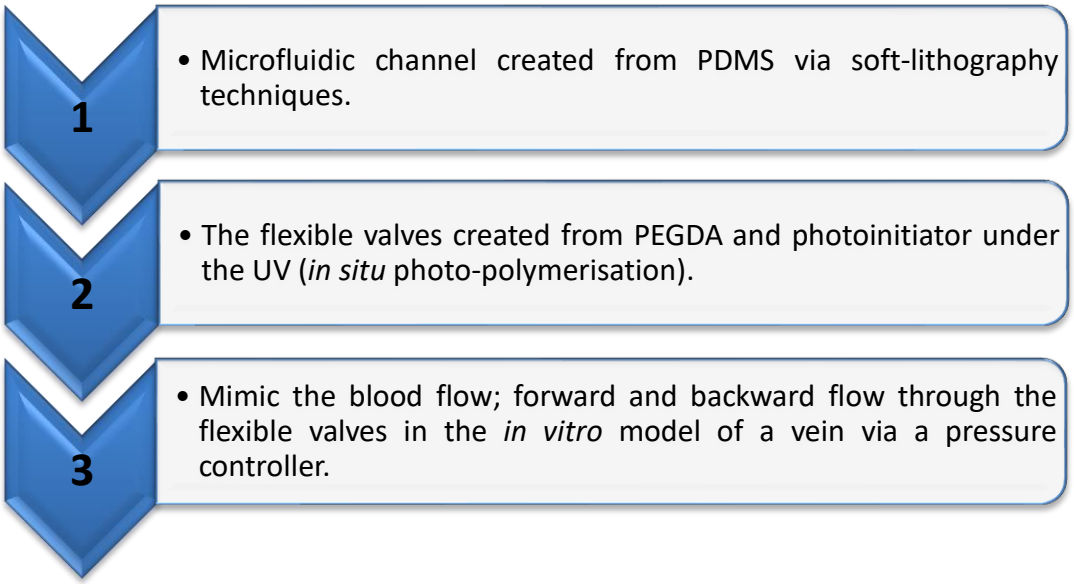

Figure 2.2. The fundamental stages involved developing a sophisticated microfluidic channel with an elastic valve.

To get the precise temperature ~ 37°C inside the PDMS microfluidic channel, temperature controller (Wavelength Electronics LFI-3551 5.0 AMP - 40W, USA) was used to control the temperature. The temperature controller was connected to a thermocouple to the stage placed on the florescence microscopy platform. The temperature of thermocouple surface was set at ~ 38°C , that promote the temperature inside the PDMS channel to be ~ 37°C with one-degree Celsius deference between the two surfaces as shown in Figure 2.3.

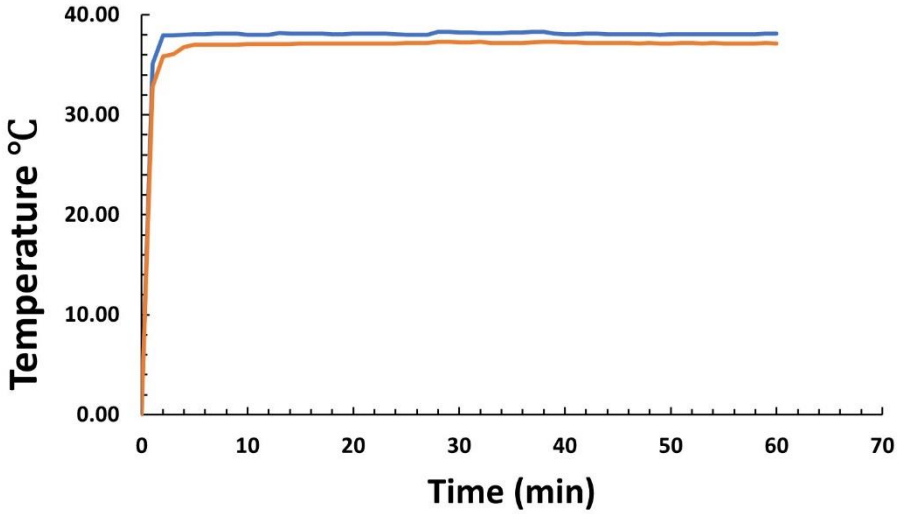

Figure 2.3. The temperature inside the PDMS channel was maintained at 37°C. The blue line indicates the temperature of the thermocouple surface, and the orange line indicates the temperature of the PDMS channel's inner surface.

2.1.2.1.2. Microfluidic devices to be coated with HUVECs monolayer.

For valve fabrication, the mixture of PEGDA (Mn ≈ 700, Sigma Aldrich, UK), 0.5% Gelatine hydrolysate Enzymatic (Sigma-Aldrich, U.S.A.) in Phosphate-Buffered Saline (PBS) and photo-initiator (2-hydroxy-2-methyl propiophenone) (Sigma Aldrich, UK) were infused into the channels. Achieving precise alignment of the photo mask involved utilising a filter with a wavelength of λ = 545 ± 25nm to freely position the valve mask within the channel without inducing polymerisation. Subsequently, the filter was switched to enable the selection of UV wavelength λ = 350 ± 50nm for curing the Poly(ethylene glycol) diacrylate (PEGDA) into the intended geometry of the valve. The entirety of this procedure was performed using x10 objectives.

The flexible valve was created using *in situ* photo polymeriza-tion by exposing the PEGDA solution to UV light (Lumencor SOLA, USA) for 400 ms through a photomask reproducing the valve geometry placed in the conjugated plane of an inverted microscope (Nikon Ti-U) (Figure 2.4). The microfluidic devices were then cleaned and sterilized with 70% ethanol.

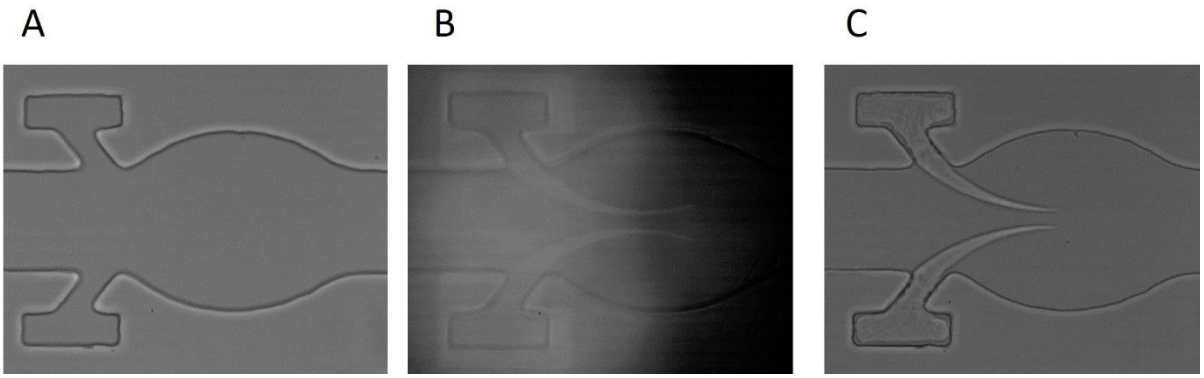

Figure 2.4. Valve fabrication, **(A)** Optical images of the microfluidic channel spotting the anchors and the valve region **(B)** Optical image of mask alignment through the fluorescent light of an inverted microscope. The mask was designed to produce the desired valve shape through a 10× objective. **(C)** Optical image of the created flexible valve. The length of the valve is about 330 µm, however this length will increase when the hydrogel swells in the growth medium, the width of each leaflet starts at about 900 µm and it narrows towards the tip.

2.1.3 Coating with HUVEC

In the experimental design, HUVECs from passages between 3 and 8 were chosen, representing a spectrum of subcultures initially derived from the primary HUVECs. HUVECs were chosen for the experiments and further development of the model due to the following reasons: 1) HUVECs have endothelium structure and morphology typical for large vein, contain Weibel-Palade bodies, express a variety of endothelium-specific elements (e.g., PECAM-1, E- and P-selectins, VE-cadherin, eNOS, vWF, ICAM-1 and VCAM-1 etc.), and produce

nitric oxide and prostacyclin, major endothelium-derived anticoagulants and platelet antagonists (Medina Leyte *et al.*, 2020), 2) HUVECs is human endothelium from a typical large vein thus representing an adequate model to study DVT (which develops in large veins), although it should be noted that the umbilical vein may still have substantial differences from veins in the limbs (Medina Leyte *et al*., 2020), 3) HUVECs are easily isolatable in high numbers by a non-invasive approach from a material designated as "medical waste" (Kocherova *et al.*, 2019), and 4) A large number of published studies have been performed on HUVECs, which allows for comparison of the obtained results (Kocherova *et al.*, 2019)

2.1.3.1 Preparation of the Human umbilical vein endothelial cells (HUVECs):

The cell culture plates (T75 flasks) were coated with 0.2 % Gelatin Hydrolysate Enzymatic (Sigma Aldrich, UK) for 20 minutes at room temperature to improve HUVECs attachment. Then, the T75 flasks were aspirated from the Gelatine solution content, and 15 mL of the previously prepared endothelial growth medium (Table 2.1) was directly added to prevent dryness to the coated flasks and maintained at 37°C in a Humidified, 5% CO2 incubator.

Table 2.1. HUVECs growth medium formulae.

Medium and supplements	**Volume**	**Source**
Medium 199, Earle's Salts	500 mL	(Gibco, UK)
Growth Medium 2 Supplement Mix	12.5 mL	(promoCell, Gemany)
Fetal bovine serum (FBS)	50 mL	(Sigma Aldrich, UK)
Penicillin and Streptomycin	5 mL	(Sigma Aldrich, UK)

HUVECs pooled donors and cryopreserved (promoCell, Germany) were prepared and seeded in T75 flasks. The medium was changed every other day till the cells' passage reached 80% confluence. After the treatment with 2X trypsin (Gibco, UK), the flasks were kept in a Humidified, 5% CO2 incubator at 37°C for 5 minutes, then the HUVECs were neutralized with the growth medium and then collected and either used directly with the experiment or stored in the liquid nitrogen to be used later.

HUVECS lose their morphological characteristics as early as the third passage. When the cells were cultured after the sixth passage, they appeared to lose their shape and size, becoming elongated, irregular, and in size, resulting in decreased cell density. These findings suggest that the HUVECs increase in cell size and volume at a later passage as a function of *in vitro* age(Bala, Ambwani and Gohil, 2011)

2.1.3.2 Functionalisation and sterilisation of the microfluidic device:

The aim of growing the HUVECs within the microfluidic channels is to create an inner monolayer of HUVECs close to the lumen blood vessels and valve leaflets. However, before seeding the microfluidic channels with the HUVECs, the PDMS layers must be sterilised and functionalised. That will increase the biocompatibility of the treated surfaces to accept the growth of human cells (HUVECs).

Firstly, to immerse the PDMS channel in 10% (3-aminopropyl)-trimethoxysilane (APTES) (Sigma-Aldrich, Singapore) diluted in 90 % ethanol, absolute, <=99.8% (Fisher Scientific™, UK) at room temperature for 15 min. Next, the APTES solution was removed, and the samples were washed with ethanol, absolute <= 99.8% (Fisher Scientific™, UK). Finally, after aspirating the liquids from the samples, the channels were left to dry for 15 minutes. 50 µl of 0.5% Hydrolysate Enzymatic (Sigma Aldrich, UK) dissolved in BPS (Sigma Aldrich, UK). Then, a

mixture of 400 µl of PEGDA 700 Mn (PEGDA; Sigma Aldrich, UK) and 0.14ul Photo initiator was added. The mixture was infused into the channels, and the flexible valve was created by using *in situ* polymerisation under UV light for 400 ms. Then the samples were washed and sterilised with 70% ethanol (Fisher Scientific™, UK). The channels were then immersed with 2% Gelatin Hydrolysate Enzymatic (Sigma Aldrich, UK) and stored at 4°C overnight. Then the devices were placed at room temperature for 1 h before the cell culture stage. Finally, the Gelatine solution was removed, and the samples were immersed in the growth medium. At this stage, the samples were ready for the cell seeding step. HUVECs were seeded with a concentration of $10^7 mL^{-1}$ into the treated channels and then were incubated at 37°C and in a 5% CO2 incubator for 4 h. The outlet and inlet were securely closed to promote cell adhesion at all the sides of the device channel and valve leaflets. To provide the HUVECs with sufficient nutrients, the growth medium was perfused into the channel under a flow rate of 1 µL min^{-1}.

A consistent flow rate of 1 µl/min is not just to provide the cells with the required nutrients but also to direct the growth and align the cells with the flow direction (Rajeeva Pandian *et al*., 2020). The work reported by Qiu Y *et al.* (2018) shows adequate evidence that endothelial cells cultivated under dynamic flow conditions manifest alignment with the flow direction. In contrast, cells grown under static conditions exhibit no actual alignment.

2.1.4. Blood preparation

All the human blood experiments were performed in accordance with the principles of the Declaration of Helsinki, ethical approval granted by University of Birmingham internal ethical review (ERN_11-0175AP20) and informed consent was obtained from all donors. Blood was drawn from healthy volunteers and immediately mixed with 3.8% sodium citrate (9:1).

Platelet rich plasma (PRP) was obtained by centrifugation of whole blood (200 g, 10 min). Washed platelets were obtained by centrifugation of PRP (1000 g, 10 min) in the presence of 10 µg prostacyclin and resuspended in modified Tyrode's-HEPES Buffer (134 mM NaCl, 0.34 mM Na2HPO4, 2.9 mM KCl, 12 mM $NaHCO_3$, 20 mM HEPES, 5 mM glucose, 1 mM $MgCl_2$; pH 7.3). In the case of experiments with untreated platelets, the platelets were labelled by Calcein Red-Orange, AM, at 1:100 ratio, at room temperature for 20 minutes, and reconstituted with the whole blood. For challenged platelets experiments, the platelets were treated first with thrombin (0.1 U/mL), eptifibatide (9 mM) or OS-1 (M3456 CTERMALHNLC, Alta Bioscience, 12 mM) peptide for 5 minutes then were labelled with Calcein Red-Orange and reconstituted with the whole blood. All microfluidics experiments were performed at 37°C.

During this project, the healthy volunteers comprised individuals aged 25 to 55 and blood group type was not considered in the selection process. Each week, three donors participated, providing three distinct blood samples. This setup allowed us to conduct about four experiments weekly.

2.1.5. Immunostaining

HUVECs within the microfluidic device were fixed with 4% paraformaldehyde for 10 minutes and washed carefully with Dulbecco's phosphate-buffered saline (DPBS). Then the HUVECs were permeabilized with 0.1% Triton X-100 (Sigma-Aldrich) in Bovine Serum Albumin (BSA)/ DPBS for 15 minutes and blocked with 1% BSA in DPBS for 1 hour at room temperature. HUVECs were labeled with CD144 (VE-cadherin) Monoclonal Antibody (16B1), eBioscience™ (Invitrogen, UK) at 1:100 dilution in 0.1% BSA, and CD31 Recombinant Rabbit Monoclonal Antibody (7) (Invitrogen, UK) at 1:100 dilution in 0.1% BSA, incubated at 4 degrees Celsius overnight. Then the HUVECs monolayer were labelled with Secondary Antibody, Alexa Fluor®

488 Goat anti-Mouse (Invitrogen) (Panel a: green), at a dilution of 1:200, and Secondary Antibody, Alexa Fluor® 568 Goat anti-rabbit (Invitrogen, UK) (Panel r: red) at a dilution of 1:200, for 60 minutes at room temperature, then the channels were washed carefully with PBS. Finally, nuclei (Panel b: blue) were stained with Hoechst 33342, trihydrochloride, trihydrate at a dilution of 1:10000 in 0.1% BSA for 10 minutes at room temperature and then were washed carefully with PBS. The images were captured at 20X magnification using Zeiss confocal microscope LSM780.

2.1.6. Imaging

Nikon Ti-U microscope was the primary instrument used in all experimental procedures. White light was employed for bright-field microscopy, providing a standard illumination source. On the other hand, an LED source possessing a UV band (SOLA, Lumencor) was utilised. Refer to Figure 2.5 for an overview of the device in the imaging condition.

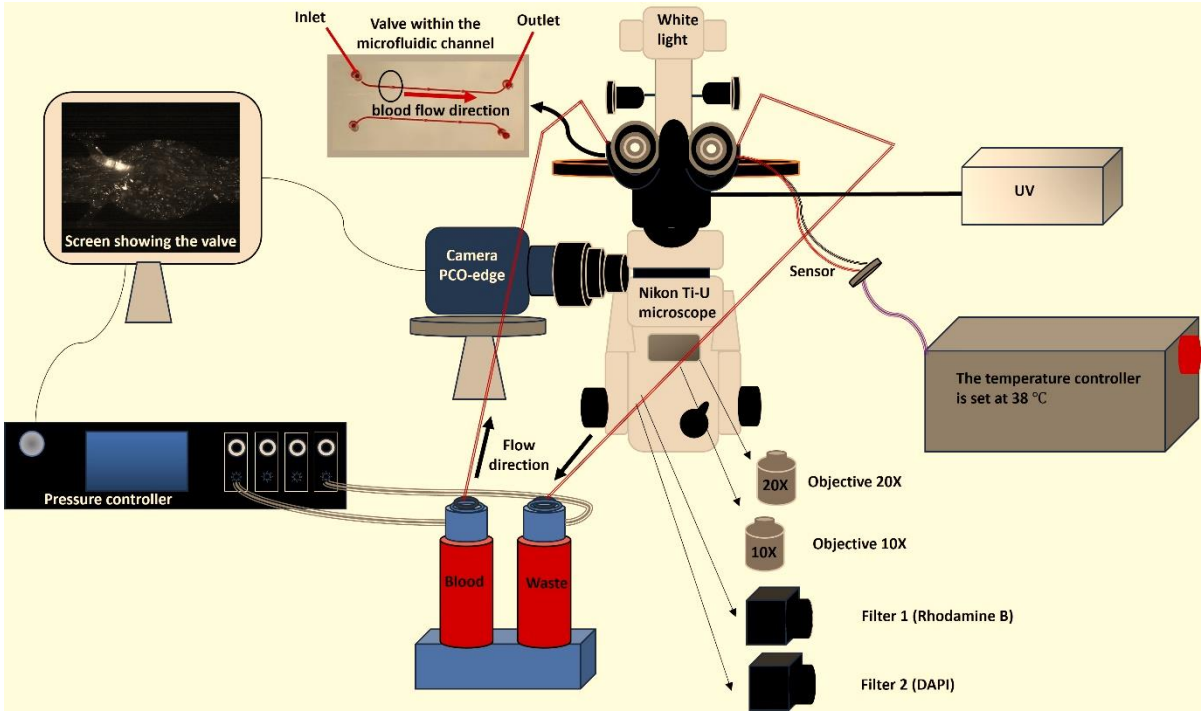

Figure 2.5. A schematic diagram illustrating the imaging configuration of the microfluidic device. After being positioned on a dedicated platform, the device was connected to a temperature controller, which maintains channel temperature at approximately 37℃. The inlet tubing links to a blood container, and the outlet tubing directs flow to a waste container. The pressure controller modulates flow rates between 0 and 120 mbar per second while maintaining a constant backflow at 60 mbar. The PCO-edge 5.5 interfaces with the fluorescence microscope and displays the valve area on-screen. A Rhodamine B filter cube (Filter 1) was employed for precise valve alignment during the microfluidic device setup. Subsequently, a DAPI filter cube (Filter 2) facilitated *in situ* polymerisation during experimentation. Two Nikon objectives contributed to the experiments: Nikon Plan Fluor 20X/0.45 and Plan Fluor 10X/0.30, each offering distinct magnification and numerical aperture characteristics for versatile imaging capabilities. Overall, the detailed setup ensures controlled temperature conditions, regulated flow dynamics, and accurate imaging procedures for robust experimentation within the microfluidic device.

In the case of fluorescence microscopy, a two-step approach was undertaken. Firstly, the valve photo mask was strategically positioned at the conjugated plane within the epi-fluorescence light path of the optical microscope, where it was subjected to UV irradiation.

Secondly, the choice between two distinct filter cubes, namely Rhodamine B and DAPI, depended upon the nature of the experiment. Further details about these filter cubes can be found in Table 2.2, providing an overview of their specifications.

2.1.6.1. Filter cubes specifications and applications:

The Rhodamine B Filter enabled the selection of the UV wavelength (λ = 545 ± 25nm) to align the valve photo mask within the microfluidic channel setup without causing any premature curing. The emitter filter was purposefully designed to transmit specific wavelengths of light while blocking others selectively (refer to Table 2.2). By eliminating the emitter filter, a broader spectrum of wavelengths reached the detector or observation system. This removal resulted in an expanded range of detectable light, significantly enhancing the visualisation of the valve photo mask during the alignment process.

Table 2.2: Fluorescence filter cube specifications

Position	**Filter cube**	**Fluorophore**	**Excitation**	**Emission**	**Dichroic**	**Light Intensity**
1	Rhodamine B	Red	545nm± 25nm	605 nm± 70 nm	565 nm	Max
2	DAPI	Blue	350 nm±50nm	460 nm± 50nm	400 nm	Low

Then, introducing the DAPI filter enabled the precise selection of the UV wavelength (λ = 350 ± 50nm) through the photomask. This strategic use facilitated the polymerisation of PEGDA,

eventually creating the PEGDA hydrogel flexible valve exactly, copying the valve photo mask shape within the microfluidic channel.

For recording the video of the microfluidic device during the experiments and specifically to capture the platelets accumulation, the Rhodamine B Filter was used, enabling the selection of the UV wavelength (λ = 545 ± 25nm) to illuminate the fluorescently labelled platelets (labelled with Calcein Red-Orange, AM), the emitter filter needed to be fitted back to Rhodamine B, this enabled the precise selection of the UV. This was essential to detect platelet accumulation during these fluorescence imaging sessions. Also, in this step, the valve photo mask had to be removed from the epi-fluorescence light path of the optical microscope.

The PCO-Edge camera was employed to capture fluorescence images and record videos of the flexible valve in action during the experiments. It was also used to capture images using microfluidic devices in bright-field microscopy. For specific camera settings, refer to Table 2.3.

Table 2.3. Camera PCO-edge settings were applied to record the experiments.

Resolution	2560 x 2160 pixels
Sensor diagonal	21.8 mm
Pixel size	6.5 x 6.5 µm
Dynamic range	16 Bit
Shutter type	Rolling Shutter
Exposure time (Fluorescence microscopy)	50 ms
Exposure time (Bright-field microscopy)	5 ms

2.1.6.2. Image Quantification and statistical analysis.

Platelet accumulations were analysed in Fiji ImageJ software (Schindelin *et al.*, 2012) by measuring the area of interest in images on a top plane, which involved measuring area µm² within a two-dimensional plane,a threshold was used to determine the fluorescent area of the platelet accumulation, where a specific intensity value was chosen to distinguish between the areas of interest (platelet accumulations) and the background.

Leaflet Region Division: For further analysis, each leaflet was divided into two main regions: the TL and TS areas.

- TL Area (Tip and Lumen side): This region represented the part of the leaflet surface located towards the tip and facing the chamber's lumen (inner cavity).
- TS Area (Tip and Sinus side): This region represented the part of the leaflet surface that faces the valve sinus.

All statistical analyses were performed using Prism (GraphPad Software Inc).

2.2. *In silico*

2.2.1. The theory of Discrete Multiphysics:

Discrete Multiphysics (DMP) is a computational approach on computational particles rather than computational mesh (Alexiadis, 2015). It links together different discrete models such as Smoothed Particle Hydrodynamics (SPH) (Alexiadis *et al*., 2017), Lattice Spring Model (LSM) (Ariane *et al.*, 2018a; Ariane *et al.*, 2018b), Discrete Element Method (DEM) (Ariane, Sommerfeld and Alexiadis, 2018), and Peridynamics (Sanfilippo *et al*., 2021), which can be used for a range of applications ranging from biological to energy application (e.g. Alexiadis *et al*., 2021; Ruiz-Riancho *et al*., 2021; Ng *et al*., 2020; Rahmat *et al*., 2020). In particular, DMP

was previously used to simulate the flow in cardiovascular (Mohammed, Ariane and Alexiadis, 2020) and venous valves (Ariane *et al*., 2017b) including the presence of emboli in the blood flow circulation (Ariane *et al.*, 2018b)

In the computational work, the hydrodynamic venous valve model of Ariane *et al.*, (2017b) and Ariane *et al.*, (2018b) was combined with the model of particle agglomeration in shear flow of Rahmat *et al*. (2020). The DMP model combines SPH for the fluid, LSM for the valve and a pseudo-Lennard-Jones potential for particle agglomeration. This section introduces the theory behind these computational methods and explains how they are combined together.

The primary modification to the original code involves converting 10% of the SPH particles into sticky particles. This was achieved by enabling the sticky particles to interact with each other based on the value of their potential energy, mainly focusing on the attractive component of the force. As a result, these particles tended to agglomerate at positions where the force reached zero, aligning with the spot of the potential energy minimum. The modified code named (Dataset Research code supporting the publication Modelling Particle Agglomeration on through Elastic Valves under Flow) was submitted to the UBIRA eData dataset repository. The code is available from the following link.

DOI: https://doi.org/10.25500/edata.bham.00001072.

2.2.1.1. Smoothed Particle Hydrodynamics (SPH)

Smoothed Particle Hydrodynamics is a computational meshless Lagrangian method independently developed by Lucy (1977) and Gingold and Monaghan (1977), which is used here to simulate the fluid dynamics. Each particle in the SPH domain represents a set of properties such as positions **r**, mass m, density ρ, pressure p, velocity **v** and viscosity μ, which are updated at each timestep. For a desired group of computational particles, the SPH

equation of motion is achieved from the discrete approximations of the Navier-Stokes's equation (R.Liu and B.Liu., 2003; Ganzenmüller and Steinhauser., 2011)

$$\mathbf{f_i} = m_i \frac{d\mathbf{v}_i}{dt} = -\sum_j m_i m_j \left(\frac{p_i}{\rho_i^2} + \frac{p_j}{\rho_j^2} + \Pi_{ij} \right) \nabla_i W_{ij}, \tag{2.1}$$

where m_i , m_j are the masses of the particle i, j respectively, $\mathbf{v}_i$ velocity of the particle i, p is the pressure, ρ_i is the density of particle *i*, $\mathbf{f}$ is the sum of all external forces applied to the system. W is the smoothing kernel function and, *W* is a bell-shaped function that describes how the interaction between particle i_{th} and j_{th} decays with their distance $|\mathbf{r}_i - \mathbf{r}_j|$. Π_{ij} is the so-called artificial viscosity (Morris *et al*., 1997)

$$\Pi_{ij=} \frac{(\mu_i + \mu_j) v_{ij}}{\rho_i \, \rho_j \, r_{ij}} \tag{2.2}$$

where μ is the dynamic viscosity and $v_{ij} = v_i - v_j$. In this work, the so-called Lucy kernel (Ganzenmüller and Steinhauser., 2011) was used

$$W(r < h) = \frac{1}{s}\left[1 + 3\frac{r}{h}\right]\left[1 - \frac{r}{h}\right]^3 \tag{2.3}$$

where h the so-called smoothing length and s is a parameter used to normalize the kernel function.

An Equation of state (EOS) is required to link the pressure *p* with the density *ρ*. In this study, the Tait's equation is used.

$$p = \frac{c_0^2 \rho_0}{7}\left[\left(\frac{\rho}{\rho_0}\right)^7 - 1\right] \tag{2.4}$$

where ρ_0 is a reference density and c_0 is a reference for fluid velocity. This formulation refers to the so-called weakly-compressible SPH. To keep the variation of the fluid density in the domain less than 1 per cent, c_0 is normally set as ten times the maximum velocity in the flow (Monaghan, 1994). This produces repulsive forces between particles aimed at approximately conserving their distance during the simulation (Lee *et al*., 2008).

2.2.1.2. Lattice Spring Model (LSM)

The elastic leaflets and moving walls of the membrane are simulated with the so-called Lattice Spring Model (LSM) or Mass Spring Models (MSM) (Kot, Nagahashi and Szymczak, 2015). The elastic body is subdivided in computational particles which are linked together by Hookean springs. The force between two particles *i* and *j* connected with a Hookean spring is given by;

$$F_{i,j} = k(|\mathbf{r}_0 - \mathbf{r}|)^2 \tag{2.5}$$

where k is the Hookean elasticity coefficient, $\mathbf{r}_0$ is the equilibrium distance between the particles and $\mathbf{r}$ their instantaneous distance. The spring coefficients is determined by the physical properties (e.g., Young modulus) of the modelled materials as discussed in Kot, Nagahashi and Szymczak (2015) and Pazdniakou and Adler (2012).

2.2.1.3. Coupling SPH and LSM (Fluid-structure interaction)

In the model, SPH is used to simulate the fluid and LSM used for the elastic structure (valve leaflets). SPH provides the forces acting between two fluid computational particles where LSM provides the forces between two solid particles. To model the fluid structure interaction, set the forces between liquid and solid computational particles was needed. These forces

must ensure no-penetration, no-slip, and continuity of stresses between the solid-liquid interface. In continuum mechanics, these conditions are often represented as

$$\left(\frac{\partial}{\partial_t}\mathbf{u} - \mathbf{v}\right) \cdot \mathbf{n} = 0\ (\text{no} - \text{penration}), \tag{2.6}$$

$$\left(\frac{\partial}{\partial_t}\mathbf{u} - \mathbf{v}\right) \times \mathbf{n} = 0\ (\text{no} - \text{slip}) \tag{2.7}$$

$$\sigma_s \mathbf{n} = \sigma_f(-|\mathbf{r}|)\ (\text{continuity of stresses}) \tag{2.8}$$

where $\mathbf{n}$ is the normal to the boundary, $\mathbf{u}$ the displacement of the solid, $\mathbf{v}$ the velocity of the liquid, σ_s the stresses in the solid and σ_f in the fluid (Alexiadis, 2015).

In DMP, these conditions need to be 'translated' in terms of forces $\mathbf{F}_{i,j}$ in order to be introduced in the model. Here it has been used the same approach employed in other DMP studies such as Schütt *et al*. (2020); Ariane *et al.* (2017a) and Alexiadis. (2015). The no-penetration conditions are implemented by means of a repulsive Lennard-Jones potential between SPH and LSM particles.

$$V(r) = K\left[\left(\frac{r^*}{r}\right)^{12} - \left(\frac{r^*}{r}\right)^{6}\right] \text{ for } r < r_{cut} \tag{2.9}$$

where $r = |\mathbf{r}|$, r^* is a reference distance between particles and K is chosen to guarantee no penetration between SPH and LSM particles.

From the potential $V(r)$, the force between two particles is calculated from the potential:

$$F(r) = -\frac{\partial V}{\partial r} \tag{2.10}$$

Figure 2.6. (A) shows the potential $V(r)$ and the force $F(r)$ applied between the SPH and LSM, with only values for $r < 2^{1/6}r^*$ being studied so that only the repulsive potential is considered.

No-slip conditions are enforced by imposing SPH-like viscous forces at the solid-liquid interface. Once both the no-penetration and no-slip boundary condition are enforced, the continuity of stress is automatically satisfied by the fact that particle methods satisfy the Newton equation of motion. The numerical scheme used to solve the resulting equations is reported in Ganzenmüller and Steinhauser (2011).

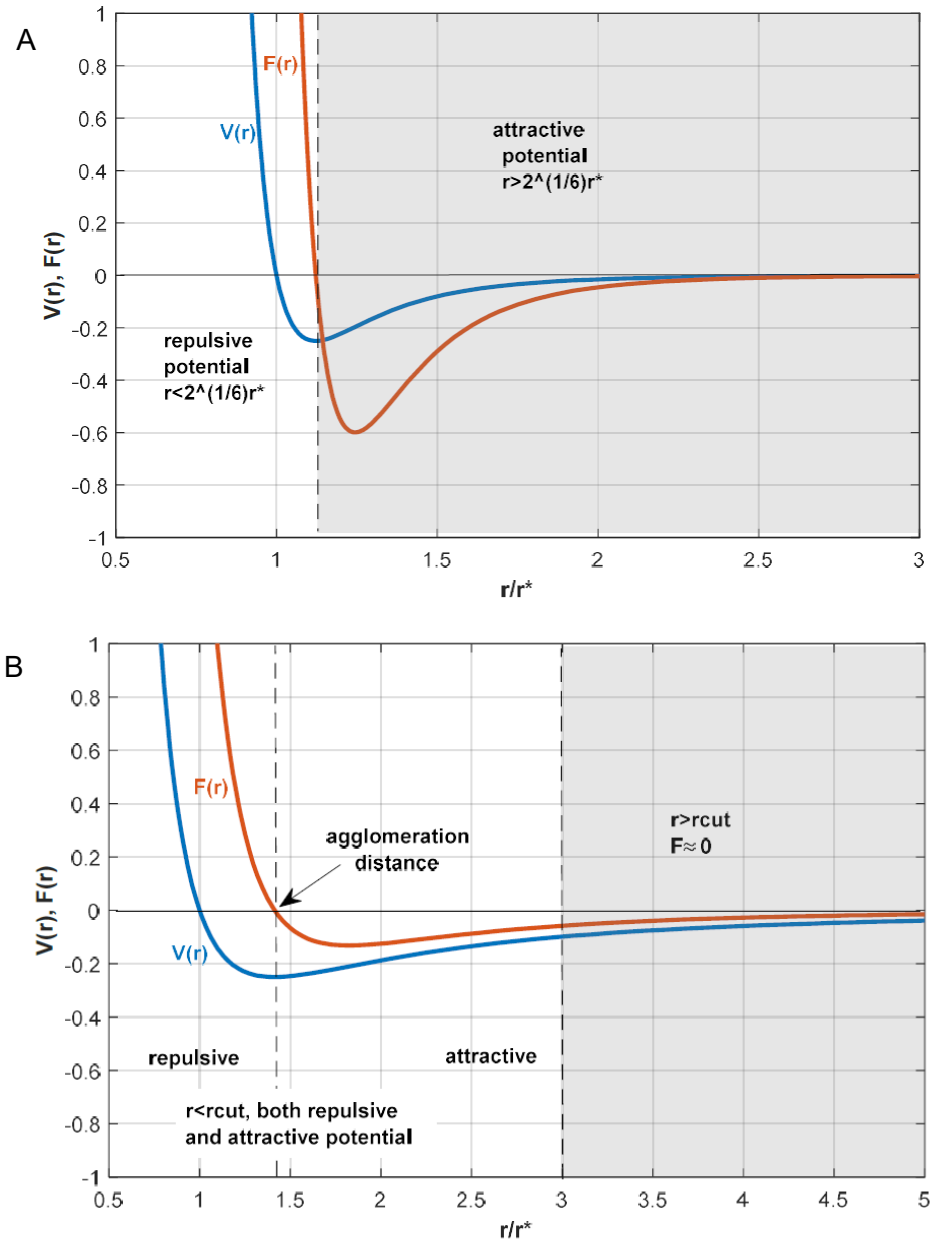

Figure 2.6. Diagram illustrating **(A)** 12-6 potential used for the no-penetration conditions and **(B)** the 4-2 potential used for particle agglomeration. In both cases, the cut-off is selected so that only the white area of the diagram is used in the potential. This implies that **(A)** is only repulsive because only the positive part is considered, while in **(B)** the negative part of the force which is attractive; particles tend to agglomerate at the location where the force is zero, which is where is the minimum of the potential is located.

2.2.1.4. Solid-solid interaction (agglomeration):

Besides fluid-structure interaction, the model also accounts for solid particles moving within the flow. These particles are 'sticky' and prone to agglomeration. To model this phenomenon, a similar approach to Rhamat *et al*. (2020) that used a soft, pseudo-Lennard Jones, potentials of the type was used

$$U(r) = 4\varepsilon\left[\left(\frac{r^*}{r}\right)^4 - \left(\frac{r^*}{r}\right)^2\right] \text{ for } r < r_{cut} \tag{2.11}$$

where ε provides the strength of the agglomeration, to model the interaction between sticky particles. In this case, both repulsive and attractive parts was considered (Figure. 2.6(B)), this produces a minimum in the potential that represents the equilibrium distance between two agglomerating particles. The value of the cut-off is selected at $3r^*$. For $r > 3r^*$, The assumption is made that $F(r) \approx 0$, which simplifies the calculations. Equation (2.11) is a numerically convenient way to implement agglomeration avoiding the sharp minima of the DLVO theory (Boström *et al*., 2006), but it does not represent a very accurate model of agglomeration. As in Rhamat *et al*. (2020) this does not constitute a problem here since the interest is not on a specific type of interaction (the actual potential among particles/platelets in Schofield *et al.* (2020) is unknown in anyway), but rather to enable particle-particle agglomeration in our virtual environment. For the same reason, ε is left as a free parameter and simulation with different values of ε are compared. For a theoretically more accurate approach based on the concept of surface energy, the reader can refer to Ariane, Sommerfeld and Alexiadis *et al*. (2018).

2.2.2. The valve model and geometry

The DMP methodology discussed previously is applied to a system of flexible valves (Figure. 2.7. a), which represents a series of venous valves distributed along a venous vessel located

in the leg. The geometry is two-dimensional and adapted from previous work by Wijeratne and Hoo (2008) and Ariane *et al*. (2018b).

Two consecutive valves are connected by a channel with flexible walls. The model is periodic, meaning that the flow exiting the system from the right boundary re-enters it from the left boundary and vice versa. Therefore, the system is composed of two valves and two flexible sections. These sections are contracted periodically to simulate pulsatile blood flow. During typical daily activities, when the muscles in the leg contract, they squeeze the blood flow which promotes blood circulation (Lurie *et al*., 2003; Wu *et al*., 2020). The pressure generated by the contraction opens the valve on the right (Figure. 2.7. b) and closes the valve on the left. This mechanism allows flow to circulate in one direction and prevents backflow. The opening and closing rate of the venous valve is around twenty rounds for each minute (Aird, 2007). To save computational time, in the model, the rhythm is slightly accelerated by considering five cycles in 15 seconds.

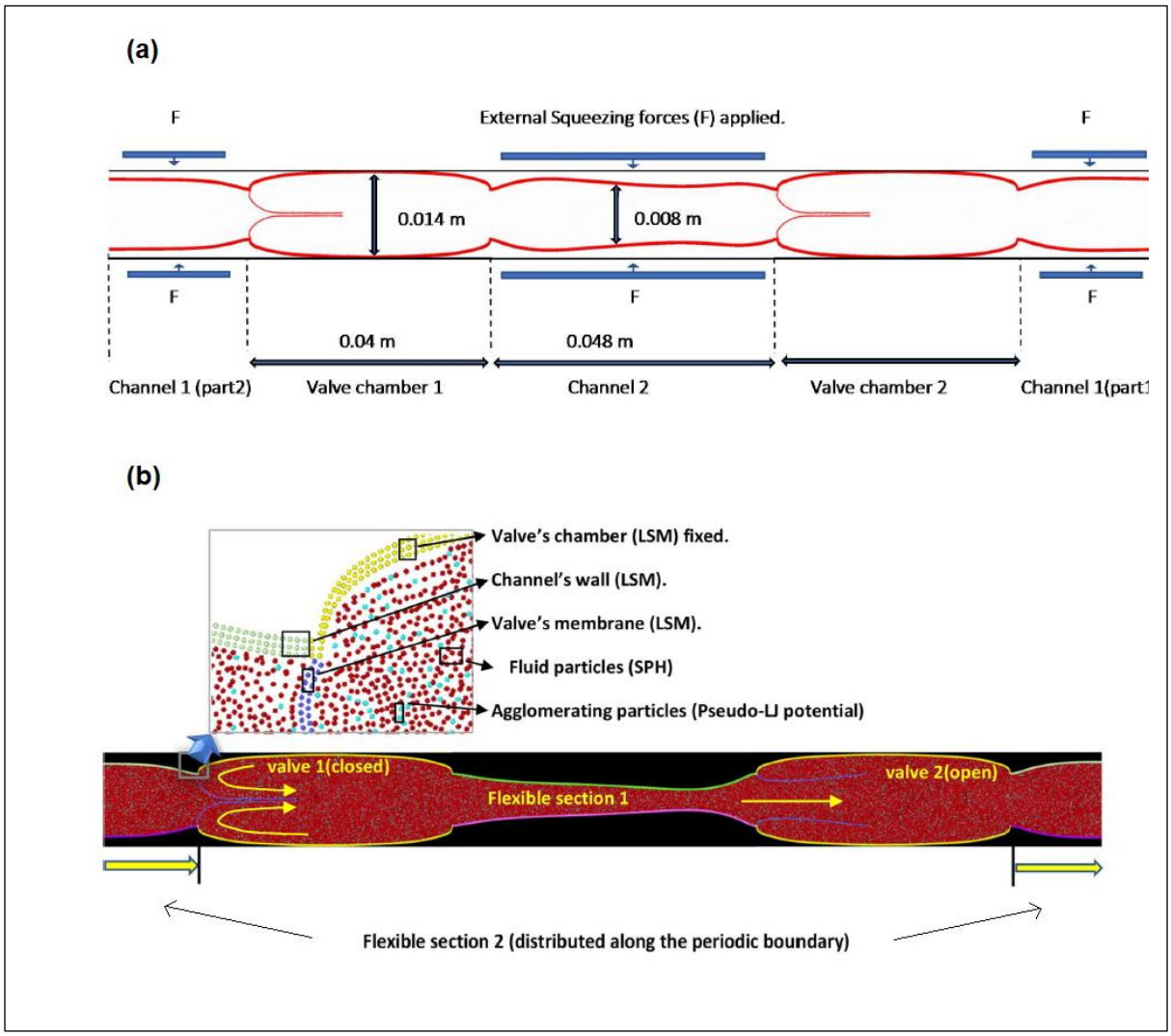

Figure 2.7. 2D geometry and structure of dual venous valve: **(a)** geometry showing the location of the contraction forces and **(b)** geometry showing the computational particles and their location in the model.

As Figure. 2.7. b, shows there are different types of computational particles in the model: SPH particles modelling the blood flow; LSM particles modelling the leaflets and the flexible sections between two valves. The walls that encase the valves are also made of solid particles, but they are fixed and do not change their position during the simulation. Additionally, a certain number of 'sticky' particles are randomly dispersed in the flow at the beginning of the simulation.

In the model the fluid is considered Newtonian and the flow laminar. Table 2.4. shows all the numerical parameters used in the simulation. The simulations were carried out with the open-source code LAMMPS (Plimpton, 1995) and the open-source code of OVITO (Stukowski, 2010) was used for the visualization and analysis of the data.

Table 2.4. Model's numerical parameters.

Parameter		Values and units
SPH		
Number of all particles that created our model domain.		168676
Number of wall stationary particles (SPH particles), three layers.		4972
Number of wall flexible particles (LSM particles), three layers.		5750
Number of the valve's particles (LSM particles), two layers.	Valve particles	1404
	Each leaflet	351
Number of SPH fluid particles		141030
Number of SPH agglomerating particles		15520
Mass of each particle (Fluid)		1.056×10^{-5} kg
Mass of each particle (Solid)		2×10^{-5} kg
Initial distance between particles Δr		10^{-4} m
Density ρ_0		1056 kg m^{-3}
Smoothing length h		2.5×10^{-4} m
Dynamic viscosity μ_0		0.0035 Pa s

Virtual sound speed c_0		10 m s^{-1}
Contraction Forces $\mathbf{F}$		0.008 N
Max velocity in the valve		0.04 m s^{-1}
Time step Δt		10^{-6} s
LSM		
Hookian coefficient $\mathrm{k_b}$	Flexible wall	1×10^5 J m^{-2}
	Valve's membrane	5×10^6 J m^{-2}
Viscous damping coefficient $\mathrm{k_v}$	Flexible wall	1 kg s^{-1}
	Valve's membrane	0.1 kg s^{-1}
Equilibrium distance r_0		10^{-4} m
Boundaries		
Repulsive radius $r*$		1×10^{-4} m
Constant k		1×10^{-4} J
Attractive forces potential		
Mass of solid particles		1.056×10^{-5} kg
Solid diameter		10^{-4} m
Particle density		1056 kg m^{-3}
Pair potential ε		2×10^{-5} J – 1×10^{-16} J

CHAPTER 3

A MICROFLUIDIC APPROACH TO INVESTIGATE DEEP VEIN THROMBOSIS

‘‘Experiments conducted by Zoe Schofield (Schofield *et al*., 2020) focused on polystyrene particles, aiming to investigate potential mechanisms of thrombus formation influenced by physical parameters such as flow conditions and valve elasticity. However, the model used in this specific stage lacked biological elements. To address this limitation, the current chapter conducted comprehensive whole-blood experiments to complement the previous findings involving nanoparticles.’’

Declaration: In the publication titled " **The Role of valve stiffness in the Insurgence of deep vein thrombosis**", I participated as a co-author. The intention was to incorporate specific content from this published work into my thesis, primarily focusing on the section related to the blood experiments that was conducted in this chapter which was a critical biological addition to the paper. This incorporation enhanced the scientific story of my thesis and supports the practical foundation of my research.

The role of valve stiffness in the insurgence of deep vein thrombosis.

Schofield, Z., **Baksamawi, H.A**., Campos, J., Alexiadis, A., Nash, G.B., Brill, A. and Vigolo, D., 2020. **Communications materials**, 1(1), p.65.

Published: 16 September 2020

DOI: https://doi.org/10.1038/s43246-020-00066-2

3.1. Introduction:

The current chapter builds upon the approach of Zoe Schofield and Daniele Vigolo, who developed a novel *in vitro* model of a vein to accurately explain the relation between cell accumulation and the role of flow geometry. This innovative approach involves the creation of a microchannel with dimensions of 300 µm width by 100 µm hight and several centimetres in length, constructed using standard soft-lithography techniques and composed of PDMS. Furthermore, this model incorporates flexible valves made of PEGDA through *in situ* photo-polymerization (see Materials and Methods). To regulate pulsed blood flow, a pressure controller was employed. These modifications allowed us to accurately replicate the blood flow, including both forward and backward flow, in the presence of valves.

Primary data revealed that symmetrical valves, with their identical mechanisms, play a pivotal role in shaping flow patterns within the microfluidic channels. In the presence of these symmetrical valves, laminar blood flow created two identical and symmetrical vortices on the valve leaflets, with a single vortex forming after each leaflet. Consequently, the hydrodynamic behaviour emerged as a central factor triggering the accumulation of blood around the valve leaflets.

Experiments involving flexible valves underscored the substantial impact of variations in the rigidity of valve leaflets on flow patterns, which were conducted by Zoe Scofield (Schofield *et al*. 2020), highlighting three key observations:

- Initial accumulation primarily occurs at the ends of valve leaflets.
- When both leaflets within a valve share identical rigidity, an increase in leaflet rigidity leads to more significant particle accumulation.

- In situations where there is a difference in leaflet rigidity within a valve, particles tend to accumulate more prominently in the leaflet pockets in the sinus area due to the created asymmetrical flow patterns.

In this chapter, the principal objective is to introduce the use of an advanced microfluidic device for exploring the potential mechanisms that initiate thrombosis. Our specific focus is finding out how the initiation of blood clot formation is manipulated by the flow hydrodynamics and the elasticity of valves within the circulatory system.

In this section of experiments conducted with flexible valves and whole blood, a parallel behaviour to our prior particle experiment was noted. Our observations underline two pivotal aspects:

- The initial accumulation of platelets primarily takes place at the tips of valve leaflets.
- When there is a variation in the rigidity of leaflets within a valve, platelets tend to accumulate more prominently within the leaflet pockets in the sinus area because of the created asymmetrical flow patterns.

A critical aspect of this microfluidic model equips with pulsatile flow, mimicking the impact of the muscle pump, which enhances blood circulation within the veins. Consequently, our study illustrates that alterations in valve stiffness have the potential to impact thrombus formation. It's important to note that in this model, the stiffness of the vessel wall itself is not considered.

3.2. Result and discussion:

3.2.1. Analysing the blood aggregation on or behind the fabricated flexible valves:

Analysing aggregate formation behaviour in microfluidic devices, the impact on blood flow, and its interaction with wall surfaces highlights the primary processes leading to clot

formation (Diamond. 2016). The study utilised two types of valves: a symmetrical valve with identical leaflets and an asymmetrical valve with one leaflet being stiffer than the other.

3.2.1.1. Symmetrical valve

In this experiment, whole blood that included fluorescently labelled platelets, refer to Chapter 2 (2.1.4. Blood preparation), was perfused through a valve featuring identical leaflets (to match the flow rate used for the aqueous suspension of PS particles, whole blood was subjected to pressure pulsing ranging from 0 to 250 mbar) created with 50% PEGDA and 4% PI. Fluorescence microscopy served as the method to detect platelet accumulation at the tips of the valve leaflet, refer to Chapter 2(2.1.6. Imaging). The findings revealed a swift build-up at the leaflet tips during the initial 60 seconds, resulting in a substantial clot formation. However, with the passage of time, the aggregation of platelets started to exhibit instability, with certain components detaching and causing a rapid reduction in the size of the blood clot (refer to Figure 3.1). Subsequently, valves with reduced stiffness (30% PEGDA and 4% PI) experienced testing under the same flow conditions, but no accumulation was observed either on the valve or within the microfluidic channel itself.

This indeed validates the pivotal role of valve flexibility in altering flow patterns and preventing the buildup of particles and platelets. Furthermore, flexible valves exhibit an instant response to changes in flow direction, with the potential to detach temporarily accumulated platelets at their tips. These findings strongly suggest that the mechanism behind platelet accumulation is predominantly determined by the flow conditions that occur due to increased valve stiffness. The primary objective of this chapter is to primarily recapitulate the interaction between pulsatile flow, characteristic of veins, and flexible valve leaflets, with less emphasis placed on replicating precise flow shear stress.

To ensure hydrodynamic similarity, such as maintaining the same Reynolds number (Re) across various veins, the flow velocity within our microfluidic device was proportionally adjusted. Hydrodynamic similarity implies that even though the absolute shear stress values vary between our device and real veins, their functional roles remain proportionally equivalent within the fluid mechanics of both systems. When assessing the influence of shear stress on platelet accumulation, it is the absolute value that carries significance. In the range of shear rates used in our study (<2500 s^{-1}), platelet accumulation mainly occurs through the interaction of GPIIbIIIa with fibrinogen, a process reliant on integrin activation by soluble agonists, which was not included in our study design (Ruggeri *et al*., 2006; Jackson, Nesbitt, and Westein, 2009; Rana *et al*., 2019). Accumulation caused by GPIb- vWF interactions, which does not need GPIb stimulations, occurs at significantly higher shear rates, with a complete transition to this mechanism at shear rates surpassing 10,000s^{-1} (Diamond, 2016).

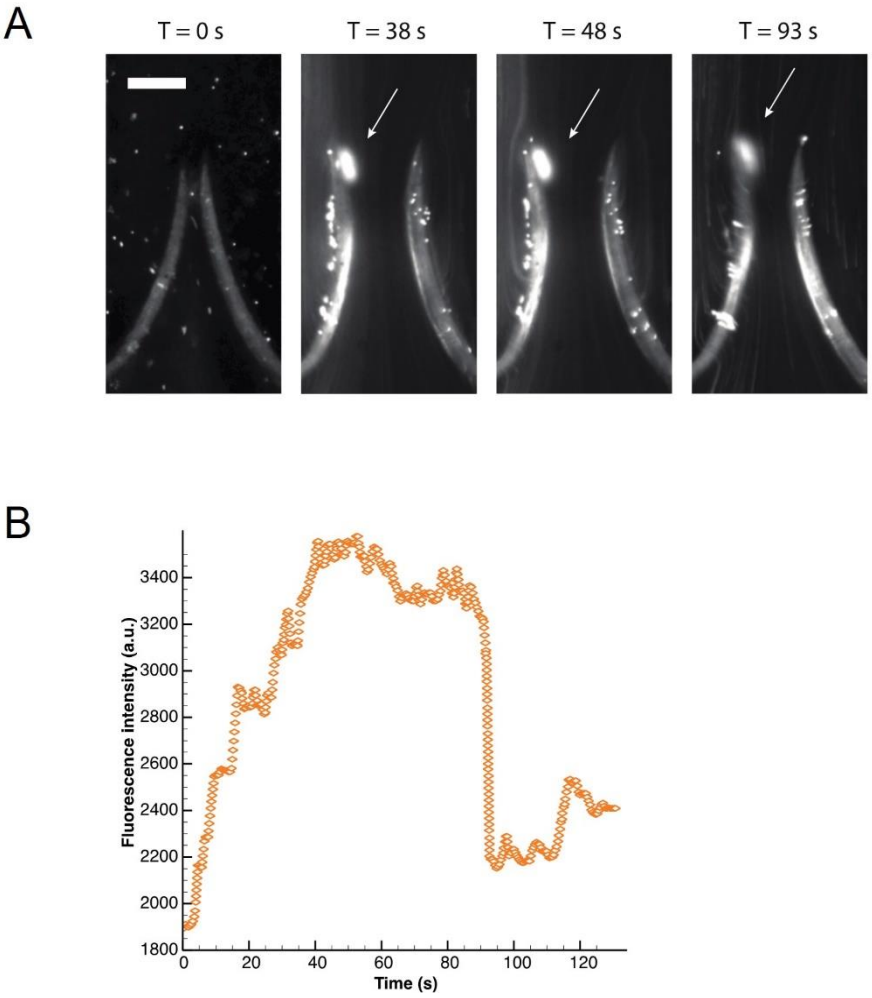

Figure 3.1. (A) Time-lapse images capture the gradual platelet accumulation on rigid, symmetrical valves. This platelet aggregate rapidly forms within 30–40 seconds under pulsed flow conditions, as indicated by the accumulation of fluorescently labelled platelets at the leaflet tips. Subsequently, it gradually grows until eventual detachment (in this instance, occurring after 93 seconds). An arrow highlights the platelet aggregate, and the scale bar represents 100 µm. **(B)** The progression of the platelet aggregate's growth over time is illustrated, with an initial rapid expansion followed by a plateau and, eventually, detachment (marked by a sudden decline in the fluorescence signal). At its maximum size, the surface area coverage extended to approximately 1200 µm² on the valve tip.

Under the same shear conditions, No formations of aggregates were observed in the case of the flexible valve.. Taken together, this indicates that the platelet accumulation detected in our study is likely not a result of shear forces; instead, hydrodynamics are the main driving factor for platelet clumping. At the same time, vWF - GPIbα interactions is involved in developing deep vein thrombosis (DVT) in the in vivo stenosis model (Brill *et al*., 2011). This may be explained by the localised release of extremely adhesive ultra-large vWF multimers from Weibel–Palade bodies, coupled with restricted availability of ADAMTS13, the enzyme responsible for cleaving vWF, caused by limited blood flow. Ultimately, the symmetry of the valve significantly influences the blood flow patterns within the channel.

3.2.1.2. Asymmetrical valve

The valve created with two different leaflets; one of the leaflets is rigid or less flexible than the other leaflets, and the valve termed to be asymmetrical valve. Studies have indicated that within a diseased vein, the leaflets of the same valve may exhibit variations in thickness and rigidity (Corcos *et al*., 2004). Additionally, the symmetry of flexible vein valves can be influenced by internal pressure and external forces, primarily affecting the lumen of the leaflets (Simão *et al*., 2016). The results regarding platelet accumulation are remarkably similar to the earlier findings conducted by Zoe Schofield with particles. These parallel observations highlight that in asymmetric scenarios, notable distinctions exist in flow patterns, ultimately leading to variations in platelet accumulation.

The primary data revealed that in the case of the asymmetrical valve, one of the leaflets exhibited greater stiffness than the other. This difference led to the formation of a distinct flow pattern downstream of the valve leaflets, consequently influencing the location of platelet aggregation, primarily occurring in the valve pocket behind one of the leaflets. This

study utilised whole blood flow, incorporating platelets labelled with fluorescence. Also, employing a fluorescence microscope to observe the platelet accumulation was necessary, refer to Chapter 2 (2.1.6. Imaging). The aggregation process started gradually behind one of the leaflets; it became visibly apparent after approximately twenty minutes and continued to grow over the subsequent twenty minutes, as illustrated in Figure 3.2. This observation highlights the critical importance of valve symmetry, as the differing stiffness of valve leaflets significantly influenced flow patterns, ultimately encouraging the formation of aggregates within the sinus zone. These results are in line with previous research indicating that the risk of deep vein thrombosis (DVT) tends to increase with age, paralleling the stiffening of valves. This suggests that circumstances where valve symmetry is not preserved may potentially heighten the risk of DVT.

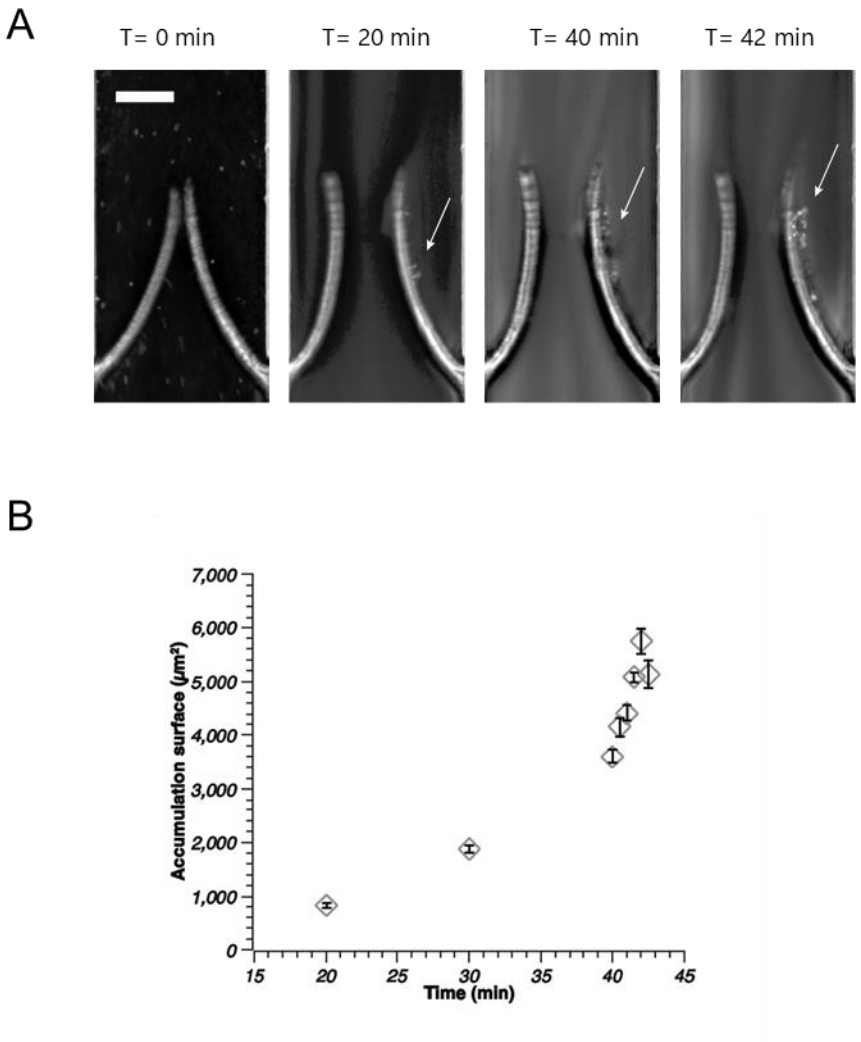

Figure 3.2. (A) Shows time-lapse images illustrating the gradual formation of blood aggregates over time on valves with asymmetrical leaflets. The accumulation process initiates slowly behind one of the leaflets. The arrow points to the primary site of agglomeration, and the scale bar corresponds to 100 µm. **(B)** The accumulation becomes noticeable after twenty minutes, and the size of the blood accumulation progressively grows, reaching its maximum extent after 40 minutes. The error bars on the graph indicates the standard error.

3.3. Summary and conclusion

Highlighting the innovative *in vitro* methodology pioneered initially by Zoe Scofield and Daniele Vigolo (Schofield *et al*., 2020), which implements in *situ* fabrication to create elastic valves with adjustable flexibility within a controlled microfluidic system. This advanced approach facilitates the generation of prothrombotic conditions. Eventually, it involves crucial valve parameters, including flexibility and controlled flow rates, vital factors responsible for platelet accumulation. Also, the experiments above were conducted with whole blood. The results confirmed the valve symmetry and stiffness asymmetry between valve leaflets, resulting in distinct patterns of platelet accumulation. Platelet accumulation on symmetrical valves predominantly occurred at the valve tips. In contrast, asymmetrical valves exhibited accumulation within the sinus area behind the valve leaflet. The asymmetry changed the flow patterns surrounding the valve and entrapped platelets within the recirculation site in the valve pocket. It is essential to note that this system does not encompass all of Virchow's triad components, such as vessel contractions and blood coagulation. Consequently, this setup enables a more straightforward explanation of the specific role of flow patterns in initiating blood clots. Nonetheless, future research activities should consider studies combining this in vitro model with the other triad components as the next step in this line of investigation.

The findings align with existing research indicating that the likelihood of developing DVT escalates as individuals grow older, according to the stiffening of valves. Moreover, the results suggest that situations where valve symmetry is not preserved may potentially elevate the risk of DVT.

The work in this chapter presents the blood experiments carried out through the microfluidic platform, which presented findings that were similar with those of particle experiments

previously completed by Zoe Schofield (Schofield *et al*., 2020). The outcome from this work suggested that the flow characteristics and valve properties triggered cell aggregation. The factors influencing flow geometry, some of which are unchangeable but testable in patients, such as valve elasticity or flow velocity and vortices, while others are adjustable, such as haematocrit or blood viscosity; this could form the basis for a more individualised prediction of the likelihood of developing a DVT.

The original version of the microfluidic model with a flexible valve established initially by Schofield *et al*. (2020), was used to conduct the blood experiments in this chapter, this offered valuable insights into the impact of physical factors on the development of blood clots, a phenomenon observed in animal models. While it is essential to acknowledge that biochemical aspects also influence thrombosis, the data presented here underlines how the physical parameters in the vein valve platform could serve as a pivotal factor that might be developed for DVT prediction. An illustrative example from the results highlights the connection between asymmetrical stiffness and the creation of a blood clot in the valve pocket behind the leaflet, a location typically observed in *in vivo* investigations of thrombosis. This parameter has not been explored previously and has a great potential to serve as an indicator of a higher risk of DVT.

CHAPTER 4

MODELLING PARTICLE AGGLOMERATION ON THROUGH ELASTIC VALVES UNDER FLOW

‘‘The results from Chapter 3 revealed that agglomeration of polystyrene particles and platelets predominantly occurs near the valve leaflets, suggesting a potential connection between altered flow and thrombus formation in venous valves. However, these findings raise a new question that could not be fully addressed through *in-vitro* experiments: Can hydrodynamics alone explain agglomeration? The current chapter addressed this question by employing an *in silico* model that simulates particles that only interact with each other, not with the leaflets. By investigating this virtual system, the aim was to determine whether, in the absence of particle-leaflet adhesion, hydrodynamics alone can account for at least a portion of the agglomeration observed in Chapter 3’’

Declaration: Some content presented in this chapter has been published.

Modelling particle agglomeration on through elastic valves under flow.

Baksamawi, H.A., Ariane, M., Brill, A., Vigolo, D. and Alexiadis, A., 2021.

ChemEngineering, 5(3), p.40. Published: 26 July 2021

DOI: https://doi.org/10.3390/chemengineering5030040

4.1 Introduction

Various 'non-return' valves are found in our leg veins (Raskob *et al*., 2021). These valves consist of two elastic leaflets that open and close in conjunction with the musculoskeletal system. When human are physically active, the muscles in the leg constantly contract and relax causing the vein valves to open, allowing blood to return to the heart, and close to avoid blood flowing back in the opposite direction (Wu *et al.*, 2020; Lurie *et al.*, 2003).

Deep Vein Thrombosis (DVT) occurs when a thrombus forms in the veins as an aggregation of blood components (Shen *et al*., 2021). One hypothesis suggests that these thrombi initially form in the venous valves (Bovill and van der Vliet., 2011), and subsequently detach from the veins and travel within the blood flow until they reach the pulmonary vascular system. Here, they cause blockage of the pulmonary artery branches, resulting in death or significant disabilities (Siegal *et al*., 2021; Das and Biradar, 2018; Payne and Brill, 2017; Cook and Crowther, 2010). Moreover, it is recognised that the lack of physical activity or long static position causes poor blood circulation, thus increasing the risk of DVT. This suggests that fluid dynamics in the valve play an important role in causing DVT (Schofield et al., 2020).

To understand the flow in venous valves, a computer simulation of various valve typologies was carried out both without (Ariane *et al.*, 2017b) and with the presence of thrombi (Ariane *et al.*, 2017a). However, the role of the flow in the initiation of the venous clot due to the aggregation of blood components is still not clear. For this reason, in a previous study conducted by Schofield *et al* (2020), an in-vitro model of DVT has been developed . The model comprises a microchannel fabricated out of PDMS by means of soft lithography. Within the microchannel, a flexible valve made of cured PEGDA was fabricated. An aqueous dispersion of polystyrene particles was perfused within the microfluidic device using pulsed flow to simulate rhythmic contractions of the leg muscles. In the in-vitro models polystyrene particles

tend to form aggregates due to Van der Waals and electrostatic interactions between themselves and the solid surfaces and this simulated the formation of aggregates. Also these results were compared with experiments of perfusing blood flow with fluorescently labelled platelets, where platelets tended to form aggregates when activated (Cattaneo, 2009; Bain, 2021).

The results show that the agglomeration of polystyrene particles and platelets occurs near the valve leaflets. These results support that a thrombus forms in the venous valves at least in part due to altered flow. However, they open a new question that could not be answered in the in-vitro experiments. Can hydrodynamic alone explain agglomeration?

In the valve, when the leaflets close, the flow streamlines converge and subsequently the probability of particles colliding enhances agglomeration. Also, both polystyrene particles and platelets accrue at the leaflets surface. Therefore, it is not clear how much of the observed agglomeration is caused by hydrodynamics and how much is simply due to the particle sticking to the leaflets surface.

Therefore, in this study Mostapha Ariane's original DVT model (Ariane *et al.*, 2017a; Ariane *et al.*, 2017b) was further developed to include particle agglomeration. Since, in the computer model, it can be arbitrarily tuned the properties of the particles, it can be accounted for 'fictional' particles that are sticky only with each other and not with the leaflets. By studying this virtual system, the research question of this paper can be answered: when removing particle-leaflets adhesion, can hydrodynamics alone explain at least part of the agglomeration observed by Schofield *et al* (2020)? If, in the virtual system set up in the computer simulations, agglomeration near the leaflets was observed, it can be concluded that hydrodynamics play a role; if not, this means that, in Schofield *et al* (2020) agglomeration is mostly due to the interaction between the particles and the leaflet surface. Thus, this study proposes a novel

model (to the best of our knowledge this is the first DVT model that accounts for agglomeration) and uses this model to answer a specific research question from a medical-related area.

This paper is organized as follows. Firstly, the general theory behind Discrete Multiphysics (DMP) is introduced, the modelling approach used to simulate the system. Then, showing how the theory is applied to the concrete case of flow in flexible valves. Lastly, the model was used to simulate particle agglomeration in the valve and show that larger clusters are formed near the leaflets.

4.2. Results and discussion

4.2.1. Hydrodynamics

The blood flow moves from left to right (Figure. 4.1) under the pressure generated by applying the force ***F*** to the flexible sections. As mentioned, ***F*** simulates the effect of muscles in the leg contracting around the vein. The higher pressure generated by ***F*** opens the valve on the left and simultaneously closes the valve on the right of the contracted section as it illustrated in Figure. 3(a) where periodic boundary conditions are applied to the system. Subsequently, the contracted section is released, and ***F*** is applied to the other section causing the open valve to

close and the closed valve to open. This prevents backflow and produces a unidirectional flow in Figure. 4.1(b) from left to right.

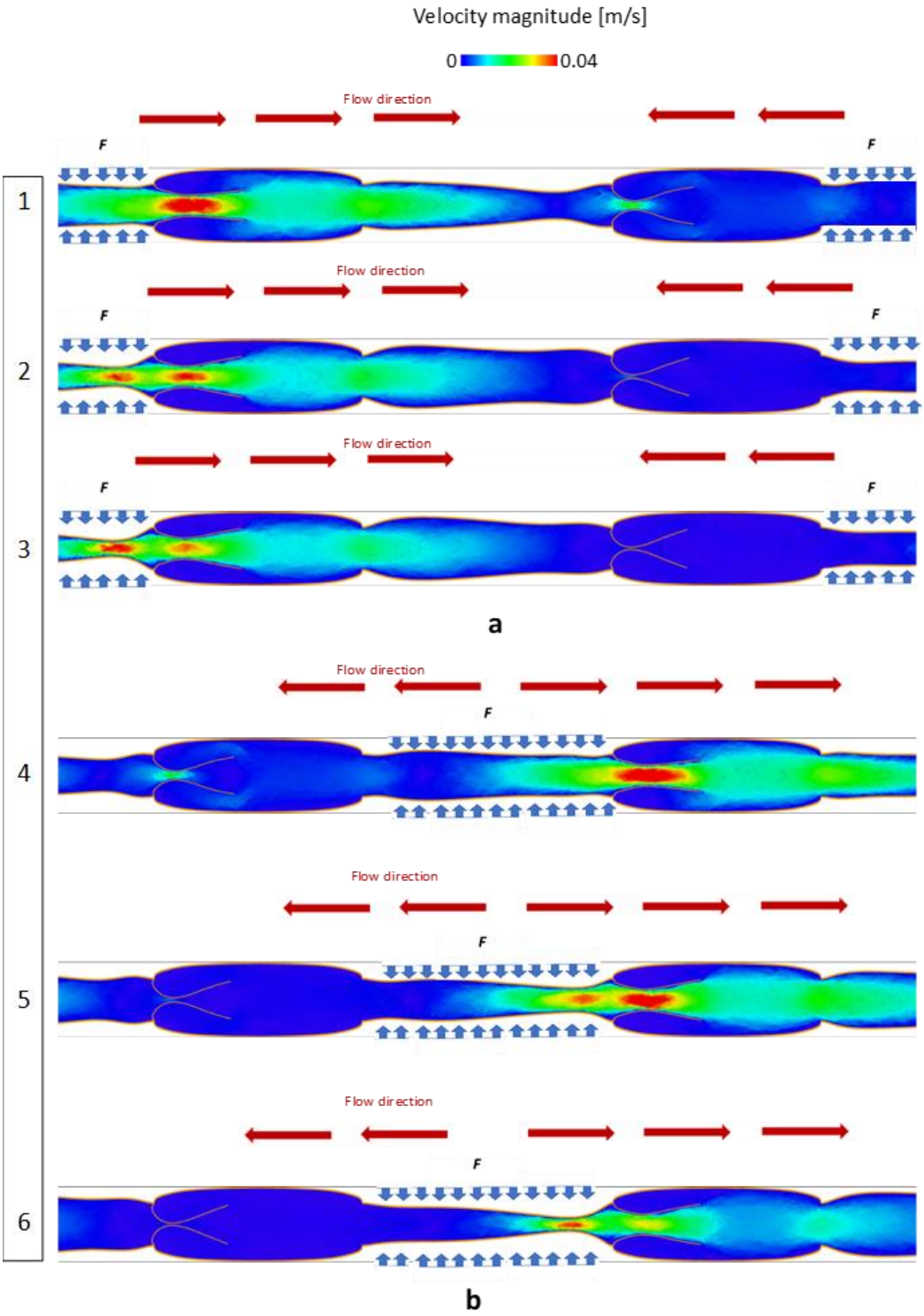

Figure 4.1. Velocity magnitude in the valve during opening and closing phases.

In our model, force ***F*** is calibrated to produce a maximal blood velocity of around 0.04 m s^{-1}, which is a reasonable value for blood flow in human veins as it can vary during average physical activity (Ariane *et al*., 2017b). The velocity magnitude during the closing and opening phases is reported in Figure 4.1. In all the simulations discussed in the next system, the system is simulated for 15 seconds representing 5 opening and closing cycles.

4.2.2. Particle agglomeration

At the beginning of the simulation, 'sticky' elemental particles are uniformly distributed in the liquid domain with concentration ~10% in the flow. When the simulation runs, these sticky particles start to aggregate in larger clusters depending on their 'stickiness', which is controlled by the value of ε in eq. (11). The goal of this study is not to replicate the physiochemical property of actual clots, but to separate the effect of hydrodynamics from the particle-wall interaction in the in-vitro experiments by Schofield *et al*. (2020) and verify that agglomeration occurs near the valve even when attractive forces between the leaflets and

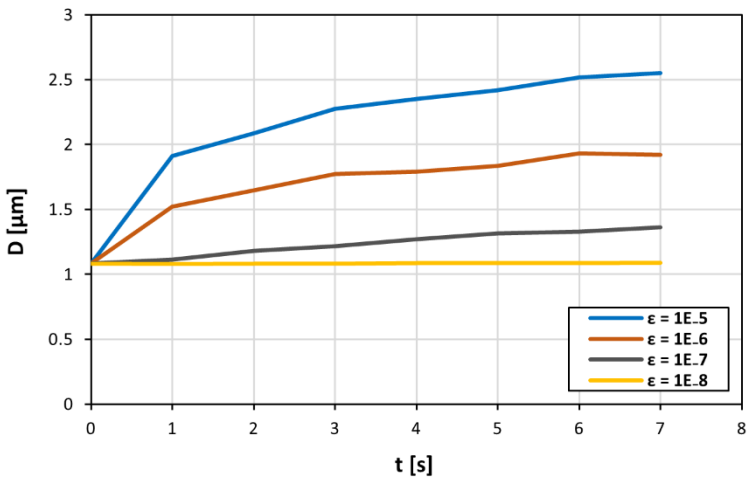

Figure 4.2. Dependence of the average size of particle agglomerates on the pair potential values between ε= 10^{-8} J and ε= 10^{-5} J as the simulation is running.

the particles are arbitrarily removed. The surface energy of the elemental particles is used in the *in vitro* experiment, and therefore, their 'stickiness', is not known. For this reason, in this study, the value of ε as a free parameter was used. Figure. 4.2 shows how the size of the average aggregate changes during the simulation.

Initially, all particles are separated, and the average size is equal to one, which represents the size of a solid single particle. As time progresses, particles randomly collide in the flow and form agglomerates. Therefore, the average size of the agglomerate increases. As particles lump into larger and larger agglomerates, the number of agglomerates in the flow decrease reducing their collision probability. Therefore, the average size tends to plateau as the simulation progresses (Figure. 4.2). An explanation for this is that there are greater attractive forces, as a result of the higher pair potential energy. However, there is a minimum pair potential energy where the attractive forces are not enough for particle agglomeration.

As expected, the higher the value of ε (and, therefore, the 'stickiness' of the particles), the higher the average size of the aggregate. Figure 4.3 shows that for small values of ε no agglomeration occurs in the flow. The particles are not sticky enough and the inertial forces generated in the flow prevent the formation of larger agglomerates. Above the value $\varepsilon = 10^{-8}$ J, agglomeration starts, and the size of the agglomerates increases linearly with $\log(\varepsilon)$ (Figure 4.3).

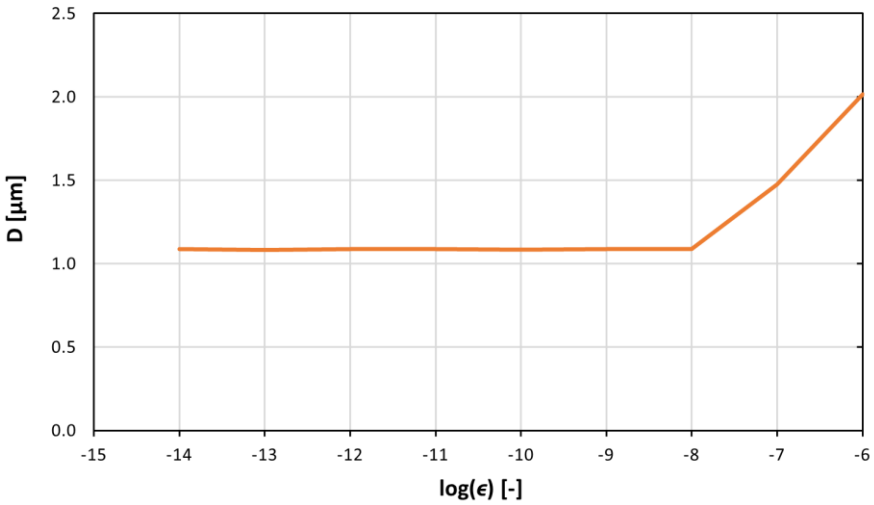

Figure 4.3. Average size of the agglomerates associated with different pair potential values between ε= 10^{-8} J and ε= 10^{-6} J at specific times (t=12.5s). Above the value of ε= 10^{-8} J, agglomeration starts, and the size of the agglomerates increases linearly with log(ε).

4.2.3. Larger agglomerates

In Figure. 4.3 the average size of the agglomerates is presented. The size distribution however is not uniform. Figure. 4.4 shows how the size is distributed in the valve during the simulation. Moreover, larger agglomerates form near the leaflets. During their motion, the leaflets temporarily reduce the section of the channel available to the flow. This increases the probability of collision between particles forming larger agglomerates. Some of the agglomerates move into the main flow, whereas others remain trapped in the valve district and accumulate in this area. This is very similar to what was observed in the experiments. Therefore, hydrodynamics plays an important role in the in-vitro model in a previous study by Schofield *et al* (2020) (Figure. 4.4)

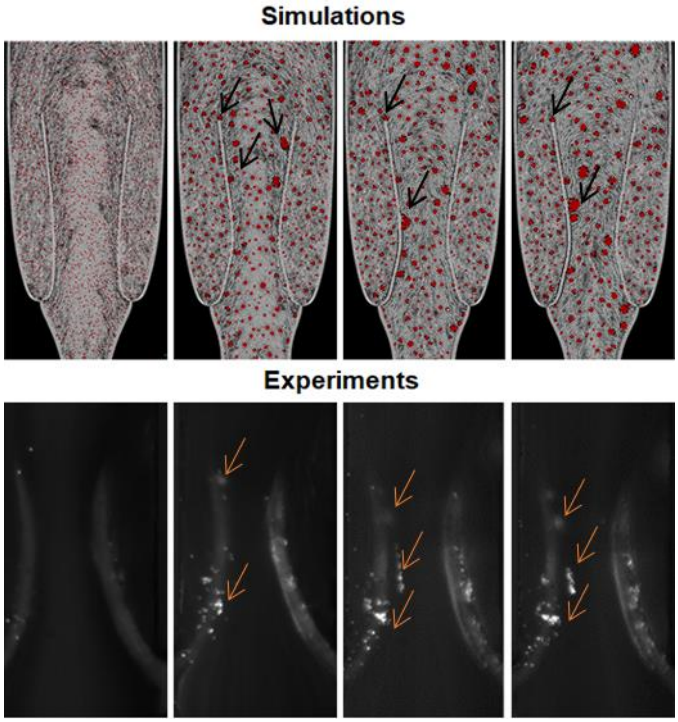

Figure 4.4. Simulation and experiment (platelets, fluorescently labelled, agglomeration in Schofield *et al*. 2020) snapshots illustrating the aggregates near the valve's leaflet at different time points. The arrows indicate the aggregates near the valve leaflets.

In theory the agglomerate can separate, since this is a particle-based simulation, particles interact by means of forces. Agglomerates form because, at a certain distance from each other, they experience attractive forces that make them stick together. Shear also exerts forces on the particles. Forces that, this time, tend to separate the particles. If shear is very high, these forces can overcome the agglomeration forces and break the aggregate. Theoretically, there is nothing that prevents this from happening in the modified code in this chapter, as the shear is way too small to break the agglomerates. Therefore, in practice, this is never going to happen.

4.3. Conclusion

In this chapter, a Discrete Multiphysics model was used and developed to combine the fluid-structure interaction model of Ariane *et al*. (2017a) and Ariane *et al*. (2017b) with the agglomeration model of Rhamat *et al*. (2020). It combines an element of novelty (first DVT model that accounts for agglomeration) with a specific research question concerning the potential role of hydrodynamics in the early stages of agglomeration in DVT.

Agglomeration around the valve leaflets was investigated, and how this is affected by the hydrodynamics. The results show that larger agglomerates are likely to form near valve leaflets even when the interaction potential between the valve leaflet and the particles is removed. This supports our previous hypothesis (Schofield *et al*., 2020) that the combination of blood hydrodynamics and the valve's mechanical characteristic is a key factor during agglomeration in venous valves.

Besides its specific results, this study is also a good example on how *in-vitro* and *in-silico* modelling can work together in research areas such as biology and medicine. In-vitro models aim at providing a physical replica of a biological system. However, it is sometimes difficult to understand all the interrelated mechanical features of this physical model. At this point, in-silico models can offer virtual replicas of the biological system where certain mechanical features can be switched on or off ad libitum. In this way, it can be somehow 'dissected' the physics of system and discern what are the most important features that regulate the system under investigation. In practice, the model can be used to assess which factors can enhance or decrease the tendency of agglomerate to form in the valve.

CHAPTER 5

CELLULAR ELASTIC VEIN VALVE (CEVV) MODEL

‘‘ Enhancing on the previous microfluidic model outlined in Chapter 3, the current chapter presents significant advancements in the development of *in-vitro* deep vein thrombosis (DVT) models. It specifically, introduces the Cellular Elastic Vein Valve (CEVV) chip, an advanced microfluidic platform designed to mimic the veins' characteristics closely. This innovative model incorporates a flexible valve integrated with endothelial cells and operates under a pulsatile flow of human blood. First and foremost, the channel structure was adapted based on clinical image of the human femoral vein, with great attention given to replicating the sinus area located behind the valve leaflets. Secondly, a key development was involved to ensure that all surfaces within the microfluidic channels were coated with human umbilical vein endothelial cells (HUVECs). This modification significantly enhanced the physiological relevance of the DVT model.’’

Declaration: Some content presented in this chapter have been published.

Platelet accumulation in an endothelium-coated elastic vein valve model of deep vein thrombosis is mediated by GPIb α—VWF interaction.

Baksamawi, H.A., Alexiadis, A., Vigolo, D. and Brill, A., 2023.

Frontiers in cardiovascular medicine, 10, p.1167884. Published: 27 April 2023

DOI: https://doi.org/10.3389/fcvm.2023.1167884

5.1 Introduction

The development of vessel on a chip is one of the innovative achievements of microfluidic models. The advantage is that the hydrodynamic microenvironment of human blood vessels is strongly mimicked (Zheng *et al*., 2012; Costa et al.,2017; Abudupataer *et al*.,2020), by downscaling the human vein from a macro-fluidic scale with a minimum size of 5 mm into a microfluidic scale (Pandian *et al*., 2018), with the range between tens and hundreds of micrometres (Streets and Huang., 2013). Moreover, the flexibility of the valve is essential to opening and closing the microfluidic channel, which is fundamental in studying the flow of the fluid (Guevara-Pantoja *et al*., 2018). The most challenging aspect of the microfluidic model for DVT research is to mimic the unique human hydrodynamic and the biological composition of the venous valve (Lehmann *et al*., 2018). Controlling the WSS and the pressure gradients at the level of human vessels is crucial to understanding the relationship between haemostasis at the level of a blood vessel and thrombosis, which is hard to achieve using animal models. In comparison, microfluidic devices are a capable platform for this type of research (Muthard and Diamond, 2013). Growing vital cells *in vitro* applications depends on the flow characteristics, mainly to mimic the parameters of human vessels, such as the shear stresses which affect the cells' survival and functions (Deroy *et al*., 2021).

The endothelium is the vital inner monolayer of blood and lymphatic vessels, consisting of endothelial cells. It is a crucial addition to the microfluidic models to simulate physiological conditions provided by endothelial cells (Grisanti *et al*., 2021). Endothelium functions in healthy vessels play a crucial role in preventing thrombosis by producing anti-thrombotic agents and facilitating binding to antithrombin molecules on their surfaces (Zhang, Oklu and Albadawi, 2017). The phenotype of endothelial cell is significantly different between the sinus

and the lumen sites of the valve (Brooks *et al*.,2009), where endothelium in the sinus site is more likely to be thromboresistant (Brooks *et al*., 2009; Rajeeva Pandian *et al*., 2020). Furthermore, ageing is one of the risk factors associated with DVT (Wendelboe and Raskob., 2016) which could change the phenotype of the endothelium layer and revise it from its thromboresistant nature (Brooks *et al*., 2009). Hence, the rotational flow or even the lack of flow is not enough to initiate thrombosis with the presence of functional endothelium in the sinus zone of the valve. The endothelial cells inhibit blood cell activation and adhesion by decreasing the expression rate of procoagulant factors (Rajeeva Pandian *et al*., 2020). However, *in vitro* studies suggest that hydrodynamics induce thrombosis in the valve sinus without the presence of ECs (Hu *et al*., 2020; Schofield *et al*.,2020). Nevertheless, venous valve microenvironment zones are the most common sites of thrombosis (Brooks *et al*., 2009; Lehmann *et al*., 2018). Thus, the ideal model for investigating thrombosis formation must include endothelial function and their interaction with the hydrodynamic forces such as blood pressure, flow type, shear rate, and shear stress (Jain *et al*., 2016).

So far, the anatomy of the human flexible vein valve and the vascular cellular monolayer has not been achieved in one model. The current study in this chapter aims to introduce a Cellular Elastic Vein Valve model (CEVV chip), an advanced microfluidic platform of veins containing a flexible valve incorporated with endothelial function under a pulsatile flow of human blood (Figure 5.1).

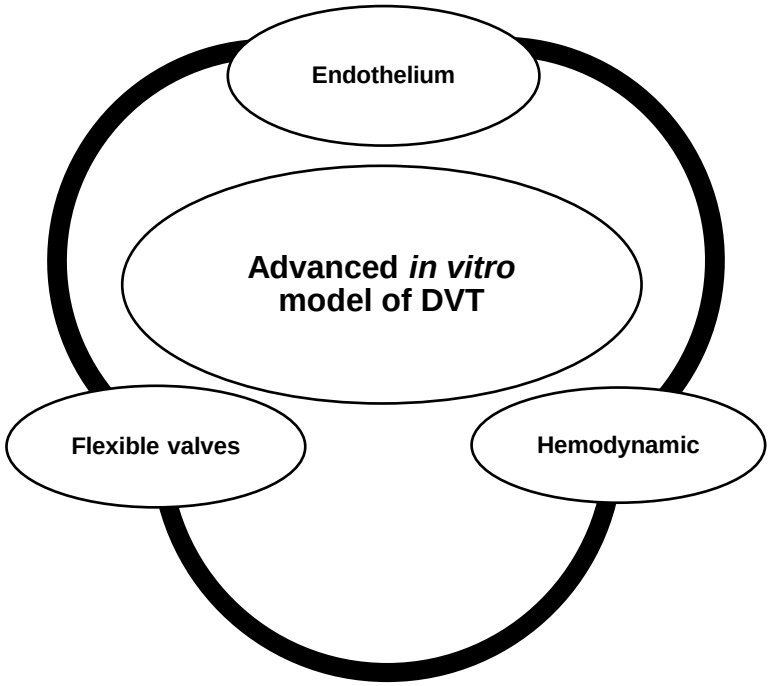

Figure 5.1. Golden standards for advancing *in vitro* deep vein thrombosis (DVT) models involve developing microfluidic channels equipped with flexible valves, ensuring all surfaces are covered with functional endothelial cells, and incorporating pulsatile flow of human blood.

5.2 Results and Discussion:

5.2.1 HUVECs growth on PDMS surfaces:

Standard techniques for functionalising the PDMS devices for cell culture were employed. These included treating the microfluidic device with absolute ethanol to clean the PDMS channels; ionising the PDMS surfaces with oxygen plasma discharge; then the PDMS was treated with (3-aminopropyl)-trimethoxysilane to improve cell attachment and proliferation, as well as, rinsing the channels with 70% ethanol for sterilising the PDMS surfaces. Coating the microfluidic channels with adhesion protein such as collagen is important to improve cell attachment during the seeding process (Mathur *et al*., 2019).

Finding an appropriate extracellular matrix protein in our approach for coating PDMS surfaces and enhancing it was essential to ensure suitability for cell adhesion in the microfluidic channel. HUVECs were seeded on multi-well plates to evaluate their growth on different PDMS samples. All multi-well plates were initially coated with a thin layer of PDMS and were prepared following the protocol detailed in Chapter 2. Followed by ionising the PDMS surfaces with a Corona discharge device (PZ2 Handheld Device, Relyon Plasma GmbH, Germany), which was used to activate the surfaces for 30 seconds, and then filled with a 1% solution of APTES for 10 minutes. PDMS samples were rinsed with 70% ethanol to sterilise their surfaces, and then the samples were kept drying in the cell culture hood. The PDMS samples were divided into four groups regarding their coating material: 0.1% Gelatine, 0.1% Modified Gelatine (PH = 9) , MaxGel™ ECM mixture, and a control group with no coating. Each group represents a different surface treatment applied to the PDMS samples for experimental purposes. The well plates were incubated for an hour in a 5% CO2 incubator, flowed by aspirating the solution from their surfaces, and then directly filled with endothelial growth medium (M199, sigma-Aldrich) where it was supplemented previously with (Growth Medium 2 Supplement Mix, Promocell) and fetal bovine serum (FBS, Sigma-Aldrich, UK) see Materials and Method. Finally, 100 µL of HUVEC cell suspension (10^7 cells mL^{-1}) was seeded into the plates and incubated overnight. HUVECs were used between passages P5 and P8.

A brightfield microscope was employed to observe the growth of HUVECs. A thoroughly developed monolayer of HUVECs was cultured on all PDMS surfaces initially coated with adhesion proteins (Figure 5.2. B, C, D). In contrast, the control PDMS samples displayed patchy growth of HUVEC (Figure 5.2. A).

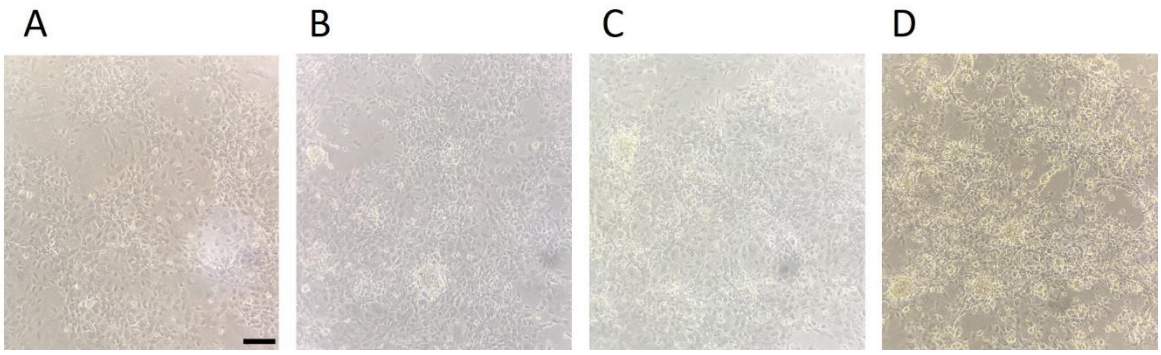

Figure 5.2. Brightfield microscopy images of HUVEC growth on different groups of samples after 16 hours of incubation. **(A)** HUVECs were cultured directly on the PDMS surface showing patches of HUVEC growth. **(B)** HUVECs were cultured on a PDMS coated with 0.1% modified Gelatine (PH =9) showing patches of HUVEC growth. **(C)** HUVECs were cultured on PDMS coated with 0.1% Gelatine showing monolayer of HUVEC growth. **(D)** HUVECs were cultured on PDMS coated with MaxGel™ ECM mixture, and the scale bar represents 100 µm showing patches of HUVEC growth.

The pH level is a contributing factor influencing the coating protein fibril formation, which forms a stable structure on PDMS surfaces that initially were functionalised by APTES. Which eventually would contribute to enhancing cell attachment and growth (Siddique *et al*., 2021).

Collagen and Gelatine are known as biocompatible proteins, suitable for a wide range of pharmaceutical applications (Liu *et al*., 2015). Enzymatic hydrolysis of raw extracted proteins with commercial proteases yields protein hydrolysates such as Gelatine hydrolysates (Zhang *et al*., 2019), which is easy to prepare and store at room temperature, whereas MaxGel™ ECM mixture should be stored at -80°C. Also, it does not require any modifications. As a result of

the HUVECs growth presented in Figure 5.2, the Gelatine hydrolysate was the most appropriate adhesion protein to be use for the HUVECs within the microfluidic experiments as sample 5.2 C reflected a higher HUVEC growth forming a uniform monolayer compared to the other samples, which displayed patchy HUVEC growth.

5.2.2 HUVECs growth within the microfluidic channels:

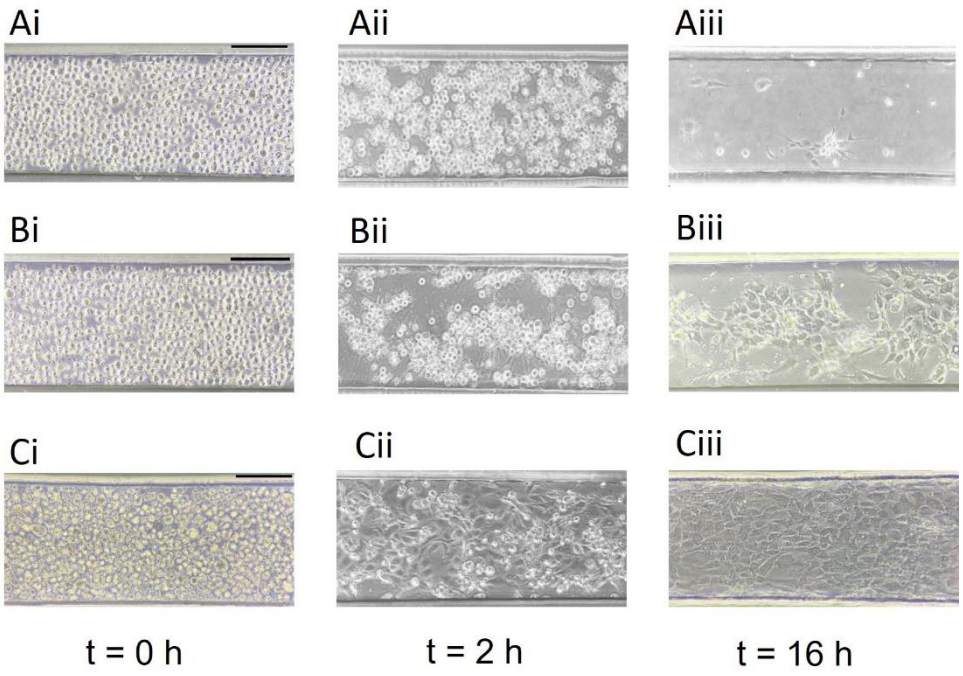

Figure 5.3. (A, B, C) Brightfield microscopy was employed to observe the growth of HUVECs and the formation of lumens within the microfluidic channel. This experiment examined three distinct protocols for treating the microfluidic channels: **(A)** channels coated solely with 1% Gelatin, **(B)** channels treated with 1% APTES for twenty minutes before Gelatin coating, and **(C)** channels subjected to a longer 1% APTES treatment duration for thirty minutes followed by Gelatin coating. **(Ai, Bi, Ci)** beginning of the cell seeding at 0 hr, **(Aii, Bii, Cii)** cells started to attach to the channel surface at 2 hrs, and **(Aiii, Biii, Ciii)** HUVEC growth after perfusing the growth medium at 1µl min^{-1}, **(Ciii)** confluence lumen formed after 16 hrs. The scale bar represents 150 µm.

The prepared microfluidic channels experienced a ten minute treatment with 1% APTES and were subsequently coated with 0.1% Gelatin hydrolysate. Growth was observed within 2 hours of seeding the channels with HUVECs (Figure 5.3 Aii). However, after 16 hours, the growth was limited, though a few cells exhibited some growth (Figure 5.3 Aiii); this suggested that the treatment process may need refinement or improvement.

PDMS is used widely as a cheap base material for microfluidic device fabrication. It is suitable for tissue engineering due to its biocompatibility (Leclerc, Sakai and Fujii, 2003). Additionally, PDMS possesses advantageous characteristics such as transparency and permeability. However, the main problem that affects the adherence of proteins on the PDMS surfaces is hydrophobicity (Chumbimuni-Torres *et al*., 2011). Oxygen plasma treatment is required to make the PDMS surfaces hydrophilic and shift it towards cytocompatibility; this makes the PDMS more suitable for cell culture applications by allowing it to accept proteins and cell attachment. It is fundamental to understand that the hydrophobicity recovery of the treated PDMS can increase either with the presence of high temperatures (Pascual *et al*., 2019) or if the PDMS samples are kept in an aqueous salt solution or de-ionised water (Chen IJ *et al*., 2007). Thus, the protocol for functionalising the PDMS channels was modified by increasing the treatment time of both oxygen plasma discharge and 1% APTES for the PDMS channels to two minutes and twenty minutes, respectively, at room temperature (Figures 5.3 B). Also, another set of PDMS channels was treated with oxygen plasma and 1% APTES of the PDMS channels for two minutes and 30 minutes, respectively, at room temperature (Figures 5.3 Ciii). The results showed a confluent monolayer of HUVECs after 16 hours of seeding the PDMS channels (Figure 5.3 Ciii), HUVECs were flat cells that grew in a monolayer and had distinct cell boundaries. While patchy growth of HUVEC within the PDMS channels was detected on the PDMS channel shown in Figure 5.3 Biii.

Increasing the plasma discharge treatment for a longer time leads to a decrease in the PDMS contact angle and improve their wettability (Ruben *et al*.,2017); and increasing the roughness of PDMS surfaces. The main concept of using plasma treatment is to improve the wettability of PDMS surfaces by replacing the methyl groups with negatively charged dipoles of the hydroxyl group (Juárez-Moreno *et al*., 2015), which leads to a shift of the PDMS surfaces to be hydrophilic and more suitable for cells attachment (Razavi *et al*., 2018). Moreover, APTES is widely used as an adhesion promoter (Aran *et al*., 2011), pre-treating the PDMS surfaces with APTES will enhance the cell attachment and growth at high fluid flow, where the shear stresses 1.16 to 9.3 Pa are induced (Siddique *et al*., 2017). The wettability of PDMS surfaces could be assessed through contact angles measurements or fluorescent probes (Pascual et al., 2019).

5.2.3 HUVECs growth within the microfluidic channels with the presence of a flexible valve:

The same protocol was applied to the microfluidic channel, incorporating a flexible valve created through *in situ* fabrication (refer to section 2.1.3). However, the results did not reveal endothelial cell growth on the valve leaflets. Moreover, the presence of the valve affected endothelial growth within the microfluidic channels (Figure 5.4 A) where The channel may hold some residue of the photoinitiator and PEGDA used in fabrication. To cleanse the channels and remove PEGDA and photo-initiator residues, 70% ethanol was initially used. While absolute ethanol is a more effective solvent, it adversely impacted the shape and size of the valve leaflet. Therefore, exploring more potent solvents or less concentrated bleaching agents is possible to enhance microfluidic channel cleaning while preserving the valve's shape and flexibility.

Sterilization of the microfluidic devices was carried out using 60% isopropanol and 2% H2O2 independently, followed by a rinse with 70% ethanol. The results demonstrated that H2O2 had a deforming effect on the shape of the valve leaflets (Figure 5.4 B). Conversely, when 60% isopropanol was employed for cleaning, a slight improvement in HUVEC growth was observed, with a few cells located around the valve area and none on the valve itself (Figure 5.4.C).

These observations indicated that the cleaning protocols employed are ineffective in

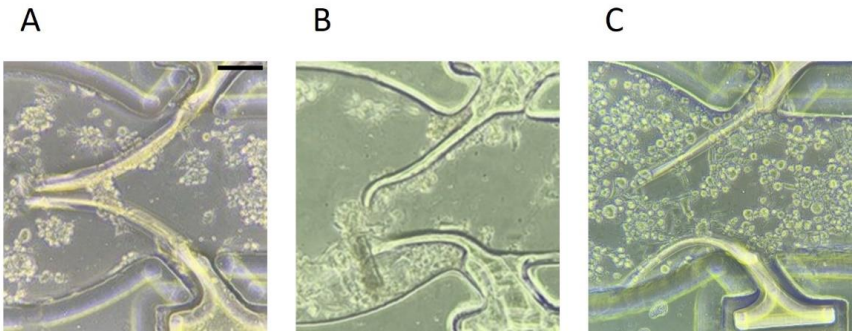

Figure 5.4. (A, B & C) Brightfield microscopy images display human umbilical vein endothelial cells (HUVECs) attachment to the microfluidic channel and the valve leaflets. Prior to cell culture, the surfaces of the microfluidic channel were treated with different solutions: **(A)** the channel was treated with 70% ethanol, **(B)** 60% isopropanol, and **(C)** hydrogen peroxide. Despite the treatments, HUVEC attachment appeared poor on all treated surfaces. The scale bar indicates 100 µm.

removing residual photo-initiator compounds, as the primary objective of these cleaning protocols was to eliminate any remaining photo-initiator residues post-polymerisation.

The surface adsorption of the valve leaflets should be highly considered, which is crucial for protein adhesion and cell attachment. Hence, a treatment involving 10% APTES for a duration of two hours was implemented. This treatment significantly improved the adsorption properties of the PEGDA hydrogel, resulting in a notable increase in cell attachment to the

valve leaflets. However, this increase in cell attachment ultimately led to undesired overgrowth on the leaflet surfaces. Furthermore, the cells grown on the channel surfaces did not exhibit stable monolayer characteristics (Figure 5.5, Ai, Bi, Ci), as they tended to detach from the channel surface during the staining process.

Remarkably, the cells on the valve leaflets exhibited a clustered pattern of HUVEC nuclei without well-defined boundaries , refer to Figure 5.5, (Dii, Diii, Div), (Eii, Eiii, Eiv) and (Fii, Fiii, Fiv). These findings highlight critical challenges faced in the protocol, particularly in achieving a confluent HUVEC growth within the microfluidic device. It becomes evident that modifications to the valve leaflet material are necessary to enhance adsorption properties and render them suitable for effective cell attachment and growth. This phase of the study represents a fundamental and required process, as changes to the valve material may impact their shape and flexibility following the polymerisation step. Thus, multiple trials will be necessary to achieve the desired outcomes in this regard.

Generally, PEGDA is a suitable material for cell culture applications due to its low toxicity, solubility in water and hydrophilicity. However, their cytocompatibility could be enhanced by adding different types of biopolymers to promote cell attachment on their surfaces (Hemmatgir, Koupaei and Poorazizi., 2022). Gelatine Hydrolysate Enzymatic (Sigma Aldrich, UK) was selected to maintain homogeneity within the microfluidic device, serving as the coating protein for PDMS channels. The optimal concentration of Gelatine Hydrolysate in the valve material was a subject of investigation. Conducting multiple trials revealed that the suitable valve composition should consist of a mixture comprising 50% PEGDA 525 *Mn*, 5% Gelatine Hydrolysate, and a photo-initiator. The PDMS microfluidic channels experienced a cleaning process, which involved washing with absolute ethanol followed by treatment with

10% APTES in absolute ethanol for twenty minutes. Subsequently, the channels were rinsed twice with BPS, and the prepared mixture was perfused through them. The hydrogel property of the valve leaflets was polymerised under UV light for a duration of 500 milliseconds. Following polymerisation and sterilisation, the channels were immersed in a 2% Gelatine solution (Sigma-Aldrich) and stored at 4 °C overnight.

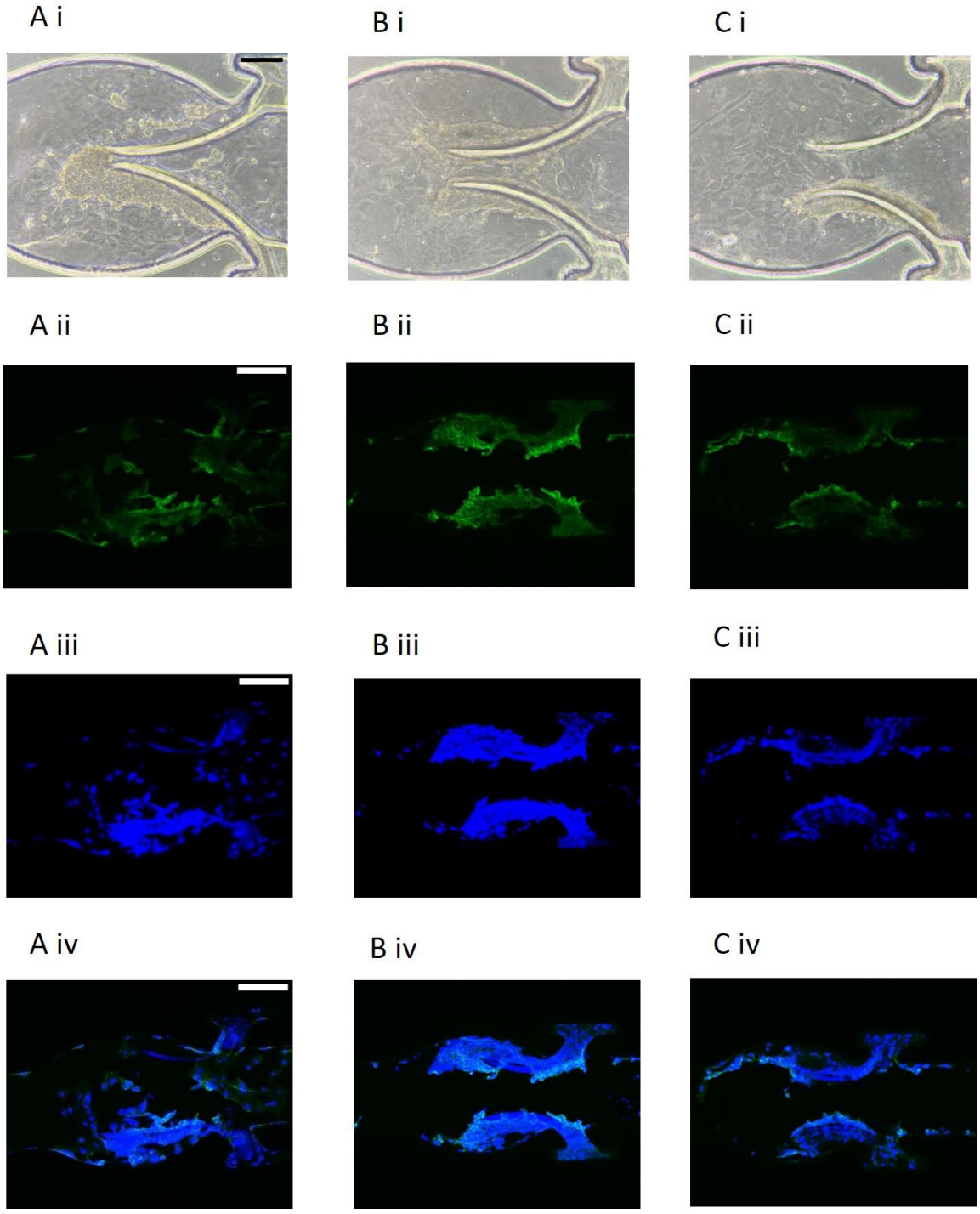

Figure 5.5. (Ai, Bi, Ci) Bright field images of HUVECs growth within the microfluidic channel and valve leaflets obtained from three microfluidic devices. The scale bar represents 100 µm. **(Dii, Diii, Div)**, **(Eii, Eiii, Eiv)** and **(Fii, Fiii, Fiv)** Confocal microscopy images of HUVECs growth within the microfluidic channel and valve leaflets, CD31 (green), and nucleus (Hoechst, blue) the cells attracted and clumped on the valve leaflets eventually died. The figures represent a single z-slice taken from the top plane. The scale bar represents 300 µm.

To prepare the devices for cell culture, they were allowed to equilibrate at room temperature for a duration of one hour. Then, after removal of the Gelatine solution, the channels were filled with the growth medium, making the microfluidic channels ready for cell seeding (as outlined in Chapter 2).

Eventually, the outcomes showed the formation of a confluent endothelial cell-lined lumen after 20 hours of cell seeding at a flow rate of 1 µl min^{-1}. The cultured HUVECs exhibited a flattened morphology, forming a monolayer with well-defined cellular boundaries and distinct nuclei, as illustrated in (Figure 5.6 C, D, E).

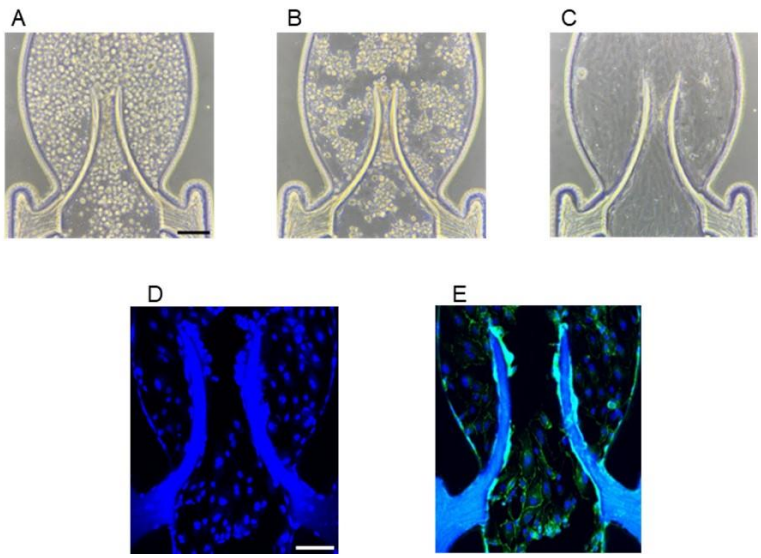

Figure 5.6. (A, B, C) Brightfield microscopy images of HUVECs growth and lumen formation within the microfluidic channel. **(A)** Beginning of the cell seeding at 0 hr, **(B)** cells started to attach and grow within the channel at 4 hrs, and growth medium perfused at 1µl min^{-1}, **(C)** confluence lumen formed after 16 hrs. **(D, E)** Confocal microscopy images of HUVECs growth within the microfluidic channel and valve leaflets. Where **(D)** shows the nucleus (Hoechst, blue) and **(E)** shows VE-Cadherin (green), and nucleus (Hoechst, blue). The scale bar represents 150 µm.

The disadvantage of this protocol is the loss of mobility in the valve leaflets (Figure 5.7). The new material of the valve leaflets (hydrogel) contains Gelatine that significantly enhances the absorption of the water from the growth medium and becomes expanded and eventually fixed in their places within the channel. Even when the percentage of Gelatine in the valve leaflets was decreased to 0.5%, this did not resolve the issue of valve leaflets swelling, as hydrogel material are known to swell in the growth medium (White, Cali and Olabisi., 2021).

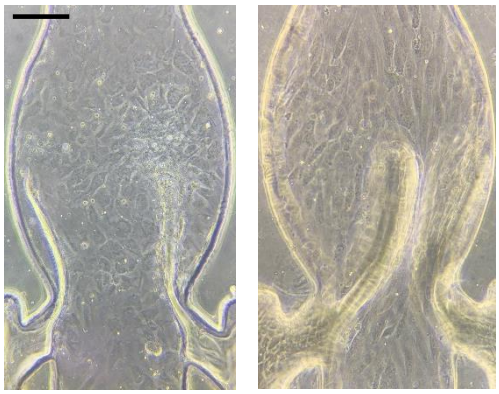

Figure 5.7. Brightfield microscopy images of HUVECs growth and lumen formation within the microfluidic channel, the valve leaflets were swollen in the growth medium and lost their mobility. The left and right images display varying degrees of deformability in the valve leaflets. The scale bar represents 150 µm.

The PEGDA molecular weight influences the density of the cross-linking; the lower the molecular weight, the higher the density and the less water content in the hydrogel structure (Makhsin *et al*., 2020). The correct choice of molecular weight of PEGDA requires further understanding of their water absorption during the polymerisation process. However, the PEGDA of the molecular weight of *Mn* 525 was replaced with the PEGDA of a higher molecular weight of *Mn* 700.

A mixture of PEGDA of molecular weight of *Mn* 700 and Gelatine hydrolysate Enzymatic with the presence of a photo-initiator (2-hydroxy-2-methylpropiophenone) was used for *in situ* photo polymerisation to obtain valve leaflets made of Gelatine/PEGDA-based hydrogels. The cured PDMS substrates were treated with oxygen plasma at thirty watts for two minutes. This was followed by immersing the PDMS channel in 10% APTES in absolute ethanol (Sigma-Aldrich, Singapore) at room temperature for fifteen minutes. APTES solution was aspirated, and the samples were washed twice in absolute ethanol. Then, vacuumed using an empty syringe, the samples were left to dry for thirty minutes. A mixture of 400 µl of PEGDA 700 *Mn*, 0.5% Gelatine hydrolysate enzymatic in BPS, and Photo initiator (2-hydroxy-2-methylpropiophenone) was infused into the channels. The flexible valve leaflet was created using *in situ* polymerisation under UV light for 500 milliseconds. Subsequently, the samples were washed and sterilised with 70% ethanol. Then, they were immersed in 70% ethanol for 60 minutes for proper sterilisation. The channels were then immersed in 2% Gelatine solution (Sigma-Aldrich) and stored at 4 °C overnight. Before cell culture, the devices were placed at room temperature for one hour before the seeding stage. The Gelatine solution was removed, and the channels were filled with the growth medium, where the PDMS microfluidic channels were ready for cell seedings.

Finally, after applying the improved treatment and modification protocol, a confluence lumen of HUVECs was formed after 20 hours of perfusing the growth medium at 1µl min^{-1} (Figure 5.8 C); they were flat cells that grew in a monolayer and have distinct cell boundaries and nuclei (Figure 5.8 D, E, F).

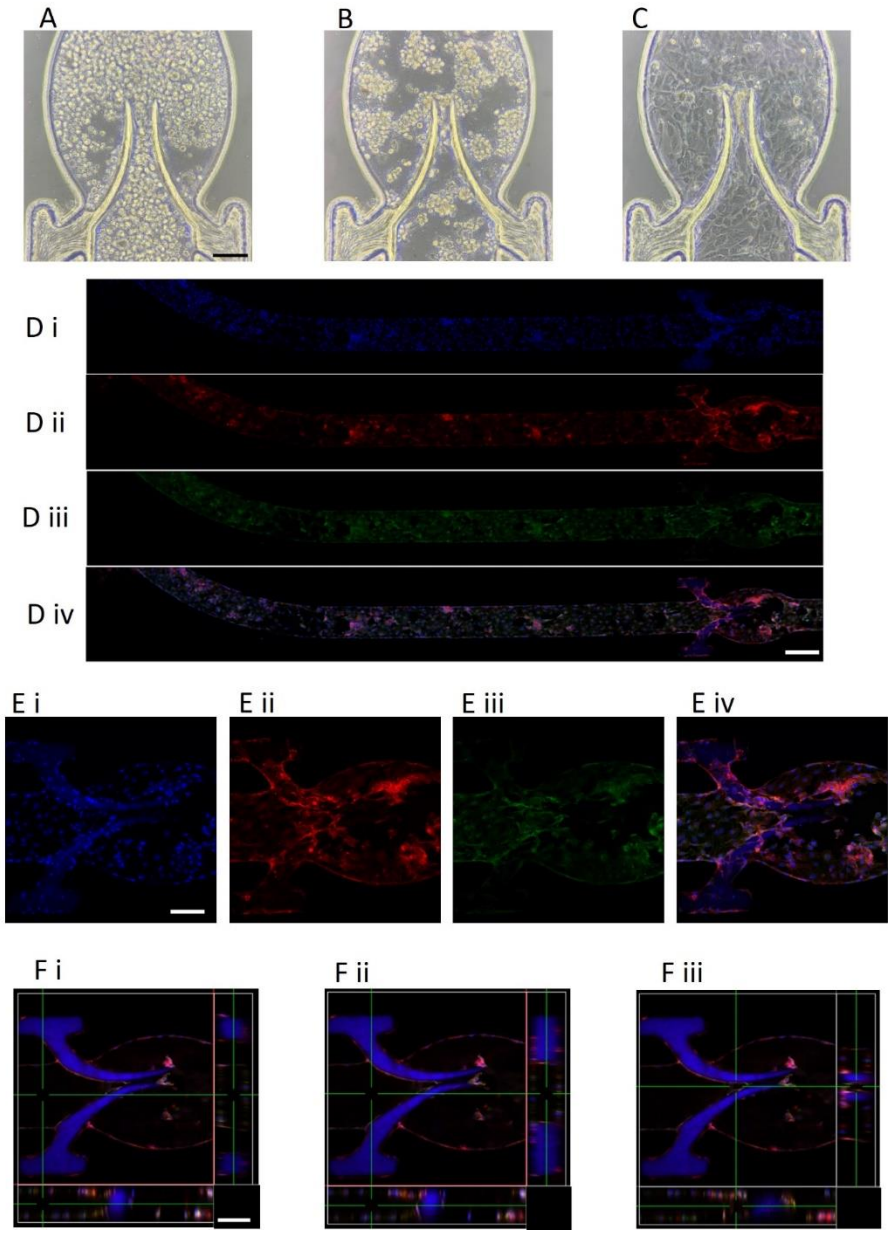

Figure 5.8. Brightfield microscopy images of HUVECs growth and lumen formation within the microfluidic channel. **(A)** beginning of the cell seeding at 0 hr, **(B)** cells started to attach and grow within the channel at 4 hrs, and growth medium perfused at 1µl min^{-1}, **(C)** confluence lumen formed after 20 hrs. scale bar represents 100 µm. **(Di, Dii, Diii, Div)** and **(Ei, Eii, Eiii, Eiv)** confocal microscopy images of HUVECs growth within the microfluidic channel and valve leaflets. **(Fi, Fii, Fiii)** showing 2D cross-sections of the 3D confocal images of the valve area. VE-Cadherin (green), nucleus (Hoechst, blue), and CD31 (red). The scale bar represents 150 µm.

Moreover, the staining process was complicated, specifically when some bubbles entered the tubing and the microfluidic channels, resulting in some cell denaturation. For this reason and to obtain clear images of the HUVEC growth within the channels and on the valve leaflets, the staining was repeated using a microfluidic device with a valve consisting of one leaflet instead of two, which was made for this purpose. In this case, the space in the valve region was more expansive, allowing the bubbles to pass freely during the staining process without any observed denaturation of the HUVEC monolayer, as shown in Figure 5.9.

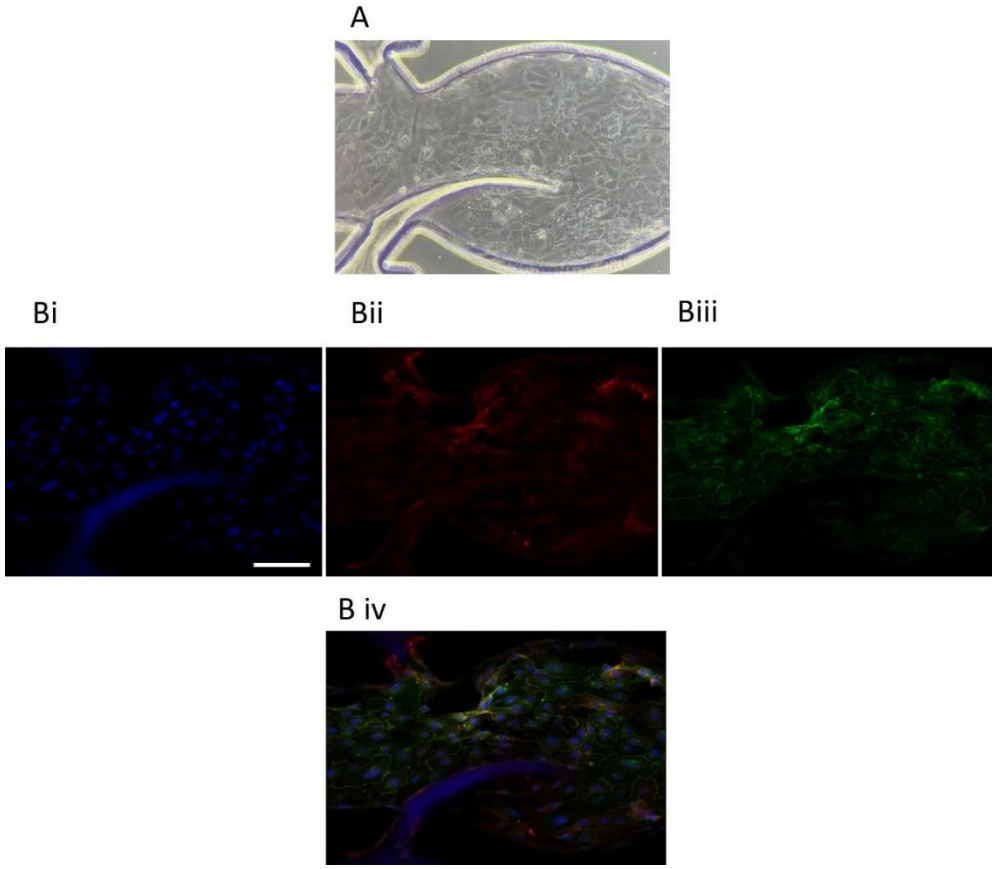

Figure 5.9. (A) Bright field and confocal microscopy images of HUVECs growth within the microfluidic channel and valve consist of one leaflet. **(Bi, Bii, Biii, and Biv)** Confocal microscopy images of HUVECs growth within the microfluidic channel and valve leaflets.VE-Cadherin (green), nucleus (Hoechst, blue), and CD31 (red) Scale bar represent 150 µm.

5.3. Capability of CEVV model for the blood experiment.

The main challenge for the created CEVV model was to endorse the flow conditions chosen to mimic the typical behaviour of blood in human veins. The whole blood was used, and the non-Newtonian shear-thinning behaviour of blood was fully captured. Thus, a lower local blood viscosity in the regions with higher shear rates was applied. However, the implementation of pulsed flow, between 0 and 120 mbar, causes dynamic variations in flow velocity and shear rate occurring within each pulse. Considering the geometry of our channel

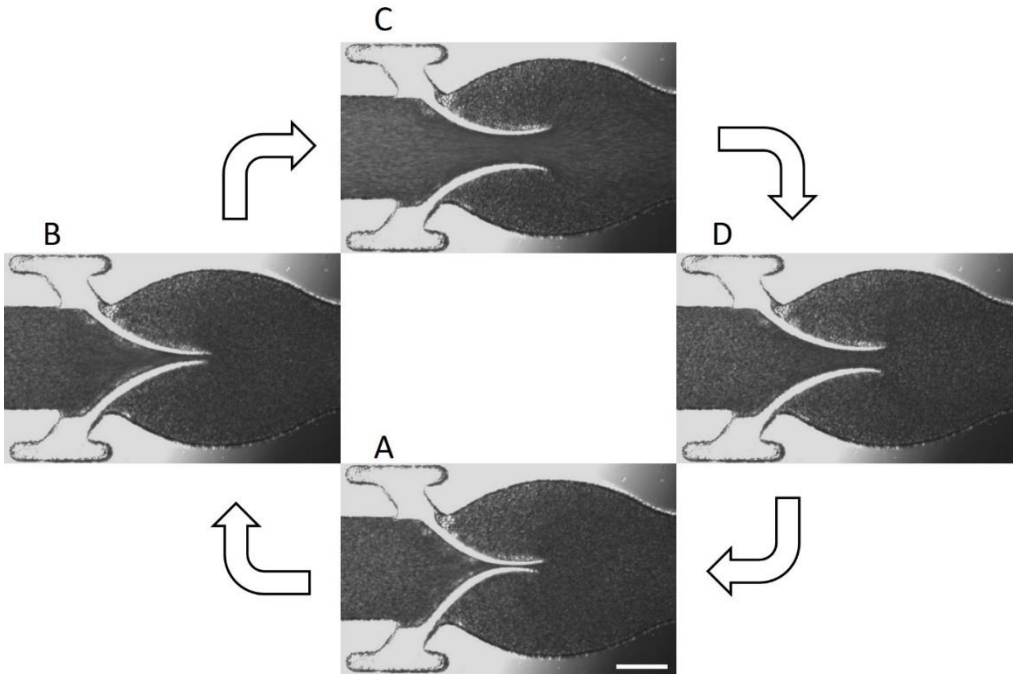

Figure 5.10. The valve opening – closing cycle at a rate of one cycle per second achieved by using pulsed blood flow between 0 and 120 mbar. Time-lapse images of the valve leaflets made of PEGDA of molecular weight of (Mn 700) and Gelatine hydrolysate Enzymatic, along with HUVECs monolayer grown within the microfluidic device and on the valve leaflets. **A-** closed phase (time = 0 s), **B-** opening phase (time = 0.25 s), **C-** equilibrium phase (time = 0.5 s) and **D-** closing phase (time = 0.75 s) then complete the cycle. The scale bar represents 150 µm.

and the typical maximum flow rate used, the maximum wall shear rate experienced in the experiments was of the order of ~100 s^{-1} . The valve opening – closing cycle is shown in Figure 5.10. After Applying all these conditions to the CEVV model for about ten minutes at

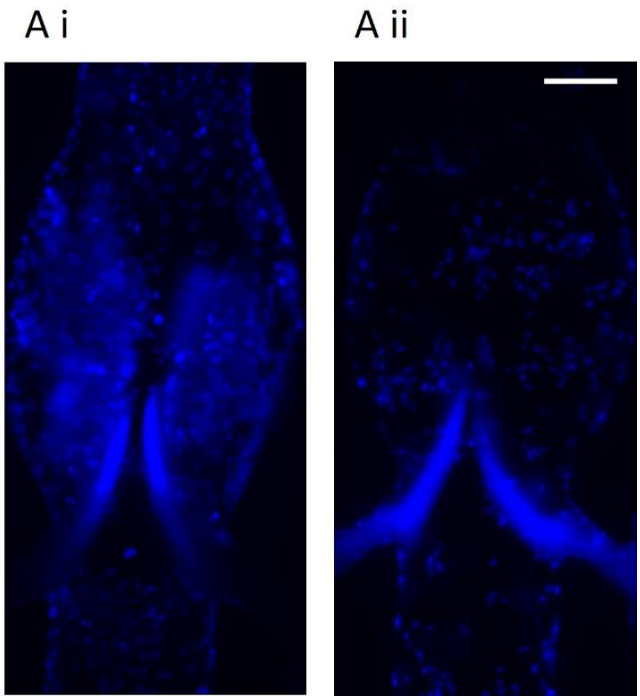

Figure 5.11. Fluorescence microscopy images of HUVECs; nucleus (Hoechst, blue). Images Ai and Aii show two distinct valves. The figures represent a single z-slice taken from the top plane. The HUVEC monolayer was stable after 10 minutes of perfusing whole blood with pulsatile flow with maximum wall shear rate of ~100 s^{-1}. The scale bar represents 150 µm.

37°C, HUVECs monolayer were stable and demonstrated a good attachment to the microfluidic channel wall and to the valve leaflets itself as shown in Figure 5.11.

Eventually, the CEVV model is an advanced *in vitro* model to conduct a wide range of *in-vitro* thrombosis research, containing the three powerful tools: biomechanical contributions of flexible venous valves, endothelium monolayer and pulsatile flow. It could be useful in the venous thrombosis research field and help diminish the use of experimental animals in accordance with the 3R ethical principles.

CHAPTER 6

PLATELET ACCUMULATION IN AN ENDOTHELIUM-COATED ELASTIC VEIN VALVE MODEL OF DEEP VEIN THROMBOSIS IS MEDIATED BY GPIBα – vWF INTERACTIONS.

''In Chapter 5, a method to grow human endothelial cells on the entire channel surface, including valve leaflets (Cellular Elastic Vein Valve model, CEVV chip), was developed. Then, in this Chapter, the CEVV model was used to carry out the following experiments: firstly, investigating the direct correlation between platelet accrual and leaflet flexibility, and secondly, examining how platelet or endothelial activation significantly enhances platelet accumulation on the valve leaflets. Furthermore, the CEVV model has the potential to reduce the need for experimental animals in thrombosis research, thereby reducing animal suffering and advancing ethical practices in scientific investigation.''

Declaration: The content presented in this chapter has been published:

Platelet accumulation in an endothelium-coated elastic vein valve model of deep vein thrombosis is mediated by GPIb α—VWF interaction.

Baksamawi, H.A., Alexiadis, A., Vigolo, D. and Brill, A., 2023.

Frontiers in cardiovascular medicine, 10, p.1167884. Published: 27 April 2023

DOI: https://doi.org/10.3389/fcvm.2023.1167884

6.1. Introduction

Venous thromboembolism (VTE) is a life-threatening condition linked to cardiovascular diseases (Cohen *et al*., 2007; Heit, 2008). VTE encompasses deep vein thrombosis (DVT), which is the formation of a thrombus in the deep veins, usually in the legs, and its most dangerous complication, pulmonary embolism (PE), which develops when the thrombus or part of it gets detached and travels to the lungs, where it occludes pulmonary circulation leading to respiratory insufficiency and even death (Wendelboe and Raskob, 2016; Khan *et al*., 2021; Lavon and Tamir, 2022).

DVT develops in the special milieu of venous flow, characterized by low shear and specific pulsatile flow patterns created by the muscle pump (Houghton *et al*., 2021). Thrombi develop in the space behind venous valve leaflets, where blood can remain for significant periods, and its flow forms two unique oppositely directed vortices (Bovill and Van Der Vliet, 2011). Excessive stagnancy of blood flow is considered one of the primary and main triggers of DVT and can result from prolonged immobilization after major surgery, limb paralysis (López and Chen, 2009); or long-haul flights (Kuipers *et al*., 2007). Recently reported evidence implies that flow reduction induces a sequence of events resembling local inflammation, with the accumulation of immune cells and platelets being an essential process preceding thrombus formation. This is further confirmed by the reduced early cell recruitment in experimental animals with mutations protecting from DVT (Brill *et al*., 2011; Payne *et al*., 2017; Ponomaryov *et al*., 2017). For example, both the recruitment of cells and thrombosis are dramatically reduced and completely absent, respectively, in mice deficient for vWF, a large pro-adhesive protein stored in platelets and Weibel-Palade bodies of the endothelium (Ponomaryov *et al*., 2017). This suggests the critical requirement of this protein for DVT initiation. Inhibition of

platelets by low doses of aspirin successfully protects against both DVT and PE, which implies the involvement of this cell type in the pathogenesis of the disease (O'Brien *et al*., 2000).

Despite extensive research in the field, which especially intensified following the US Surgeon General's Call to Action to Prevent Deep Vein Thrombosis and Pulmonary Embolism (Galson SK., 2008), the pathogenesis of DVT remains incompletely understood. One of the reasons for this is the lack of a reliable high throughput DVT model to explore mechanisms of its initiation and propagation as well as to test the efficacy of new anti-thrombotic drugs. The existing animal (mice) models (Wrobleski *et al*., 2011; Payne and Brill, 2017), in which DVT is usually induced by artificial blood flow reduction in a large vein, despite their exceptional importance, have certain limitations, such as ethical issues, differences between human and rodent genomes, horizontal rather than an upright posture, and the high cost of animal purchase and maintenance. Thus, despite a number of advantages of *in vivo* models, such as the presence of multiple unrecognisable (unknown) factors affecting the outcome, the possibility to work with genetically modified animals, and explore not only acute but also chronic thrombosis, the development of an *in vitro* approach that would recapitulate factors promoting DVT in all their complexity, is highly relevant and important.

Most currently used *in vitro* models of thrombosis are primarily based on a parallel plate flow chamber, used to study cell adhesion and deposition on a surface under shear conditions (Fredrickson *et al*., 1998; Bacabac *et al*., 2005; Van Kruchten, Cosemans and Heemskerk, 2012; Sakariassen, Orning and Turitto, 2015; Coenen, Mastenbroek and Cosemans, 2017). However, these models do not recapitulate the specificity of flow geometry in veins, which is defined mainly by flexible valves preventing backflow of the blood (Rajeeva Pandian *et al*., 2020). Recently developed microfluidic technology has an advantage in terms of the low blood

volume and number of cells needed for experiments (Westein *et al*., 2012; Rajeeva Pandian *et al*., 2020).

Vessel-on-a-chip models mimicking the hemodynamic microenvironment of human blood vessels are cutting-edge technology in thrombosis research (Zheng *et al*., 2012; Costa *et al*., 2017; Abudupataer *et al*., 2020). The thrombosis-on-a-chip approach, recapitulating the venous environment such as specific flow patterns and endothelium, is a promising method to address mechanisms of venous thrombosis (Pandian *et al*., 2018). In a recently published elegant study (Lehmann *et al*., 2018), authors demonstrated the initial formation of fibrin gel, followed by accumulation and activation of procoagulant platelets and thrombus growth in a microfluidics device, which combines biological (blood, tissue factor) and hemodynamic factors (valve leaflets steadily fixed at different angles) inducing thrombosis in a vein. it has been recently reported a new microfluidics model with mobile valves and a pulsatile flow pattern typical for veins (Schofield *et al*., 2020) and was validated by our *in-silico* model (Baksamawi *et al*., 2021). In the Chapter 5, a method to grow human endothelial cells on the entire surface of the channel, including valve leaflets (Cellular Elastic Vein Valve model, CEVV chip) was developed. Then CEVV model was used to carry out the following experiments 1)investigating the direct correlation between platelet accrual and leaflet flexibility, and 2) examining how platelet or endothelial activation significantly enhances platelet accumulation on the valve leaflets.

6.2. Results

6.2.1. Cellular elastic vein valve model

The microfluidic device used in the experiments has some advantages vs. our previous model (Schofield *et al*., 2020). Based on the human femoral vein valve duplex image showing the

valve leaflets and the valvular pocket (Dalsing and Kistner., 2019), the sinus area in the microfluidic design was expanded to be closer to the real shape of human veins (for more details about the measurements of the device channel and valve with the respect of the human femoral vein valve duplex image refer to chapter 2, Figure 2.1). Briefly, it was composed of a microchannel made of PDMS incorporating a flexible valve made of PEGDA fabricated by *in-situ* photo-polymerization to mimic the geometry and elasticity of venous valves.

The general overview of the device is presented in Figure 2.5. Platelet accumulation on basal surface (TS area, representing the valve leaflet surface facing the valve sinus) and luminal surface (TL area, representing the valve leaflet surface facing the lumen) of the valve leaflets

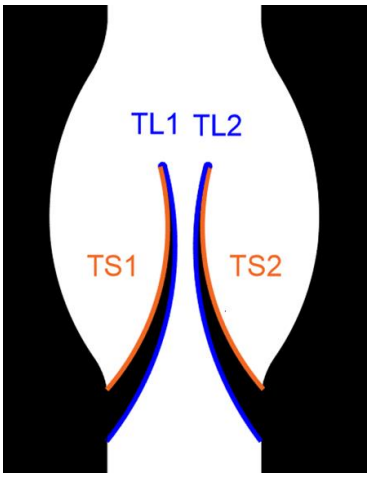

Figure 6.1. Subdivision of the valve into four areas (two for each leaflet) for quantitation, TL represent the leaflet's tip and luminal side, TS represent the leaflet's tip and sinus side.

(as shown in Figure 6.1) was quantitated separately and analysed as described in Chapter 2 (2.1.6.2. Image Quantification and statistical analysis).

The microfluidic device was coated with HUVECs for 24 h (see Chapter 2) to reach a confluent monolayer on both the walls of the microchannel and the valve leaflets. The monolayer's

continuity was confirmed by both brightfield microscopy (Figures 5.8A–C) and staining for endothelial markers, VE-Cadherin and PECAM-1(CD31) (Figures 5.8D, E, F). The cell monolayer was sufficiently stable to endure the shear stress used in the experiments without visible denudation.

6.2.2. Unchallenged platelets accumulate at the luminal side of leaflet tips.

To delineate the impact of leaflet flexibility, two types of valves were fabricated: either with both leaflets flexible (although not to an identical extent, three independent observers were evaluated the flexibility of moving leaflets using ImageJ software), designated as "symmetrical", or with one leaflet flexible and another one completely rigid, defined as "non-symmetrical". Platelet accumulation started immediately when shear was applied and reached its peak within 1 minute. Perfusion of reconstituted blood through a symmetrical valve resulted in the accumulation of platelets at the luminal side of the tip, with more platelets accruing at the more flexible leaflet [area under curve (AUC) 4,126 ± 405 vs. 1,994 ± 310, $p < 0.02$; TL area, Figures 6.2 A, D]. In the non-symmetrical valve, robust platelet deposition was also observed in the TL area exclusively of the flexible leaflet (AUC 26,296 ± 2,875 vs. 9,848 ± 946, $p < 0.006$; Figures 6.2B, E). There was no platelet accumulation directly attached to the leaflets surface in the TS area in both types of valves (Figures 6.2A, B, D, E; appendix figure A.1(A, B). Conformational change of GPIIb-IIIa (αIIbβ3 integrin), resulting in acquiring an ability to bind fibrinogen, is a well-known hallmark of platelet activation by various agonists including thrombin. This facilitates the formation of a fibrinogen bridge linking adjacent platelets together, which underlies platelet aggregation (Ma, Qin and Plow., 2007). Therefore, it was the next to assess whether this interaction mediates platelet recruitment to the leaflets. Inhibition of αIIbβ3 integrin by eptifibatide did not reduce but

rather moderately enhanced platelet deposition (more flexible leaflet of symmetrical valve, AUC 4,126 ± 405 vs. 6,660 ± 513, $p < 0.02$; Figures 6.2C, F, G; AUC of TL and TS areas is presented in appendix figure A.1(C). In accordance with this, platelet passage through the microfluidics system did not induce platelet activation, as judged by unchanged expression of P-selectin, phosphatidylserine, the ability to bind PAC-1 antibody, and lack of GPIbα shedding (appendix figure A.2). Thus, similarly to the microchannel without endothelial cells (Schofield *et al*., 2020), platelet accumulation correlated with the degree of leaflet mobility, this correlation suggests that higher leaflet flexibility corresponds to increased platelet accumulation, indicating a potential connection between leaflet mobility and platelet behaviour.

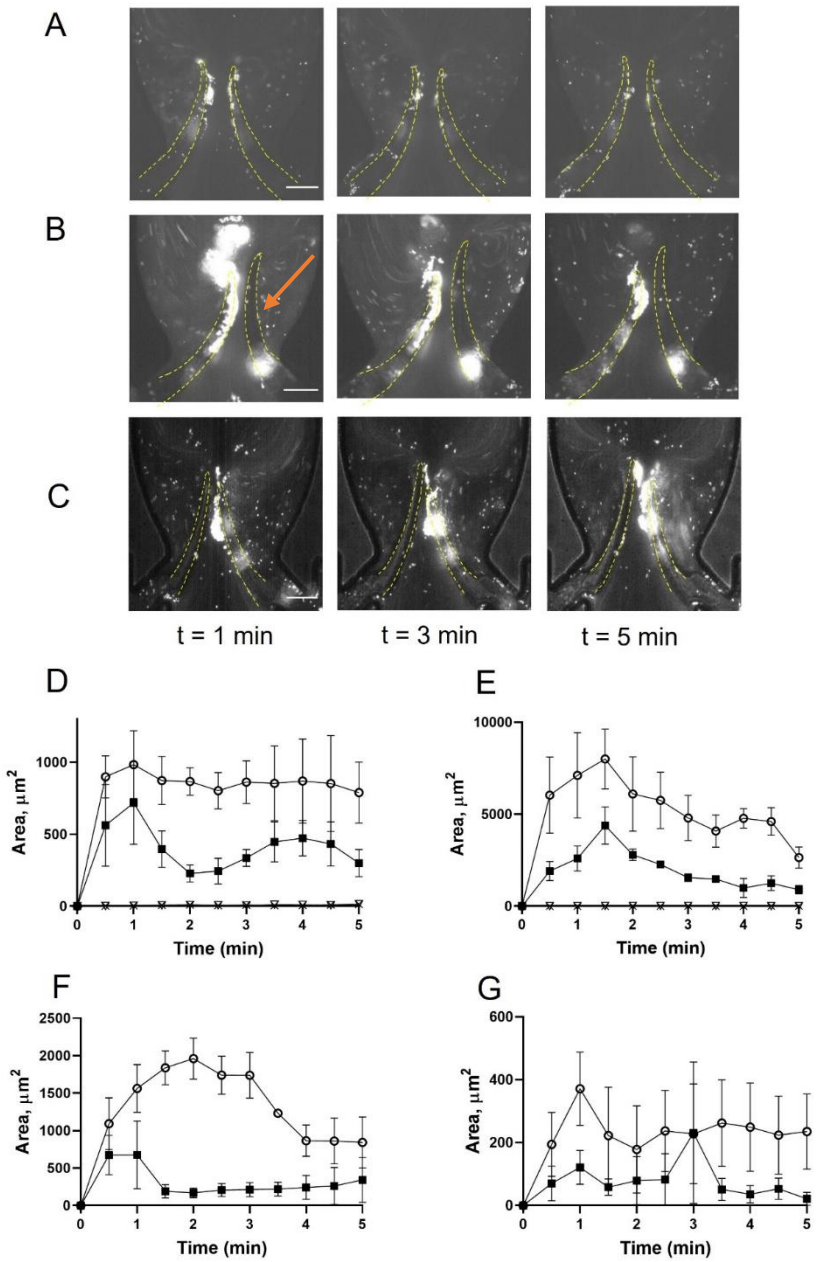

Figure 6.2. Deposition of unchallenged platelets on symmetrical, non-symmetrical valves and deposition of platelets treated with eptifibatide. Blood reconstituted with fluorescently labelled platelets was perfused through either symmetrical **(A)** or non-symmetrical, the arrow points to the rigid leaflet**(B)** valves, and resting platelets were preincubated with 9 mM eptifibatide **(C)** through a symmetrical valve for 5 min. Quantitation of resting platelet accumulation on more flexible (TL area, circles; TS area, open triangles) and less flexible/immobile (TL area, squares; TS area, Xs) leaflets of the symmetrical **(D)** or non-symmetrical **(E)** valve. **(F, G)** Quantitation of eptifibatide-treated platelet accumulation at the TL **(F)** and TS **(G)** regions. Scale bar 100 µm. Error bars represent SEM, n = 3.

6.2.3. Thrombin activation enhances platelet accumulation.

Pre-activation of platelets with thrombin resulted in their clumping in the flowing blood and the formation of massive “caps” on the leaflet tips (Figures 6.3A, C; AUC of TL and TS areas is presented in appendix figure A.1(D). The maximal TL area of the more flexible leaflet of symmetrical valve covered by platelets exceeded that for the resting platelets by ∼2 fold (AUC 4,126 ± 405 vs. 9,517 ± 896, $p < 0.006$). Thrombin-activated platelet adherence was observed also in the TS area of the leaflet (AUC 3,690 ± 578 vs. zero in resting platelets). Platelet masses remained anchored to the leaflets throughout the entire course of the experiments.

6.2.4. Accumulation of activated platelets depends on GPIbα—vWF A1 domain interaction.

Pre-treatment of thrombin-activated platelets with eptifibatide did not reduce platelet depositions (TL area of more flexible leaflet of symmetrical valve, AUC 9,517 ± 896 vs. 10,892 ± 2,044, $p = 0.57$; Figures 6.3B, D). Moreover, similar to resting cells, in the presence of eptifibatide, thrombin-activated platelets also accumulated behind the leaflets (TS areas; AUC of TL and TS areas is presented in appendix figure A.1(E).

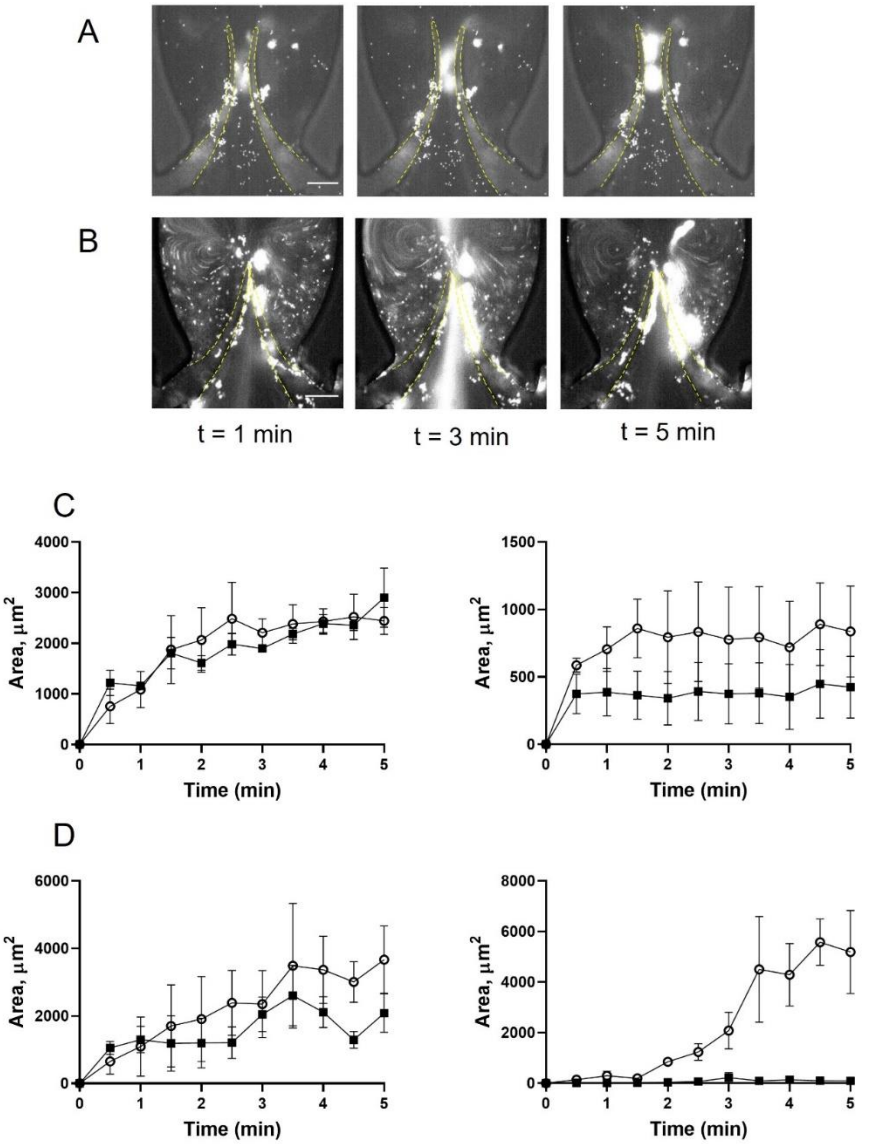

Figure 6.3. Deposition of platelets is increased by thrombin. Platelets were preincubated with 0.1 U/ml thrombin **(A, C)**, and with 0.1 U/ml thrombin + 9 µM eptifibatide **(B, D)**, Blood reconstituted with fluorescently labelled platelets was perfused through a symmetrical valve for 5 min. **(C, D)**, left row represents TL region, and the right row represents TS region; (TL, circles; TS, open triangles). Scale bar 100 µm. Error bars represent SEM, n = 3

This finding suggests the involvement of another mechanism of platelet accumulation under these conditions. Inhibition of the interaction of platelet GPIbα with vWF A1 domain with OS-1 peptide (Colicchia *et al*., 2022) of either resting or thrombin-activated platelets resulted in

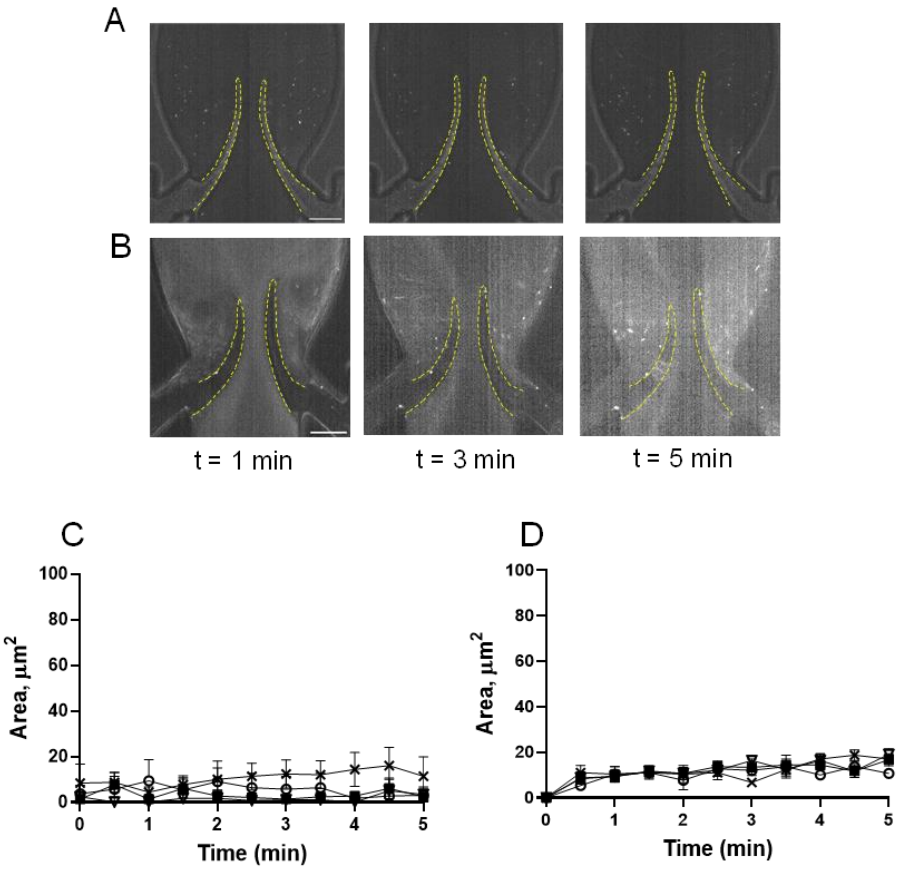

Figure 6.4. Deposition of platelets is mediated by the VWF-GPIbα axis. Platelets were preincubated with OS-1 peptide (M3456 CTERMALHNLC, Alta Bioscience, 12 µM) **(A)**, or with 0.1 U/ml thrombin + OS-1 peptide **(B)** for 5 min, fluorescently labelled platelets , reconstituted with whole blood, and perfused through a symmetrical valve for 5 min. **(C,D)**, Quantitation of platelet accumulation on more flexible (TL area, circles; TS area, open triangles) and less flexible (TL area, squares; TS area, Xs) leaflets. Scale bar 100 µm. Error bars represent SEM, n = 3.

complete abolishment of platelet deposition on all parts of the leaflets (Figures 6.4A–D; AUC of TL and TS areas is presented in appendix figure A.1(F, G).

6.2.5. Endothelial activation promotes platelet accumulation at the space behind valve leaflets.

A key role of the endothelium in DVT initiation has been recently demonstrated in preclinical studies (Brill *et al*., 2011; von Bruhl *et al*., 2012). Therefore the effect of histamine was tested, one of the most potent natural secretagogues of endothelial Weibel-Palade bodies, on platelet behavior in our system. Histamine treatment did not result in significant platelet accrual changes at the leaflets front side and their tips (TL area, AUC 4,126 ± 405 vs. 4,617 ± 1,119, p = 0.55). However, after histamine treatment, platelet aggregates developed predominantly at the valve pocket (TS area), where a thrombus is usually found in humans (AUC zero vs. 4,149 ± 505; Figures 6.5A–C; AUC of TL and TS areas is presented in appendix figure A.1(H). Thus, in sharp contrast to the system with unchallenged cells, platelet accumulation in the zone behind valve leaflets is likely not mediated by flow geometry only but requires either platelet or endothelial activation and Weibel-Palade body release as a critical component of its mechanism.

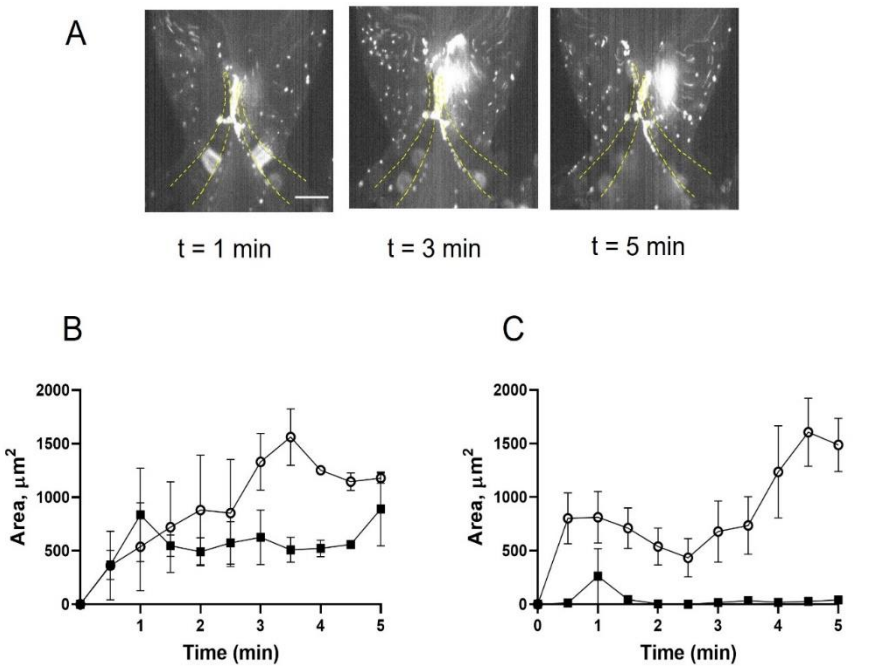

Figure 6.5. Histamine increases platelet deposition in the valve pockets (TS area). **(A)** HUVECs inside the chamber were incubated with histamine (10 µM, 15 min), and whole blood reconstituted with resting platelets was perfused through a symmetrical valve for 5 min. **(B, C)** quantitation of platelet accumulation on more flexible (circles) and less flexible (squares) leaflets, TL and TS region, respectively. Scale bar 100 µm. Error bars represent SEM, n = 3.

6.3. Discussion.

A model that combines mobile valve leaflets and pulsatile flow, characteristic of human veins, with the presence of an endothelial monolayer has been presented in chapter 5. This model recapitulates hemodynamics specific for venous flow and contains endothelium as a critical biological component involved in thrombosis prevention under physiological conditions and thrombosis initiation when prothrombotic stimuli start to prevail. The endothelial monolayer remains present and morphologically unchanged in human DVT (Sevitt, 1974), which implies that DVT is triggered by functional changes in the endothelial and blood cells rather than endothelial denudation, typical for thrombosis in arteries. Both the vessel wall and the blood

cells also produce tissue factor (TF), an important component of the blood coagulation cascade involved in thrombosis. The investigation of the impact of TF on DVT using microfluidics would require further development of the model and should become a goal of future studies.

Hemodynamics in our model shares pivotal flow features in the presence of valves, such as two vortices described in another microfluidics model (Lehmann *et al*., 2018). The area around the second ("inner") vortex has substantially lower oxygen level than the other vessel areas (Lehmann *et al*., 2018), which suggests that both endothelium and blood cells are exposed to hypoxia (Bovill and Van Der Vliet, 2011; Hamer *et al*., 1981). This results in endothelial activation, the release of Weibel-Palade bodies and recruitment of various cells including platelets, a process critical for thrombosis initiation (Brill *et al*., 2011; Payne *et al*., 2017). Platelet (C-type lectin-like receptor 2) CLEC-2 is crucial for experimental DVT (Payne *et al*., 2017), whereas platelet depletion prevents venous thrombosis development in mice (von Brühl *et al*., 2012). Also, procoagulant platelets, expressing phosphatidylserine, trigger blood clotting essential for thrombosis both in patients and *in vitro* (Denorme and Campbell, 2022). Thus, platelet deposition has been chosen as a readout representing the prothrombotic trend. Platelets were reconstituted in whole blood to create shear forces necessary for thrombus development (Lehmann *et al*., 2018). A pulsatile flow was utilized to mimic the flow pattern specific for veins and mainly generated due to the muscle pump, the dysfunction of which is associated with elevated risk for DVT (Houghton *et al*., 2021). The involvement of this back-and-forth flow pattern, and especially its reflux component, in removal of forming fibrin and, as a result, in regulation of thrombus growth has recently been demonstrated (Hu *et al*., 2020). Passage of reconstituted blood with resting platelets resulted in their accumulation predominantly at the tips and luminal part of the leaflets. Interestingly, shear stress,

constantly changing both its direction and strength, did not destroy the aggregates suggesting their stability is likely based on receptor-ligand rather than simple electrostatic interactions. The kinetics of platelet deposition was remarkably similar to thrombus formation *in vivo* in the laser injury model, with rapid initial accumulation followed by gradual decrease (e.g., Figures 6.2E, F). Although the mechanism of this phenomenon remains incompletely understood, it is likely that insufficient fibrin formation cannot support stability of the growing clot. Of note, a strong correlation between stabilized platelet accumulation and maximal platelet accumulation was revealed, which implies that both platelet accretion and subsequent loss of some platelets are tightly regulated processes (Sim *et al*., 2004). Inhibition of αIIbβ3 integrin with eptifibatide did not prevent deposition. This implies that the fibrinogen bridge between αIIbβ3 integrins on two adjacent platelets, a mechanism involved in platelet aggregation by most agonists, is not implicated in platelet accumulation in our system. This is corroborated by the lack of platelet activation (including lack of activation of GPIIb-IIIa) following blood passage through the microfluidics chamber. Activation of platelets with thrombin strongly increased platelet deposition on both leaflets of the symmetrical valve. Thrombin-activated platelets also accrued at the TS area of the leaflet, where human thrombi are usually found. Similar to resting platelets, deposition of activated cells not only was not reduced by inhibiting αIIbβ3 integrin, but instead led to increased accumulation. This suggests that the exclusion of the αIIbβ3-dependent mechanism likely increases the number of non-aggregated platelets available for adhesion (de Groot and Sixma, 1997). Increased platelet adhesion to a thrombogenic surface after blockade of the integrin has been reported, where inhibiting αIIbβ3 integrin receptor leads to antithrombotic effects without significantly impacting adherent properties (Andre *et al*., 1996). Inhibition of αIIbβ3 by several antagonists including eptifibatide also increases the proportion of “coated” (collagen and thrombin-

activated) platelets (Hamilton *et al*., 2004). Coated platelets are a fraction of the highly pro-thrombotic cell fragments that form after simultaneous agonist activation of platelets with thrombin and collagen and express various procoagulant proteins, such as fibrinogen and vWF on their surface (Dale, 2005). Our findings also demonstrate that hydrodynamics define the mechanism of platelet adhesion as an essential role of αIIbβ3 in platelet deposition on HUVEC was reported under static conditions (Bombeli, Schwartz and Harlan, 1998). Lack of involvement of αIIbβ3 in platelet recruitment in our model suggests the existence of another mechanism. Indeed, neutralization of GPIbα bending to the vWF A1 domain completely abolished the accumulation of activated platelets on both sides of the leaflets. This finding corroborates the previously published critical role of this interaction for DVT in mice (Brill *et al*., 2011). vWF is stored in both platelets and endothelial granules known as Weibel-Palade bodies. Activation of endothelial cells and Weibel-Palade body release are known prerequisites for venous thrombus development (Brill *et al*., 2011; Payne *et al*., 2017). Local vein stimulation with histamine induces thrombosis even in mast cell-deficient mice, which are completely protected from DVT (Ponomaryov *et al*., 2017). In our model, histamine promoted platelet accumulation at the TS side of the leaflets, an effect likely mediated by endothelium-derived vWF and, potentially, other Weibel-Palade body constituents, such as P-selectin, whose role in experimental DVT has been reported (von Brühl *et al*., 2012). These data also suggest that results obtained in our *in vitro* model match reasonably well data from *in vivo* approaches. It is intriguing why histamine treatment did not affect platelet deposition at the TL area. The likely reason for this is a dramatic difference in shear stress between TL and TS areas, with the latter being prone to vortex formation. The flow passing through the valve leaflets generates a primary vortex when a part of the bloodstream curves into the valve pocket. This primary vortex, in turn, gives rise to a smaller secondary vortex that rotates in the

opposite direction at the bottom of the valvular sinus (Bovill and Van Der Vliet, 2011). vWF cleavage by ADAMTS13 requires its unravelling by shear forces (Crawley *et al*., 2011; DeYoung, Singh and Kretz, 2022), which are much higher at the TL area. Also, blood exchange in the valvular pocket (TS area) is slower than between the leaflets (TL area), which leads to reduced supply of new portions of ADAMTS13 to the TS area. This results in accelerated cleavage of endothelium derived vWF ultra-large vWF multimers at the TL area thereby reducing the effect of histamine on platelet accrual. Interestingly, shear microgradient-induced formation of a thrombus consisting of only minimally activated discoid platelets has been reported (Nesbitt *et al*., 2009). In this chapter, platelet accumulation was induced solely by flow dynamics and was likely independent of soluble platelet agonists, such ADP, thromboxane A2 and thrombin, and not associated with platelet shape change or degranulation, although these parameters was not assessed directly. Blood coagulation plays a central role in venous thrombosis making anticoagulants a critical line of defense against DVT. Platelet trigger the coagulation cascade by expressing phosphatidylserine (PS), which provides a surface for clotting factor and thereby propagating thrombin generation and fibrin formation (Heemskerk, Mattheij and Cosemans, 2013). Platelets also form a scaffold for fibrin fibers and modulate clot retraction (Monroe, Hoffman and Roberts, 2002; Jurk and Kehrel, 2005). Under low shear conditions, GPIbα—vWF interaction results in amplified PS expression, recruitment of coagulation factors, and accumulation of fibrin fibers at the platelet surface (Cosemans *et al*., 2011). Thus, enhanced platelet deposition observed in our experiments could trigger blood clotting leading to thrombus development, although the impact of this factor could be reduced since citrated (i.e., with low calcium level) blood was used. Although PS expression on resting platelets remained unchanged after passage through the flow system, the kinetics of fibrin formation and its dependency on platelets in our model is an interesting scientific

question that should be addressed in future studies and, possibly, using alternative anticoagulants.

Venous valve flexibility is one of the essential characteristics affecting hemodynamics in the vein. Leaflet stiffness can increase because of diseases, such as phlebitis, in which increased deposition of connective tissue components, for example, collagen and elastin, makes the leaflet more rigid leading to its dysfunction and insufficiency (Liu and Liu, 2019). This could result in venous hypertension and reduced venous return to the heart directly affecting cardiac output (Meissner *et al*., 2007). Moreover, stiffening of a valve may negatively affect hemodynamics at the neighboring healthy valve (Soifer *et al*., 2017). Therefore platelet deposition on the valve leaflets with different ability to bend was explored. Interestingly, preferable localization of adherent platelets depended on their activation status with resting platelets predominantly accruing at the luminal part of the more flexible leaflet, whereas accumulation of thrombin-activated platelets was moderately higher at the more rigid one. This finding suggests that increased rigidity of the leaflet renders it more prothrombotic when combined with hyperactivated platelets.

6.4. Conclusion

Deep vein thrombosis is a life-threatening disease that takes millions of people's lives worldwide. Given both technical and ethical issues of using animals in research, it is necessary to develop an appropriate *in vitro* model that would recapitulate the conditions of venous thrombus development. A novel microfluidics vein-on-a-chip with moving valve leaflets was created (refer to chapter 5), to mimic the hydrodynamics in a vein, and Human Umbilical Vein Endothelial Cell (HUVEC) monolayer. A pulsatile flow pattern, typical for veins, was used in the experiments. Unstimulated human platelets, reconstituted with the whole blood,

accumulated at the luminal side of the leaflet tips proportionally to the leaflet flexibility. Platelet activation by thrombin induced robust platelet accrual at the leaflet tips. Inhibition of glycoprotein (GP) IIb-IIIa did not decrease but, paradoxically, slightly increased platelet accumulation. In contrast, blockade of the interaction between platelet GPIbα and A1 domain of vWF completely abolished platelet deposition. Stimulation of the endothelium with histamine, a known secretagogue of Weibel-Palade bodies, promoted platelet accrual at the basal side of the leaflets, where human thrombi are usually observed. Thus, Stimulation of either platelets or endothelium upregulates platelet deposition through a mechanism involving platelet-vWF interaction. This model could be useful in the venous thrombosis research field and help diminish the use of experimental animals in accordance with the 3R ethical principles.

CHAPTER 7

GENERAL CONCLUSIONS AND FURTHER WORK

7.1. Summary and conclusion:

Venous thromboembolism (VTE) carries significant clinical concerns and encloses both deep vein thrombosis (DVT) and pulmonary embolism (PE) (DeRoo et al., 2023). DVT occurs when a blood clot forms in deep veins, often in the legs (Raskob et al., 2021); then, when this clot becomes loose, it breaks and travels within the bloodstream, with the potential of blocking branches of the pulmonary artery, possibly leading to sudden death, this condition known as PE (Siegal et al., 2021). The initiation of thrombosis in blood vessels is prompted by critical factors, including hypercoagulability, dysfunction of blood vessel walls, and blood flow stasis (Sasano et al., 2021); these factors are grouped within Virchow's triad (Byrnes and Wolberg, 2017). Yet, our understanding of the underlying mechanisms of DVT formation still needs more investigations to develop targeted therapies and prophylactic strategies (DeRoo et al., 2023), especially highlighting the roles of physical parameters of the valves and flow pattern in DVT initiation (Schofield et al., 2020). Animal models have been widely used to explore the mechanisms of thrombosis, haemostasis, and to evaluate the efficiency and safety of antithrombotic drugs for potential human treatments (Dörffler-Melly et al., 2000). Ethical considerations deliver a foundation for promoting animal research's reliable and moral use. The direct priority is to ensure the well-being of animals and actively explore alternative methodologies to enhance scientific research while maintaining ethical standards (Olsson et al., 2012). The National Centre for the Replacement, Refinement, and Reduction of Animals in Research (NC3Rs) funds this project. NC3Rs is a scientific organisation established by the UK government to explore, advance, and advocate novel scientific methods aligned with replacement, reduction, and refinement of the utilisation of animals in research (Prescott and

Lidster, 2017). Therefore, this project aimed to develop a new technique to avoid animal usage in DVT research.

Firstly, this thesis adopted a novel approach to creating a microfluidic device, including a straight channel with *in-situ* fabricated flexible valves. The flexibility of the valve leaflets is precisely controlled during fabrication, producing either symmetrical valves with varying degrees of flexibility or asymmetrical valves. In the case of asymmetrical valves, there exists variability between the two leaflets, with one being flexible and the other being rigid.

The initial data from the experiments involving human whole blood with fluorescently labelled platelets was perfused through the microfluidic channel with pulsatile flow between 0 and 250 mbar per second (refer to Chapter 3). In the case of symmetrical valves, blood accumulation was observed when the fluorescently labelled platelets tended to gather at the tips of the valve leaflets. On the contrary, in asymmetrical valves, blood accumulates behind one of the leaflets, highlighting the significance of the unique flow patterns generated by the rhythm of valve leaflets' movement. Similarly, in the nanoparticle experiments that were conducted previously by Zoe Schofield (Schofield et al., 2020), Polystyrene particles (PS) were distributed in water and perfused through a microfluidic channel, experiencing pulsatile flow between 0-100 mbar per second. Notably, particle accumulation occurred behind one of the leaflets when dealing with an asymmetrical valve. In the case of symmetrical valves, the PS tended to gather at the tip of the leaflets. However, the blood experiment further clarified the impact of changes in flow patterns around valve leaflets on clot formation, specifically when PS accumulation can be explained by Van der Waals and electrostatic interactions between the PS themselves and the solid surfaces of the microfluidic device. This observation sheds light on a previously unexplored relationship between asymmetrical stiffness and the

formation of aggregates behind valve leaflets, a phenomenon consistently recognised in *in vivo* studies (Bovill and Van Der Vliet, 2011). This newfound parameter emerges as a novel indicator potentially associated with an elevated risk of DVT, prompting further investigation.

Secondly, *In vitro,* experiments alone could not confirm whether hydrodynamics can explain cell agglomeration, so the need for computational simulations has arisen as a powerful tool to explore the effects of hydrodynamics on the particle's agglomerations. Chapter 4 presents the development and utilisation of a Discrete Multiphysics model, combining the fluid-structure interaction model from Ariane et al. (2017a) and Ariane et al. (2017b) with the agglomeration model introduced by Rhamat et al. (2020). This integration represents a novel approach, representing the first DVT model to consider agglomeration. The latest outcomes from the *in-silico* model corroborate and validate the results obtained from the *in vitro* model (Schofield et al., 2020). The results show larger agglomerates are likely to form near valve leaflets even when the interaction potential between the valve leaflet and the particles is removed. The study investigates the potential impact of hydrodynamics in the early stages of agglomeration in DVT. Specifically, the investigation explores agglomeration phenomena around the valve leaflets and discusses how hydrodynamics influence these processes. Also, this numerical simulation shows how it is beneficial to combine *in silico* and *in vitro* approaches in biological research. This implies that certain mechanical features in the virtual models can be controlled and adjusted according to the researcher's preferences or requirements. In practice, the model can be used to assess which factors can increase or decrease the tendency of agglomerates to form on the valve.

Thirdly, a novel microfluidic model was developed to closely replicate the essential characteristics of human veins: pulsatile flow, flexible valves, and an endothelial monolayer

(refer to Chapter 5). Adding an endothelial monolayer to the microfluidic channels and the flexible valves was vital in distinguishing the CEVV model and making it more advanced compared to previous models (Sanchez *et al*., 2022; Schofield *et al*., 2020; Hu *et al*., 2020; Rajeeva Pandian *et al*., 2020; Lehmann *et al*., 2018). The challenge in developing the CEVV model was to reproduce the typical behaviour of blood in human veins. Implementing the pulsatile flow pulsing between 0 and 120 mbar per second induces dynamic variations in flow velocity and shear rate occurring within each pulse. However, the maximum wall shear rate generated under such conditions was approximately ~100 s^{-1}, where the HUVECs showed suitable attachment to the microfluidic channel wall and valve leaflets. The CEVV model holds promise as a valuable tool in venous thrombosis research and aligns with ethical principles advocating for the reduction, refinement, and replacement (3R) of animal experimentation.

Finally, refer to Chapter 6, a CEVV on a chip was used to conduct the human blood experiments, where human endothelial cells grew on the entire surface of the microfluidic channel. Outlining the impact of leaflet flexibility, two types of valves were fabricated: symmetrical and non-symmetrical. The results obtained using whole human blood with fluorescently labelled platelets showed a direct correlation between platelet accumulation at the tips and luminal part of the leaflets of the valve and leaflet flexibility. Specifically, a higher accumulation of platelets was observed on the more flexible leaflet. However, there was no platelet accumulation at the sinus area in either type of valve.

Additional experiments were conducted to determine which platelet receptor could be involved in platelet accumulation. GPIIb-IIIa (αIIbβ3 integrin) is a platelet receptor that links platelets together and contributes to platelet aggregation (Ma, Qin, and Plow, 2007). Conversely, inhibiting the αIIbβ3 integrin with eptifibatide did not decrease platelet

accumulation; instead, it moderately increased it. So, the absence of αIIbβ3 involvement in platelet recruitment in the CEVV model indicates the presence of an alternative mechanism. Inhibition of GPIbα-VWF A1 domain interaction by using OS-1 peptide (Colicchia et al., 2022) eliminated the accumulation of either resting or thrombin-activated platelets on both sides of the leaflets. This observation confirms the crucial role of this interaction in deep vein thrombosis (DVT) in mice, as previously reported (Brill et al., 2011). Also, recent studies have highlighted the significant role of the endothelium in initiating DVT (Brill et al., 2011; von Bruhl et al., 2012). Therefore, the impact of histamine on platelet aggregation was investigated using the CEVV model. The findings showed that following the treatment of the endothelial cells with histamine platelet aggregation largely formed at the sinus area, a spot typically associated with thrombus formation in humans.

In summary, the investigation of platelet deposition on valve leaflets with varying flexibility revealed that resting platelets mainly adhered to the luminal part of flexible leaflets, while thrombin-activated platelets showed higher accumulation on rigid ones; this suggests that increased leaflet rigidity enhances thrombotic risk with hyperactivated platelets. Furthermore, the activation of platelets or endothelial cells directs the platelet deposition on specific areas of the valve leaflets, primarily mediated by the interaction between platelets and the von Willebrand factor.

7.2. Further work

The data presented in this thesis pave the way for new future research experiments. Here are some potential experiment suggestions for consideration:

- Valve flexibility: additional experiments are needed to determine the Young's modulus of the new valve material, comprising PEGDA (Mn ≈ 700), 0.5% Gelatine hydrolysate in PBS,

and PI (2-hydroxy-2-methyl propiophenone). Accordingly, the change in flow rate will deflect more or less the valve and by studying how the deflection changes with the flow rate it is possible to extrapolate the Young's modulus of that particular valve composition. The experimental setups needs to be established to quantify the deflection of the valve material across various flow rates within the microfluidic channel. This process could adopt a methodology similar to that described by Wexler et al. in 2013, where the bending of elastic fibres in viscous flows was studied. Likewise, Schofield et al. 2020 investigated the flexibility of valves made up of PEGDA (Mn ≈575) and PI. This technique could be applied to assess the flexibility of the new valve material utilised in the in situ fabrication of the CEVV chip that was used throughout Chapters 5 and 6.

The experimental procedure involves 1) Preparing samples with simpler geometry than the valve, typically only one straight thin fibre; otherwise with a complex geometry it will be impossible to extract the Young's modulus. Materials with varying compositions, including different proportions of PEGDA (Mn ≈700), Gelatin, and PI, and potentially altering cross-linking densities. 2) Utilise a pump to regulate a constant flow rate of fluid passing through the microfluidic channel, with corresponding flow rates recorded for each experiment. 3) Employ appropriate techniques, such as ImageJ software, to measure the deformation of the valve material in response to the flowing fluid. Then, record deformation measurements alongside the corresponding flow rates for each experiment. Finally, by studying the small deformations at relatively low flow rates, it is possible to extract a linear dependence. This will be used to calculate Young's modulus.

Hence, by performing the experiments outlined above, a valuable understanding of the valve material's mechanical behaviour, precisely its flexibility and response to varying flow rates, can be assessed.

- Investigating the initiation and progression of DVT using a microfluidic platform equipped with three valves, or more if it is achievable, this can yield valuable insights into the dynamics of blood clot formation, including its initial development on the first valve and the potential developments of embolus detachment, as well as its impact on the formation of subsequent blood clots on the subsequent valves. A comprehensive analysis of platelet accumulation across all valves within the microfluidic channel, with specific attention to the last valve, would be highly recommended.

- Personalising the CEVV chip model is a vital approach. Personalisation should begin with biological considerations, such as using primary cells and blood from the same individual to develop the microfluidic device and run the experiment. Furthermore, the investigation should consider personal health records (Van Den Berg *et al*., 2019) likewise, there would be significant benefits in using human blood to isolate and generate blood outgrowth ECs (Ormiston *et al*., 2015; Mathur *et al*., 2019)
- Growing the HUVECs within the microfluidic channels under pulsatile flow. The suggestion is to introduce a pulsatile flow regimen during the growth phase instead of a continuous flow. This dynamic flow pattern subjects the endothelial cells on the valve leaflets to rhythmic movements throughout the growth process. Over time, these cells experience adaptation to both the fluidic motion and the pressure exerted by the leaflets during the closing phase.
- Using alternative anticoagulants such as heparin, hirudin or PPACK, all of them are very potent inhibitors of thrombin, so using these anticoagulants will make evaluation of platelets more ‘‘clean’’ but will not allow for testing thrombin/fibrin generation.

- An investigation of the of other receptors (e.g., GPVI) including inhibitory receptors (e.g., PECAM-1) on platelet surface. For this, mutant mouse blood will be ideal, but it undermines the idea of replacing animals in research.
- Explore the role of procoagulant platelets in the system.
- Study differences between young and old platelets in their ability to accumulate around the valves.
- Check the efficacy of currently used anti-platelet drugs and anticoagulants used to prevent and treat VTE (e.g., direct thrombin inhibitors - dabigatran, FXa inhibitors - rivaroxaban, apixaban etc.).
- Verify the applicability of the device to test new drugs and therefore be useful in drug development.
- Using non-thrombin inhibitors as anticoagulants and recalcified plasma: study thrombin and fibrin generation and interactions of platelets with the layers of formed fibrin.
- Studying cells other than platelets, for example, neutrophils, the role of neutrophil extracellular traps (NETs) using DNASe-I that destroys NET or inhibitors of PAD4 that inhibit NETosis; monocytes, main producers of tissue factor, an key activator of the extrinsic pathway of coagulation. Cells can be retrieved for staining or stained in situ, or for RNA seq/single cell RNAseq.
- Explore different environmental conditions, for example, in the presence of LPS (lipopolysaccharides) or bacteria to mimic sepsis, or DAMPs (Damage-Associated Molecular Patterns) such as S100A8/A9 molecules.
- Test platelets from patients with VTE as well as other diseases predisposing to DVT (e.g., stroke, paresis/paralysis, sepsis, genetic predisposition to venous thrombosis, trauma etc.).

- Check the possibility of the approach to predict chances of DVT development, which is a very important potential application.

CHAPTER 8

LIST OF REFERENCES

Abudupataer, M., Chen, N., Yan, S., Alam, F., Shi, Y., Wang, L., Lai, H., Li, J., Zhu, K. and Wang, C. (2020) 'Bioprinting a 3D vascular construct for engineering a vessel-on-a-chip', *Biomedical Microdevices*, *22*, pp.1-10.

Adair, B.D., Alonso, J.L., van Agthoven, J., Hayes, V., Ahn, H.S., Yu, I.S., Lin, S.W., Xiong, J.P., Poncz, M. and Arnaout, M.A. (2020) 'Structure-guided design of pure orthosteric inhibitors of αIIbβ3 that prevent thrombosis but preserve hemostasis', *Nature Communications*, *11*(1), p.398.

Ageno, W., Becattini, C., Brighton, T., Selby, R. and Kamphuisen, P.W. (2008) 'Cardiovascular risk factors and venous thromboembolism: a meta-analysis', *Circulation*, *117*(1), pp.93-102.

Aird, W.C. (2005) 'Spatial and temporal dynamics of the endothelium', *Journal of Thrombosis and Haemostasis*, 3(7), pp.1392-1406.

Aird, W.C. (2007) 'Vascular bed-specific thrombosis', *Journal of Thrombosis and Haemostasis*, *5*, pp.283-291.

Alexiadis, A. (2015) 'The discrete multi-hybrid system for the simulation of solid-liquid flows', *PloS One*, *10*(5), p.e0124678.

Alexiadis, A., Simmons, M.J.H., Stamatopoulos, K., Batchelor, H.K. and Moulitsas, I. (2021) 'The virtual physiological human gets nerves! How to account for the action of the nervous system in multiphysics simulations of human organs', *Journal of the Royal Society Interface*, *18*(177), p.20201024.

Alexiadis, A., Stamatopoulos, K., Wen, W., Batchelor, H.K., Bakalis, S., Barigou, M. and Simmons, M.J.H. (2017) 'Using discrete multi-physics for detailed exploration of hydrodynamics in an in vitro colon system', *Computers in Biology and Medicine*, *81*, pp.188-198.

Amelirad, A., Shamsasenjan, K., Akbarzadehlaleh, P. and Sarvar, D.P. (2019) 'Signaling pathways of receptors involved in platelet activation and shedding of these receptors in stored platelets', Advanced Pharmaceutical Bulletin, 9(1), p.38.

André, P., Arbeille, B., Drouet, V., Hainaud, P., Bal dit Sollier, C., Caen, J.P. and Drouet, L.O. (1996) 'Optimal antagonism of GPIIb/IIIa favors platelet adhesion by inhibiting thrombus growth: an ex vivo capillary perfusion chamber study in the guinea pig', *Arteriosclerosis, Thrombosis, and Vascular Biology*, *16*(1), pp.56-63.

Andrews, R. K. and Berndt, M. C. (2008) 'Platelet adhesion: A game of catch and release', Journal of Clinical Investigation, 118(9), pp. 3009–3011. doi: 10.1172/JCI36883.

Ashorobi, D., Ameer, M. A., & Fernandez, R. (2023) *Thrombosis*. *In StatPearls. StatPearls* Publishing.

Arachiche, A., Mumaw, M.M., de la Fuente, M. and Nieman, M.T. (2013) 'Protease-activated receptor 1 (PAR1) and PAR4 heterodimers are required for PAR1-enhanced cleavage of PAR4 by α-thrombin', *Journal of Biological Chemistry*, *288*(45), pp.32553-32562.

Aran, K., Fok, A., Sasso, L.A., Kamdar, N., Guan, Y., Sun, Q., Ündar, A. and Zahn, J.D. (2011) 'Microfiltration platform for continuous blood plasma protein extraction from whole blood during cardiac surgery', *Lab on a Chip*, *11*(17), pp.2858-2868.

Ariane, M., Allouche, M.H., Bussone, M., Giacosa, F., Bernard, F., Barigou, M. and Alexiadis, A. (2017a) 'Discrete multi-physics: A mesh-free model of blood flow in flexible biological valve including solid aggregate formation', *PloS One*, *12*(4), p.e0174795.

Ariane, M., Kassinos, S., Velaga, S. and Alexiadis, A. (2018a) 'Discrete multi-physics simulations of diffusive and convective mass transfer in boundary layers containing motile cilia in lungs', *Computers in Biology and Medicine*, *95*, pp.34-42.

Ariane, M., Sommerfeld, M. and Alexiadis, A. (2018) 'Wall collision and drug-carrier detachment in dry powder inhalers: Using DEM to devise a sub-scale model for CFD calculations', *Powder Technology*, *334*, pp.65-75.

Ariane, M., Vigolo, D., Brill, A., Nash, F.G.B., Barigou, M. and Alexiadis, A. (2018b) 'Using Discrete Multi-Physics for studying the dynamics of emboli in flexible venous valves', *Computers & Fluids*, *166*, pp.57-63.

Ariane, M., Wen, W., Vigolo, D., Brill, A., Nash, F.G.B., Barigou, M. and Alexiadis, A. (2017b) 'Modelling and simulation of flow and agglomeration in deep veins valves using discrete multi physics', *Computers in Biology and Medicine*, *89*, pp.96-103.

Asquith, N.L., Duval, C., Zhmurov, A., Baker, S.R., McPherson, H.R., Domingues, M.M., Connell, S.D., Barsegov, V. and Ariëns, R.A. (2022) 'Fibrin protofibril packing and clot stability are enhanced by extended knob-hole interactions and catch-slip bonds', *Blood Advances*, *6*(13), pp.4015-4027.

Audu, C.O., Wakefield, T.W. and Coleman, D.M. (2019) 'Pediatric deep venous thrombosis', *Journal of Vascular Surgery: Venous and Lymphatic Disorders*, *7*(3), pp.452-462.

Auton, M., Sowa, K.E., Smith, S.M., Sedlák, E., Vijayan, K.V. and Cruz, M.A. (2010) 'Destabilization of the A1 domain in von Willebrand factor dissociates the A1A2A3 tri-domain and provokes spontaneous binding to glycoprotein Ibα and platelet activation under shear stress', *Journal of Biological Chemistry*, *285*(30), pp.22831-22839.

Bacabac, R.G., Smit, T.H., Cowin, S.C., Van Loon, J.J., Nieuwstadt, F.T., Heethaar, R. and Klein-Nulend, J. (2005) 'Dynamic shear stress in parallel-plate flow chambers', *Journal of Biomechanics*, *38*(1), pp.159-167.

Badimon, L. (2018) 'Pathogenesis of ST-Elevation Myocardial Infarction', *Coronary Microvascular Obstruction in Acute Myocardial Infarction,* (pp. 1-13). Academic Press.

Bagot, C.N. and Arya, R. (2008) 'Virchow and his triad: a question of attribution', *British journal of Haematology*, *143*(2), pp.180-190.

Bailey, K., Astbury, W.T. and Rudall, K.M. (1943) 'Fibrinogen and fibrin as members of the keratin-myosin group', *Nature*, *151*(3843), pp.716-717.

Bain, B.J. (2021) 'Structure and function of red and white blood cells and platelets', *Medicine*, *49*(4), pp.183-188.

Baksamawi, H.A., Ariane, M., Brill, A., Vigolo, D. and Alexiadis, A. (2021) 'Modelling particle agglomeration on through elastic valves under flow', *ChemEngineering*, *5*(3), p.40.

Bala, K., Ambwani, K. and Gohil, N.K. (2011) 'Effect of different mitogens and serum concentration on HUVEC morphology and characteristics: implication on use of higher passage cells', *Tissue and Cell*, *43*(4), pp.216-222.

Bayne, K., Ramachandra, G.S., Rivera, E.A. and Wang, J. (2015) 'The evolution of animal welfare and the 3Rs in Brazil, China, and India', *Journal of the American Association for Laboratory Animal Science*, *54*(2), pp.181-191.

Bazigou, E. and Makinen, T. (2013) 'Flow control in our vessels: vascular valves make sure there is no way back', *Cellular and Molecular Life Sciences*, *70*, pp.1055-1066.

Bentzon, J.F., Otsuka, F., Virmani, R. and Falk, E. (2014) 'Mechanisms of plaque formation and rupture', *Circulation research*, *114*(12), pp.1852-1866.

Bevers, E.M., Comfurius, P. and Zwaal, R.F. (1983) 'Changes in membrane phospholipid distribution during platelet activation', *Biochimica et Biophysica Acta (BBA)-Biomembranes*, *736*(1), pp.57-66.

Bevers, E.M. and Williamson, P.L. (2016) 'Getting to the outer leaflet: physiology of phosphatidylserine exposure at the plasma membrane', *Physiological Reviews*, *96*(2), pp.605-645.

Blair, T.A., Michelson, A.D. and Frelinger III, A.L. (2018) 'Mass cytometry reveals distinct platelet subtypes in healthy subjects and novel alterations in surface glycoproteins in Glanzmann thrombasthenia', *Scientific Reports*, *8*(1), p.10300.

Bombeli, T., Schwartz, B.R. and Harlan, J.M. (1998) 'Adhesion of activated platelets to endothelial cells: evidence for a GPIIbIIIa-dependent bridging mechanism and novel roles for endothelial intercellular adhesion molecule 1 (ICAM-1), αvβ3 integrin, and GPIbα', *The Journal of Experimental Medicine*, *187*(3), pp.329-339.

Bonnefoy, A., Liu, Q., Legrand, C. and Frojmovic, M.M. (2000) 'Efficiency of platelet adhesion to fibrinogen depends on both cell activation and flow', *Biophysical Journal*, *78*(6), pp.2834-2843.

Boström, M., Deniz, V., Franks, G.V. and Ninham, B.W. (2006) 'Extended DLVO theory: Electrostatic and non-electrostatic forces in oxide suspensions', *Advances in Colloid and Interface Science*, *123*, pp.5-15.

Bovill, E.G. and van der Vliet, A. (2011) 'Venous valvular stasis–associated hypoxia and thrombosis: what is the link?', *Annual Review of Physiology*, *73*, pp.527-545.

Brandt, M., Schönfelder, T., Schwenk, M., Becker, C., Jäckel, S., Reinhardt, C., Stark, K., Massberg, S., Münzel, T., von Brühl, M.L. and Wenzel, P. (2014) 'Deep vein thrombus formation induced by flow reduction in mice is determined by venous side branches', *Clinical Hemorheology and Microcirculation*, *56*(2), pp.145-152.

Brill, A., Fuchs, T.A., Chauhan, A.K., Yang, J.J., De Meyer, S.F., Köllnberger, M., Wakefield, T.W., Lämmle, B., Massberg, S. and Wagner, D.D. (2011) 'von Willebrand factor–mediated platelet adhesion is critical for deep vein thrombosis in mouse models', *Blood, The Journal of the American Society of Hematology*, *117*(4), pp.1400-1407.

Brink, A., Elf, J., Svensson, P.J., Engström, G., Melander, O. and Zöller, B. (2023) 'Sex-specific risk factors for deep venous thrombosis and pulmonary embolism in a population-based historical cohort study of middle-aged and older individuals', *Journal of the American Heart Association*, *12*(5), p.e027502.

Brooks, E.G., Trotman, W., Wadsworth, M.P., Taatjes, D.J., Evans, M.F., Ittleman, F.P., Callas, P.W., Esmon, C.T. and Bovill, E.G. (2009) 'Valves of the deep venous system: an overlooked risk factor', *Blood, The Journal of the American Society of Hematology*, *114*(6), pp.1276-1279.

Brozovich, F.V., Nicholson, C.J., Degen, C.V., Gao, Y.Z., Aggarwal, M. and Morgan, K. (2016) 'Mechanisms of vascular smooth muscle contraction and the basis for pharmacologic treatment of smooth muscle disorders', *Pharmacological Reviews*, *68*(2), pp.476-532.

Budnik, I. and Brill, A. (2018) 'Immune factors in deep vein thrombosis initiation', *Trends in Immunology*, *39*(8), pp.610-623.

Byrnes, J.R. and Wolberg, A.S. (2017) 'New findings on venous thrombogenesis', *Hämostaseologie*, *37*(01), pp.25-35.

Caggiati, A., Phillips, M., Lametschwandtner, A. and Allegra, C. (2006) 'Valves in small veins and venules', *European Journal of Vascular and Endovascular Surgery*, *32*(4), pp.447-452.

Camenzind, S. and Eggel, M. (2022) 'The 3Rs principles and genetic pain disenhancement', *Animal Welfare*, *31*(4), pp.495-503.

Campos, J. and Brill, A. (2020) 'By word of mouse: using animal models in venous thrombosis research', *Platelets*, *31*(4), pp.447-454.

Cattaneo M. (2009) 'Light transmission aggregometry and ATP release for the diagnostic assessment of platelet function', *Seminars in Thrombosis and Hemostasis*, *35*(2), 158–167.

Chaudhry, R., Miao, J. H., and Rehman, A. (2022) *Physiology, Cardiovascular*. In StatPearls. StatPearls Publishing.

Chen, I.J. and Lindner, E. (2007) 'The stability of radio-frequency plasma-treated polydimethylsiloxane surfaces. *Langmuir*, *23*(6), pp.3118-3122.

Chen, Y., Tang, B., Nie, M., Qi, X., Wang, F. and Wang, H. (2023) 'The incidence, risk factors, characteristics, and prognosis of recurrent deep venous thrombosis in the contralateral lower extremity', *Journal of Vascular Surgery: Venous and Lymphatic Disorders*, *11*(1), pp.52-60.

Chernysh, I.N., Nagaswami, C., Kosolapova, S., Peshkova, A.D., Cuker, A., Cines, D.B., Cambor, C.L., Litvinov, R.I. and Weisel, J.W. (2020) 'The distinctive structure and composition of arterial and venous thrombi and pulmonary emboli', *Scientific Reports*, *10*(1), p.5112.

Chi, G., Goldhaber, S.Z., Hull, R.D., Hernandez, A.F., Kerneis, M., Al Khalfan, F., Cohen, A.T., Harrington, R.A. and Gibson, C.M. (2017) 'Thrombus burden of deep vein thrombosis and its association with thromboprophylaxis and D-dimer measurement: insights from the APEX trial', *Thrombosis and Haemostasis*, *117*(12), pp.2389-2395.

Chumbimuni-Torres, K.Y., Coronado, R.E., Mfuh, A.M., Castro-Guerrero, C., Silva, M.F., Negrete, G.R., Bizios, R. and Garcia, C.D. (2011) 'Adsorption of proteins to thin-films of PDMS and its effect on the adhesion of human endothelial cells', *RSC Advances*, *1*(4), pp.706-714.

Clay, E., Jamotte, A., Verhamme, P., Cohen, A.T., Van Hout, B.A. and Gumbs, P. (2018) 'Cost-effectiveness of edoxaban compared to warfarin for the treatment and secondary prevention of venous thromboembolism in the UK', *Journal of Market Access & Health Policy*, *6*(1), p.1495974.

Coenen, D.M., Mastenbroek, T.G. and Cosemans, J.M. (2017) 'Platelet interaction with activated endothelium: mechanistic insights from microfluidics', *Blood, The Journal of the American Society of Hematology*, *130*(26), pp.2819-2828.

Cohen, I. (1985) *The mechanism of clot retraction.* In Platelet membrane glycoproteins (pp. 299-323). Boston, MA: Springer US.

Cohen AT, Agnelli G, Anderson FA, Arcelus JI, Bergqvist D, Brecht JG, Greer IA, Heit JA, Hutchinson JL, Kakkar AK, Mottier D, Oger E, Samama MM, Spannagl M; VTE Impact Assessment Group in Europe (VITAE) (2007) 'Venous thromboembolism (VTE) in Europe. The number of VTE events and associated morbidity and mortality' ,*Thrombosis and Haemostasis,* 98(4):756-64.

Colicchia, M., Schrottmaier, W.C., Perrella, G., Reyat, J.S., Begum, J., Slater, A., Price, J., Clark, J.C., Zhi, Z., Simpson, M.J. and Bourne, J.H. (2022) 'S100A8/A9 drives the formation of procoagulant platelets through GPIbα', *Blood, The Journal of the American Society of Hematology*, *140*(24), pp.2626-2643.

Cook, D., Attia, J., Weaver, B., McDonald, E., Meade, M. and Crowther, M. (2000) 'Venous thromboembolic disease: an observational study in medical-surgical intensive care unit patients', *Journal of Critical Care*, *15*(4), pp.127-132.

Cook, D.J. and Crowther, M.A. (2010) 'Thromboprophylaxis in the intensive care unit: Focus on medical–surgical patients', *Critical Care Medicine*, *38*, pp.S76-S82.

Corcos, L., De Anna, D., Dini, M., Macchi, C., Ferrari, P.A. and Dini, S. (2004) 'Histopathology of great saphenous vein valves in primary venous insufficiency', *Phlebolymphology*, *47*, pp.304-311.

Cosemans, J.M., Schols, S.E., Stefanini, L., de Witt, S., Feijge, M.A., Hamulyák, K., Deckmyn, H., Bergmeier, W. and Heemskerk, J.W. (2011) 'Key role of glycoprotein Ib/V/IX and von Willebrand factor in platelet activation-dependent fibrin formation at low shear flow', *Blood, The Journal of the American Society of Hematology*, *117*(2), pp.651-660.

Costa, P.F., Albers, H.J., Linssen, J.E., Middelkamp, H.H., Van Der Hout, L., Passier, R., Van Den Berg, A., Malda, J. and Van Der Meer, A.D. (2017) 'Mimicking arterial thrombosis in a 3D-printed microfluidic in vitro vascular model based on computed tomography angiography data', *Lab on a Chip*, *17*(16), pp.2785-2792.

Cowman, J., Müllers, S., Dunne, E., Ralph, A., Ricco, A.J., Malone, F.D. and Kenny, D. (2017) 'Platelet behaviour on von Willebrand factor changes in pregnancy: consequences of haemodilution and intrinsic changes in platelet function', *Scientific Reports*, *7*(1), p.6354.

Crawley, J.T., de Groot, R., Xiang, Y., Luken, B.M. and Lane, D.A. (2011) 'Unraveling the scissile bond: how ADAMTS13 recognizes and cleaves von Willebrand factor', *Blood, The Journal of the American Society of Hematology*, *118*(12), pp.3212-3221.

Crowther, M.A. and Warkentin, T.E. (2008) 'Bleeding risk and the management of bleeding complications in patients undergoing anticoagulant therapy: focus on new anticoagulant agents', *Blood, The Journal of the American Society of Hematology*, *111*(10), pp.4871-4879.

Cushman, M. (2007) *Epidemiology and risk factors for venous thrombosis*. In Seminars in Hematology, 44(2), pp. 62-69. WB Saunders. doi: 10.1053/j.seminhematol.2007.02.004

Dale, G.L. (2005) 'Coated-platelets: an emerging component of the procoagulant response', *Journal of Thrombosis and Haemostasis*, *3*(10), pp.2185-2192.

Dalsing, M.C. and Kistner, R.L. (2019) *Deep Venous Incompetence and Valve Repair*. In Atlas of Endovascular Venous Surgery (pp. 517-545). Elsevier. doi: 10.1016/B978-0-323-51139-1.00019-X

Das, K. and Biradar, M.S. eds. (2018). *Hypoxia and Anoxia*. BoD–Books on Demand. doi: 10.5772/intechopen.73765.

Das, T. and Stickle, W.B. (1993) 'Sensitivity of crabs Callinectes sapidus and C. similis and the gastropod Stramonita haemastoma to hypoxia and anoxia', *Marine Ecology-Progress Series*, *98*, pp.263-263.

Date, K., Ettelaie, C. and Maraveyas, A. (2017) 'Tissue factor-bearing microparticles and inflammation: a potential mechanism for the development of venous thromboembolism in cancer', *Journal of Thrombosis and Haemostasis*, *15*(12), pp.2289-2299.

Dautaj, A., Krasi, G., Bushati, V., Precone, V., Gheza, M., Fioretti, F., Sartori, M., Costantini, A., Benedetti, S. and Bertelli, M. (2019) 'Hereditary thrombophilia', *Acta Bio Medica: Atenei Parmensis*, *90*(Suppl 10), p.44.

Delbosc, S., Bayles, R.G., Laschet, J., Ollivier, V., Ho-Tin-Noé, B., Touat, Z., Deschildre, C., Morvan, M., Louedec, L., Gouya, L. and Guedj, K. (2017) 'Erythrocyte efferocytosis by the arterial wall promotes oxidation in early-stage atheroma in humans', *Frontiers in Cardiovascular Medicine*, *4*, p.43.

Denorme, F. and Campbell, R.A. (2022) 'Procoagulant platelets: novel players in thromboinflammation', *American Journal of Physiology-Cell Physiology*, *323*(4), pp.C951-C958.

Deppermann, C., Cherpokova, D., Nurden, P., Schulz, J.N., Thielmann, I., Kraft, P., Vögtle, T., Kleinschnitz, C., Dütting, S., Krohne, G. and Eming, S.A. (2013) 'Gray platelet syndrome and defective thrombo-inflammation in Nbeal2-deficient mice', *The Journal of Clinical Investigation*, *123*(8), pp.3331-3342.

DeRoo, E., Zhou, T., Yang, H., Stranz, A., Henke, P. and Liu, B. (2023) 'A vein wall cell atlas of murine venous thrombosis determined by single-cell RNA sequencing', *Communications Biology*, *6*(1), p.130.

Deroy, C., Stovall-Kurtz, N., Nebuloni, F., Soitu, C., Cook, P.R. and Walsh, E.J. (2021) 'Predicting flows through microfluidic circuits with fluid walls', *Microsystems & Nanoengineering*, *7*(1), p.93.

Dexter, L. (1973) 'The chair and venous thrombosis', *Transactions of the American Clinical and Climatological Association*, *84*, pp.1–15.

DeYoung, V., Singh, K. and Kretz, C.A. (2022) 'Mechanisms of ADAMTS13 regulation', *Journal of Thrombosis and Haemostasis*, *20*(12), pp.2722-2732.

Diamond, S.L. (2016) 'Systems analysis of thrombus formation', *Circulation Research*, *118*(9), pp.1348-1362.

Diaz, J.A., Obi, A.T., Myers Jr, D.D., Wrobleski, S.K., Henke, P.K., Mackman, N. and Wakefield, T.W. (2012) 'Critical review of mouse models of venous thrombosis', *Arteriosclerosis, Thrombosis, and Vascular Biology*, *32*(3), pp.556-562.

Diaz, J.A., Farris, D.M., Wrobleski, S.K., Myers, D.D. and Wakefield, T.W. (2015) 'Inferior vena cava branch variations in C57BL/6 mice have an impact on thrombus size in an IVC ligation (stasis) model', *Journal of Thrombosis and Haemostasis*, *13*(4), pp.660-664.

Diaz, J.A., Saha, P., Cooley, B., Palmer, O.R., Grover, S.P., Mackman, N., Wakefield, T.W., Henke, P.K., Smith, A. and Lal, B.K. (2019) 'Choosing a mouse model of venous thrombosis: a consensus assessment of utility and application', *Arteriosclerosis, Thrombosis, and Vascular Biology*, *39*(3), pp.311-318.

Do, H.N., Haldane, A., Levy, R.M. and Miao, Y. (2022) 'Unique features of different classes of G-protein-coupled receptors revealed from sequence coevolutionary and structural analysis', *Proteins: Structure, Function, and Bioinformatics*, *90*(2), pp.601-614.

Dogru, S., Aydemir, D., Salman, N., Ulusu, N.N. and Alaca, B.E. (2020) 'Impact of PDMS surface treatment in cell-mechanics applications', *Journal of the Mechanical Behavior of Biomedical Materials*, *103*, p.103538.

Dong, C., Lee, J., Kim, S., Lai, W., Webb III, E.B., Oztekin, A., Zhang, X.F. and Im, W. (2018) 'Long-ranged protein-glycan interactions stabilize von Willebrand factor A2 domain from mechanical unfolding', *Scientific Reports*, *8*(1), p.16017.

Dörffler-Melly, J., Schwarte, L.A., Ince, C. and Levi, M. (2000) 'Mouse models of focal arterial and venous thrombosis', *Basic Research in Cardiology*, *95*, pp.503-509.

Dorsam, R.T. and Kunapuli, S.P. (2004) 'Central role of the P2Y 12 receptor in platelet activation', *The Journal of Clinical Investigation*, *113*(3), pp.340-345.

Du, Y., Goddi, A., Bortolotto, C., Shen, Y., Dell'Era, A., Calliada, F. and Zhu, L. (2020) 'Wall shear stress measurements based on ultrasound vector flow imaging: theoretical studies and clinical examples', *Journal of Ultrasound in Medicine*, *39*(8), pp.1649-1664.

Duffy, D.C., McDonald, J.C., Schueller, O.J. and Whitesides, G.M. (1998) 'Rapid prototyping of microfluidic systems in poly (dimethylsiloxane)', *Analytical Chemistry*, *70*(23), pp.4974-4984.

Duprat, C., Berthet, H., Wexler, J.S., Du Roure, O. and Lindner, A. (2015) 'Microfluidic in situ mechanical testing of photopolymerized gels', *Lab on a Chip*, *15*(1), pp.244-252.

Dyer, M.R., Chen, Q., Haldeman, S., Yazdani, H., Hoffman, R., Loughran, P., Tsung, A., Zuckerbraun, B.S., Simmons, R.L. and Neal, M.D. (2018) 'Deep vein thrombosis in mice is regulated by platelet HMGB1 through release of neutrophil-extracellular traps and DNA', *Scientific Reports*, *8*(1), p.2068.

Emeis, J.J., Jirouskova, M., MUCHITSCH, E.M., Shet, A.S., Smyth, S.S. and Johnson, G.J. (2007) 'A guide to murine coagulation factor structure, function, assays, and genetic alterations', *Journal of Thrombosis and Haemostasis*, *5*(4), pp.670-679.

Fang, X.Z., Wang, Y.X., Xu, J.Q., He, Y.J., Peng, Z.K. and Shang, Y. (2021) 'Immunothrombosis in acute respiratory dysfunction of COVID-19', *Frontiers in Immunology*, *12*, p.651545.

Feitsma, L.J., Brondijk, H.C., Jarvis, G.E., Hagemans, D., Bihan, D., Jerah, N., Versteeg, M., Farndale, R.W. and Huizinga, E.G. (2022) 'Structural insights into collagen binding by platelet receptor glycoprotein VI', *Blood, The Journal of the American Society of Hematology*, *139*(20), pp.3087-3098.

Fiddes, L.K., Raz, N., Srigunapalan, S., Tumarkan, E., Simmons, C.A., Wheeler, A.R. and Kumacheva, E. (2010) 'A circular cross-section PDMS microfluidics system for replication of cardiovascular flow conditions', *Biomaterials*, *31*(13), pp.3459-3464.

Fogelson, A.L. and Neeves, K.B. (2015) 'Fluid mechanics of blood clot formation', *Annual Review of Fluid Mechanics*, *47*, pp.377-403.

Franchini, M. and Mannucci, P.M. (2008) 'Venous and arterial thrombosis: different sides of the same coin?', *European Journal of Internal Medicine*, *19*(7), pp.476-481.

Fredrickson, B.J., Dong, J.F., McIntire, L.V. and López, J.A. (1998) 'Shear-dependent rolling on von Willebrand factor of mammalian cells expressing the platelet glycoprotein Ib-IX-V complex', *Blood, The Journal of the American Society of Hematology*, *92*(10), pp.3684-3693.

Galanaud, J.P., Laroche, J.P. and Righini, M. (2013) 'The history and historical treatments of deep vein thrombosis', *Journal of Thrombosis and Haemostasis*, *11*(3), pp.402-411.

Galbraith, K., Collin, J., Morris, P.J. and Wood, R.F. (1985) 'Recent experience with arterial embolism of the limbs in a vascular unit', *Annals of the Royal College of Surgeons of England*, *67*(1), p.30–33.

Galson, S.K. (2008) 'Prevention of deep vein thrombosis and pulmonary embolism', *Public Health Reports*, *123*(4), pp.420-421.

Ganzenmüller, G.C.; Steinhauser, M.O.; Van Liedekerke, P.; Leuven, K.U. (2011) 'The implementation of Smooth Particle Hydrodynamics in LAMMPS', *Paul Van Liedekerke Kathol. Univ. Leuven*, *1*, 1–26.

Gershom, E.S., Sutherland, M.R., Lollar, P. and Pryzdial, E.L.G. (2010) 'Involvement of the contact phase and intrinsic pathway in herpes simplex virus-initiated plasma coagulation', *Journal of Thrombosis and Haemostasis*, *8*(5), pp.1037-1043.

Gil, M.R. (2019) *Overview of the coagulation system*. In Transfusion Medicine and Hemostasis (pp. 559-564). Elsevier. DOI: 10.1016/B978-0-12-813726-0.00091-X

Gingold, R.A. and Monaghan, J.J. (1977) 'Smoothed particle hydrodynamics: theory and application to non-spherical stars', *Monthly Notices of the Royal Astronomical Society*, *181*(3), pp.375-389.

Ginsberg, M.H. (2014) 'Integrin activation', *BMB reports*, *47*(12), p.655–659. doi: 10.5483/bmbrep.2014.47.12.241

Godat, L.N., Haut, E.R., Moore, E.E., Knudson, M.M. and Costantini, T.W. (2023) 'Venous thromboembolism risk after spinal cord injury: A secondary analysis of the CLOTT study', *Journal of Trauma and Acute Care Surgery*, *94*(1), pp.23-29.

Goudswaard, L.J., Williams, C.M., Khalil, J., Burley, K.L., Hamilton, F., Arnold, D., Milne, A., Lewis, P.A., Heesom, K.J., Mundell, S.J. and Davidson, A.D. (2023) 'Alterations in platelet proteome signature and impaired platelet integrin αIIbβ3 activation in patients with COVID-19', *Journal of Thrombosis and Haemostasis*, *21*(5), pp.1307-1321.

Van De Graaff, E. and Steinhubl, S.R. (2001) 'Complications of oral antiplatelet medications', *Current Cardiology Reports*, *3*(5), pp.371-379.

Green, D. (2006) 'Coagulation cascade', *Hemodialysis International*, *10*(S2), pp.S2-S4. DOI: 10.1111/j.1542-4758.2006.00119.x

Grimsey, N., Soto, A.G. and Trejo, J. (2011) 'Regulation of protease-activated receptor signaling by post-translational modifications', *IUBMB life*, *63*(6), pp.403-411.

Grisanti, G. *et al.* (2021) 'A microfluidic platform for cavitation-enhanced drug delivery', *Micromachines*, 12(6), pp. 1–17. doi: 10.3390/mi12060658.

de Groot, P.G. and Sixma, J.J. (1997) 'Role of glycoprotein IIb: IIIa in the adhesion of platelets to collagen under flow conditions', *Blood*, *89*(5), pp.1837-1837.

Guerrero, J.A., Bennett, C., van der Weyden, L., McKinney, H., Chin, M., Nurden, P., McIntyre, Z., Cambridge, E.L., Estabel, J., Wardle-Jones, H. and Speak, A.O. (2014) 'Gray platelet syndrome: proinflammatory megakaryocytes and α-granule loss cause myelofibrosis and confer metastasis resistance in mice', *Blood, The Journal of the American Society of Hematology*, *124*(24), pp.3624-3635.

Guevara-Pantoja, P.E., Jiménez-Valdés, R.J., García-Cordero, J.L. and Caballero-Robledo, G.A., (2018) 'Pressure-actuated monolithic acrylic microfluidic valves and pumps', *Lab on a Chip*, *18*(4), pp.662-669.

Hally, K., Fauteux-Daniel, S., Hamzeh-Cognasse, H., Larsen, P. and Cognasse, F. (2020) Revisiting 'platelets and toll-like receptors (TLRs): at the interface of vascular immunity and thrombosis', *International Journal of Molecular Sciences*, *21*(17), p.6150.

Hamer, J.D., Malone, P.C. and Silver, I.A. (1981) 'The PO2 in venous valve pockets: its possible bearing on thrombogenesis', *British Journal of Surgery*, *68*(3), pp.166-170.

Hamilton, S.F., Miller, M.W., Thompson, C.A. and Dale, G.L. (2004) 'Glycoprotein IIb/IIIa inhibitors increase COAT-platelet production in vitro', *Journal of Laboratory and Clinical Medicine*, *143*(5), pp.320-326.

Han, X., Nieman, M.T. and Kerlin, B.A. (2021) 'Protease-activated receptors: An illustrated review', *Research and Practice in Thrombosis and Haemostasis*, *5*(1), pp.17-26.

Heemskerk, J.W.M., Mattheij, N.J.A. and Cosemans, J.M.E.M. (2013) 'Platelet-based coagulation: different populations, different functions', *Journal of Thrombosis and Haemostasis*, *11*(1), pp.2-16.

Heit, J.A. (2008) 'The epidemiology of venous thromboembolism in the community', *Arteriosclerosis, Thrombosis, and Vascular Biology*, *28*(3), pp.370-372.

Heit, J.A., Silverstein, M.D., Mohr, D.N., Petterson, T.M., O'Fallon, W.M. and Melton, L.J. (1999) 'Predictors of survival after deep vein thrombosis and pulmonary embolism: a population-based, cohort study', *Archives of Internal Medicine*, *159*(5), pp.445-453.

Heit, J.A., Spencer, F.A. and White, R.H. (2016) 'The epidemiology of venous thromboembolism', *Journal of Thrombosis and Thrombolysis*, *41*, pp.3-14.

Heit, J.A., O'Fallon, W.M., Petterson, T.M., Lohse, C.M., Silverstein, M.D., Mohr, D.N. and Melton, L.J. (2002) 'Relative impact of risk factors for deep vein thrombosis and pulmonary embolism: a population-based study', *Archives of Internal Medicine*, *162*(11), pp.1245-1248.

Hemmatgir, F., Koupaei, N. and Poorazizi, E. (2022) 'Characterization of a novel semi-interpenetrating hydrogel network fabricated by polyethylene glycol diacrylate/polyvinyl alcohol/tragacanth gum as a wound dressing', *Burns*, *48*(1), pp.146-155.

Henke, P.K. and Wakefield, T. (2009) 'Thrombus resolution and vein wall injury: dependence on chemokines and leukocytes', *Thrombosis Research*, *123*, pp.S72-S78.

Herrmann, K. (2019) *Refinement on the way towards replacement: Are we doing what we can?*. In Animal experimentation: Working towards a paradigm change (pp. 3-64). Brill. doi:10.1163/9789004391192_002

Hoffman, M. (2003) 'Remodeling the blood coagulation cascade', *Journal of Thrombosis and Thrombolysis*, *16*, pp.17-20.

Hou, G., Wang, J. and Layton, A. (2012) 'Numerical methods for fluid-structure interaction—a review', *Communications in Computational Physics*, *12*(2), pp.337-377.

Houghton, D.E., Ashrani, A., Liedl, D., Mehta, R.A., Hodge, D.O., Rooke, T., Wennberg, P., Wysokinski, W. and McBane, R. (2021) 'Reduced calf muscle pump function is a risk factor for venous thromboembolism: a population-based cohort study', *Blood, The Journal of the American Society of Hematology*, *137*(23), pp.3284-3290.

Hu, X., Li, Y., Li, J. and Chen, H. (2020) 'Effects of altered blood flow induced by the muscle pump on thrombosis in a microfluidic venous valve model', *Lab on a Chip*, *20*(14), pp.2473-2481.

Huang, J., Li, X., Shi, X., Zhu, M., Wang, J., Huang, S., Huang, X., Wang, H., Li, L., Deng, H. and Zhou, Y. (2019) 'Platelet integrin αIIbβ3: signal transduction, regulation, and its therapeutic targeting', *Journal of Hematology & Oncology*, *12*, pp.1-22.

Huffman, J.E., De Vries, P.S., Morrison, A.C., Sabater-Lleal, M., Kacprowski, T., Auer, P.L., Brody, J.A., Chasman, D.I., Chen, M.H., Guo, X. and Lin, L.A. (2015) 'Rare and low-frequency variants and their association with plasma levels of fibrinogen, FVII, FVIII, and vWF', *Blood, The Journal of the American Society of Hematology*, *126*(11), pp.e19-e29.

Hunt, B.J. (2009) 'The prevention of hospital-acquired venous thromboembolism in the United Kingdom', *British Journal of Haematology*, *144*(5), pp.642-652.

Italiano Jr, J.E., Bergmeier, W., Tiwari, S., Falet, H., Hartwig, J.H., Hoffmeister, K.M., André, P., Wagner, D.D. and Shivdasani, R.A. (2003) 'Mechanisms and implications of platelet discoid shape', *Blood*, *101*(12), pp.4789-4796.

Jackson, S.P., Nesbitt, W.S. and Westein, E. (2009) 'Dynamics of platelet thrombus formation', *Journal of thrombosis and Haemostasis*, *7*, pp.17-20.

Jagadeeswaran, P., Cooley, B.C., Gross, P.L. and Mackman, N. (2016) 'Animal models of thrombosis from zebrafish to nonhuman primates: use in the elucidation of new pathologic pathways and the development of antithrombotic drugs', *Circulation Research*, *118*(9), pp.1363-1379.

Jain, A., Barrile, R., van der Meer, A.D., Mammoto, A., Mammoto, T., De Ceunynck, K., Aisiku, O., Otieno, M.A., Louden, C.S., Hamilton, G.A. and Flaumenhaft, R. (2018) 'Primary human lung alveolus-on-a-chip model of intravascular thrombosis for assessment of therapeutics', *Clinical Pharmacology & Therapeutics*, *103*(2), pp.332-340.

Jagadeeswaran, P., Kulkarni, V., Carrillo, M. and Kim, S. (2007) 'Zebrafish: from hematology to hydrology', *Journal of Thrombosis and Haemostasis*, *5*, pp.300-304.

Jagadeeswaran, P., Cooley, B.C., Gross, P.L. and Mackman, N. (2016) 'Animal models of thrombosis from zebrafish to nonhuman primates: use in the elucidation of new pathologic pathways and the development of antithrombotic drugs', *Circulation Research*, *118*(9), pp.1363-1379.

Jennings, L.K. and Phillips, D.R. (1982) 'Purification of glycoproteins IIb and III from human platelet plasma membranes and characterization of a calcium-dependent glycoprotein IIb-III complex', *Journal of Biological Chemistry*, *257*(17), pp.10458-10466.

Jin, N.Z. and Gopinath, S.C. (2016) 'Potential blood clotting factors and anticoagulants', Biomedicine *& Pharmacotherapy*, *84*, pp.356-365.

Jouda, H., Larrea Murillo, L. and Wang, T. (2022) 'Current progress in vascular engineering and its clinical applications', *Cells*, *11*(3), p.493.

Juárez-Moreno, J.A., Ávila-Ortega, A., Oliva, A.I., Avilés, F. and Cauich-Rodríguez, J.V. (2015) 'Effect of wettability and surface roughness on the adhesion properties of collagen on PDMS films treated by capacitively coupled oxygen plasma', *Applied Surface Science*, *349*, pp.763-773.

Jurk, K., and Kehrel, B. E. (2005) 'Platelets: physiology and biochemistry', *Seminars in Thrombosis and Hemostasis*, *31*(4), 381–392. Doi: 10.1055/s-2005-916671.

Kang, C., Bonneau, M., Brouland, J.P., dit Sollier, C.B. and Drouet, L. (2003) 'In vivo pig models of venous thrombosis mimicking human disease', *Thrombosis and Haemostasis*, *89*(02), pp.256-263.

Kang, I., Raghavachari, M., Hofmann, C.M. and Marchant, R.E. (2007) 'Surface-dependent expression in the platelet GPIb binding domain within human von Willebrand factor studied by atomic force microscopy', *Thrombosis Research*, *119*(6), pp.731-740.

Kanke, M., Matsueda, G.R., Strauss, H.W., Yasuda, T., Liau, C.S. and Khaw, B.A. (1991) 'Localization and visualization of pulmonary emboli with radiolabeled fibrin-specific monoclonal antibody', *Journal of Nuclear Medicine*, *32*(6), pp.1254-1260.

Kattula, S., Byrnes, J.R. and Wolberg, A.S. (2017) 'Fibrinogen and fibrin in hemostasis and thrombosis', *Arteriosclerosis, Thrombosis, and Vascular Biology*, *37*(3), pp.e13-e21.

Kemp, M., Chan, A.H.Y., Harrison, J., Rogers, H., Zhao, A., Kaur, H., Tang, G., Yang, E. and Beyene, K. (2023) 'Formal and informal venous thromboembolism risk assessment and impact on prescribing of thromboprophylaxis: a retrospective cohort study', *International Journal of Clinical Pharmacy*, pp.1-11.

Khan, F., Tritschler, T., Kahn, S.R. and Rodger, M.A. (2021) 'Venous thromboembolism', *The Lancet*, *398*(10294), pp.64-77.

Khursigara, M.R., Schlam, D., Noone, D.G., Bruno, V., Ortiz-Sandoval, C.G., Pluthero, F.G., Kahr, W.H., Bowman, M.L., James, P., Grinstein, S. and Licht, C. (2020) 'Vascular endothelial cells evade complement-mediated membrane injury via Weibel-Palade body mobilization', *Journal of Thrombosis and Haemostasis*, *18*(6), pp.1484-1494.

Klaeske, K., Brade, A., Eifert, S., Jawad, K., Saeed, D., Haunschild, J., Sieg, F., Borger, M.A. and Dieterlen, M.T. (2023) 'The Glycoprotein (GP) Ib-IX-V Complex on Platelets: GPIbα Protein Expression Is Reduced in HeartMate 3 Patients with Bleeding Complications within the First 3 Months', *International Journal of Molecular Sciences*, *24*(6), p.5639.

Knight, L.C., Baidoo, K.E., Romano, J.E., Gabriel, J.L. and Maurer, A.H. (2000) 'Imaging pulmonary emboli and deep venous thrombi with 99mTc-bitistatin, a platelet-binding polypeptide from viper venom', *Journal of Nuclear Medicine*, *41*(6), pp.1056-1064.

Knight, L.C., Maurer, A.H. and Romano, J.E. (1996) 'Comparison of iodine-123-disintegrins for imaging thrombi and emboli in a canine model', *Journal of Nuclear Medicine*, *37*(3), pp.476-482.

Kocherova, I., Bryja, A., Mozdziak, P., Angelova Volponi, A., Dyszkiewicz-Konwińska, M., Piotrowska-Kempisty, H., Antosik, P., Bukowska, D., Bruska, M., Iżycki, D. and Zabel, M. (2019) 'Human umbilical vein endothelial cells (HUVECs) co-culture with osteogenic cells: from molecular communication to engineering prevascularised bone grafts', *Journal of Clinical Medicine*, *8*(10), p.1602.

Kot, M., Nagahashi, H. and Szymczak, P. (2015) 'Elastic moduli of simple mass spring models', *The Visual Computer*, *31*, pp.1339-1350.

Kuipers, S., Schreijer, A.J.M., Cannegieter, S.C., Büller, H.R., Rosendaal, F.R. and Middeldorp, S. (2007) 'Travel and venous thrombosis: a systematic review', *Journal of Internal Medicine*, *262*(6), pp.615-634.

Lapointe, C., Vincent, L., Giguère, H., Auger-Messier, M., Schwertani, A., Jin, D., Takai, S., Pejler, G., Sirois, M.G., Tinel, H. and Heitmeier, S. (2023) 'Chymase Inhibition Resolves and Prevents Deep Vein Thrombosis Without Increasing Bleeding Time in the Mouse Model', *Journal of the American Heart Association*, *12*(4), p.e028056.

Lavon, O. and Tamir, T. (2022) 'Evaluation of the Padua Prediction Score ability to predict venous thromboembolism in Israeli non-surgical hospitalized patients using electronic medical records', *Scientific Reports*, *12*(1), p.6121.

Lecut, C., Schoolmeester, A., Kuijpers, M.J., Broers, J.L., van Zandvoort, M.A., Vanhoorelbeke, K., Deckmyn, H., Jandrot-Perrus, M. and Heemskerk, J.W. (2004) 'Principal role of glycoprotein VI in α2β1 and αIIbβ3 activation during collagen-induced thrombus formation', *Arteriosclerosis, Thrombosis, and Vascular Biology*, *24*(9), pp.1727-1733.

Lee, E.S., Moulinec, C., Xu, R., Violeau, D., Laurence, D. and Stansby, P. (2008) 'Comparisons of weakly compressible and truly incompressible algorithms for the SPH mesh free particle method', *Journal of Computational Physics*, *227*(18), pp.8417-8436.

Lee, M., Rodansky, E.S., Smith, J.K. and Rodgers, G.M. (2012) 'ADAMTS13 promotes angiogenesis and modulates VEGF-induced angiogenesis', *Microvascular Research*, *84*(2), pp.109-115.

Lehmann, M., Schoeman, R.M., Krohl, P.J., Wallbank, A.M., Samaniuk, J.R., Jandrot-Perrus, M. and Neeves, K.B. (2018) 'Platelets drive thrombus propagation in a hematocrit and glycoprotein VI–dependent manner in an in vitro venous thrombosis model', *Arteriosclerosis, Thrombosis, and Vascular Biology*, *38*(5), pp.1052-1062.

Li, S.H. and Hui, R.T. (2009) 'Reduced contractile capacity of vascular smooth muscle: Another mechanism of hypertension?', *Medical Hypotheses*, *73*(1), pp.62-64.

Libby, P. and Simon, D.I. (2001) 'Inflammation and thrombosis: the clot thickens', *Circulation*, *103*(13), pp.1718-1720.

Libby, P. and Hansson, G.K. (2019) 'From focal lipid storage to systemic inflammation: JACC review topic of the week', *Journal of the American College of Cardiology*, *74*(12), pp.1594-1607.

Litvinov, R.I. and Weisel, J.W. (2023) 'Blood clot contraction: Mechanisms, pathophysiology, and disease', *Research and Practice in Thrombosis and Haemostasis*, *7*(1), p.100023.

Liu, X., Sun, L., Wang, M., Li, B. and Liu, L. (2020) 'Modeling and Simulation of Valve Cycle in Vein Using an Immersed Finite Element Method', *CMES-Computer Modeling in Engineering & Sciences*, *123*(1) pp. 153–183.

Leclerc, E., Sakai, Y. and Fujii, T. (2003) 'Cell culture in 3-dimensional microfluidic structure of PDMS (polydimethylsiloxane)', *Biomedical Microdevices*, *5*, pp.109-114.

Lehmann, M., Schoeman, R.M., Krohl, P.J., Wallbank, A.M., Samaniuk, J.R., Jandrot-Perrus, M. and Neeves, K.B. (2018) 'Platelets drive thrombus propagation in a hematocrit and glycoprotein VI–dependent manner in an in vitro venous thrombosis model', *Arteriosclerosis, Thrombosis, and Vascular Biology*, *38*(5), pp.1052-1062.

Liu, G.R. and Liu, M.B. (2003) *Smoothed particle hydrodynamics: a meshfree particle method*. World scientific, Singapore.

Liu, X. and Liu, L. (2019) 'Effect of valve lesion on venous valve cycle: A modified immersed finite element modeling', *PLoS One*, *14*(3), p.e0213012.

López, J.A. and Chen, J. (2009) 'Pathophysiology of venous thrombosis', *Thrombosis Research*, *123*, pp.S30-S34.

Lowe, G.D. (2003) 'Virchow's triad revisited: abnormal flow', *Pathophysiology of Haemostasis and Thrombosis*, *33*(5-6), pp.455-457.

Lu, J., Zhang, C., Shi, S., Li, S., Liu, J., Wu, J., Huang, C. and Lei, M. (2023) 'Stoichiometry and architecture of the platelet membrane complex glycoprotein Ib-IX-V', *Biological Chemistry*, (0). DOI: 10.1515/hsz-2022-0227.

Lucy, L.B. (1977) 'A numerical approach to the testing of the fission hypothesis', *Astronomical Journal, vol. 82, Dec. 1977, p. 1013-1024.*, *82*, pp.1013-1024.

Lurie, F., Kistner, R.L., Eklof, B. and Kessler, D. (2003) 'Mechanism of venous valve closure and role of the valve in circulation: a new concept', *Journal of Vascular Surgery*, *38*(5), pp.955-961.

Lurie, J.M., Png, C.M., Subramaniam, S., Chen, S., Chapman, E., Aboubakr, A., Marin, M., Faries, P. and Ting, W. (2019) 'Virchow's triad in "silent" deep vein thrombosis', *Journal of Vascular Surgery: Venous and Lymphatic Disorders*, *7*(5), pp.640-645.

Lutsey, P.L. and Zakai, N.A. (2023) 'Epidemiology and prevention of venous thromboembolism', *Nature Reviews Cardiology*, *20*(4), pp.248-262.

Ma, Y.Q., Qin, J. and Plow, E.F. (2007) 'Platelet integrin αIIbβ3: activation mechanisms', *Journal of Thrombosis and Haemostasis*, *5*(7), pp.1345-1352.

MacColl, E. and Khalil, R.A. (2015) 'Matrix metalloproteinases as regulators of vein structure and function: implications in chronic venous disease', *Journal of Pharmacology and Experimental Therapeutics*, *355*(3), pp.410-428.

Machlus, K.R. and Italiano Jr, J.E. (2013) 'The incredible journey: From megakaryocyte development to platelet formation', *Journal of Cell Biology*, *201*(6), pp.785-796.

MacInnes, D.C. and Miller, K.M. (1984) 'Fatal coronary artery thrombosis associated with cannabis smoking', *The Journal of the Royal College of General Practitioners*, *34*(267), p.575.

Mackman, N. (2008) 'Triggers, targets and treatments for thrombosis', *Nature*, *451*(7181), pp.914-918.

Mackman, N. (2012) 'New insights into the mechanisms of venous thrombosis', *The Journal of clinical investigation*, *122*(7), pp.2331-2336.

Malone, P.C. and Agutter, P.S. (2016) 'Deep venous thrombosis: the valve cusp hypoxia thesis and its incompatibility with modern orthodoxy', *Medical Hypotheses*, *86*, pp.60-66.

Mammadova-Bach, E., Gil-Pulido, J., Sarukhanyan, E., Burkard, P., Shityakov, S., Schonhart, C., Stegner, D., Remer, K., Nurden, P., Nurden, A.T. and Dandekar, T. (2020) 'Platelet glycoprotein VI promotes metastasis through interaction with cancer cell–derived galectin-3', *Blood, The Journal of the American Society of Hematology*, *135*(14), pp.1146-1160.

Marom, G. (2015) 'Numerical methods for fluid–structure interaction models of aortic valves', *Archives of Computational Methods in Engineering*, *22*, pp.595-620.

Martin-Ventura, J.L., Rodrigues-Diez, R., Martinez-Lopez, D., Salaices, M., Blanco-Colio, L.M. and Briones, A.M. (2017) 'Oxidative stress in human atherothrombosis: sources, markers and therapeutic targets', *International journal of molecular sciences*, *18*(11), p.2315.

Martin, C., Morales, L.D. and Cruz, M.A. (2007) 'Purified A2 domain of von Willebrand factor binds to the active conformation of von Willebrand factor and blocks the interaction with platelet glycoprotein Ibα', *Journal of Thrombosis and Haemostasis*, *5*(7), pp.1363-1370.

Martínez-Revelles, S., García-Redondo, A.B., Avendaño, M.S., Varona, S., Palao, T., Orriols, M., Roque, F.R., Fortuño, A., Touyz, R.M., Martínez-González, J. and Salaices, M. (2017) 'Lysyl oxidase induces vascular oxidative stress and contributes to arterial stiffness and abnormal elastin structure in hypertension: role of p38MAPK', *Antioxidants & Redox Signaling*, *27*(7), pp.379-397.

Massberg, S., Brand, K., Grüner, S., Page, S., Müller, E., Müller, I., Bergmeier, W., Richter, T., Lorenz, M., Konrad, I. and Nieswandt, B. (2002) 'A critical role of platelet adhesion in the initiation of atherosclerotic lesion formation', *The Journal of Experimental Medicine*, *196*(7), pp.887-896.

Mathur, T., Singh, K.A., Pandian, N.K., Tsai, S.H., Hein, T.W., Gaharwar, A.K., Flanagan, J.M. and Jain, A. (2019) 'Organ-on-chips made of blood: endothelial progenitor cells from blood reconstitute vascular thromboinflammation in vessel-chips', *Lab on a Chip*, *19*(15), pp.2500-2511.

Makhsin, S.R., Goddard, N.J., Gupta, R., Gardner, P. and Scully, P.J. (2020) 'Optimization synthesis and biosensing performance of an acrylate-based hydrogel as an optical waveguiding sensing film', *Analytical Chemistry*, *92*(22), pp.14907-14914.

Maxwell, M.J., Westein, E., Nesbitt, W.S., Giuliano, S., Dopheide, S.M. and Jackson, S.P. (2007) 'Identification of a 2-stage platelet aggregation process mediating shear-dependent thrombus formation', *Blood*, *109*(2), pp.566-576.

Mazzolai, L., Aboyans, V., Ageno, W., Agnelli, G., Alatri, A., Bauersachs, R., Brekelmans, M.P., Büller, H.R., Elias, A., Farge, D. and Konstantinides, S. (2018) 'Diagnosis and management of acute deep vein thrombosis: a joint consensus document from the European Society of Cardiology working groups of aorta and peripheral vascular diseases and pulmonary circulation and right ventricular function', *European Heart Journal*, *39*(47), pp.4208-4218.

Mazzolai, L., Ageno, W., Alatri, A., Bauersachs, R., Becattini, C., Brodmann, M., Emmerich, J., Konstantinides, S., Meyer, G., Middeldorp, S. and Monreal, M. (2022) 'Second consensus document on diagnosis and management of acute deep vein thrombosis: updated document elaborated by the ESC Working Group on aorta and peripheral vascular diseases and the ESC Working Group on pulmonary circulation and right ventricular function', *European Journal of Preventive Cardiology*, *29*(8), pp.1248-1263.

Mccarty, O.J., Calaminus, S.D.J., Berndt, M.C., Machesky, L.M. and Watson, S.P. (2006) 'von Willebrand factor mediates platelet spreading through glycoprotein Ib and αIIbβ3 in the presence of botrocetin and ristocetin, respectively', *Journal of Thrombosis and Haemostasis*, *4*(6), pp.1367-1378.

McLachlin, A.D., McLachlin, J.A., Jory, T.A. and Rawling, E.G. (1960) 'Venous stasis in the lower extremities', *Annals of Surgery*, *152*(4), p.678.

McLendon, K., Goyal, A. and Attia, M. (2023) *Deep venous thrombosis risk factors*. Treasure Island (FL): StatPearls Publishing.

Medina-Leyte, D.J., Domínguez-Pérez, M., Mercado, I., Villarreal-Molina, M.T. and Jacobo-Albavera, L. (2020) 'Use of human umbilical vein endothelial cells (HUVEC) as a model to study cardiovascular disease: A review', *Applied Sciences*, *10*(3), p.938.

Meissner, M.H., Gloviczki, P., Bergan, J., Kistner, R.L., Morrison, N., Pannier, F., Pappas, P.J., Rabe, E., Raju, S. and Villavicencio, J.L. (2007) 'Primary chronic venous disorders', *Journal of Vascular Surgery*, *46*(6), pp.S54-S67.

Michelson, A.D. and Barnard, M.R. (1987) 'Thrombin-induced changes in platelet membrane glycoproteins Ib, IX, and IIb-IIIa complex', *Blood. American Society of Hematology,* 70(5), pp. 1673–1678.

Miziara, I.D., Magalhães, A.T.D.M., Santos, M.D.A., Gomes, É.F. and Oliveira, R.A.D. (2012) 'Ética da pesquisa em modelos animais', *Brazilian Journal of Otorhinolaryngology*, *78*, pp.128-131.

Mohammed, A.M., Ariane, M. and Alexiadis, A. (2020) 'Using discrete multiphysics modelling to assess the effect of calcification on hemodynamic and mechanical deformation of aortic valve', *ChemEngineering*, *4*(3), p.48.

Monaghan, J.J. (1994) 'Simulating free surface flows with SPH', *Journal of Computational Physics*, *110*(2), pp.399-406.

Monroe, D.M., Hoffman, M. and Roberts, H.R. (2002) 'Platelets and thrombin generation', *Arteriosclerosis, Thrombosis, and Vascular Biology*, *22*(9), pp.1381-1389.

Morris, J.P., Fox, P.J. and Zhu, Y. (1997) 'Modeling low Reynolds number incompressible flows using SPH', *Journal of Computational Physics*, *136*(1), pp.214-226.

Muthard, R.W. and Diamond, S.L. (2013) 'Side view thrombosis microfluidic device with controllable wall shear rate and transthrombus pressure gradient', *Lab on a Chip*, *13*(10), pp.1883-1891.

Nauli, S.M., Kawanabe, Y., Kaminski, J.J., Pearce, W.J., Ingber, D.E. and Zhou, J. (2008) 'Endothelial cilia are fluid shear sensors that regulate calcium signaling and nitric oxide production through polycystin-1', *Circulation*, *117*(9), pp.1161-1171.

Nesbitt, W.S., Westein, E., Tovar-Lopez, F.J., Tolouei, E., Mitchell, A., Fu, J., Carberry, J., Fouras, A. and Jackson, S.P. (2009) 'A shear gradient–dependent platelet aggregation mechanism drives thrombus formation', *Nature Medicine*, *15*(6), pp.665-673.

Neubauer, K. and Zieger, B. (2022) 'Endothelial cells and coagulation', *Cell and Tissue Research*, *387*(3), pp.391-398.

Ng, K.C., Alexiadis, A., Chen, H. and Sheu, T.W.H. (2020) 'A coupled smoothed particle hydrodynamics-volume compensated particle method (SPH-VCPM) for fluid structure interaction (FSI) modelling', *Ocean Engineering*, *218*, p.107923.

Nieswandt, B., Brakebusch, C., Bergmeier, W., Schulte, V., Bouvard, D., Mokhtari-Nejad, R., Lindhout, T., Heemskerk, J.W., Zirngibl, H. and Fässler, R. (2001) 'Glycoprotein VI but not α2β1

integrin is essential for platelet interaction with collagen', *The EMBO Journal*, *20*(9), pp.2120-2130.

Nieswandt, B. and Watson, S.P. (2003) 'Platelet-collagen interaction: is GPVI the central receptor?', *Blood*, *102*(2), pp.449-461.

Nishiwaki, S., Morita, Y., Yamashita, Y., Morimoto, T., Amano, H., Takase, T., Hiramori, S., Kim, K., Oi, M., Akao, M. and Kobayashi, Y. (2021) 'Impact of no, distal, and proximal deep vein thrombosis on clinical outcomes in patients with acute pulmonary embolism: from the COMMAND VTE registry', *Journal of cardiology*, 77(4), pp.395-403.

Nuñez-Borque, E., Fernandez-Bravo, S., Yuste-Montalvo, A. and Esteban, V. (2022) 'Pathophysiological, cellular, and molecular events of the vascular system in anaphylaxis', *Frontiers in Immunology*, *13*, p.836222.

O'Brien, J., Duncan, H., Kirsh, G., Allen, V., King, P., Hargraves, R., Mendes, L., Perera, T., Catto, P., Schofield, S. and Ploschke, H. (2000) 'Prevention of pulmonary embolism and deep vein thrombosis with low dose aspirin: Pulmonary Embolism Prevention (PEP) trial', *Lancet*, *355*(9212).

Ormiston, M.L., Toshner, M.R., Kiskin, F.N., Huang, C.J., Groves, E., Morrell, N.W. and Rana, A.A. (2015) 'Generation and culture of blood outgrowth endothelial cells from human peripheral blood', *JoVE (Journal of Visualized Experiments)*, (106), p.e53384.

Pandian, N.K., Mannino, R.G., Lam, W.A. and Jain, A. (2018) 'Thrombosis-on-a-chip: Prospective impact of microphysiological models of vascular thrombosis', *Current Opinion in Biomedical Engineering*, *5*, pp.29-34.

Panteleev, M.A., Korin, N., Reesink, K.D., Bark, D.L., Cosemans, J.M., Gardiner, E.E. and Mangin, P.H. (2021) 'Wall shear rates in human and mouse arteries: Standardization of hemodynamics for in vitro blood flow assays: Communication from the ISTH SSC subcommittee on biorheology', *Journal of Thrombosis and Haemostasis*, *19*(2), pp.588-595.

Pascual, M., Kerdraon, M., Rezard, Q., Jullien, M.C. and Champougny, L. (2019) 'Wettability patterning in microfluidic devices using thermally-enhanced hydrophobic recovery of PDMS', *Soft Matter*, *15*(45), pp.9253-9260.

Patrono, C., Morais, J., Baigent, C., Collet, J.P., Fitzgerald, D., Halvorsen, S., Rocca, B., Siegbahn, A., Storey, R.F. and Vilahur, G. (2017) 'Antiplatelet agents for the treatment and prevention of coronary atherothrombosis', *Journal of the American College of Cardiology*, *70*(14), pp.1760-1776.

Payne, H. and Brill, A. (2017) 'Stenosis of the inferior vena cava: a murine model of deep vein thrombosis', *JoVE (Journal of Visualized Experiments)*, (130), p.e56697.

Payne, H., Ponomaryov, T., Watson, S.P. and Brill, A. (2017) 'Mice with a deficiency in CLEC-2 are protected against deep vein thrombosis', *Blood, The Journal of the American Society of Hematology*, *129*(14), pp.2013-2020.

Pazdniakou, A. and Adler, P.M. (2012) 'Lattice spring models', *Transport in Porous Media*, *93*(2), pp.243-262.

Phillips, M.N., Jones, G.T., Van Rij, A.M. and Zhang, M. (2004) 'Micro-venous valves in the superficial veins of the human lower limb', *Clinical Anatomy: The Official Journal of the American Association of Clinical Anatomists and the British Association of Clinical Anatomists*, *17*(1), pp.55-60.

Plimpton, S. (1995) 'Fast parallel algorithms for short-range molecular dynamics', *Journal of Computational Physics*, *117*(1), pp.1-19.

Pohl, A., Spaulding, A.C., Brennan, E.R., Stauffer, J., Hussain, W.A., Muraleedharan, D., Colibaseanu, D.T. and Edwards, M.A. (2023) 'Risk adjusted venous thromboembolism prophylaxis following pancreatic surgery', *Journal of Thrombosis and Thrombolysis*, (55), pp.604-616.

Ponomaryov, T., Payne, H., Fabritz, L., Wagner, D.D. and Brill, A. (2017) 'Mast cells granular contents are crucial for deep vein thrombosis in mice', *Circulation Research*, *121*(8), pp.941-950.

Potters, W.V., Marquering, H.A., VanBavel, E. and Nederveen, A.J. (2014) 'Measuring wall shear stress using velocity-encoded MRI', *Current Cardiovascular Imaging Reports*, *7*, 9257.

Prandoni, P. (2009) 'Venous and arterial thrombosis: two aspects of the same disease?', *Clinical Epidemiology*, pp.1-6.

Prescott, M.J. and Lidster, K. (2017) 'Improving quality of science through better animal welfare: the NC3Rs strategy', *Lab Animal*, *46*(4), pp.152-156.

Pugsley, M.K. and Tabrizchi, R. (2000) 'The vascular system: An overview of structure and function', *Journal of Pharmacological and Toxicological Methods*, *44*(2), pp.333-340.

Pusztaszeri, M.P., Seelentag, W. and Bosman, F.T. (2006) 'Immunohistochemical expression of endothelial markers CD31, CD34, von Willebrand factor, and Fli-1 in normal human tissues', *Journal of Histochemistry & Cytochemistry*, *54*(4), pp.385-395.

Qiu Y, Ahn B, Sakurai Y, Hansen CE, Tran R, Mimche PN, Mannino RG, Ciciliano JC, Lamb TJ, Joiner CH, Ofori-Acquah SF, Lam WA. (2018) 'Microvasculature-on-a-chip for the long-term study of endothelial barrier dysfunction and microvascular obstruction in disease', *Nat Biomed Eng*, 2:453-463.

Qiu, Y., Ciciliano, J., Myers, D.R., Tran, R. and Lam, W.A. (2015) 'Platelets and physics: How platelets "feel" and respond to their mechanical microenvironment', *Blood Reviews*, *29*(6), pp.377-386.

Rahmat, A., Weston, D., Madden, D., Usher, S., Barigou, M. and Alexiadis, A. (2020) 'Modeling the agglomeration of settling particles in a dewatering process', *Physics of Fluids*, *32*(12).

Rajeeva Pandian, N.K. and Jain, A. (2022) 'In silico analyses of blood flow and oxygen transport in human micro-veins and valves', *Clinical Hemorheology and Microcirculation*, *81*(1), pp.81-96.

Rajeeva Pandian, N.K., Walther, B.K., Suresh, R., Cooke, J.P. and Jain, A. (2020) 'Microengineered human vein-chip recreates venous valve architecture and its contribution to thrombosis', *Small*, *16*(49), e.2003401.

Rajendran, P., Rengarajan, T., Thangavel, J., Nishigaki, Y., Sakthisekaran, D., Sethi, G. and Nishigaki, I. (2013) 'The vascular endothelium and human diseases', *International Journal of Biological Sciences*, *9*(10), p.1057 –1069.

Rana, A., Westein, E., Niego, B.E. and Hagemeyer, C.E. (2019) 'Shear-dependent platelet aggregation: mechanisms and therapeutic opportunities', *Frontiers in Cardiovascular Medicine*, *6*, p.141.

Rashidi, F., Barco, S., Kamangar, F., Heresi, G.A., Emadi, A., Kaymaz, C., Jansa, P., Reis, A., Rashidi, A., Taghizadieh, A. and Rezaeifar, P. (2021) 'Incidence of symptomatic venous thromboembolism following hospitalization for coronavirus disease 2019: prospective results from a multi-center study', *Thrombosis Research*, *198*, pp.135-138.

Raskob, G.E., Spyropoulos, A.C., Cohen, A.T., Weitz, J.I., Ageno, W., De Sanctis, Y., Lu, W., Xu, J., Albanese, J., Sugarmann, C. and Weber, T. (2021) 'Association between asymptomatic proximal deep vein thrombosis and mortality in acutely ill medical patients', *Journal of the American Heart Association*, *10*(5), p.e019459.

Raskob, G.E., Angchaisuksiri, P., Blanco, A.N., Buller, H., Gallus, A., Hunt, B.J., Hylek, E.M., Kakkar, A., Konstantinides, S.V., McCumber, M. and Ozaki, Y. (2014) 'Thrombosis: a major contributor to global disease burden', *Arteriosclerosis, Thrombosis, and Vascular Biology*, *34*(11), pp.2363-2371.

Raskob, G.E., Spyropoulos, A.C., Cohen, A.T., Weitz, J.I., Ageno, W., De Sanctis, Y., Lu, W., Xu, J., Albanese, J., Sugarmann, C. and Weber, T. (2021) 'Association between asymptomatic proximal deep vein thrombosis and mortality in acutely ill medical patients', *Journal of the American Heart Association*, *10*(5), p.e019459.

Razavi, M. and Thakor, A.S. (2018) 'An oxygen plasma treated poly (dimethylsiloxane) bioscaffold coated with polydopamine for stem cell therapy', *Journal of Materials Science: Materials in Medicine*, *29*, pp.1-14.

Reneman, R.S., Arts, T. and Hoeks, A.P. (2006) 'Wall shear stress–an important determinant of endothelial cell function and structure–in the arterial system in vivo: discrepancies with theory', *Journal of Vascular Research*, *43*(3), pp.251-269.

Rivera, J., Lozano, M.L., Navarro-Núñez, L. and Vicente, V. (2009) 'Platelet receptors and signaling in the dynamics of thrombus formation', *Haematologica*, *94*(5), p.700–711.

Ruben, B., Elisa, M., Leandro, L., Victor, M., Gloria, G., Marina, S., Mian K, S., Pandiyan, R. and Nadhira, L. (2017) 'Oxygen plasma treatments of polydimethylsiloxane surfaces: effect of the atomic oxygen on capillary flow in the microchannels', *Micro & Nano Letters*, *12*(10), pp.754-757.

Ruggeri, Z.M., Orje, J.N., Habermann, R., Federici, A.B. and Reininger, A.J. (2006) 'Activation-independent platelet adhesion and aggregation under elevated shear stress', *Blood*, *108*(6), pp.1903-1910.

Ruggeri, Z.M. and Mendolicchio, G.L. (2007) 'Adhesion mechanisms in platelet function', *Circulation Research*, *100*(12), pp.1673-1685.

Ruiz-Riancho, I.N., Alexiadis, A., Zhang, Z. and Garcia Hernandez, A. (2021) 'A discrete multi-physics model to simulate fluid structure interaction and breakage of capsules filled with liquid under coaxial load', *Processes*, *9*(2), p.354.

Russell, W.M.S. and Burch, R.L. (1959) *The principles of humane experimental technique*. Methuen: London, UK.

Rys, R.N., Blostein, M.D. and Lemarié, C.A. (2018) 'Deep vein thrombosis induced by stasis in mice monitored by high frequency ultrasonography', *JoVE (Journal of Visualized Experiments)*, 13;(134):57392.

Sache, A., Reymond, P., Brina, O., Jung, B., Farhat, M. and Vargas, M.I. (2023) 'Near-wall hemodynamic parameters quantification in in vitro intracranial aneurysms with 7 T PC-MRI', *Magnetic Resonance Materials in Physics, Biology and Medicine*, *36*(2), pp.295-308.

Sakariassen, K.S., Orning, L. and Turitto, V.T. (2015) 'The impact of blood shear rate on arterial thrombus formation', *Future Science OA*, *1*(4).

Sanchez, Z.A.C., Vijayananda, V., Virassammy, D.M., Rosenfeld, L. and Ramasubramanian, A.K. (2022) 'The interaction of vortical flows with red cells in venous valve mimics', *Biomicrofluidics*, 3;16(2):024103.

Sanfilippo, D., Ghiassi, B., Alexiadis, A. and Hernandez, A.G. (2021) 'Combined peridynamics and discrete multiphysics to study the effects of air voids and freeze-thaw on the mechanical properties of asphalt', *Materials*, *14*(7), p.1579.

Sasano, T., Cho, M.S., Rodriguez-Aguayo, C., Bayraktar, E., Taki, M., Afshar-Kharghan, V. and Sood, A.K. (2021) 'Role of tissue-factor bearing extracellular vesicles released from ovarian cancer cells in platelet aggregation in vitro and venous thrombosis in mice', *Thrombosis Update*, *2*, p.100020.

Savage, B., Saldívar, E. and Ruggeri, Z.M. (1996) 'Initiation of platelet adhesion by arrest onto fibrinogen or translocation on von Willebrand factor', *Cell*, *84*(2), pp.289-297.

Schecter, A.D., Giesen, P.L., Taby, O., Rosenfield, C.L., Rossikhina, M., Fyfe, B.S., Kohtz, D.S., Fallon, J.T., Nemerson, Y. and Taubman, M.B. (1997) 'Tissue factor expression in human arterial smooth muscle cells. TF is present in three cellular pools after growth factor stimulation', *The Journal of Clinical Investigation*, *100*(9), pp.2276-2285.

Schillemans, M., Karampini, E., van den Eshof, B.L., Gangaev, A., Hofman, M., van Breevoort, D., Meems, H., Janssen, H., Mulder, A.A., Jost, C.R. and Escher, J.C. (2018) 'Weibel-Palade body localized syntaxin-3 modulates von Willebrand factor secretion from endothelial cells', *Arteriosclerosis, Thrombosis, and Vascular Biology*, *38*(7), pp.1549-1561.

Schindelin, J., Arganda-Carreras, I., Frise, E., Kaynig, V., Longair, M., Pietzsch, T., Preibisch, S., Rueden, C., Saalfeld, S., Schmid, B. and Tinevez, J.Y. (2012) 'Fiji: an open-source platform for biological-image analysis', *Nature Methods*, *9*(7), pp.676-682.

Schofield, Z., Baksamawi, H.A., Campos, J., Alexiadis, A., Nash, G.B., Brill, A. and Vigolo, D. (2020) 'The role of valve stiffness in the insurgence of deep vein thrombosis', *Communications Materials*, *1*(1), p.65.

Schönfelder, T., Jäckel, S. and Wenzel, P. (2017) 'Mausmodelle der tiefen Venenthrombose', *Gefässchirurgie*, *22*, pp.28-33.

Schulman, S., Kearon, C. and Subcommittee on Control of Anticoagulation of the Scientific and Standardization Committee of the International Society on Thrombosis and Haemostasis. (2005) 'Definition of major bleeding in clinical investigations of antihemostatic medicinal products in non-surgical patients', *Journal of Thrombosis and Haemostasis*, *3*(4), pp.692-694.

Schütt, M., Stamatopoulos, K., Simmons, M.J.H., Batchelor, H.K. and Alexiadis, A. (2020) 'Modelling and simulation of the hydrodynamics and mixing profiles in the human proximal colon using Discrete Multiphysics', *Computers in Biology and Medicine*, *121*, p.103819.

Sevitt, S. (1974) 'The structure and growth of valve-pocket thrombi in femoral veins', *Journal of Clinical Pathology*, *27*(7), pp.517-528.

Shaydakov ME, Sigmon DF, Blebea J. (2023) *Thromboelastography*. Treasure Island (FL): StatPearls Publishing.

Shaydakov, M.E., Ting, W., Sadek, M., Aziz, F., Diaz, J.A., Comerota, A.J., Lurie, F., Blebea, J., Eklöf, B.G., Lugli, M. and De Maeseneer, M.G. (2022) 'Extended anticoagulation for venous thromboembolism: A survey of the American Venous Forum and the European Venous Forum', *Journal of Vascular Surgery: Venous and Lymphatic Disorders*, *10*(5), pp.1012-1020.

She, K., Zhang, X., Yin, J., Cheng, G., Chen, X. and Zhang, Y. (2020) 'Case report: lateral axillary-profunda femoris artery bypass for acute lower limb ischemia due to thrombosis after bilateral axillofemoral bypass', *Journal of Cardiothoracic Surgery*, *15*, pp.1-8.

Shen, R., Gao, M., Tao, Y., Chen, Q., Wu, G., Guo, X., Xia, Z., You, G., Hong, Z. and Huang, K. (2021) 'Prognostic nomogram for 30-day mortality of deep vein thrombosis patients in intensive care unit', *BMC Cardiovascular Disorders*, *21*(1), pp.1-14.

Siddique, A., Meckel, T., Stark, R.W. and Narayan, S. (2017) 'Improved cell adhesion under shear stress in PDMS microfluidic devices', *Colloids and Surfaces B: Biointerfaces*, *150*, pp.456-464.

Siddique, A., Pause, I., Narayan, S., Kruse, L. and Stark, R.W. (2021) 'Endothelialization of PDMS-based microfluidic devices under high shear stress conditions', *Colloids and Surfaces B: Biointerfaces*, *197*, p.111394.

Siegal, D.M., Eikelboom, J.W., Lee, S.F., Rangarajan, S., Bosch, J., Zhu, J., Yusuf, S. and Venous Thromboembolism Collaboration. (2021) 'Variations in incidence of venous thromboembolism in low-, middle-, and high-income countries', *Cardiovascular Research*, *117*(2), pp.576-584.

Sim, D.S., Merrill-Skoloff, G., Furie, B.C., Furie, B. and Flaumenhaft, R. (2004) 'Initial accumulation of platelets during arterial thrombus formation in vivo is inhibited by elevation of basal cAMP levels', *Blood*, *103*(6), pp.2127-2134.

Simão, M., Ferreira, J.M., Mora-Rodriguez, J. and Ramos, H.M. (2016) 'Identification of DVT diseases using numerical simulations', *Medical & Biological Engineering & Computing*, *54*, pp.1591-1609.

Skilbeck, C.A., Walker, P.G., David, T. and Nash, G.B. (2004) 'Disturbed flow promotes deposition of leucocytes from flowing whole blood in a model of a damaged vessel wall', *British Journal of Haematology*, *126*(3), pp.418-427.

Soifer, E., Weiss, D., Marom, G. and Einav, S. (2017) 'The effect of pathologic venous valve on neighboring valves: fluid–structure interactions modeling', *Medical & Biological Engineering & Computing*, *55*, pp.991-999.

Sorrentino, S., Studt, J.D., Medalia, O. and Sapra, K.T. (2015) 'Roll, adhere, spread and contract: structural mechanics of platelet function', *European Journal of Cell Biology*, *94*(3-4), pp.129-138.

Stewart, G.J., Ritchie, W.G. and Lynch, P.R. (1974) 'Venous endothelial damage produced by massive sticking and emigration of leukocytes', *The American Journal of Pathology*, *74*(3), p.507–532.

Streets, A.M. and Huang, Y. (2013) 'Chip in a lab: Microfluidics for next generation life science research', Biomicrofluidics, 7(1), p. 11302

Stukowski, A. (2009) 'Visualization and analysis of atomistic simulation data with OVITO–the Open Visualization Tool', *Modelling and Simulation in Materials Science and Engineering*, *18*(1), p.015012.

Takhviji, V., Zibara, K., Maleki, A., Azizi, E., Hommayoun, S., Tabatabaei, M., Ahmadi, S.E., Soleymani, M., Ghalesardi, O.K., Farokhian, M. and Davari, A. (2021) 'A case-control study on factor V Leiden: an independent, gender-dependent risk factor for venous thromboembolism', *Thrombosis Journal*, *19*, pp.1-9.

Tang, P., Wang, Y., Yang, X., Wu, Z., Chen, W., Ye, Y., Jiang, Y., Lin, L., Lin, B. and Lin, B. (2023) 'Protective Role of Endothelial SIRT1 in Deep Vein Thrombosis and Hypoxia-induced Endothelial Dysfunction Mediated by NF-κB Deacetylation', *Inflammation*, pp.1-14.

Taylor, A.M. and Bordoni, B. (2020) *Histology, blood vascular system*. Treasure Island (FL): StatPearls Publishing.

Teixeira, A.L., Padilla, J. and Vianna, L.C. (2017) 'Impaired popliteal artery flow-mediated dilation caused by reduced daily physical activity is prevented by increased shear stress', *Journal of Applied Physiology*, *123*(1), pp.49-54.

Terpos, E., Ntanasis-Stathopoulos, I., Elalamy, I., Kastritis, E., Sergentanis, T.N., Politou, M., Psaltopoulou, T., Gerotziafas, G. and Dimopoulos, M.A. (2020) 'Hematological findings and complications of COVID-19', *American Journal of Hematology*, *95*(7), pp.834-847.

Thomas, G.M., Brill, A., Mezouar, S., Crescence, L., Gallant, M., Dubois, C. and Wagner, D.D. (2015) 'Tissue factor expressed by circulating cancer cell-derived microparticles drastically increases the incidence of deep vein thrombosis in mice', *Journal of Thrombosis and Haemostasis*, *13*(7), pp.1310-1319.

Thomas, S.G. (2019) 'The structure of resting and activated platelets', *Platelets*, pp.47-77.

Tischer, A., Moon-Tasson, L. and Auton, M. (2023) 'Removal of the vicinal disulfide enhances the platelet-capturing function of von Willebrand factor', *Blood, The Journal of the American Society of Hematology*, *141*(12), pp.1469-1473.

Tsao, C.W., Aday, A.W., Almarzooq, Z.I., Anderson, C.A., Arora, P., Avery, C.L., Baker-Smith, C.M., Beaton, A.Z., Boehme, A.K., Buxton, A.E. and Commodore-Mensah, Y. (2023) 'Heart disease and stroke statistics—2023 update: a report from the American Heart Association', *Circulation*, *147*(8), pp.e93-e621.

Tucker WD, Arora Y, Mahajan K. (2023) *Anatomy, Blood Vessels*. Treasure Island (FL): StatPearls Publishing.

Tutwiler, V., Litvinov, R.I., Lozhkin, A.P., Peshkova, A.D., Lebedeva, T., Ataullakhanov, F.I., Spiller, K.L., Cines, D.B. and Weisel, J.W. (2016) 'Kinetics and mechanics of clot contraction are governed by the molecular and cellular composition of the blood', *Blood, The Journal of the American Society of Hematology*, *127*(1), pp.149-159.

Valentijn, K.M., Sadler, J.E., Valentijn, J.A., Voorberg, J. and Eikenboom, J. (2011) 'Functional architecture of Weibel-Palade bodies', *Blood, The Journal of the American Society of Hematology*, *117*(19), pp.5033-5043.

Van Den Berg, A., Mummery, C.L., Passier, R. and Van der Meer, A.D. (2019) 'Personalised organs-on-chips: functional testing for precision medicine', *Lab on a Chip*, *19*(2), pp.198-205.

Van Der Loop, F.T., Gabbiani, G., Kohnen, G., Ramaekers, F.C. and van Eys, G.J. (1997) 'Differentiation of smooth muscle cells in human blood vessels as defined by smoothelin, a novel marker for the contractile phenotype', *Arteriosclerosis, Thrombosis, and Vascular Biology*, *17*(4), pp.665-671.

Van Kruchten, R., Cosemans, J.M. and Heemskerk, J.W. (2012) 'Measurement of whole blood thrombus formation using parallel-plate flow chambers–a practical guide', *Platelets*, *23*(3), pp.229-242.

Vedovati, M.C., Giustozzi, M., Munoz, A., Bertoletti, L., Cohen, A.T., Klok, F.A., Connors, J.M., Bauersachs, R., Brenner, B., Campanini, M. and Becattini, C. (2023) 'Risk factors for recurrence and major bleeding in patients with cancer-associated venous thromboembolism', *European Journal of Internal Medicine*, *112*, pp.29-36.

Vella, M.A., Dumas, R.P., Chreiman, K., Wasser, T., Smith, B.P., Reilly, P.M., Seamon, M.J. and Shiroff, A. (2020) 'Epidural catheters are associated with an increased risk of venous thromboembolism in trauma', *Journal of Thrombosis and Thrombolysis*, *49*, pp.420-425.

von Brühl, M.L., Stark, K., Steinhart, A., Chandraratne, S., Konrad, I., Lorenz, M., Khandoga, A., Tirniceriu, A., Coletti, R., Köllnberger, M. and Byrne, R.A. (2012) 'Monocytes, neutrophils, and platelets cooperate to initiate and propagate venous thrombosis in mice in vivo', *Journal of Experimental Medicine*, *209*(4), pp.819-835.

Vyas V, Goyal A. (2022) *Acute Pulmonary Embolism*. Treasure Island (FL): StatPearls Publishing.

Wakefield, T.W., Wrobleski, S.K., Sarpa, M.S., Taylor Jr, F.B., Esmon, C.T., Cheng, A. and Greenfield, L.J. (1991) 'Deep venous thrombosis in the baboon: an experimental model', *Journal of Vascular Surgery*, *14*(5), pp.588-598.

Wang, J., Huang, W., Zhou, Y., Han, F., Ke, D. and Lee, C. (2020) 'Hemodynamic analysis of VenaTech convertible vena cava filter using computational fluid dynamics', *Frontiers in Bioengineering and Biotechnology*, *8*, p.556110.

Weintraub, N.L. (2009) 'Understanding abdominal aortic aneurysm', *The New England journal of Medicine*, *361*(11), p.1114–1116.

Weitz, J.I., Jaffer, I.H. and Fredenburgh, J.C. (2017) 'Recent advances in the treatment of venous thromboembolism in the era of the direct oral anticoagulants', *F1000Research*, *6*(0).

Wendelboe, A.M. and Raskob, G.E. (2016) 'Global burden of thrombosis: epidemiologic aspects', *Circulation Research*, *118*(9), pp.1340-1347.

Westein, E., de Witt, S., Lamers, M., Cosemans, J.M. and Heemskerk, J.W. (2012) 'Monitoring in vitro thrombus formation with novel microfluidic devices', *Platelets*, *23*(7), pp.501-509.

Westling, A., Bergqvist, D., Boström, A., Karacagil, S. and Gustavsson, S. (2002) 'Incidence of deep venous thrombosis in patients undergoing obesity surgery', *World Journal of Surgery*, *26*, pp.470-473.

White, K.A., Cali, V.J. and Olabisi, R.M. (2021) 'Micropatterning biomineralization with immobilized mother of pearl proteins', *Scientific Reports*, *11*(1), p.2141.

White, R.H. (2003) 'The epidemiology of venous thromboembolism', *Circulation*, 107(23_suppl_1), pp.I-4–8.

Wijeratne, N.S. and Hoo, K.A. (2008) 'Numerical studies on the hemodynamics in the human vein and venous valve', *American Control Conference, Seattle, WA, USA, pp. 147-152*. doi: 10.1109/ACC.2008.4586482.

Winter, W.E., Flax, S.D. and Harris, N.S. (2017) 'Coagulation testing in the core laboratory', *Laboratory Medicine*, *48*(4), pp.295-313.

Wrobleski, S.K., Farris, D.M., Diaz, J.A., Myers Jr, D.D. and Wakefield, T.W. (2011) 'Mouse complete stasis model of inferior vena cava thrombosis', *JoVE (Journal of Visualized Experiments)*, (52), p.e2738.

Wu, B., Du, F., Wenjing, A., Liu, F., Liu, Y., Zheng, W., Li, G. and Wang, X. (2022) 'Graphene-ophicalcite heterogeneous composite sponge for rapid hemostasis', *Colloids and Surfaces B: Biointerfaces*, *216*, p.112596.

Wu, W.T., Zhussupbekov, M., Aubry, N., Antaki, J.F. and Massoudi, M. (2020) 'Simulation of thrombosis in a stenotic microchannel: The effects of vWF-enhanced shear activation of platelets', *International Journal of Engineering Science*, *147*, p.103206.

Yakusheva, A.A., Butov, K.R., Bykov, G.A., Závodszky, G., Eckly, A., Ataullakhanov, F.I., Gachet, C., Panteleev, M.A. and Mangin, P.H. (2022) 'Traumatic vessel injuries initiating hemostasis generate high shear conditions', *Blood Advances*, *6*(16), pp.4834-4846.

Yesudasan, S. and Averett, R.D. (2019) 'Recent advances in computational modeling of fibrin clot formation: A review', *Computational Biology and Chemistry*, *83*, p.107148.

Zhang, P., Leger, A.J., Baleja, J.D., Rana, R., Corlin, T., Nguyen, N., Koukos, G., Bohm, A., Covic, L. and Kuliopulos, A. (2015) 'Allosteric activation of a G protein-coupled receptor with cell-penetrating receptor mimetics', *Journal of Biological Chemistry*, *290*(25), pp.15785-15798.

Zhang, Y.S., Oklu, R. and Albadawi, H. (2017) 'Bioengineered in vitro models of thrombosis: methods and techniques', *Cardiovascular Diagnosis and Therapy*, *7*(Suppl 3), p.S329.

Zhang, Y., Tu, D., Shen, Q. and Dai, Z. (2019) 'Fish scale valorization by hydrothermal pretreatment followed by enzymatic hydrolysis for gelatin hydrolysate production', *Molecules*, *24*(16), p.2998.

Zheng, W., Jiang, B., Wang, D., Zhang, W., Wang, Z. and Jiang, X. (2012) 'A microfluidic flow-stretch chip for investigating blood vessel biomechanics', *Lab on a Chip*, *12*(18), pp.3441-3450.

Ziliotto, N., Bernardi, F. and Piazza, F. (2021) 'Hemostasis components in cerebral amyloid angiopathy and Alzheimer's disease', *Neurological Sciences*, *42*(8), pp.3177-3188.

APPENDIX

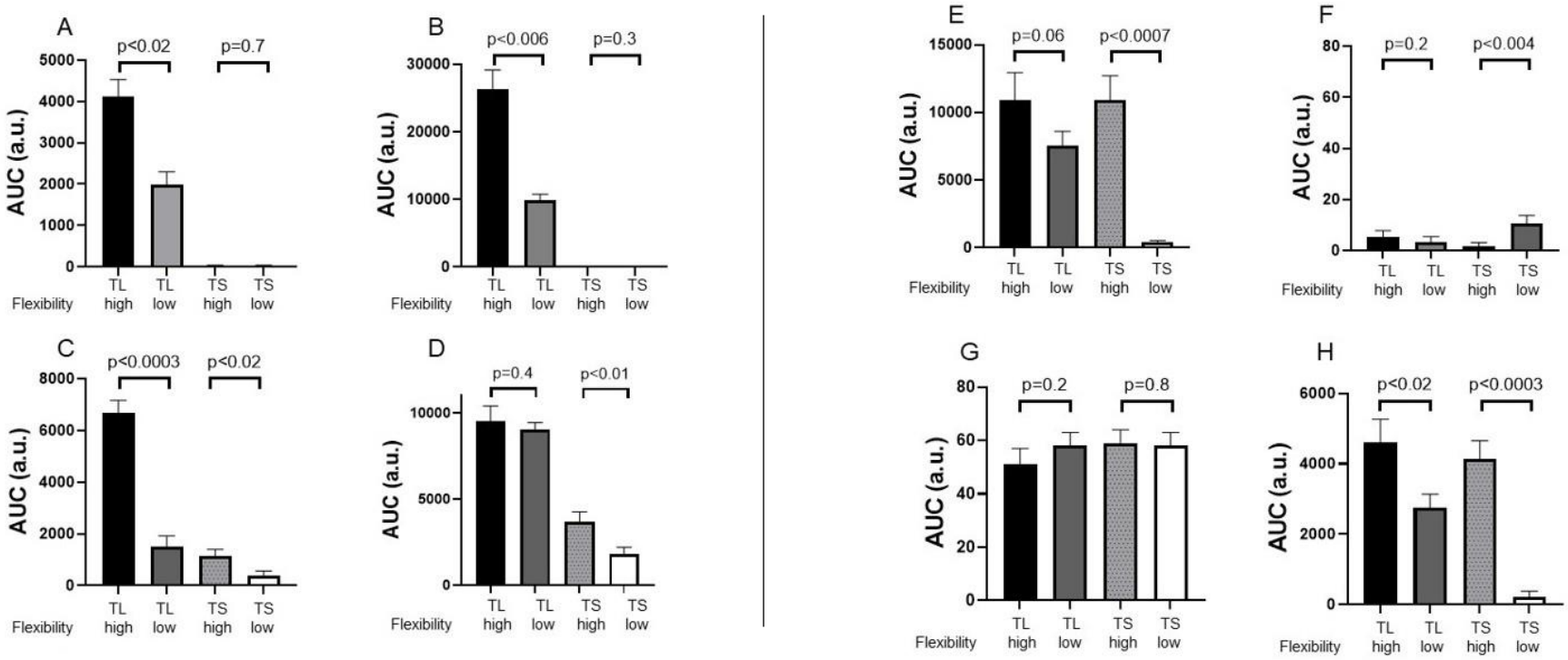

Figure A.1: AUC at TL and TS areas of flexible and less/non-flexible leaflets. AUC of platelets deposited at the TL and TS areas of **(A)** symmetrical valve, **(B)** non-symmetrical valve, **(C)** resting platelets + eptifibatide, **(D)** thrombin-activated platelets, **(E)** thrombin-activated platelets + eptifibatide, **(F)** resting platelets treated with OS-1, **(G)** thrombin-activated platelets treated with OS-1, and **(H)** histamine-treated HUVECs is presented as mean ± SD. Statistical comparison was performed by unpaired Student's t-test.

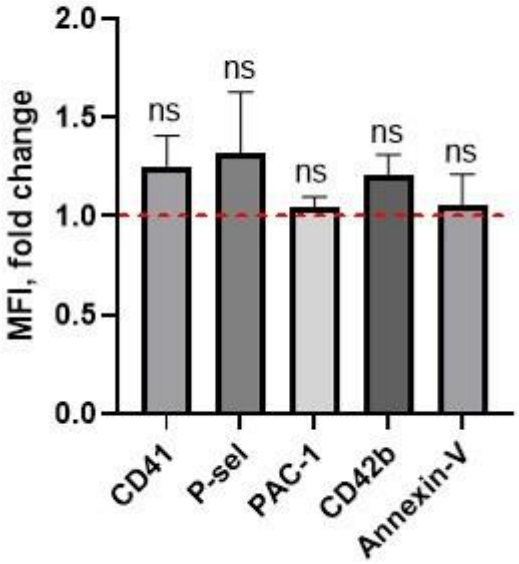

Figure A.2: Passage through the flow system does not activate platelets. Expression of CD41/GPIIb-IIIa, P-selectin, active CD41/GPIIb/IIIa (PAC-1), CD42b/GPIba and phosphatidylserine (annexin V) on platelets in the whole blood was analyzed before and after passage through the microfluidics chamber. Red dashed line represents the level of expression before the passage. Bars represent mean fluorescence intensity (MFI), mean ± SD. Statistical comparison was performed by unpaired Student's t-test.